Publications

Strypsteen, G., Van Rijn, L.C. and Rauwoens, P. (2019). On the relation between predicted and observed aeolian transport rates: a field study at the Belgian coast. *Aeolian Research* (under review).

Strypsteen, G., Houthuys, R. and Rauwoens, P. (2019). Dune evolution at decadal timescales and its relation with potential aeolian transport. Submitted to: *Journal of Marine Science and Engineering, 7(10), 357.*

Strypsteen, G., De Sloover, L., De Wulf, A., and Rauwoens, P. (2019). Downwind evolution of aeolian saltation across an artificially constructed coastal berm. Submitted to: *Aeolian Research.*

Strypsteen, G., and Rauwoens, P. (2019). Aeolian sand transport across a shell-fragmented beach: a field study. Submitted to: *Journal of Coastal Research.*

Van Rijn, L.C. and **Strypsteen, G.** (2019). A fully predictive model for aeolian sand transport. *Coastal Engineering* (accepted).

Restoration and maintenance of coastal beach and dune systems requires knowledge of aeolian sediment transport processes for the prediction of system response to wind forces over short to long-term timescales. This allows for appropriate management of storms in addition to seasonal and decadal variations. Accurate aeolian sediment transport equations are of utmost importance for modern geomorphology and coastal engineering practices. Although sand transport by wind is easily observable, reliable and accurate data sets of sand transport rates are of scarcity due to measuring difficulties. Field monitoring is essential to understand its impact in the overall sediment budgets and long-term coastal dune behavior. The main objective of this thesis is unravelling the nature of aeolian sand transport on the Belgian coast, enlarging the knowledge with the aim to improve long-term aeolian sediment transport estimates. The overall aim of the thesis is based on analyzing collected data from field experiments carried out between 2016 and 2018. This work is performed within the framework of the project CREST (Climate REsilient coaST), funded by the Strategic Basic Research (SBO) program of Flanders Innovation & Entrepreneurship, Belgium. Within the project, it is aimed to further the knowledge of coastal processes on land and under water.

Monitoring and Modelling Aeolian Sand Transport at the Belgian Coast

Glenn Strypsteen

Monitoring and Modelling Aeolian Sand Transport at the Belgian Coast

Glenn Strypsteen

About the author

Glenn Strypsteen was born in Bruges, Belgium on November 7, 1990. After graduating from high school in 2009, he attended KU Leuven where he graduated as a Civil Engineer in 2013. During his last year of university, he studied in Brno, Czech Republic for 6 months where he finished his Master's dissertation entitled "Process of Aeolian transport using the EIS-method" under the supervision of Prof. dr. ir. Björn Van de Walle and Prof dr. ing. Jana Parilkova. His research focused on examining influence of moisture on aeolian sediment transport in a small lab-scale wind tunnel. There, he developed an early passion for science and aeolian sediment processes. Subsequent to finishing his Master's, he worked with his father in construction for one year. Despite enjoying this adventure, he missed the stimulating and intellectual atmosphere university and academia offers and returned to start his academic career as a research assistant in 2014. One year later, he started a PhD, supervised by Prof. dr. ir. Pieter Rauwoens, on this thesis entitled "Monitoring and Modelling Aeolian Sand Transport at the Belgian Coast". It felt for him a natural choice, since he always wanted to do embark on a PhD. Furthermore, this topic holds societal relevance as well as contextual relevance for the prevalence of large storms and rising sea levels. In his doctoral thesis, he made qualitative contributions to the aeolian research field where he focused on the nature of aeolian sand transport at the Belgian coast. Glenn is known for being an enthusiastic, driven and adventurous person. His personal hobbies include climbing, bouldering, "vanlife", hiking, traveling and landscape photography.



FACULTY OF ENGINEERING TECHNOLOGY.
DEPARTMENT OF CIVIL ENIGINEERING
TECHNOLOGY CLUSER CONSTRUCTION
Spoorwegstraat 12,
B-8200 Brugge
glenn.strypsteen@kuleuven.be
https://iiw.kuleuven.be/onderzoek/kustwaterbouw-grondmechanica/kustwaterbouw-grondmechanica

Glenn STRYPSTEEN

MONITORING AND MODELLING AEOLIAN SAND TRANSPORT AT THE BELGIAN COAST

December 2019

KU LEUVEN

ARENBERG DOCTORAL SCHOOL
Faculty of Engineering Technology

Monitoring and Modelling Aeolian Sand Transport at the Belgian Coast

Glenn Strypsteen

Supervisor:
Prof. dr. ir. Pieter Rauwoens

Dissertation presented in partial fulfilment of the requirements for the degree of Doctor of Engineering Technology (PhD)

December 2019

Monitoring and Modelling Aeolian Sand Transport at the Belgian Coast

GLENN STRYPSTEEN

© 2019 KU Leuven – Faculty of Engineering Technology
Uitgegeven in eigen beheer, Glenn Strypsteen, Celestijnenlaan 200A box 2402, B-3001 Leuven (Belgium)

Alle rechten voorbehouden. Niets uit deze uitgave mag worden vermenigvuldigd en/of openbaar gemaakt worden door middel van druk, fotokopie, microfilm, elektronisch of op welke andere wijze ook zonder voorafgaande schriftelijke toestemming van de uitgever.

All rights reserved. No part of the publication may be reproduced in any form by print, photoprint, microfilm, electronic or any other means without written permission from the publisher.

Monitoring and Modelling Aeolian Sand Transport at the Belgian Coast

DISSERTATION

presented in partial fulfillment
of the requirements for the degree of
Doctor of Engineering Technology (PhD)

by

Glenn STRYPSTEEN
Born on 7 November 1990
in Bruges, Belgium

The dissertation has been approved by the promotor prof. dr. ir. Pieter Rauwoens.

Composition of the examination committee:

Prof. dr. ir. Liesbet Van der Perre	Chairman (KU Leuven)
Prof. dr. ir. Pieter Rauwoens	Promotor (KU Leuven)

Assessor (member of supervisory committee):

Prof. dr. Gerard Govers	KU Leuven
Prof. dr. ir. Jaak Monbaliu	Secretary (KU Leuven)
Ir. Daphné Thoon	MOW-MDK
Dr. ir. Thijs Lanckriet	Fluves

Additional members:

Prof. dr. Irene Delgado-Fernandez	Edge Hill University, UK
Dr. ir. Sierd De Vries	TU Delft, The Netherlands
Prof. dr. Margaret Chen	VUB, Belgium

December 2019

"Most impossible goals can be met simply by breaking them down into bite size chunks, writing them down, believing them and going full speed ahead as if they were routine."

Don Lancaster

Preface

After working in my dad's construction company for one year, I started my academic career as a research assistant in 2014 in the research group RecyCon (Recycling in Construction) of the Department of Civil Engineering, Faculty of Engineering Technology, Technology Cluster Construction, KU Leuven. Science has always piqued my curiosity and it seemed a respectable opportunity to give my curiosity a purpose. One year later my supervisor, Prof. dr. ir. Pieter Rauwoens, started as a new professor in the coastal engineering research group of the Technology Cluster and was fortuitously searching for PhD candidates. Of the various topics being offered, 'Monitoring and Modelling Aeolian Sand Transport at the Belgian Coast' felt serendipitous given my MSc. dissertation was in the same research field and a PhD was an achievement I would always have envisioned for myself. Furthermore, this topic holds societal value and is contextually relevant for the prevalence of large storms and rising sea levels.

During these four years as a PhD student, I have experienced the multifaceted nature of research. Initially when I started, I was understandably enthusiastic, but was soon confronted with my own lack of knowledge. Meeting and working with people in the same field helped with motivation and formulation of novel ideas which can be fulfilling especially if beneficial for other researchers alike.

Many people are deserving of my gratitude - whom without, this thesis would not have been possible. Firstly, I would like to thank my supervisor, Prof. dr. ir. Pieter Rauwoens, for giving me the opportunity to join his research group 'Coastal Engineering & Geotechnics' and introducing me to coastal research. But mostly for having confidence in me during my employment as a PhD student and allowing me freedom. Given I am an adventurous person and travel a lot, I was glad to have had opportunities to attend international conferences, research stays and summer schools. This was of value to my research and personal motivation.

Several people have made notable contributions in various stages during this research period. Thank you to the members of my supervisory committee, Prof. dr. ir. Jaak Monbaliu, Prof. dr. Gerard Govers, dr. ir. Thijs Lanckriet and ir. Daphné Thoon for you interest and useful comments.

I have very good memories of the numerous aeolian field campaigns I conducted in the past four years and special memories of the very first one on 13th May 2016. A lot of work, a lot of planning and many discussions made it a very success. It illustrates how a group of enthusiastic researchers are able to build a beautiful monitoring set-up where lots of qualitative data can be gathered. Therefore, special thanks goes to researchers and students from the VUB, Ghent University, Flanders Hydraulics Research, University of Twente, and other institutions for the planning, help, and data-processing during the measurement campaigns: Annelies Vandenbulcke, Alain De Wulf, Lars De Sloover, Jeffrey Verbeurgt, Bart De Wit, Samuel Van Ackere, Evelien Brand, Pieter Rauwoens, Vincent Gruwez, Ine Vandebeek, Anne-Lise Montreuil, Toon Verwaest, Francesca Ortenzio, Sebastiaan Dan, Matthias Wyffels, Janus Van Massenhove, Stijn Willemse, Eva De Grande, Tanguy De Moor, Tina Mertens, Margaret Chen, Sander Vos, Leonardo Duarte Campos, Kathelijne Wijnberg, Ellen Bastiaensen, Kathleen Van Meel, and Lia De Bruyn.

I thank the support of VLIZ (Flanders Marine Institute) for the use of their research infrastructure, the maintenance of the research infrastructure, and the help for manufacturing the meteorological stations. The people responsible for this are: Andre Cattrijse, Jan Vermaut, Tim Deckmyn, Robin Houthoofdt, Michiel T'Jampens, Dries Vandewoude, and Wim Versteeg.

I would also like to thank the municipalities of Ostend and Koksijde to make it possible to do the much-needed research on their beaches. My sincere gratitude goes to the people of the surfclub 'Windekind' in Koksijde. Thanks for the opportunity to use your facilities and to store our research instrumentation. Sven Fransen and Julie Monseweyer, thank you.

The support of Coastal Division of the Flemish Government, Department of Mobility and Public Works cannot be forgotten. Thank you to make it possible to use the data of dune volume and wind.

Thanks to the people at TU Delft, Utrecht University, University of Twente, Edge Hill University, University of Algarve and other institutions for the inspiring talks and great feedback. It was enjoyable to talk to people with similar research objectives or research experience. Susana Costas, André Pacheco, Sierd de Vries, Irene Delgado-Fernandez, Nicholas O'Keeffe, Tom Doyle, Kathelijne Wijnberg, Leonardo Duarte Campos, Filipe Galiforni Silva, Isaac Williams, Gerben Ruessink, Winnie de Winter, Pam Hage, Yvonne Smit, Jasper Donker, Bas Hoonhout, Bas Arens, Dano Roelvink, Rik Houthuys, Andreas Baas, and the anonymous reviewers for the little pieces of the puzzle that made up this thesis.

Special thanks to Prof. dr. Leo van Rijn, who has greatly contributed to the design and actualisation of this research. Even having met during the last months of my PhD research, I feel that with our many discussions and phone

calls, a lot of feedback and qualitative information resulted from it. I hope to continue work with you in the future.

I would like to thank my fellow KU Leuven PhD colleagues, especially my best friend and office mate, Zeger Sierens, for the much-needed talks when I really needed it. Thanks to Bart Roest for the help with Matlab, to make beautiful graphs and figures, and the interesting discussions we had about the Belgian coast. Thanks to PhD-colleagues, Brecht Devolder, Brecht Vandevyvere, Xiaoguang Chen, Jiawei Tan, Yuelin Li, and Inti Vanmechelen to put a smile on my face.

Huge thanks to my close friends Adriaan Vandenbrande, Koen Surmont, Johanna Bendas, and Jamie Vandenberghe for their motivating talks about past, present and future. Hopefully we can continue doing that for the rest of our lives.

Nevertheless, thanks to all the people from the climbing gym 'Biover' where I always could "hang" out with. It was and it still is a good way to rest my brain and thoughts.

Special thanks to Naadirah Moola for proofreading this thesis, without you there would be still grammatical errors in the text which I could not forgive myself.

I would like to finish with thanking my parents, sisters and family for their contribution, support and guidance throughout these past years. I cannot describe how much I appreciate your help.

Glenn Strypsteen
Brugge, September 2019



Abstract

Restoration and maintenance of coastal beach and dune systems requires knowledge of aeolian sediment transport processes for the prediction of system response to wind forces over short to long-term timescales. This allows for appropriate management of storms in addition to seasonal and decadal variations. Accurate aeolian sediment transport equations are of utmost importance for modern geomorphology and coastal engineering practices. Although sand transport by wind is easily observable, reliable and accurate data sets of sand transport rates are of scarcity due to measuring difficulties. Field monitoring is essential to understand its impact in the overall sediment budgets and long-term coastal dune behavior. The main objective of this thesis is unravelling the nature of aeolian sand transport on the Belgian coast, enlarging the knowledge with the aim to improve long-term aeolian sediment transport estimates. The overall aim of the thesis is based on analyzing collected data from field experiments carried out between 2016 and 2018. This work is performed within the framework of the project CREST (Climate REsilient coaST), funded by the Strategic Basic Research (SBO) program of Flanders Innovation & Entrepreneurship, Belgium. Within the project, it is aimed to further the knowledge of coastal processes on land and under water.

To gain initial insight into the relationship between aeolian sand transport rates and wind speed, simultaneous monitoring of meteorological conditions and aeolian sand transport rates, using Modified Wilson And Cook (MWAC) sand traps, was carried out on the subaerial beach of two study sites in Belgium. The study sites comprise the natural beach-dune system of Koksijde and the managed beach-dyke system of Mariakerke. Six aeolian mathematical models, each predicting saturated transport rates, are used for objective testing. Some of the models are frequently used for long-term budget calculations. Recently, new models have been proposed in literature that require validation from qualitative field measurements. The key parameter in all these aeolian models is the shear velocity, u_*. Shear velocities are calculated using vertical wind profile data from meteorological stations located on the beach. A modified Bagnold model was able to produce a strong one-to-one relation between observed and predicted transport rates. The other aeolian models produced poor results, underestimating and/or overestimating sediment transport rates.

While short-term aeolian sediment transport rates and wind speed are correlated by a modified Bagnold model, it seems of particular interest to study its relationship with annual to decadal dune behavior. To gain insight in dune behavior and the processes covering dune growth, long-term changes in dune volume at the Belgian coast are analyzed based on measured data by airborne surveys. The Belgian government has been monitoring the eastern part of the coastline since 1979, and since 1983 the entire coastline by annually or bi-annually surveying cross-shore bathymetric profiles and collecting airborne photogrammetric and, since 1999, airborne Laser Scanner (LiDAR) data. For most of the 65 km long coastal stretch, a linearly dune growth is found. It varies between 0-12.3 $m^3/m/year$ with an average linear dune growth of 6.2 $m^3/m/year$, featuring large spatial variations in longshore directions. The dune volume is defined as the volume of sand above the dune foot level. The dune foot level along the Belgian coast is defined at +6.89 m TAW (Belgium Ordnance Datum). In this thesis, the longshore spatial and temporal variations in dune volume changes are derived and correlated with potential sediment transport. Based on a wind data set from the period between 2000 and 2017, it is found that potential aeolian sediment transport has its main drift from west to south-west direction (onshore to oblique onshore). Based on the modified Bagnold model, onshore potential aeolian sediment transport ranges maximum to 9 $m^3/m/year$, while longshore potential aeolian sediment transport could reach up to 20 $m^3/m/year$. An important correlation is found between observed and predicted dune development at decadal timescales when zones with dune managing activities are excluded. Most of the predicted data are within a factor 2 of the measured values. The variability in potential transport is well related to the variability in dune volume changes at the considered spatial–temporal scale, suggesting that natural dune growth is primarily caused by aeolian sediment transport from the beach. It also suggests that annual differences in forcing and transport limiting conditions (wind and moisture) only have a modest effect on the overall variability of dune volume trends.

At the Belgian coast, the beach profile is also regularly altered by human intervention to limit aeolian sand towards the hinterland as it often results in large depositions of sand on neighboring roads and tram tracks. Each year, the municipalities do large investments in the maintenance of their streets and sewer systems. A field experiment was designed to carry out simultaneous measurements of wind and sediment transport across a human-constructed high berm with a steep seaward cliff that is backed by a dyke. In front of the dyke, a trench is excavated to prevent aeolian sand being blown to the hinterland. Two sets of measurements were carried out, one with oblique onshore and one with winds directly onshore. Over-steepened velocity profiles and thus large shear velocities were measured at the steep cliff during the onshore wind event compared to the back beach due to flow compression and acceleration. The fetch effect has been measured across the flat berm where maximum transport was achieved at a distance of 20 to 35 m of the berm lip. The fetch effect is characterized with an overshoot during the oblique onshore wind event. Sand

flux rapidly increased towards a maximum value followed by a decrease to a lower equilibrium value which was approximately half of the maximum mass flux obtained at the critical fetch distance. The evolution of the vertical mass flux profiles downwind caused the grain distribution above the surface (decay rate) to increase almost linear with increasing fetch length further away from the berm lip, until an equilibrium is achieved. This means that the distribution of particle trajectories changed similar until it was stable for different transport events on a flat dry beach surface. Based on this study, the steep cliff in front of the human-constructed coastal berm is very sensitive to erosion due to aeolian sand transport. Sand being eroded from the berm lip is deposited in front of the dyke and in the trench.

When studying aeolian sediment transport in coastal zones, often a location is chosen where the number of supply-limiting factors is minimal (e.g. moisture, shells, vegetation) to ensure better comparison between predicted and observed values. However, as is often the case in a natural coastal environment, the beach contains bed irregularities caused by wind action, patches of pebbles, beach wrack, shells and shell-fragments, vegetation and beach litter. The effect of these small-scale bed features is frequently disregarded when conducting field experiments, even sometimes called insignificant. Therefore, the effect of largely scattered shell pavement on aeolian sand transport on the upper beach of a natural beach-dune system was studied during a short-term field experiment in the winter of 2016 in Belgium. The coverage of shell pavement on the upper beach increased towards the dunes and was highest just in front of the dune foot. Continuous sand transport occurred during strong highly oblique onshore wind and was measured during two experiments. During the two experiments, spatial variations in aeolian sand transport indicate that there was a consistent decrease in transport rate with distance downwind. Within 162 m, aeolian sand transport decreased by factor of 10 from the high waterline in the direction of the dunes. The negative gradient in transport caused local deposition of sand on the upper beach in the form of mobile rippled sand strips. This accumulation of sand acted as a new source area for aeolian transport to the dunes when the intertidal beach was inundated. However, as this region is also very sensitive to wave run-up, the accumulated sand may be removed again from the upper beach. The vertical distribution and median grain size of airborne sand particles across the shell-fragmented beach remained constant.

The main conclusions of this research are that on a short-time scale (hours to days), aeolian sediment transport rate is cubic related with wind speed by a modified Bagnold model. On decadal timescales, an important correlation between observed and predicted dune development is also found. This indicates that dune growth is primarily caused by aeolian sediment transport from the beach and that annual differences in forcing and transport limiting conditions only have a slight effect on the overall variability of dune volume trends. It also suggests that the modified Bagnold model proves to perform strong on longer timescales. During moderate onshore and oblique onshore wind, measurements

on a high flat berm with a steep seaward cliff indicate the presence of the fetch and overshoot effect. It was observed that the evolution of the vertical mass flux profiles downwind causes the exponential decay rate to increase almost linear with increasing fetch length until an equilibrium decay rate is achieved. The effect of shell pavement and moisture on a beach is significant and cannot be disregarded. Aeolian sand transport can be reduced by a factor 10 within a short distance downwind, causing local accumulation of sand which is not entering the dunes directly. Though, shells do not have an influence on the vertical distribution and grain size of airborne sand particles downwind. Further research should focus on better quantifying aeolian sediment transport rates by more innovative monitoring techniques, especially when long-term monitoring is required. Further research should also focus more on the influence of bed roughness and its feedback to the wind shear velocity on aeolian sediment transport. Additionally, a change in decadal dune behavior due to climate change is also very relevant to study.

Samenvatting

Om met stormperiodes, seizoens- en decadale variaties om te gaan, vereist het herstel en onderhoud van strand- en duinsystemen kennis van eolische sedimenttransportprocessen. Dit is nodig om het gedrag van het strand- en duinsysteem op windactie op korte tot lange termijn te voorspellen. Nauwkeurige eolische sedimenttransport voorspellingen zijn van het grootste belang voor de moderne geomorfologie en kustmanagement. Hoewel zandtransport door wind gemakkelijk waarneembaar is, zijn betrouwbare en nauwkeurige datasets van zandtransporthoeveelheden nauwelijks beschikbaar vanwege de meetmoeilijkheden. Veldmonitoring is essentieel om de impact ervan op de algehele sedimentbegrotingen en het gedrag van duinen op lange termijn te begrijpen. Het hoofddoel van dit proefschrift is het verkennen van de aard van eolisch zandtransport aan de Belgische kust, om de kennis te vergroten met als doel het verbeteren van voorspellingen van eolisch sedimenttransport op lange termijn. Het algemene doel van het proefschrift is gebaseerd op het analyseren van verzamelde data van veldexperimenten uitgevoerd tussen 2016 en 2018. Dit werk wordt uitgevoerd in het kader van het project CREST (Climate REsilient coaST), gefinancierd door het Strategisch Basis Onderzoek programma (SBO) van het Agentschap Innoveren en Ondernemen, België. De doelstelling van het project is het vergroten van de kennis van kustprocessen op land en onder water.

Om een eerste inzicht te krijgen in de relatie tussen eolische zandtransporthoeveelheden en windsnelheid, werd gelijktijdige monitoring van meteorologische condities en eolische zandtransporthoeveelheden, met behulp van Modified Wilson And Cook (MWAC) zandvangers, uitgevoerd op het strand van twee onderzoekslocaties in België. De studielocaties omvatten het natuurlijke strand-duinsysteem van Koksijde en het beheerde strand-dijksysteem van Mariakerke. Zes eolische wiskundige modellen, die elk verzadigde transporthoeveelheden voorspellen, werden getest. Sommige modellen worden vaak gebruikt voor budgetberekeningen op lange termijn. Recent worden in de literatuur echter nieuwe modellen voorgesteld die gevalideerd moeten worden op basis van kwalitatieve veldmetingen. De belangrijkste parameter in al deze eolische modellen is de sleepsnelheid, u_*. Sleepsnelheden werden berekend met behulp van verticale windprofielgegevens van op het strand gepositioneerde

meteorologische stations. Een aangepast Bagnold-model was in staat een sterke één-op-één-relatie tot stand te brengen tussen waargenomen en voorspelde transporthoeveelheden. De andere eolische modellen leverden minder goede resultaten op, waarbij de transporthoeveelheden werden onderschat en/of overschat.

Hoewel eolische sedimenttransporthoeveelheden en windsnelheid op korte termijn worden gecorreleerd met een aangepast Bagnold-model, lijkt het van bijzonder belang om de relatie met jaarlijks tot decadaal duingedrag te bestuderen. Om inzicht te krijgen in het duingedrag en de processen die de duingroei bestrijken, werden langetermijnveranderingen in duinvolume aan de Belgische kust geanalyseerd op basis van topografische metingen. Sinds 1979 monitort de Belgische overheid het oostelijke deel van de kustlijn en sinds 1983 de gehele kustlijn door jaarlijks of tweejaarlijks cross-shore bathymetrische profielen te meten en fotogrammetrische gegevens te verzamelen. Sinds 1999, worden Airborne Laser Scanner (LiDAR) gegevens verzameld. Voor het grootste deel van de 65 km lange kustlijn werd een lineair positieve trend in duinvolumeverandering gevonden. Duingroei varieert tussen 0-12.3 $m^3/m/jaar$ met een gemiddelde van 6.2 $m^3/m/jaar$, met grote ruimtelijke kustlangse variaties. Het duinvolume wordt gedefinieerd als het volume zand boven het duinvoetniveau. Het duinvoetniveau langs de Belgische kust is gedefinieerd op +6.89 m TAW. In dit proefschrift worden de kustlangse ruimtelijke en temporele variaties in duinvolumeveranderingen afgeleid en gecorreleerd met potentieel sedimenttransport. Op basis van een winddataset uit de periode 2000 tot 2017 blijkt dat potentieel eolisch sedimenttransport zijn belangrijkste koers heeft uit west en zuidwestelijke richting (richting onshore tot schuin-onshore). Gebaseerd op het aangepaste Bagnold-model varieert onshore potentieel eolisch sediment-transport tot maximaal 9 $m^3/m/jaar$, terwijl het kustlangs kan oplopen tot 20 $m^3/m/jaar$. Een belangrijk verband werd gevonden tussen waargenomen en voorspelde duinontwikkeling op decadale tijdschalen wanneer zones met duinbeheeractiviteiten werden uitgesloten. De meeste voorspelde waarden liggen binnen een factor 2 van de gemeten waarden. De variabiliteit in potentieel transport is goed gerelateerd aan de variabiliteit in duinvolume-veranderingen op de beschouwde ruimtelijk-temporele schaal. Dit suggereert dat duingroei voornamelijk wordt veroorzaakt door eolisch sedimenttransport vanaf het strand. Het suggereert eveneens dat jaarlijkse verschillen in wind condities en transportbeperkende omstandigheden (windsnelheid en vocht) slechts een gering effect hebben op de algehele variabiliteit in duinvolumetrends.

Aan de Belgische kust wordt het strandprofiel ook regelmatig gewijzigd door menselijk ingrijpen om eolisch zand naar het achterland te beperken, omdat het vaak resulteert in grote afzettingen op aangrenzende wegen en tramsporen. Elk jaar doen de gemeenten grote investeringen in het onderhoud van hun straten en rioleringen. Een veldexperiment werd ontworpen om gelijktijdige metingen van wind- en sedimenttransport uit te voeren over een door mensen geconstrueerde hoge berm met een steile zeewaartse klif die wordt afgeschermd

door een dijk. Voor de dijk werd een geul uitgegraven om te voorkomen dat eolisch zand naar het achterland wordt geblazen. Twee reeksen metingen werden uitgevoerd, één met schuin aanlandige wind en één met winden meteen aanlandig. Steilere snelheidsprofielen en dus grotere sleepsnelheden werden gemeten aan de klif tijdens het aanlandig windevent dan op het achterstrand als gevolg van stromingscompressie en versnelling. Het "fetch-effect" werd gemeten over de vlakke berm waar maximaal transport werd bereikt op een afstand van 20 tot 35 m van de bermlip. Het "fetch-effect" werd gekenmerkt door een "overshoot" tijdens het schuine windevenement. Zandflux nam snel toe naar een maximale waarde gevolgd door een afname naar een lagere evenwichtswaarde die ongeveer de helft was van de maximale massaflux verkregen op de kritische fetch-afstand. De evolutie van de verticale massafluxprofielen windafwaarts zorgt ervoor dat de zandkorreldistributie boven het zandoppervlak bijna lineair toeneemt met toenemende fetchlengte verder weg van de bermlip, totdat een evenwicht wordt bereikt. Hierin is saltatie volledig ontwikkeld waar zanddeeltjes een relatief stabiele verdeling vertonen. Op basis van deze studie is de steile zeewaartse klif zeer gevoelig voor erosie door eolisch zandtransport. Zand dat wordt geërodeerd aan de bermlip wordt afgezet voor de dijk en in de geul.

Bij het bestuderen van eolisch sedimenttransport in kustgebieden wordt vaak een locatie gekozen waar het aantal transportbeperkende factoren minimaal is (bijv. vocht, schelpen, vegetatie), om een betere vergelijking tussen voorspelde en waargenomen waarden te garanderen. Echter, zoals vaak het geval is in een natuurlijke kustomgeving, bevat het strand bed-onregelmatigheden veroorzaakt door windwerking, stukken kiezelstenen, strandwrak, schelpen en schelpfragmenten, vegetatie en strandafval. Het effect van deze kleinschalige bedkenmerken wordt vaak buiten beschouwing gelaten bij het uitvoeren van veldexperimenten, zelfs soms insignificant genoemd. Het effect van schelpen op eolisch zandtransport op het droogstrand van een natuurlijk strand-duinsysteem werd daarom onderzocht tijdens een kortdurig veldexperiment in de winter van 2016 in België. De dekking van de schelpen op het droogstrand nam toe richting de duinen en was het hoogst vlak voor de duinvoet. Continu zandtransport vond plaats tijdens sterke, zeer schuin aanlandige wind en werd gemeten tijdens twee experimenten. Tijdens de twee experimenten gaven ruimtelijke variaties in eolisch zandtransport aan dat er sprake is van een consistente afname in transporthoeveelheid windafwaarts. Binnen 162 m nam het eolisch zandtransport met een factor 10 af vanaf de hoogwaterlijn in de richting van de duinen. De negatieve gradiënt in transport veroorzaakte lokale afzetting van zand op het droogstrand in de vorm van mobiele golvende zandstroken. Deze ophoping van zand fungeerde als een nieuw brongebied voor eolisch transport naar de duinen wanneer het getijdenstrand onder water stond. Omdat dit gebied echter ook zeer gevoelig is voor golfoploop, kan het afgezette zand weer van het droogstrand worden verwijderd. De verticale distributie en korrelgrootte van de windgedreven zanddeeltjes over het strand met schelpen wijzigt niet.

De belangrijkste conclusies van dit onderzoek zijn dat op korte tijdsschaal (uren tot dagen) eolische sedimenttransport kubisch is gerelateerd aan de windsnelheid en dat het kan geformuleerd worden via een aangepast Bagnold-model. Op decadale tijdschaal werd ook een belangrijke correlatie gevonden tussen waargenomen en voorspelde duinontwikkeling. Dit geeft aan dat duingroei voornamelijk wordt veroorzaakt door eolisch sedimenttransport vanaf het strand en dat jaarlijkse verschillen in windcondities en transportbeperkende omstandigheden slechts een gering effect hebben op de algehele variabiliteit in duinvolumetrends. Het suggereert ook dat het aangepast Bagnold-model sterk blijkt te presteren op langere tijdschalen. Tijdens aanlandige wind geven metingen op een vlakke berm met een steile zeewaartse klif aan op de aanwezigheid van het fetch- en overshooteffect. Er werd waargenomen dat de evolutie van de verticale massaflux-profielen windafwaarts ervoor zorgt dat de verticale zandkorreldistributie bijna lineair toeneemt met toenemende fetchlengte verder weg van de bermlip, totdat een evenwicht wordt bereikt. Het effect van schelpen en vocht op een strand is aanzienlijk en kan niet worden genegeerd. Eolisch zandtransport kan windafwaarts binnen een korte afstand met een factor 10 worden verminderd, waardoor plaatselijke zandophoping ontstaat dat niet rechtstreeks de duinen binnendringt. Schelpen hebben echter geen invloed op de verticale verdeling en korrelgrootte van windgedreven zanddeeltjes windafwaarts. Verder onderzoek moet gericht zijn op een betere kwantificering van eolisch sedimenttransport door meer innovatieve monitoringstechnieken, vooral wanneer monitoring op lange termijn vereist is. Verder onderzoek moet zich ook meer richten op de invloed van bedruwheid en de feedback ervan op de windsnelheid op het eolische sedimenttransport. Bovendien is een verandering in het decadale duingedrag als gevolg van klimaatverandering ook zeer relevant voor studie.

Contents

Preface i

Abstract v

Samenvatting ix

Contents xiii

Definitions xvii

List of Figures xix

List of Tables xxvii

1 Introduction 1

1.1 Motivation and relevance ... 1
1.2 Aeolian sand transport in coastal environments: the fundamentals ... 3
1.3 Review of existing aeolian sediment transport models ... 7
1.4 Research Objectives ... 10
1.5 Methodology ... 12
1.5.1 General Approach ... 12
1.5.2 Aeolian Research Monitoring Techniques ... 13
1.6 Thesis outline ... 16

2 On the relation between predicted and observed aeolian transport rates: a field study at the Belgian coast 17

2.1 Introduction ... 18
2.2 Aeolian sand transport models ... 19
2.3 Study sites ... 24
2.4 Experimental setup ... 25
2.4.1 Instrumentation and data collection ... 25
2.5 Analysis method ... 27
2.5.1 Calculation of shear velocities ... 27

2.5.2 Calculation of aeolian sediment fluxes....27
2.6 Results and discussion....28
2.6.1 Results from the Belgian study sites....28
2.6.2 Results from other sites....33
2.7 Conclusions....38
2.8 Acknowledgements....38

3 Dune evolution at decadal timescales and its relation with potential aeolian transport 41

3.1 Introduction....42
3.2 Regional setting....44
3.3 Methods....48
3.3.1 Dune volume changes along the Belgian coast....48
3.3.2 Calculation procedure of potential transport....50
3.4 Results and discussion....53
3.4.1 Spatial-temporal variability in dune volume changes: linear trends....53
3.4.2 Typical management strategies and their effect on dune behavior....55
3.4.3 Potential aeolian sediment transport....60
3.4.4 Correlation between potential transport and dune volume changes....64
3.5 Conclusions....67
3.6 Acknowledgments....68

4 Downwind evolution of aeolian saltation across an artificially constructed coastal berm 69

4.1 Introduction....70
4.2 Methods....71
4.2.1 Study site....71
4.2.2 Experimental design....74
4.2.3 Vertical distribution of aeolian mass flux....76
4.3 Results and discussion....78
4.3.1 Grain sizes....78
4.3.2 Aeolian sand transport events....79
4.3.3 Wind flow across an artificially constructed coastal flat berm....81
4.3.4 Vertical flux profile characterization....83
4.3.5 Fetch effect across a human-constructed coastal flat berm 84
4.3.6 Downwind evolution of vertical flux profiles....89
4.4 Conclusions....93
4.5 Acknowledgments....94

5 Aeolian sand transport across a shell-fragmented beach: a field study **95**

5.1 Introduction 96
5.2 Study site 97
5.3 Methodology 99
5.3.1 Instrumentation 99
5.3.2 Data analysis 101
5.4 Results and discussion 102
5.5 Conclusions 109
5.6 Acknowledgements 110

6 Conclusions **111**

7 Future Research **119**

7.1 Recommendations for future monitoring techniques 119
7.2 A comprehensive predictive model for aeolian sand transport 121
7.2.1 Introduction 121
7.2.2 General predictive roughness model 122
7.2.3 Modelling other effects 123
7.3 Dune behavior due to climate change 127

A Dune behavior along the Belgian coast **129**

References **165**

Curriculum Vitae **181**

List of publications **183**

Definitions

Aeolian sediment processes. Derived from *Aeolus*, the Greek god of the winds, can be defined as the processes which involve wind action. The main processes are erosion, transport and deposition caused by the movement of air across the Earth's surface.

Aerodynamic surface roughness, z_0. The height above the surface at which the wind speed theoretically becomes zero.

Beach nourishment. The supply of sand to the shore to increase the recreational value and/or to secure the beach against shore erosion by feeding sand on the beach.

Cup anemometer. Usually installed on a meteorological station to measure the wind velocity at a certain height above the surface.

Effective bed roughness, k_s. Used to simulate the roughness of arbitrary roughness elements, e.g. ripples, shell and/or shell-fragments.

Fetch effect. An increase in sediment transport rate in the downwind direction until an equilibrium is reached.

Hinterland. The land or area behind the coast.

Long-term timescale. Timescale of interest for coastal development and management studies. It mostly represents decadal timescales.

MWAC sand trap. A Modified Wilson And Cook sand trap is a vertical mechanical trap, containing seven bottles above the surface, which is used to measure aeolian sediment transport rates.

RTK GPS. Real-Time Kinematic positioning system to measure topography in x,y,z coordinates.

Saltation. Dominant mode in aeolian transport. Particles move forward by making ballistic jumps from one place to another (size range = 70-500 µm).

Saltiphone (#impact/s). An acoustic impact device to measure aeolian sediment transport intensities.

Saturated sediment transport (kg/m/s). The maximum amount of sediment that can be transported by wind.

Sediment transport rate (kg/m/s). The total amount of sediment transport by wind across a surface.

Shear velocity, u_* (m/s). Or friction velocity is a form by which shear stress of a fluid can be rewritten in velocity units. It has an advantage of being independent of height above the surface compared to the actual measured velocity.

Short-term timescale. Timescale of interest for studying for example the physical processes of aeolian sediment transport. It mostly represents timescales of hours to days.

Spatial-temporal. Aeolian sediment processes can vary not only in space, but also in time. This makes aeolian processes very complex.

Subaerial beach. Or upper beach is the volume of beach above the high-water level.

Surface creep. Particles which do not lose contact with the surface and move by rolling or sliding along the surface (> 500 µm).

Suspension. Very small particles are transported in suspension by turbulent eddies (< 70 µm).

Threshold shear velocity, u_{*_T} (m/s). The critical shear velocity upon particles beginning to move by movement of air. It depends on bed surface properties, e.g. roughness, moisture, and salt.

Vertical flux profile. The vertical distribution of sediment above the surface. It is mostly an exponential decay curve characterized by the decay rate β (m^{-1}).

List of Figures

Figure 1-1. Aeolian sand transport towards the hinterland of Ostend, Belgium resulting in large depositions of sand on neighboring roads and tram tracks. Image taken during storm Eleanor between 2-3 January 2018..... 3

Figure 1-2. Scheme showing the main principles of coastal dynamics in a beach-dune system. Image obtained from Poortinga (2015)..... 6

Figure 1-3. Different aeolian sediment transport modes. Image obtained from Walter (2012). 6

Figure 1-4. Combined meteorological station with eight anemometers, a wind vane and a temperature sensor.....13

Figure 1-5. The Modified Wilson And Cook sand trap (MWAC), measuring sand transport on the beach of Koksijde, November 2016.....14

Figure 1-6. Array of saltiphone sensors during an aeolian measurement campaign on the beach of Mariakerke-Bad, November 2016.....15

Figure 1-7. Topographical survey with a mobile laser scanner on the beach of Mariakerke-Bad, September 2016.....16

Figure 2-1. Comparison of six aeolian models based on shear velocity. The median grain size is 310 µm. The original Bagnold model (1937) only calculates transport rates above the threshold of motion (0.31 m/s) and is indicated by the black solid line. 24

Figure 2-2. Location of the study areas. Study site 1, Mariakerke, is located next to Oostende at the central part of the Belgian coastline. Study site 2, at Koksijde, is located at the southwestern part of the coastline, near the border of France. 25

Figure 2-3. a) Meteorological station with four anemometers, a wind vane and a temperature sensor. b) MWAC sand trap deployed at the beach surface. 26

Figure 2-4. Example of velocity profiles during sand transport with a distinct focal point as measured on 24th November 2016 in Koksijde. 29

Figure 2-5. Bed roughness for different wind velocities at the Belgian study sites. 29

Figure 2-6. Grain size distribution of surface samples, and median grain size of trapped sand with height above the surface for Sand transport rates 30

Figure 2-7. Examples of sand transport fluxes as function of elevation above the surface and best fit exponential decay functions 31

Figure 2-8. Vertical mesh sand trap covering a height of 30 cm. Image taken on 24/11/2016 on the subaerial beach of Koksijde. 32

Figure 2-9. Comparison between observed and predicted sand transport rates for six aeolian models; all data sets. Diagonal lines represent the one-to-one correspondence. All transport rates are in kg/m/hr. Blue dots correspond to the measurements in Mariakerke. Yellow dots correspond to the measurements in Koksijde 35

Figure 2-10. Relation between standard deviation of observed transport rates and shear velocity 37

Figure 3-1. The 65 km long Belgian coast is located at the North Sea, between the French and the Dutch border and is divided into 254 coastal sections. The river 'IJzer' flows into the North Sea at Nieuwpoort. The green areas indicate the locations with vegetated coastal dunes 44

Figure 3-2. Coastal orientation of the Belgian coast. It represents the orientation of foredunes or dykes. The mean coastal orientation is 62° with respect to the North (red line). 45

Figure 3-3. A) Average beach width along the Belgian coast based on airborne surveys from 2000–2017. Beach width is the horizontal distance between the average low-water level and the dune foot. Upper beach width is the horizontal distance between the average high-water level and the dune foot or a hard defense structure. B) Average beach slope along the Belgian coast based on airborne surveys

from 2000–2017. Error bars indicate the standard deviation. 46

Figure 3-4. The grain size variation along the Belgian coast. There is an increase from France (0 km) to the Netherlands (65 km)....47

Figure 3-5. Typical sights at the Belgian coast. Left: natural beach-dune system at Koksijde (11 km from the French border). Right: managed beach-dyke system at Mariakerke (26 km from the French border)....47

Figure 3-6. The definition of the dune volume (number 3), where the dune foot level starts at +6.89 m TAW. Figure adapted from Vandebroek et al. (2017). 49

Figure 3-7. Overview of available data on dune volume with respect to the first survey along the Belgian coast, based on the annual surveys (positive values = deposition; negative values = erosion; 0 = stable). The term dune volume has been defined purely based on bounding planes. Dune volume can also be calculated in areas with a seawall or with artificially raised touristic berms, where no vegetated dunes are found....50

Figure 3-8. Orientation (O) of the Belgian coastline and calculation procedure of potential transport. The orange arrow shows the onshore direction of sediment transport towards the dunes and is used to explain dune behavior. The angle α is the wind direction (with respect to the north) and the angle dd_j is the difference between the wind direction and coastal orientation O....53

Figure 3-9. Example of dune volume in time combined with a linear fit (correlation of determination R^2 = 0.99) for coastal section 50 (natural dunes)....54

Figure 3-10. Density of occurrence of linear dune behavior. Of the dune sections, 80% show correlation coefficients larger than or equal to 0.9. 54

Figure 3-11. Dune behavior along the Belgian coast. Red bars indicate the places where the correlation coefficient of the linear trend analysis is higher than or equal to 0.9. The red dashed line represents the average annual dune growth for correlations higher than or equal to 0.9....55

Figure 3-12. Decadal dune evolution of the coastal dunes at section 8. 56

Figure 3-13. Concrete revetment and wall, built to reinforce the dune foot in section 8.....56

Figure 3-14. Decadal dune evolution of the coastal dunes at section 36. The solid magenta line indicates the recent dune trend.....57

Figure 3-15. Dune blowouts at sections 36 to 38.....57

Figure 3-16. Decadal dune evolution of the coastal dunes at section 72. The solid magenta line indicates the recent dune trend.....58

Figure 3-17. Concrete wall as a dune foot protection measure in section 72.....58

Figure 3-18. Decadal dune evolution of the coastal dunes at section 160. The solid magenta line indicates the recent dune trend.....59

Figure 3-19. The dunes at section 160, showing the plantation of brushwood fences.....59

Figure 3-20. Tidal channel 'the Zwingeul' (sections 254 and 255).....60

Figure 3-21. Decadal dune evolution of the coastal dunes at section 254. The solid magenta line indicates the recent dune trend.....60

Figure 3-22. Measured wind speed (W_s) and wind direction at Ostend Airport weather station for the period 2000–2017. The red line represents the Belgian coastline direction. The potential transport drift is also given.....61

Figure 3-23. A) Annual potential longshore transport for the period 2000-2017. B) Annual potential cross-shore (or normal) transport for the period 2000-2017. Positive is offshore transport, negative is onshore transport. C) Annual potential transport (PT) for the period 2000–2017. All transport rates are given in $m^3/m/year$. D) The angle of potential transport is fairly constant with an average value of 260 degrees to the north.....62

Figure 3-24. Decadal evolution of potential dune growth at Section 50 of the Belgian coast.....63

Figure 3-25. Annual potential longshore and onshore aeolian sediment transport, based on the period between 2000-2017.....63

Figure 3-26. Comparison between observed and predicted linear dune development. Diagonal lines represent the one-to-one correspondence. Red dashed lines show the factor of two

variance. Yellow dots represent the locations where managing activities are carried out. 66

Figure 3-27. Annual predicted and observed dune volume change along the Belgian coast on a decadal timescale. Red and black bars indicate the observed and predicted values of dune development, respectively..... 67

Figure 4-1. Location of the study area. 72

Figure 4-2. Topography before and after preparation of the study area against winter storms. Excavators and bulldozers manipulate the upper beach by removing an excess of sand from the upper beach seawards and digging a trench at the dyke toe..... 73

Figure 4-3. Left panel shows the trench at the dyke toe. Right panel shows the study site at Mariakerke with aeolian sand transport during strong onshore winds. (Photograph taken on 12 November 2017)..... 73

Figure 4-4. Plan view of the study site with the location of the equipment. 12 Modified Wilson And Cook (MWAC) sand traps were placed at the upper beach together with two meteorological stations and two saltiphones. Coordinates refer to the Lambert 72 coordinate system. The topography is from field surveys conducted on November 7, 2017..... 75

Figure 4-5. a) Meteorological station with four anemometers, a wind vane and a temperature sensor. b) Saltiphone sensor. c) MWAC sand trap deployed at the beach surface..... 76

Figure 4-6. Grain size distribution of surface samples, and median grain size of trapped sand with height above the surface at the study site for sand traps Z_6 and Z_7..... 79

Figure 4-7. A) 10-min average records of wind speed at 2 m. The dashed line represents the threshold of movement (6 m/s). B) 10-min average records of wind direction. Offshore winds occur when wind direction is between 53 and 233 degrees. Wind speed and direction refers to the data obtained from M_{cliff}. C) Precipitation and cumulative precipitation. D) Saltation intensity at M_{dyke} and $M_{cliff,}$ 10 cm above the surface, recorded once every 20 seconds. Two aeolian transport events were measured with the MWAC sand traps (Event 1 and Event 2)..... 80

Figure 4-8. Selected vertical wind profiles for Event 1 and 2 at 15:00 on 12/11/2017..... 82

Figure 4-9. Shear velocities during Event 1 and 2 using the regression procedure of the logarithmic law of Equation (4.1).....83

Figure 4-10. Vertical flux profiles for MWAC Z_1 during Event 1. The left figure shows the regression line from the four-point exponential decay model (Equation (4.2)), where elevation is the independent variable. The right figure shows the regression based on the exponential decay model and log-linear model. Herein is elevation the dependent variable. 84

Figure 4-11. Evolution of sand transport downwind from the lip of the berm for Event 1 and Event 2.....87

Figure 4-12. Topographic elevation changes caused by transport Event 1 and Event 2. Red color indicates erosion, while blue color indicates deposition. 88

Figure 4-13. Relationship between the vertical decay rate, β, and cross-shore distance. 0 m is the location of the dyke crest. 89

Figure 4-14. Variation of the vertical decay rate, β, and fetch distance during longshore winds on 29 September 2016 on the study site.....91

Figure 4-15. The increase of decay rate as a function of increasing fetch length (β_c=27 m^{-1}).....92

Figure 4-16. Vertical flux profile development for Event 1 and Event 2 in the transect $Z_1 - Z_6$ and $Z_7 - Z_{12}$. Trap 1 corresponds with the most upwind sand trap, while Trap 6 corresponds with the most downwind sand trap. 92

Figure 5-1. Location and orientation of the study site. 98

Figure 5-2. Meteorological station with eight anemometers, a wind vane and a temperature sensor connected to a buried CR800 Campbell Scientific datalogger. On the beach surface, many shell hash and fragments are present of different size (crushed, small and large). 98

Figure 5-3. Overview of measurement locations. The topography is obtained from the LiDAR flight three weeks after the campaign (14/12/2016). All the instruments are located on the upper beach. The meteorological station is located in the middle of the experiment near the embryo dunes. The dotted lines represent the high waterline (+4 m TAW) and dune region. The MWAC sand traps are positioned parallel with the wind direction. During the

whole experiment, the wind direction was from northeast, highly oblique onshore.....100

Figure 5-4. The Modified Wilson And Cook sand trap (MWAC) and saltiphones, measuring sand transport on the beach of Koksijde, 24 November 2016. Note the presence of different sized shell fragments. 101

Figure 5-5. 10-minute time series of wind speed, shear velocity, wind direction, tide and saltation impacts over the entire field experiment conducted on November 24-25, 2016.....103

Figure 5-6. Comparison between the registrations of the two saltiphones. 104

Figure 5-7. Aeolian sand transport commences directly at the high waterline on November 24, 2016 during Experiment 1.....105

Figure 5-8. Bed roughness for different shear velocities during the entire experiment. 105

Figure 5-9. Relation between overall particle count and potential transport. 106

Figure 5-10. Upper graph shows the measured mass fluxes downwind during Experiment 1 and 2. Left to right is MWAC 10 to MWAC 1. Middle graph shows the calculated decay coefficient β based on Equation (1.3) and median grain size d_{50}. Lower graph shows the beach profile at the beginning of the field campaign together with the variation of surface moisture. 108

Figure 5-11. Deposition of sand on the upper beach in the form of large rippled sand strips visible on top of the shell pavement.....109

List of Tables

Table 1-1. A summary of the representative published sand transport models (after Dong et al., 2003). 8

Table 2-1. Summary of data of the field experiments in Mariakerke (period 2016-2018); s_Q is the standard deviation of sand transport. 31

Table 2-2. Summary of data of the field experiments in Koksijde (period 2016-2018). The italic values represent the data set obtained by Campos (2018). s_Q is the standard deviation of sand transport 32

Table 2-3. Summary of data of the field experiments conducted by Sherman et al. (1998). Only the results of Tower 1 and 2 are given 33

Table 2-4. Summary of results comparing observed transport rates with predicted transport rates for different aeolian models, only data of the two Belgian sites (Mariakerke and Koksijde). 34

Table 2-5. Summary of all results comparing observed transport rates with predicted transport rates for different aeolian models, all data sets. 35

Table 4-1. Regression parameters for the non-linear exponential regression procedure and total mass flux for Event 1 and Event 2 85

Chapter I

Introduction

The introduction starts with a short overview of the societal importance and relevance of studying aeolian sand transport on sandy coastlines. Then the fundamental, theoretical background of aeolian sediment transport in coastal areas is concisely given. Subsequently, the problems and objectives are addressed in this thesis. The outline of the thesis will be drawn at the end of this chapter.

1.1 Motivation and relevance

Being a coastal planet, Earth has about 1.6 million kilometers of coastlines, which is equivalent to about 40 times around the equator (World Recourses Institute, 2019). Approximately 83% of all countries in the world have coastlines in different forms and shapes, with different climates and ecosystems ("Countries of the world ordered by coastline," 2019). It is estimated that nearly one-third of the total human population lives within 100 km of a coastline (Nasa, 2019). With a growing population, more people are living along the coast. Currently, coastal populations are growing faster than inland populations and face increasing challenges as a result of coastal erosion, sea-level rise, and an increased risk of flooding.

At the Belgian coast, many management activities are carried out primarily in the form of beach nourishments to account for future flood risks or hazards. Despite these coherent management activities, the movement of large quantities of sand along the Belgian coastline remains a daily reality. Sediment transport and beach erosion in relation to coastal safety has been a subject for research for decades. However, most studies about sediment budget calculations have been focusing on the marine processes controlling the dynamics of the coast. Nevertheless, a non-negligible part of controlling the coastal dynamics is attributed by aeolian sediment transport processes (Figure 1-1). Aeolian sand transport is the movement of sand particles by wind, resulting in an interaction between beach and dune systems. Aeolian sand transport has the ability to change beach and dune morphology in space and time. Aeolian sand could also

reach the hinterland resulting in large maintenance and cleaning costs for the neighboring coastal municipalities.

Coastal dunes approximately cover half of the Belgian coastline, where they provide safety against flooding during extreme storm events (Lebbe et al., 2008). Compared to hard engineering structures like sea dikes, coastal dunes are very efficient and are in favor because they are being built by natural aeolian processes (Nickling & Davidson-Arnott, 1990; Delgado-Fernandez & Davidson-Arnott, 2009; Baas et al., 2006). However, natural coastal dunes are not fixed, they are dynamic and the downside; therefore, is that the provided safety level varies in time (de Vries et al., 2012). In global sandy coastal environments, understanding how these natural occurring aeolian processes work is necessary for a variety of reasons including dealing with storms, seasonal and decadal variations and for the restoration and maintenance of coastal beach and dune systems. These require knowledge of aeolian sediment transport processes for the prediction of system response to wind forces over short to long-term timescales (Houser et al., 2015).

Until recently, accurate quantitative data on the amount of aeolian sand transport flux was not available at the Belgian coast with only a few qualitative studies studying aeolian sand transport at the Belgian coast (Teurlincx et al., 2009 and Snacken, 1956). However, at the neighboring French coast, Anthony et al. (2006) studied aeolian sand transport and found that significant sand transport takes place from the shoreface to the dune area. Knowledge of beach and dune development processes by wind, unfortunately, lacks scientific background and contrastingly, accurate aeolian sediment transport equations are of utmost importance for modern geomorphology and coastal engineering practices. Aeolian sediment transport models describe the transport rate due to wind action. Most of these models tend to overpredict the actual aeolian accumulated volumes in coastal environments (Sherman et al., 1998; Sherman et al., 2013; Horikawa et al., 1984; Liu et al., 2006). Reasons for discrepancies between observed and predicted values are discussed in detail by Sherman et al. (2013). Important sources of error are the grain size and composition of the bed (uniform versus graded), horizontally non-uniform sand surface conditions related to grain size, relief, crusting and shells, moisture variations and fetch effect (Houser, 2009; de Vries et al., 2014; Delgado-Fernandez, 2010; Hoonhout & de Vries, 2017).

Although sand transport by wind is easily observable, reliable and accurate data sets of sand transport rates are still scarcely available due to measuring difficulties. For the most part, relatively simple mechanical trapping systems are being used, but reported efficiencies vary and are often below 50% (Goossens & Offer, 2000), differing from site to site and sometimes even unknown. Field monitoring is essential to understand the impact of aeolian sediment in the overall sediment budgets and long-term coastal dune behavior. In the past decades, a substantial amount of research has been carried out on dune erosion

which can be simulated with good accuracy. Yet, predictions on aeolian sediment transport from the beach towards the dunes, leading to dune recovery, are still difficult to make (Vellinga, 1986; Steetzel, 1993; van Rijn, 2013; Delgado-Fernandez, 2011).



Figure 1-1. *Aeolian sand transport towards the hinterland of Ostend, Belgium resulting in large depositions of sand on neighboring roads and tram tracks. Image taken during storm Eleanor between 2-3 January 2018.*

This thesis unravels the nature of aeolian sand transport with the Belgian coast as study area, broadening the knowledge with the aim to improve long-term aeolian sediment transport estimates. The overall aim of the thesis is based on analyzing collected data from field experiments. The data includes morphological data, topographical data, meteorological data and aeolian transport data. Field measurement techniques have improved over time, allowing us to focus on identifying and measuring key variables like: wind speed, wind direction, fetch distance and surface moisture content. This work is performed within the framework of project CREST (Climate REsilient coaST), funded by the Strategic Basic Research (SBO) program of Flanders Innovation & Entrepreneurship, Belgium. The project aims to increase the knowledge of coastal processes near the coast and on land.

1.2 Aeolian sand transport in coastal environments: the fundamentals

Aeolian sand transport in coastal environments is defined as the wind-driven transport of sand on beaches and dunes. This process is very dynamic and acts at a spatial-temporal scale, capable of inducing both rapid and gradual morphological changes. During storm surges (hydrodynamic forces), when water levels are higher than the dune foot, large amounts of sand are sometimes eroded from the beach and dune system (see Figure 1-2). In between storms, aeolian sand transport is crucial for the restoration of dunes as they are naturally

supplied with sand from the intertidal area. Loosely packed and mixed sand from the intertidal area is a crucial source for aeolian sediment transport where it again becomes part of the beach-dune system. The sand entering the dune system contributes to the growth of vegetation which in turn stimulates sand trapping. However, dune behavior is a function of the supply of sand in the nearshore environment (Hoonhout & Vries, 2016). The total amount of sand from the beach to the dune system is dependent on wind, waves, tidal range and beach morphology (Pye, 1983; Hesp, 1999).

Generally, when wind velocity is higher than the threshold wind velocity, sand is transported along the wind direction. The dominant transport mode of aeolian sediment transport is saltation. For sand particles in the size range of 70 to 500 μm, it involves sand grains following ballistic trajectories as they hop from one place to another across the beach surface. For increasing wind speeds, the particles are lifted from the bed, primarily dominated by gravitational and aerodynamical forces. The impact of the saltating particles with the sand surface may result in a rebound, but may also mobilize and eject other particles into saltation (Figure 1-3). Very small particles (fine sand fraction), smaller than 70 μm, are mostly transported in suspension by turbulent eddies. The largest particles (coarse sand fraction), larger than 500 μm, are transported by sliding and rolling as surface creep. The combined transport of particles by rolling, sliding, and small hops (saltations) due to wind action can be defined as bed load transport of particles with near continuous contact with the bed. Bed load transport of particles in a thin transport layer is the dominant mode of wind-blown transport for sand particles. Observations in wind tunnels and in nature show that most of the transport occurs in a thin layer (< 0.05 m) above the sand surface (Ho, 2012).

The total amount of aeolian sediment transport during saturated conditions is mainly dependent on the wind velocity when exposed to wind action. Many researchers have proposed models for aeolian sand transport under ideal conditions with uniform and steady wind obeying the law of the wall, with almost uniform (size, composition) and dry sand on a horizontal sand surface without vegetation and other obstacles (Sherman & Hotta, 1990). One of the first and most widely used models for ideal conditions has been formulated by Bagnold (1941). Bagnold (1941), who did an extensive survey on desert aeolian transport in the 1930's, found that the potential amount of transport is a cubic power function of the wind velocity. On the Belgian coast, and generally in all sandy coastal environments, these conditions are mostly violated. Therefore the actual rate of sand transport is mostly lower than transport estimates.

On most beaches, the primary controls of aeolian sediment transport are wind speed, wind direction, beach morphology, and sediment moisture content. Other factors that have the potential to influence aeolian transport on beaches can usually be ignored but is not always the case. The significance of these variables is reviewed by several researchers (Horikawa, 1988; Sherman & Hotta, 1990;

Nickling & Davidson-Arnott, 1990; Pye & Tsoar, 2009). Topographical features due to managing activities or human interference by built structures, walking or driving, and removing storm deposits also modify aeolian sand transport potential (Nordstrom, 1994; Jackson & Nordstrom, 2011). The influences of the primary controls of aeolian sediment transport are:

- Wind speed and wind direction have a direct influence on the total amount of sand being transported from the beach to the dune region. However, high wind speeds usually coincides with rainfall and beach inundation, limiting the supply of available sand (Delgado-Fernandez, 2011). Large fetch lengths will generate large amounts of sand transport compared to onshore winds where the fetch effect becomes important. Delgado-Fernandez (2010) described the fetch effect as an increase in sediment transport rate in the downwind direction until steady-state conditions are reached (saturated).

- Beach morphology, like changes in slopes, grain size, ripples and shell-fragments, have a direct influence on wind velocity and wind shear velocity and thus, potential aeolian transport. Complex interaction occurs between different grain sizes, but under ideal conditions, larger grain sizes are transported with more difficulty than smaller ones (Bagnold, 1941). Slope effects are relatively minor for angles less than approximately 10 degrees on sandy coastlines (Sherman et al., 2005).

- A lot of research has been carried out on the influence of surface moisture as it is one of the main controls of the threshold velocity (Arens, 1996; Bauer et al., 2009; Han et al., 2011; Jackson & Nordstrom, 1998). Beach sand becomes moist or wet due to precipitation, tidal cycles or capillary rise from the water table. Moist sand sticks, making it more difficult to transport than dry sand.

An important aspect of aeolian sediment transport in coastal environments is variation in the interaction between topography, wind flow and primary controls in time and space. This makes aeolian sediment transport processes very complex and dynamic (Ellis & Sherman, 2013).

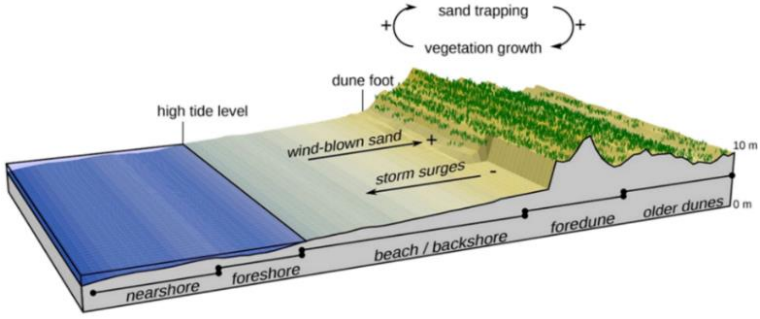

Figure 1-2. *Scheme showing the main principles of coastal dynamics in a beach-dune system. Image obtained from Poortinga (2015).*

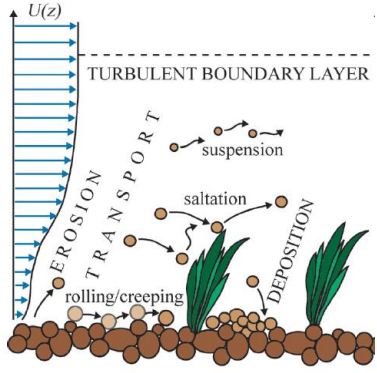

Figure 1-3. *Different aeolian sediment transport modes. Image obtained from Walter (2012).*

1.3 Review of existing aeolian sediment transport models

Numerous authors have developed aeolian models, predicting saturated mass transport rates that are proportional, to some power (mostly 2 or 3), of the shear velocity or wind velocity. Most of these models can be divided into three categories: process-based models, numerical models and statistical models. Most process-based models are based on the momentum transfer between moving sand particles and the airstream and relate sediment transport rate with wind shear velocity and/or threshold shear velocity (Bagnold, 1954; Zingg, 1953; Owen, 1964; Lettau & Lettau, 1978). Most of these process-based models include empirical constants derived from environmental assumptions in wind tunnel tests or field experiments. The output of numerical models contains sediment transport rates often by incorporating subprocesses in aeolian sand transport. These subprocesses include the grain-bed collision, sediment transport in air, adaptation of the air stream due to wind-blown sand, interaction with vegetation, and supply-limitations (Anderson & Haff, 1991; McEwan & Willetts, 1994; Hoonhout & Vries, 2016). Therefore, numerical aeolian models require many valuable input parameters obtained by field experiments and wind tunnel tests. The third category, statistical aeolian models, usually establishes an empirical relationship between sediment transport rate and wind velocity based on many field and wind tunnel experiments. They are very site specific and often fail when used at other locations or situations (Sherman et al., 1998). In the past century, many empirical relationships have been established and they all have the same limitation where most empirical models cannot be properly supported by theoretical equations.

Aeolian sediment transport models can generally be divided into five groups. Table 1-1 summarizes some representative aeolian sediment transport models. The Bagnold type equations relate sediment transport rate directly with the shear velocity. Moreover, they also predict sediment transport rate when the shear velocity is lower than the threshold shear velocity. Thus, the modified Bagnold type equations account for this inconvenience and predict only sediment transport when sand is moving. However, the (modified) Bagnold type equations do require the shear velocity term; therefore, measurement of the vertical wind profile is necessary. In the O'Brien-Rindlaub type equations, sediment transport rate is directly related to wind velocity measured at a given height above the surface. However, they suffer the same limitations as the Bagnold type equations. In the modified O'Brien-Rindlaub type equations, the threshold velocity term is added only to make them meaningful when the wind velocity is higher than the threshold velocity. The complex type numerical equations usually have several parameters which need to be defined by experimental studies. Usually they lack theoretical background and therefore, the Bagnold and modified Bagnold type equations are preferred. The advantage

of these pragmatic models is that only one empirical constant, C, has to be determined.

Table 1-1. *A summary of the representative published sand transport models (after Dong et al., 2003).*

Basic form	Equation	Authors	Eq. no.
Bagnold type $Q = BU_*^3$	$Q = C\sqrt{\frac{d}{D}}\frac{\rho_a}{g}U_*^3$	Bagnold (1941)	(1.1)
	$Q = C\frac{\rho_a}{g}U_*^3$	Chepil (1945)	(1.2)
	$Q = C_z\left(\frac{d}{D}\right)^{\frac{3}{4}}\frac{\rho_a}{g}U_*^3$	Zingg (1953)	(1.3)
	$Q = \left(\frac{1}{gd}\right)^{\frac{3}{2}}e^{(4{,}97d-0{,}47)}U_*^3$	Hsu (1974)	(1.4)
Modified Bagnold type $Q = Bf(U_{*t})U_*^3$	$Q = C\sqrt{\frac{d}{D}}\frac{\rho_a}{g}(U_* - U_{*t})^3$	Bagnold (1954)	(1.5)
	$Q = C\left(1-\frac{U_{*t}}{U_*}\right)\left(1+\frac{U_{*t}}{U_*}\right)^2\frac{\rho_a}{g}U_*^3$	Kawamura, (1951); White (1979)	(1.6)
	$Q = \left(0{,}25+0{,}33\frac{U_{*t}}{U_*}K_t\right)\left(1-\left(\frac{U_{*t}}{U_*}\right)^2\right)\frac{\rho_a}{g}U_*^3$	Owen (1964)	(1.7)
	$Q = CK_t\left(1-\frac{U_{*t}}{U_*}\right)\frac{\rho_a}{g}U_*^3$	Iversen et al. (1976)	(1.8)
	$Q = C\left(1-\left(\frac{U_{*t}}{U_*}\right)^2\right)\frac{\rho_a}{g}U_*^3$	Kind (1976)	(1.9)
	$Q = C\left(\frac{d}{D}\right)^{\frac{3}{4}}\left(1-\left(\frac{U_{*t}}{U_*}\right)^2\right)\frac{\rho_a}{g}U_*^3$	Maegley (1976)	(1.10)
	$Q = C\sqrt{\frac{d}{D}}\left(1-\frac{U_{*t}}{U_*}\right)\frac{\rho_a}{g}U_*^3$	Lettau & Lettau (1978)	(1.11)
	$Q = C\frac{1}{A^2\frac{U_{*t}}{U_*}}\left(1-\frac{U_{*t}}{U_*}\right)\frac{\rho_a}{g}U_*^3$	Lyles et al. (1979) quoted by Greeley & Iversen (1985)	(1.12)
	$Q = C\frac{\rho_{air}}{g}U_{*t}(U_*^2 - U_{*t}^2)$	Kok et al. (2012)	(1.13)
	$Q = C\sqrt{\frac{d_{50}}{D}}\left(\frac{\rho_{air}}{g}\right)(U_*^3 - U_{*t}^3)$	Van Rijn (2018)	(1.14)

O'Brien-Rindlaub type $Q = BU^3$	$Q = CU^3, C = 0{,}03$	O'Brien & Rindlaub (1936)	(1.15)
Modified O'Brien-Rindlaub type $Q = Bf(U_t)U^3$	$Q = C\left(1-\frac{U}{U_t}\right)\frac{\rho_a}{g}U^3$	Dymin (1954) quoted by Greeley & Iversen (1985)	(1.16)
	$Q = C\left(1-\left(\frac{U}{U_t}\right)^3\right)\frac{\rho_a}{g}U^3$	Kuhlman (1958)	(1.17)
	$Q = C\left(1-\frac{U}{U_t}\right)^3\frac{\rho_a}{g}U^3$	Dymin (1954) quoted by Greeley & Iversen (1985)	(1.18)
Complex type	$Q = \emptyset(\rho_s g)\sqrt{\frac{(\rho_s-\rho_a)}{\rho_a}gd^3}$	Kadib (1965)	(1.19)
	$Q = e^{(a+bU)}$	Radok (1977)	(1.20)
	$Q = d\rho_s\left\{N_1\left[\frac{U_*}{gd}\left(\frac{\rho_a}{\rho_s}\right)\right]^{0,8}-N_2\right\}U_*$	Nakashima (1979)	(1.21)
	$Q = C[(U_*-U_{*t})(U_*+U_{*t})^2]H_1+(3U_*^2+2U_*U_{*t}-U_{*t}^2)H_2+(3U_*+U_{*t})H_3\left(\frac{\rho_a}{g}\right)$	Horikawa et al. (1984)	(1.22)
	$Q = K_1U_*(U_*-U_{*t})(K_2U_*+K_3U_{*t}+K_4)$	Sorensen (1991)	(1.23)

A: Bagnold's threshold coefficient, or square root of Shield's parameter; a, b: empirical coefficients; B, C: proportionality coefficients; D: reference grain diameter, 0.25 mm; d: mean grain diameter; g: acceleration due to gravity (9.81 m/s²); H_1, H_2, H_3: integrals of the normal distribution function; K_1, K_2, K_3, K_4: parameters related to particle trajectory, collisions, and airflow; K_t: U_w/U_{*t}, U_w is the particle settling velocity; N_1, N_2: empirical coefficients; U: wind velocity at given reference height; U_t: threshold wind velocity at given reference height; U_*: shear velocity; U_{*t}: threshold shear velocity; $\emptyset$: a transport intensity function based on Einstein's bed-load transport model; ρ_a: the air density; ρ_s: density of the sand particle (after Dong et al., 2003).

1.4 Research Objectives

The main objective of this thesis is exploring the nature of aeolian sand transport on the Belgian coast, enlarging knowledge with the aim to improve long-term aeolian sediment transport estimates. This thesis is divided into five research objectives. Research objectives A, B, C, D and E are elaborated in several research questions which are addressed in the concluding chapter of this thesis (Chapter 6). The research objectives and questions are formulated as:

A. Evaluating the relationship between aeolian sand transport rate and wind speed on the Belgian coast (Chapter 2).

   1. *Which mathematical aeolian model can be proposed, showing a good relation between observed and predicted saturated sand transport rates?*
   2. *Which often used aeolian models perform poor in the relation between observed and predicted saturated sand transport rates?*

B. Characterizing the temporal variability and relative magnitude of annual aeolian sediment transport on the Belgian coast (Chapter 3).

   1. *What is the amount of potential annual cross- and longshore aeolian sediment transport along the Belgian coast?*
   2. *What is the main direction of annual aeolian sediment transport along the Belgian coast?*
   3. *What is the frequency and variation of aeolian sediment transport events along the Belgian coast?*

C. Identifying trends in dune behavior on the Belgian coast (Chapter 3).

   1. *What is the spatial-temporal variability in dune volume changes along the Belgian coast?*
   2. *What is the correlation between observed and predicted dune volume on an annual timescale along the Belgian coast?*
   3. *What is the correlation between observed and predicted dune volume on decadal timescales along the Belgian coast?*
   4. *What are the longshore variations of the correlations by distinguishing between 'natural' and 'managed' beach sections of the Belgian coast featuring dunes?*

D. Examining the downwind evolution of aeolian saltation across an artificially constructed coastal high berm with a steep seaward cliff, backed by a dyke (Chapter 4).

    1. *How does the total mass flux of aeolian sand vary over a flat beach with increasing fetch length?*
    2. *What is the relationship between the vertical decay coefficient β of the flux profile and the fetch length?*
    3. *What is the influence of the steep cliff and dyke structure?*

E. Studying the effect of shells on aeolian sand transport across a shell-fragmented beach (Chapter 5).

    1. *What is the downwind evolution of the total mass flux of aeolian sand across a shell-fragmented beach?*
    2. *How does the vertical distribution and grain size of airborne sand particles vary across a shell-fragmented beach?*

1.5 Methodology

1.5.1 General Approach

To answer the different research questions and research objectives, an analysis of field data from different sources are being used. The following methods are applied for each research objective:

A. The first research objective was achieved using short-term simultaneous monitoring of meteorological variables and aeolian sand transport rates on the subaerial beach of two study sites in Belgium. The field measurements were conducted between 2016 and 2018. The main focus was to get insight into the relationship between aeolian sand transport rate and wind speed. Six aeolian models, each predicting saturated transport rates, were used for objective testing.

B. To answer the second research objective, the best relationship between aeolian sand transport and wind speed, found in the first research objective, is being applied on the entire Belgian coast. A meteorological data set of 17 years at an hourly basis, including wind speed and wind direction, between 2000 and 2017 is analyzed and used to calculate potential aeolian sand transport. In the calculation procedure of potential transport, the median grain size and coastal orientation per coastal section is taken into account.

C. The third research objective is being answered by using a unique 38-year data set, containing annually or bi-annually airborne photogrammetric and airborne Laser Scanner (LiDAR) topographical data. Spatial and temporal variability in dune behavior is then correlated with potential sediment input from the beach.

D. The answer to the fourth research objective, is achieved using detailed field data on the managed beach of Mariakerke in Belgium during a two-week monitoring campaign in November, 2017. The field data included measurements of aeolian sand fluxes, aeolian transport intensity, topographical changes, wind speed, wind direction and precipitation.

E. The fifth research objective is being answered by using a short-term (two day) field experiment in the winter of 2016 on the natural upper beach of Koksijde, Belgium. The field data included measurements of aeolian sand fluxes, aeolian transport intensity, topography, and environmental conditions.

1.5.2 Aeolian Research Monitoring Techniques

The core of this thesis is built around field monitoring aeolian sand transport under different environmental conditions with different wind speeds and wind directions by using a unique instrument set-up. The instrument set-up changed for each measurement campaign depending on the intended objectives and research questions. Across a number of fixed measurement stations on the beach, data of meteorological conditions, topography, and wind-driven sand transport events were collected. A brief summary of the different monitoring techniques, used in this thesis, is described.

1.5.2.1 Meteorological stations

Wind speed and wind direction were measured using four cup anemometers (Vector Instruments A100R) and a wind vane (Vector Instruments W200P) on a 3 m high meteorological stations, positioned at one or two locations on the beach (Figure 1.4). Mostly, the meteorological stations were positioned on the subaerial beach or in the dunes. The cup anemometers were positioned at four elevations above the surface, at 15 cm, 30 cm, 51 cm and 195 cm respectively. The wind speed data, recorded once every 20 seconds, were averaged over one-minute periods and saved on a CR800 Campbell Scientific datalogger. The wind vane was installed at an elevation of 2 m. The wind speed measurements were used to calculate the aerodynamic roughness length, z_0, and wind shear velocity, u_*, derived from the vertical wind profile. Furthermore, measurements on air temperature were performed at 10-minute intervals. Time series of rainfall and tides were taken from nearby measuring stations.



Figure 1-4. *Combined meteorological station with eight anemometers, a wind vane and a temperature sensor.*

1.5.2.2 Modified Wilson And Cook sand traps

Measuring of sediment transport rates typically employ passive vertical sediment traps (e.g. Leatherman, 1978; Nickling & Davidson-Arnott, 1990; Goossens & Offer, 2000). During the measurement campaigns, 12 Modified

Wilson And Cook (MWAC) vertical sand traps were exposed to the wind to determine the rate of aeolian sand transport (Figure 1.5). These sand traps have been extensively used in numerous studies where efficiencies of between 42% and 120% were reported (e.g. Van Pelt et al., 2009; Sterk & Raats, 1996; Goossens & Offer, 2000; Poortinga et al., 2013; Youssef et al., 2008). Trap efficiency is defined as the relative ratio of trapped sand to the actual quantity of blown sand (Chepil & Milne, 1941). The sand trap is equipped with a vane to ensure that the bottle inlet was always orientated towards the wind. The traps collect sediment in seven plastic bottles from 0.065 to 1.00 m above the surface. When aeolian sand transport occurs, the saltating layer seldom reaches heights above 25 cm (Van Dijk et al., 1996; Poortinga et al., 2014). Therefore, four bottles were placed in the MWAC sand trap array at a of height 6.5, 13.5, 21.0 and 28.5 cm above the surface. Each bottle had a glass inlet and outlet tube with a diameter of 8 mm ($\approx$ 50 mm^2 or 5.10^{-5} m^2). The mass of sand collected in the bottle was divided by the inlet tube area and exposed time (in minutes) to provide transport rates in $kg/m^2/min$. An exponential decay curve fitted through the flux results of the four measuring points was the basis used to calculate the total horizontal sediment flux per meter beach width (kg/m/min) (Poortinga et al., 2014; Bauer & Davidson-Arnott, 2014). The trap values were not corrected by an efficiency factor. Sediment samples were taken from the upper layer of the beach surface (thickness of 10 mm) at each MWAC location. Both these surface samples and the samples collected in the MWAC bottles were analyzed for grain size distribution.



Figure 1-5. *The Modified Wilson And Cook sand trap (MWAC), measuring sand transport on the beach of Koksijde, November 2016.*

1.5.2.3 Saltiphone

In the last decade, electronic impact sensors have become increasingly popular to measure aeolian sand transport. Saltating sand grains were counted using two high-frequency saltiphone sensors. A saltiphone sensor detects sediment transport by a microphone on an area that is only 1-2 cm in diameter, attached

to a stainless-steel tube which counts the number of impacts of sand grains. The instruments only detect a small (vertical) portion of the horizontal flux. Two vanes at the back of the tube ensure proper positioning of the microphone in the wind. The sensor is adjustable in height between 0-50 cm. The saltiphones were placed at 5 cm and 15 cm above the sand surface, see Figure 1.6. Saltating particles larger than 50 microns would mostly hit the microphone and produce high-frequency noise, which could be distinguished from other noises caused by wind and rain. Every 20 seconds, the cumulative number of impacts was recorded and stored on the Campbell datalogger. Detailed descriptions about its design, testing and deployment are given by Spaan & Van Den Abeele (1991). Tests done by Poortinga et al. (2013) show that the output from saltiphones placed side by side varied from one instrument to another. However, no relationship was determined between the two instruments as they were only used to register transport events. Saturation of the impact sensor (oversampling) may occur in specific conditions: very close to the bed and/or in strong wind conditions with high particle concentrations. At low wind conditions, the transport layer may be so small (thin), that most of the particles would pass underneath the location of the lowest sensor (undersampling).



Figure 1-6. *Array of saltiphone sensors during an aeolian measurement campaign on the beach of Mariakerke-Bad, November 2016.*

1.5.2.4 Topographical measurements

Topography was regularly surveyed by Ghent University with a mobile laser scanner equipped SPV (Special Purpose Vehicle) in combination with a high-grade INS (Inertial Navigation System) and an RTK-GNSS covering the upper beach and intertidal zone to determine changes in height before and after aeolian transport events (Figure 1.7).



Figure 1-7. *Topographical survey with a mobile laser scanner on the beach of Mariakerke-Bad, September 2016.*

1.6 Thesis outline

The core of the thesis is built around four article manuscripts and constitutes seven chapters. The introduction (Chapter 1) is followed by Chapter 2, which presents the relation between predicted and observed aeolian transport rates based on six aeolian models using short-term transport rate data sets. The validation of the best aeolian model on a short time-scale gave inspiration to do an analysis of decadal dune behavior at the Belgian coast and its relation with potential sediment input from the beach. This work is presented in Chapter 3. Chapter 4 describes the downwind evolution of aeolian saltation across a human-constructed coastal berm. The effect of largely scattered shell pavement and moisture on aeolian sand transport on the upper beach of a natural beach-dune system is studied during a short-term field experiment and is described in Chapter 5. Chapters 2, 3, 4 and 5 each start with the main highlights and findings of the chapter. In Chapter 6, the overall conclusions are summed up by addressing the research objectives and questions. Chapter 7 gives some recommendations for future research.

Chapter II

On the relation between predicted and observed aeolian transport rates: a field study at the Belgian coast

Abstract

Between 2016 and 2018, simultaneous monitoring of meteorological variables and aeolian sand transport rates, using MWAC sand traps, was carried out on the subaerial beach of two study sites in Belgium. The aim of the field study was to get insight into the relationship between aeolian sand transport rate and wind speed. In addition, other field data sets have been analyzed. Six aeolian models, each predicting saturated transport rates, are used for data comparison. The models of Bagnold (1937); Kawamura (1951); Bagnold (1954); Hsu (1974); Kok et al. (2012) and the modified Bagnold model proposed by Van Rijn (2018) are evaluated. The key parameter in all these aeolian models is the shear velocity, u_*. Shear velocities are calculated using vertical wind profile data from on the beach located meteorological stations. Mean shear velocities ranged from 0.29-0.54 m/s. Transport rates of dry sand ranged from 7.2 and 121.8 kg/m/hr. The modified Bagnold model of Van Rijn (2018) produces a strong one-to-one relation between observed and predicted transport rates. The model of Kok et al. (2012) also gives good results. The model of Bagnold (1954) and the model of Kawamura (1951) produce the poorest results. Bagnold (1954) underestimates transport rates, while the Kawamura (1951) overestimates transport rates.

Keywords: Aeolian transport, Subaerial beach, Field measurements, Transport equation, Dry sand, Belgium

Chapter under review as: Strypsteen, G., Van Rijn, L.C. and Rauwoens, P. (2019). On the relation between predicted and observed aeolian transport rates: a field study at the Belgian coast. *Aeolian Research*.

2.1 Introduction

The restoration and maintenance of beach and dune systems require accurate knowledge of aeolian sediment transport processes for the prediction of the system response to wind forces on the timescale of storms, seasons and decades. Accurate predictions of aeolian sediment transport from the beach towards the foredune is central in the development of physically-based models of long-term coastal evolution (Arens, 1996; Delgado-Fernandez & Davidson-Arnott, 2009; Sherman & Bauer, 1993; Short & Hesp, 1982). Natural and anthropogenically-modified coastal dunes offer protection against storm inundation (Nordstrom, 2001) and sea-level rise (de Winter & Ruessink, 2017), and studying short-term aeolian processes elucidate the development and evolution of these natural coastal barriers. Understanding how dunes will develop is only possible when the physics and mechanisms of aeolian processes are known. Aeolian sediment transport is usually studied by measuring transport rates, sediment flux variations, and vertical distribution of flux profiles in relation to the underlying physical principles (Anderson & Haff, 1991; Bagnold, 1954; Greeley & Iversen, 1985; Pye & Tsoar, 2013; Livingstone & Warren, 1996). Under ideal conditions, most of these issues have been extensively studied through wind tunnel tests and laboratory work. Physically-based models are derived for steady, uniform flows with a logarithmic velocity profile over a flat surface composed of dry uniform sand (Bauer et al., 1990). Bagnold (1937) developed the first aeolian model, based on physics, laboratory tests and field experiments. He and other researchers (Ho, 2012; Han et al., 2011; Yang et al., 2019) have shown that most of the sand transport takes place in a thin layer close to sand bed. Many researchers developed similar models which were calibrated against laboratory data to determine new empirical constants (Sarre, 1989; Sherman & Hotta, 1990; Tsoar et al., 1996). Most of these models are based on the momentum transfer between moving sand particles and airstream and relate sediment transport rate with wind shear velocity and/or threshold shear velocity. Comparative studies show that many of these models are not in agreement when compared to the observed transport values in field conditions (Sherman et al., 1998; Sherman & Li, 2012). Transport rate models are typically proportional to power two or three with wind speed. Furthermore, these models are developed for equilibrium conditions yet these conditions are rarely encountered in coastal environments. On beaches and dunes, the transport of sand by wind can be limited by rainfall, surface moisture, fetch effect, vegetation, beach geometry, and sediment supply effects (Nickling & Davidson-Arnott, 1990; Sherman & Hotta, 1990; Arens, 1996; Hesse & Simpson, 2006; Davidson-Arnott et al., 2005; Ruz & Meur-Ferec, 2004; Hoonhout & de Vries, 2017). These factors are disregarded in transport models which are typically derived for only dry sand. Existing transport equations must be able to predict transport rates with sufficient accuracy when the sand is dry and source and fetch are infinite. If so, they can serve as base model for long-term aeolian sand transport predictions in analytical or numerical calculations (Hoonhout & Vries, 2016; Kok et al.,

2012; Delgado-Fernandez & Davidson-Arnott, 2011; van Rijn, 2018). In the last decade, new attempts were made to develop modified aeolian models with improved reliability and accuracy for the prediction of the transport of dry sand in saturated (equilibrium) conditions (Kok et al., 2012; van Rijn, 2018).

With respect to the understanding of long-term dune behavior at the Belgian coast, various short-term aeolian field campaigns between 2016 and 2018, were conducted at two Belgian sites. The field experiments were designed to study aeolian sediment transport processes across the beach and dune system through the simultaneous measurement of meteorological conditions and sediment transport rates. In this paper, these new field data sets are combined with existing data sets from international literature to test various popular, older models and two recently proposed models. Based on a rigorous analysis, the quality of each model in terms of accurate equilibrium sand flux is judged.

2.2 Aeolian sand transport models

Sand transport occurs when the threshold for motion is exceeded. The dominant mode of transport for sand particles in the size range of 70 to 500 μm is saltation ballistic trajectories. Very fine sand smaller than 70 μm is mostly transported in suspension by turbulent eddies. The coarse sand particles ($>$ 500 μm) are transported by sliding and rolling as surface creep for wind velocities of 12 to 20 m/s (Yang et al., 2019). Very coarse particles can be transported as saltating particles during extreme wind velocities $>$ 20 m/s. Observations in wind tunnels and in nature show that most of the transport occurs in a thin layer ($<$ 0.03 m) above the bed surface (Bagnold, 1937; Ho, 2012; Han et al., 2011). In this thin transport layer, the layer-averaged particle velocity is almost insensitive to the external wind velocity above the transport layer. Particle concentration is so high that the wind velocity is strongly reduced (Kok et al., 2012). An increase of the wind velocity results in an increase of the particle concentration which in turn leads to a decrease of the wind flow speed close to the bed such that the new equilibrium particle velocity remains almost unchanged (Valance et al., 2015).

The sand transport of dry sand close to the bed in both water and air can be described by a set of dimensionless parameters (Yalin, 1977; van Rijn, 1993; van Rijn, 2018), being:

- dimensionless transport rate, ϕ:

$$\phi = \frac{Q_{s,\,mass}}{\rho_s \cdot \sqrt{(s\text{-}1) \cdot g \cdot d_{50}^3}} \tag{2.1}$$

- dimensionless grain size, D_*:

$$D_* = \left[(s\text{-}1) \cdot \frac{g}{\upsilon^2}\right]^{\frac{1}{3}} \cdot d_{50} \tag{2.2}$$

- dimensionless bed-shear stress, defined by the Shields parameter, θ:

$$\theta = \frac{u_*{}^2}{(s\text{-}1) \cdot g \cdot d_{50}} \tag{2.3}$$

- and dimensionless density, s:

$$s = \frac{\rho_s}{\rho_{air}} \tag{2.4}$$

where $Q_{s,mass}$ is the mass sand transport (in kg/m/s); ρ_s is the sediment density (2650 kg/m^3); ρ_{air} is the air density (1.2 kg/m^3); d_{50} represents the median grain size (in m); υ is the kinematic viscosity of air ($1.33 \cdot 10^{-5}$ m^2/s for 0 °C and $1.5 \cdot 10^{-5}$ m^2/s for 20 °C); u_* is the bed-shear velocity (in m/s).

The dimensionless sand transport equation can be formulated as (Yalin, 1977; Van Rijn, 1993):

$$\phi = \alpha \cdot D_*{}^{\beta} \cdot (\theta - \theta_{th})^{\gamma} \tag{2.5}$$

with α, β and γ being coefficients. Equation (2.5) is a universal equation for sand transport in water based on dimension analysis (Yalin, 1977; Van Rijn, 1993). It is assumed that Equation (2.5) is also valid for sand transport in air. Bagnold (1941) and Meyer-Peter & Müller (1948) found that $\gamma \cong 1.5$ for sand transport in air and sand transport in water close to the bed respectively. Meyer-Peter & Müller (1948) have found that bed load transport of very coarse sand in water is independent of grain size ($\beta = 0$). Van Rijn (2007) has found that bed load transport of coarser sand particles in water is related to $(d_{50})^{0.5}$; thus $\beta = 0.5$. Bagnold (1941) has found a similar power for wind-blown sand transport taking place in a very thin layer close to bed. Therefore, it is assumed that $\beta = 0.5$. We introduce a reference grain diameter D to convert Equation (2.5) into a Bagnold type expression.

Substitution of Equations (2.1), (2.2) and (2.3) in (2.5) and s-1 ≅ s for sand in air, and using: s = 2650/1.2 = 2208, $\upsilon = 1.4 \cdot 10^{-5}$ m^2/s, D = 250 µm, $\beta = 0.5$, $\gamma = 1.5$, yields:

$$Q_{s,\,mass} = 3.5 \cdot \alpha \cdot \sqrt{\frac{d_{50}}{D}} \cdot \left(\frac{\rho_{air}}{g}\right) \cdot \left(u_*^2 - u_{*,th}^2\right)^{1.5} \tag{2.6}$$

$$Q_{s,\,mass} \cong \alpha_B \cdot \sqrt{\frac{d_{50}}{D}} \cdot \left(\frac{\rho_{air}}{g}\right) \cdot \left(u_*^3 - u_{*,th}^3\right) \tag{2.7}$$

which is a modified Bagnold-equation for saturated (equilibrium) transport of dry sand in air. Equation (2.6) includes the term $(u_*^2\text{-}u_{*,th}^2)^{1.5}$ which can be replaced by the term $(u_*^3\text{-}u_{*,th}^3)$ as the error involved is negligible. Based on the work of Bagnold: $\alpha_B = 3.5 \cdot \alpha \cong 2$. This derivation shows that a modified Bagnold model can be derived from general dimensional analysis. Bagnold (1941) also formulated the bed-shear velocity for threshold conditions as:

$$u_{*,th} = A \cdot \sqrt{\left[\left(\frac{\rho_s}{\rho_{air}} - 1\right) \cdot g \cdot d_{50}\right]} \tag{2.8}$$

where A is an empirical constant taken as 0.11 based on more recent data of Shao et al. (2000) and Han et al. (2011).

Numerous authors developed mathematical aeolian models, predicting mass transport rates that are proportional to some power of the shear velocity or wind velocity. Most of these models include empirical constants, derived from environmental assumptions. Sherman et al. (1998) and Sherman & Li (2012) tested the performance of eight aeolian transport models to field observations on a sandy beach: Bagnold (1954); Kawamura (1951); Zingg (1953); Owen (1964); Kadib (1965); Hsu (1974); Lettau & Lettau (1978) and Sørensen (2004). Based on evaluations made by comparing slopes and intercepts of best fit lines and RMSE, they concluded that predictions made by the Bagnold (1937) model is the best match from their observations. The models of Kadib (1965), Hsu (1974) and Lettau & Lettau (1978) showed reasonable performance. The model of Kawamura (1951) produced relatively poor results.

Based on the findings of Sherman et al. (1998) and Sherman & Li (2012), we evaluate the models of Bagnold (1937); Kawamura (1951); Bagnold (1954); Hsu (1974) and some of the more recently used models found in literature: Kok et al. (2012) and the modified Bagnold model expressed by Equation (2.7) (Van Rijn, 2018).

Hereafter, the models of Bagnold (1937), Kawamura (1951), Bagnold (1954), Hsu (1974) and Kok et al. (2012) are briefly described. In all of formulations, sand transport rate is presented by Q_s, with unit kg/m/s. All parameters are considered to be constant, except the wind speed (shear velocity). This makes the variability in transport solely dependent on variability in wind speed.

Original Bagnold (1937)

One of the most cited benchmark equations, concerning aeolian transport calculations, is that from Bagnold (1937). He based his formulation on boundary-layer theory and physical approach and validated it by wind tunnel and field experiments. Calibrated for uniform dry sand with a diameter of 0.25 mm, in its simplest form his expression can be described by:

$$Q_s = \begin{cases} C_B \cdot \sqrt{\frac{d_{50}}{D}} \cdot \frac{\rho_{air}}{g} u_*^3, & u_* > u_{*,th} \\ 0, & u_* \leq u_{*,th} \end{cases} \tag{2.9}$$

Where D is a reference grain diameter of 0.25 mm, d is the median grain diameter of the sand, and C_B is a constant with a value of 1.5 for nearly uniform sand, 1.8 for naturally graded sands, 2.8 for poorly sorted sand with a wide range of grain sizes, and 3.5 for pebble surfaces. In this study, $C_B = 2$, is used. ρ_{air} is the air density (taken as 1.2 kg/m^3), g is the gravity constant (taken as 9.81 m/s^2) and u_* is the shear velocity. Bagnold's expression is typically valid for grain sizes within the range of 0.1-1.0 mm and is only used when the threshold of motion is exceeded.

Kawamura (1951)

Kawamura (1951) was the first to develop a transport equation which takes into account the threshold shear velocity term.

$$Q_s = C_{kw} \cdot \frac{\rho_{air}}{g} \cdot (u_* - u_{*,th}) \cdot (u_* + u_{*,th})^2 \tag{2.10}$$

Where C_{kw} is a constant equal to 2.78 derived from wind tunnel experiments. Field measurements showed that this constant ranges from 2.3 to 3.1 on sandy beaches for grain sizes between 0.1-0.8 mm. The threshold velocity $u_{*,th}$ is given by Equation (2.8).

Bagnold (1954)

Bagnold (1954) corrected his model with the threshold velocity term and suggested a modified equation. This expression is described as:

$$Q_s = C_B \cdot \sqrt{\frac{d}{D}} \cdot \frac{\rho_{air}}{g} (u_* - u_{*,th})^3 \tag{2.11}$$

The empirical constants are the same as those used in his initial model (Equation (2.9)).

Hsu (1974)

A different method for calculating sand transport rates was developed by Hsu (1974), who related sand transport to the third power of the friction Froude number:

$$Q_s = C_{Hsu} \cdot \left(\frac{u*}{\sqrt{g \cdot d}} \right)^3 \tag{2.12}$$

Where C_{Hsu} (in kg/m/s) equals:

$$C_{Hsu} = \frac{\exp(-0.47 + 4.97 \cdot d) \cdot 10^{-4}}{10} \tag{2.13}$$

Note that the unit of the grain diameter, d, is in mm for the calculation of the empirical constant.

Kok et al. (2012)

Kok et al. (2012) proposed a different mathematical relationship between wind velocity and mass flux which is in fact a coupled equation from Kok & Renno (2007) and Durán et al. (2011). Based on the momentum balance in the saltation layer, scaling of the particle's hop length with the threshold shear velocity, and particle speed scaling with wind velocity in the saltation layer, the following expression is given:

$$Q_s = C_{DK} \cdot \frac{\rho_{air}}{g} \cdot u_{*,th} \cdot \left(u_*^2 - u_{*,th}^2 \right) \tag{2.14}$$

Experiments and numerical simulations suggest that, for sand with an average diameter of 250 µm, the empirical constant C_{DK} is equal to 5.

Figure 2-1 shows a theoretical comparison between the models based on shear velocities ranging between 0 and 1.4 m/s for sand with a median grain size of 310 µm. The threshold shear velocity is 0.31 m/s based on Equation (2.8). Each model is valid for saturated dry conditions and uses the empirical constants specified by the original authors. Potential transport rates vary significantly near the threshold of motion. In Figure 2-1, it is observed that the performance of the original model of Bagnold (1937) and the modified Bagnold model proposed by Van Rijn (2018) are similar at shear velocities much higher than the threshold. The model of Kawamura (1951) produces the highest transport

rates compared to the other selected models only when shear velocities are greater than approximately 0.31 m/s. The model of Bagnold (1954) produces the smallest transport rates; almost factor 10 smaller than those of the original Bagnold model.

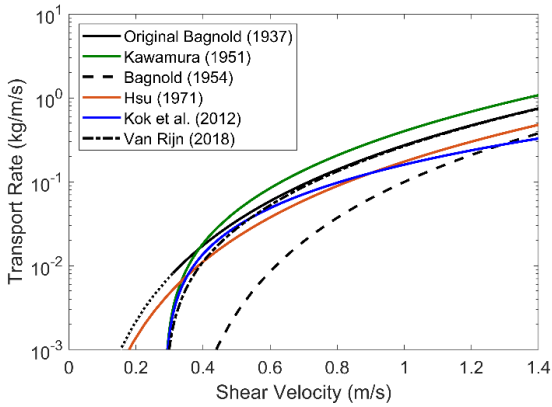

Figure 2-1. *Comparison of six aeolian models based on shear velocity. The median grain size is 310 µm. The original Bagnold model (1937) only calculates transport rates above the threshold of motion (0.31 m/s) and is indicated by the black solid line.*

2.3 Study sites

New experiments have been conducted at two study sites situated on the Belgian coast. The SW-NE oriented Belgian coastline, stretching between the borders of France and the Netherlands, is 65 km long and is part of the southern sandy North Sea coastline. The orientation is parallel to the frequently blowing southwesterly winds characterized by wind speeds of 3-15 m/s, inducing a northeastern aeolian drift. The climate is temperate with an annual average temperature of 10.6°C and average rainfall of about 748 mm (Statbel., 2017). The coast is situated in a macro-tidal regime, ranging from 3.5 m at neap tide to 5 m at spring tide. The wave climate is from low to medium energy with typical wave heights of 0.5-1 m (Haerens et al., 2012). Detailed measurements on aeolian sand transport were performed on two sites. The locations of the sites are shown in Figure 2-2.

Study site 1, Mariakerke beach is characterized by a flat, dissipative sandy beach exceeding a width of 250 m and protected landward by a dyke (> 9 m TAW). The median grain size, d_{50}, is 310 µm and a threshold velocity is 0.31 m/s based on Equation (2.8). Other human interferences in Mariakerke beach include a groin field and regular beach nourishments. No vegetation is present on the beach, which is also invariant in longshore direction.

Site 2, Koksijde beach is a natural sandy beach with a median grain size, d_{50}, of 220 µm and a threshold velocity is 0.26 m/s based on Equation (2.8). It is situated in a dissipative macro-tidal environment. The beach is flat and is characterized by ridge and runnels topography, ranging between 250-500 m (Speybroeck et al., 2004; Voulgarist et al., 1998). All the experiments discussed in this paper were carried out on the subaerial dry beach with winds almost parallel to the beach, excluding possible fetch effects.

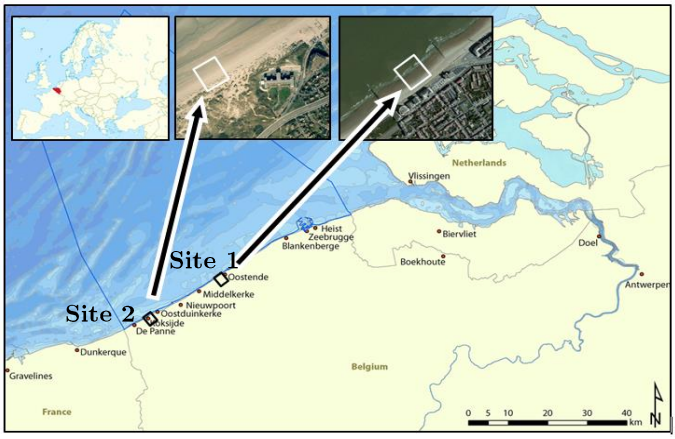

Figure 2-2. *Location of the study areas. Study site 1, Mariakerke, is located next to Oostende at the central part of the Belgian coastline. Study site 2, at Koksijde, is located at the southwestern part of the coastline, near the border of France.*

2.4 Experimental setup

The measurement campaigns, conducted between 2016 and 2018, were designed to measure simultaneous sand transport rates and shear velocities. This allows us to have a unique data set to evaluate the performance of most common and recently used transport models.

2.4.1 Instrumentation and data collection

2.4.1.1 Meteorological stations

Wind speed and direction were mainly measured using four cup anemometers (Vector Instruments A100R) and a wind vane (Vector Instruments W200P) on one or two locations on the dry beach in the study area (Figure 2-3a). Cup anemometers were positioned at 0.15, 0.30, 0.51 and 1.95 m respectively in mast 1 and in mast 2. The wind vane was installed at 2 m above the surface. Wind

speed was recorded at 1 Hz and averaged over 1 minute. Air temperature was recorded at 10-minute intervals. Occasionally, one mast was positioned on the dry beach where all eight anemometers were used with positions at 0.04, 0.22, 0.49, 0.91, 1.29, 1.67, 2.02 and 2.40 m above the surface. Time series of rainfall and tides were from nearby measuring stations.

2.4.1.2 MWAC sand traps

Modified Wilson And Cook (MWAC) sand traps were exposed to the wind for minutes to sometimes hours to determine the rate of aeolian sand transport (Figure 2-3b). These sand traps have been extensively used in numerous studies in which efficiencies of between 42% and 120% were reported (e.g. Van Pelt et al., 2009; Sterk & Raats, 1996; Goossens & Offer, 2000; Poortinga et al., 2013; Youssef et al., 2008). The trap collected sediment in seven plastic bottles from 6.5 to 100 cm above the surface. Aeolian sand transport is dominated by saltation, which involves sand grains following ballistic trajectories as they hop intermittently across the sediment surface. When aeolian sand transport occurs, the saltating layer seldom reaches heights above 25 cm (Van Dijk et al., 1996). Therefore, four bottles were placed in the MWAC sand trap array in the near-bed layer at a of height 6.5, 13.5, 21.0 and 28.5 cm above the surface. The total horizontal sediment flux per meter beach width is determined by fitting an exponential decay curve through the flux results of the four measuring points and extrapolating this curve to the bed (Poortinga et al., 2014; Bauer & Davidson-Arnott, 2014). The trap values were not corrected by an efficiency factor. As the traps were only used in dry weather conditions (dry sand), clogging of the intake nozzles did not occur.

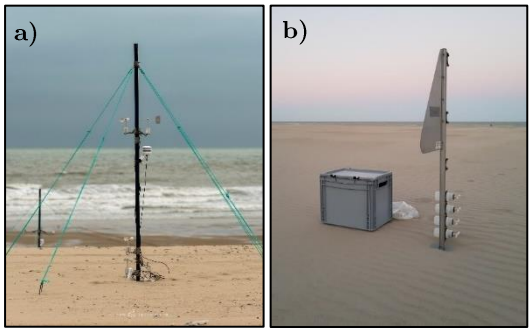

Figure 2-3. *a) Meteorological station with four anemometers, a wind vane and a temperature sensor. b) MWAC sand trap deployed at the beach surface.*

2.5 Analysis method

2.5.1 Calculation of shear velocities

One of the main forcing parameters in the selected aeolian models is the shear velocity. The shear velocity has the advantage of being independent of the height of the velocity measurement above the surface. Accurate shear velocities can be determined by using wind speeds at minimum three or more heights above the surface (Bauer et al., 1992). The wind velocity distribution over the boundary layer is described by:

$$u_z = \frac{u_*}{\varkappa} \cdot \ln\left(\frac{z}{z_0}\right) \tag{2.15}$$

Where u_z is the wind speed at elevation z above the surface, $\varkappa$ is the von Karman's constant (taken as 0.4), and z_0 is the roughness length of the surface. Log-linear regression is used to obtain the optimal parameter set (u_* and z_0), corresponding to the best-fit line through the wind velocities at each elevation. Elevation is used as the independent variable and wind speed as the dependent variable as suggested by the guidelines of Bauer et al. (1992).

2.5.2 Calculation of aeolian sediment fluxes

The vertical distribution of sediment saltation transport, derived from the MWAC sand traps is described by an empirical exponential decay function (Horikawa & Shen, 1960; Williams, 1964):

$$q_z = q_0 \cdot e^{-\beta \cdot z} \tag{2.16}$$

Where q_z is the sediment mass transported at height z above the surface ($kg/m^2/s$), q_o is the extrapolated saltating sediment mass transported at the surface ($kg/m^2/s$) and β is the decay rate (m^{-1}), a measure of the vertical concentration gradient (Van Dijk et al., 1996). To obtain the sediment mass per unit area and time, q_z, the amount of sand captured in one bottle is divided by the inlet area (diameter 8 mm) and exposed time. Generally, this non-linear multiparameter decay model yields high correlation coefficients ($R^2 > 0.9$), because the fitted coefficients (q_o and β) are only weakly related to physical aeolian parameters such as grain size, roughness, and shear velocity (Bauer & Davidson-Arnott, 2014). The total saltating mass transport can be obtained by the integration of Equation (2.16):

$$Q_s = \int_0^\infty q_z \cdot dz = \frac{q_0}{\beta} \tag{2.17}$$

where Q_s is the total mass transported by saltation (kg/m/s), assuming that saltating particles start moving immediately above the surface, z = 0 (Horikawa & Shen, 1960).

2.6 Results and discussion

2.6.1 Results from the Belgian study sites

2.6.1.1 Velocity profiles, shear velocities and roughness lengths

Figure 2-4 shows typical results of measured velocity profiles and corresponding regression lines to determine the shear velocity and the roughness length parameter at the site of Koksijde. Surface conditions were in the form of small ripples for wind velocities up to 14 m/s. Steeper profiles correspond to higher shear velocities. During transport events, the wind profiles intercept with each other in a fixed focal point (Bagnold, 1954), as can be seen in Figure 2-4. The height of the focal point is about 0.045 m, which is about 150 particle diameters and in reasonable agreement with values measured by Pye & Tsoar (2009).

Figure 2-5 shows that the bed roughness height (k_s) varies between 0.1 and 100 mm at the beach of Mariakerke and between 10 and 100 mm at the beach of Koksijde. Figure 2-5 indicates that the roughness height increases with wind speed at 2 m above the sand surface (U_{2m}). The scatter is relatively large for smaller wind speeds < 7 m/s as values averaged over 20 seconds are shown. The scatter reduces significantly for larger wind speeds between 7 and 14 m/s. Field & Pelletier (2018) found that the aerodynamic roughness increases as a power law with shear velocity.

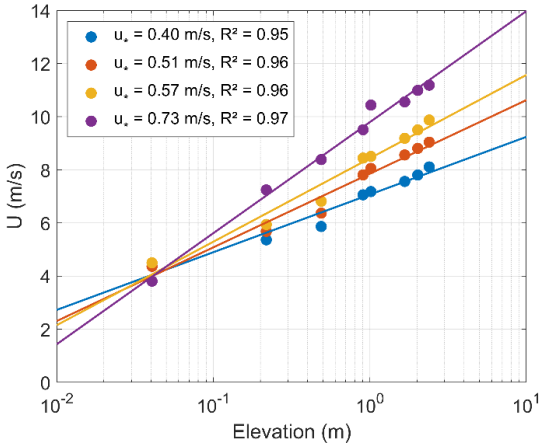

Figure 2-4. *Example of velocity profiles during sand transport with a distinct focal point as measured on 24th November 2016 in Koksijde.*

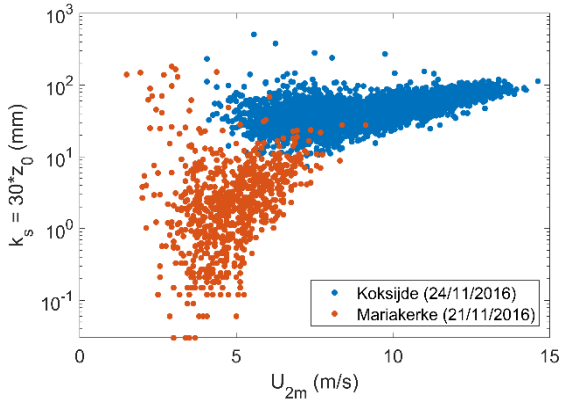

Figure 2-5. *Bed roughness for different wind velocities at the Belgian study sites.*

2.6.1.2 Grain sizes

During the aeolian measurement campaigns, samples were taken from the trapped sand and sand surface beneath the traps in order to determine particle size distribution. The median grain size for both study sites differs as the beach of Mariakerke was nourished in 2014 with slightly coarser sand and shows a larger grain size distribution. Figure 2-6 shows the grain size distribution at Koksijde beach (d_{50} = 220 ± 15 µm) and Mariakerke beach (d_{50} = 310 ± 14 µm). The grain size of the trapped sand varies with elevation above the surface and is not equal to the surface grain size. The grain size of trapped sand seems

to decrease just above the surface. Higher above the surface, grain size tends to increase again. Similar conclusions are made by Farrell et al. (2012) and Yang et al. (2019). They found that an inflection point occurs between 4 to 40 cm above the surface. The height of the inflection point above the surface tends to increase with wind velocity by a power function (Yang et al., 2019).

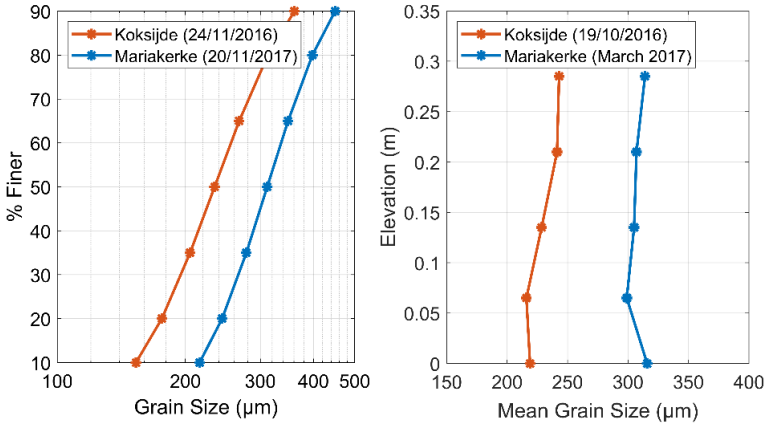

Figure 2-6. *Grain size distribution of surface samples, and median grain size of trapped sand with height above the surface for Sand transport rates.*

2.6.1.3 Aeolian sand transport rates

Three field data sets are used, (1) measurements by the authors at two Belgian beach sites (Koksijde and Mariakerke), (2) measurements by Campos (2018) at a Belgian beach (Koksijde) and (3) measurements reported in Sherman et al. (1998) to evaluate the predicting ability of six different aeolian transport models.

40 data sets on aeolian sand transport at the Belgian sites were obtained based on many deployments of the sand traps. A summary of the data is presented in Table 2-1 for Mariakerke and Table 2-2 for Koksijde. Table 2-1 and Table 2-2 show the average shear velocity, median grain diameter, average regression parameters from Equation (2.16) with corresponding correlation coefficient and average transport flux. The overbar means a spatial-averaged value. Each experiment is a combination of 12 MWAC sand trap measurements, which were positioned at different locations on the dry beach. Usually, the sand traps were deployed in a two by six array.

Figure 2-7 shows typical results of the vertical distribution of sediment transport fluxes derived from the MWAC sand traps. The correlation coefficients of the exponential regression analysis of transport flux show mostly values above 0.90. The weight of the trapped sand in each MWAC sand trap was standardized

according to the inlet opening and run duration. Based on these results, the depth-integrated sand transport rate was determined and the standard deviation of the 12 trap measurements was computed (last two columns of Table 2-1 and Table 2-2). The transport fluxes varied between 7.2 and 84 kg/m/hr for Mariakerke and between 12.6 and 121.8 kg/m/hr for Koksijde. The highest transport rates were measured on Koksijde beach with peaking wind speeds up to 16 m/s. The ratio (s_Q/Q) of the standard deviation and the mean transport rate varies in the range of 0.25 to 0.9 for the site Mariakerke and in the range of 0.45 to 1.1 for Koksijde. The standard error of the mean value is much smaller ($s_Q/n^{0.5}$ with n = number samples = 12).

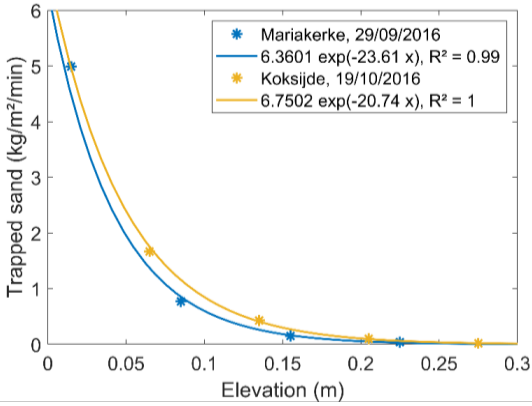

Figure 2-7. *Examples of sand transport fluxes as function of elevation above the surface and best fit exponential decay functions.*

Table 2-1. *Summary of data of the field experiments in Mariakerke (period 2016-2018); s_Q is the standard deviation of sand transport.*

Date	Exp.	$\overline{u_*}$ (m/s)	$\overline{d_{50}}$ (mm)	$\overline{q_0}$ (kg/m²/hr)	$\overline{\beta}$ (1/m)	R^2	$\overline{Q_s}$ (kg/m/hr)	s_Q (kg/m/hr)
13/05/'16	1	0.39	0.31	453.0	21.06	0.998	21.6	16.8
29/09/'16	1	0.29	0.31	201.6	28.57	0.995	7.2	1.8
	2	0.29	0.31	184.8	25.82	0.981	7.2	3.6
17/03/'17	1	0.32	0.31	283.2	21.00	0.954	13.8	4.8
18/03/'17	1	0.42	0.31	466.2	19.84	0.956	23.4	11.4
19/03/'17	1	0.44	0.31	1904.4	20.01	0.990	95.4	41.4
	2	0.47	0.31	1648.8	17.47	0.967	94.2	71.4
	3	0.45	0.31	1608.6	16.62	0.975	96.6	61.2
	4	0.43	0.31	966.6	17.07	0.989	56.4	24
20/03/'17	1	0.27	0.31	505.2	17.23	0.987	29.4	14.4
21/03/'17	1	0.29	0.31	132.0	15.73	0.965	8.4	4.2
	2	0.36	0.31	357.6	23.89	0.973	15	10.8
22/03/'17	1	0.32	0.31	321.6	23.05	0.969	13.8	10.2
12/11/'17	1	0.56	0.31	1179.0	14.06	0.967	84	73.2
18/11/'17	1	0.30	0.31	260.4	23.08	0.972	11.4	6.6

25/04/'18	1	0.39	0.31	418.8	17.72	0.975	23.4	3.6
	2	0.41	0.31	645.6	24.42	0.955	26.4	19.8
26/04/'18	1	0.38	0.31	709.8	22.29	0.949	31.8	22.2
	2	0.37	0.31	642.6	23.64	0.983	27	17.4
27/04/'18	1	0.34	0.31	952.2	21.73	0.897	43.8	22.8

Table 2-2. *Summary of data of the field experiments in Koksijde (period 2016-2018). The italic values represent the data set obtained by Campos (2018).* s_Q *is the standard deviation of sand transport.*

Date	Exp.	$\overline{u_*}$ (m/s)	$\overline{d_{50}}$ (mm)	$\overline{q_0}$ (kg/m²/hr)	$\overline{\beta}$ (1/m)	R^2	$\overline{Q_s}$ (kg/m/hr)	s_Q (kg/m/hr)
19/10/'16	1	0.45	0.22	379.2	15.57	0.963	24.6	16.8
	2	0.41	0.22	193.8	15.44	0.991	12.6	8.4
24/11/'16	1	0.47	0.22	1740.0	22.75	0.985	76.8	63.0
	2	0.52	0.22	1908.0	21.60	0.991	88.2	55.8
	3	0.45	0.22	861.6	17.23	0.976	49.8	59.4
	4	0.49	0.22	1365.6	18.58	0.996	73.8	31.8
	5	0.52	0.22	1708.8	16.90	0.994	101.4	43.8
	6	0.54	0.22	2050.2	16.80	0.996	121.8	53.4
24/11/'16	*1*	*0.53*	*0.22*	*912.6*	*23.72*	*0.997*	*38.4*	-
	2	*0.43*	*0.22*	*983.4*	*19.71*	*0.989*	*49.8*	-
	3	*0.40*	*0.22*	*1342.2*	*19.89*	*0.994*	*67.2*	-
	4	*0.52*	*0.22*	*1276.8*	*18.67*	*0.996*	*68.4*	-
	5	*0.47*	*0.22*	*1647.6*	*18.89*	*0.996*	*87.0*	-
	6	*0.49*	*0.22*	*1620.0*	*18.36*	*0.997*	*88.2*	-
	7	*0.44*	*0.22*	*1273.8*	*19.59*	*0.986*	*64.8*	-
	8	*0.48*	*0.22*	*1444.2*	*18.25*	*0.997*	*79.2*	-
	9	*0.47*	*0.22*	*1209.6*	*18.13*	*0.993*	*66.6*	-
29/01/'18	1	0.51	0.22	1155.6	17.96	0.973	64.2	31.8
	2	0.45	0.22	1253.4	16.81	0.968	74.4	82.2
	3	0.53	0.22	2161.2	16.05	0.989	134.4	101.4

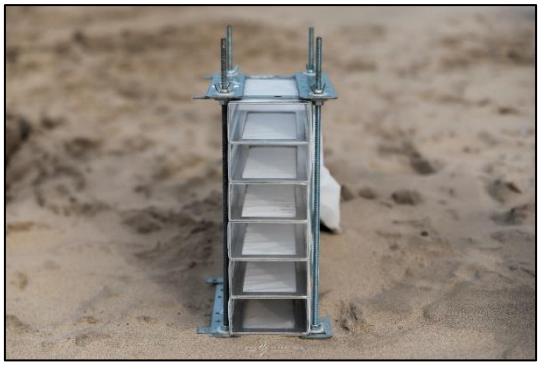

Figure 2-8. *Vertical mesh sand trap covering a height of 30 cm. Image taken on 24/11/2016 on the subaerial beach of Koksijde.*

Table 2-2 includes the results of the sand transport rate measurements conducted by Campos (2018) on the subaerial beach of Koksijde. These measurements were carried out simultaneously with the author's measurements on 24th November 2016. Campos (2018) did nine sand transport measurements in conditions with wind speeds between 7.2 and 9.2 m/s using vertically stacked mesh traps (Sherman et al., 2014). The sand trap consists of an array of six subdivided nylon mesh traps covering a height of 30 cm. Each mesh trap is 10 cm wide, 25 cm long and 5 cm high (Figure 2-8). These traps are oriented to the wind direction. The advantage of these traps is that they can trap large amounts of sand, even sand which is being transported over the first five centimeters above the surface. This is not the case when MWAC sand traps are used as the lower bottle has an elevation of 6.5 cm above the surface. Additional details of his measurements is presented in Campos (2018).

2.6.2 Results from other sites

Table 2-3 presents the results of the sand transport rate measurements conducted by Sherman et al. (1998) in April, 1994 on the foreshore and back beach of a dissipative beach on Inch Spit in Dingle Bay on the southwestern coast of Ireland. They measured wind conditions at five locations across the beach. Wind velocities were measured at four elevations above the surface to determine shear velocities: 0.25, 0.50, 0.75, and 1.00 m. The meteorological towers were spaced 10 to 15 m from each other, starting from the dune foot at the upper beach perpendicular towards the lower beach. Sand transport rates were measured with co-located cylindrical traps with apertures 40 mm wide and 450 mm high (Leatherman, 1978; Rosen, 1979; Nordstrom et al., 2006). The traps are not self-orienting and thus have to be manually oriented to the wind direction. More information about the experimental design is presented in Sherman et al. (1998).

Table 2-3. *Summary of data of the field experiments conducted by* Sherman et al. (1998). *Only the results of Tower 1 and 2 are given.*

Date	Time	Location	$\overline{u_*}$ (m/s)	$\overline{z_0}$ (mm)	w (%)	$\overline{d_{50}}$ (mm)	$\overline{Q_s}$ (kg/m/hr)
24/04/1994	11:11	Tower 1	0.4897	1.9429	5.43	0.17	27.76
Run 1		Tower 2	0.5068	0.8477	4.84	0.17	27.68
24/04/1994	11:42	Tower 1	0.4757	1.9213	5.24	0.17	24.81
Run 2		Tower 2	0.5125	1.0344	5.83	0.17	23.41
24/04/1994	12:27	Tower 1	0.3908	0.7983	4.10	0.17	22.90
Run 3		Tower 2	0.4352	0.5841	2.91	0.17	28.24
24/04/1994	12:57	Tower 1	0.5767	2.7162	6.78	0.17	50.55
Run 4		Tower 2	0.6540	2.8073	5.41	0.17	39.12
26/04/1994	10:58	Tower 1	0.6069	3.1223	7.14	0.17	35.04
Run 5		Tower 2	0.5001	0.7227	5.38	0.17	34.96
26/04/1994	11:29	Tower 1	0.6361	3.6258	2.98	0.17	26.41
Run 6		Tower 2	0.5652	1.3985	3.24	0.17	29.93
26/04/1994	12:27	Tower 1	0.5788	3.3658	2.72	0.17	14.46

Run 7		Tower 2	0.4958	0.9233	3.70	0.17	18.08
26/04/1994	15:28	Tower 1	0.4494	1.7280	0.13	0.17	6.78
Run 8		Tower 2	0.3596	0.2756	1.05	0.17	6.93
28/04/1994	13:14	Tower 1	0.4635	1.3730	5.05	0.17	12.19
Run 9		Tower 2	0.3670	0.1026	4.67	0.17	13.07
28/04/1994	13:43	Tower 1	0.4282	0.7918	5.34	0.17	10.54
Run 10		Tower 2	0.3753	0.1061	4.32	0.17	9.25
28/04/1994	14:29	Tower 1	0.4738	1.3151	5.15	0.17	21.67
Run 11		Tower 2	0.3844	0.0963	4.29	0.17	27.52
28/04/1994	15:29	Tower 1	0.4481	1.2406	1.48	0.17	17.40
Run 12		Tower 2	0.3824	0.1555	2.27	0.17	16.90
28/04/1994	17:14	Tower 1	0.3178	1.6087	0.63	0.17	0.78
Run 13		Tower 2	0.2730	0.2361	2.21	0.17	1.02
28/04/1994	18:00	Tower 1	0.2785	1.8583	0.49	0.17	0.34
Run 14		Tower 2	0.2299	0.2458	1.56	0.17	0.73

The median grain size on the beach during the field experiment of Sherman et al. (1998) was approximately 170 µm, resulting in a threshold velocity of 0.21 m/s based on Equation (2.8). All of their data is not used in our performance analysis. Compared to the author's mostly longshore measurements, their measurements were conducted during onshore to oblique onshore winds. This means that the fetch effect plays an important role in the amount of trapped sand. Sherman et al. (1998) observed that the highest rates of transport were found at the dune foot and the lowest in the foreshore (lower beach zone), indicating that most of the sand supply comes from the foreshore. Tower 1 and 2 were located on the upper beach and measured maximum transport rates for all but two events. Therefore, only the results from tower 1 and 2 are averaged and used in this study.

In order to compare observed with predicted transport rates from the different models, linear regression analysis is used: $Q_{predicted} = m.Q_{observed}$. Correlation coefficients (R^2), root mean square errors (RMSE), and best fit line slope values are computed. Table 2-4 shows the results of all models for the measurements of the two Belgian sites. Table 2-5 shows the results for all transport rate measurements. Figure 2-9 shows the comparison between observed and predicted transport rates for the six aeolian models including all data sets.

Table 2-4. *Summary of results comparing observed transport rates with predicted transport rates for different aeolian models, only data of the two Belgian sites (Mariakerke and Koksijde).*

Model	Slope (m)	R^2	RMSE (kg/m/min)
Original Bagnold (1937)	1.21	0.35	0.52
Kawamura (1951)	1.68	0.61	1.17
Threshold Bagnold (1954)	0.14	0.53	0.92
Hsu (1971)	0.69	0.44	0.42
Kok et al. (2012)	1.13	0.57	0.45
Modified Bagnold (2018)	1.01	0.60	0.40

Table 2-5. *Summary of all results comparing observed transport rates with predicted transport rates for different aeolian models, all data sets.*

Model	Slope (m)	R^2	RMSE (kg/m/min)
Original Bagnold (1937)	1.26	0.19	0.56
Kawamura (1951)	1.96	0.31	1.28
Threshold Bagnold (1954)	0.15	0.36	0.80
Hsu (1971)	0.72	0.08	0.41
Kok et al. (2012)	1.19	0.26	0.55
Modified Bagnold (2018)	1.06	0.42	0.45

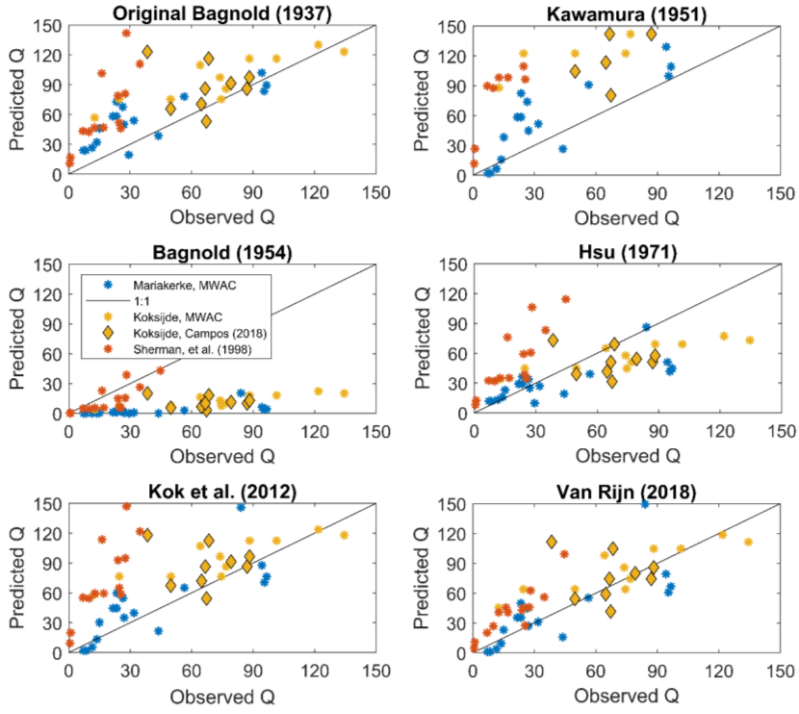

Figure 2-9. *Comparison between observed and predicted sand transport rates for six aeolian models; all data sets. Diagonal lines represent the one-to-one correspondence. All transport rates are in kg/m/hr. Blue dots correspond to the measurements in Mariakerke. Yellow dots correspond to the measurements in Koksijde.*

Analysis of the results shows that the modified Bagnold model based on Equation (2.2) (Van Rijn, 2018) yields the best performance when observed transport rates are compared to predicted transport rates. The modified Bagnold model has the best fit line slope to 1, a high R^2, and the lowest RMSE.

The model of Kok et al. (2012) also performs very good but shows a slightly weaker statistical relationship between observed and predicted rates of transport. The model of Kawamura (1951) is in contrast as it does not produce a one-to-one prediction and has the largest RMSE. Our results suggest that the Kawamura model overestimates transport substantially. The Kawamura model also displayed a poor performance in the evaluation of Sherman et al. (1998) and Sherman & Li (2012). The model of Bagnold (1954) also displays a poor result. The best fit line is close to zero, indicating a large underestimation of transport rate. It also has a relatively large RMSE. However, this model is frequently used in long-term sediment budget calculations. E.g. Hoonhout & Vries (2016) used it as the benchmark model to calculate saturated transport conditions in the numerical model 'Aeolis'. The other models perform intermediately and display similar predictive results. When considering only the data sets of the two Belgian sites, the models perform slightly better. This could be attributed to the use of different sand traps with different trap efficiencies. Trap efficiency is defined as the relative ratio of trapped sand to the actual quantity of blown sand (Chepil & Milne, 1941). Sherman et al. (1998) used cylindrical sand traps with efficiencies ranging from 30% to 70%, which are different from the trap efficiencies of the MWAC sand traps ranging from 35% to 120%. Furthermore, they are not self-oriented compared to the MWAC sand traps. It is possible that the cylindrical traps capture less sand than the MWAC sand traps due to its mechanical structure. The transport rates measured with the vertical nylon mesh traps, used in the study of Campos (2018), show similar results as the transport rates measured with the MWAC sand traps during the same wind conditions on the subaerial beach of Koksijde.

The general variability between observed and predicted transport rates could thus be partly attributed to the use of different mechanical sand traps. Variation between observed and predicted transport rates could also be attributed to the effect of moisture. As sand was trapped during dry conditions, little to no moisture was present in the samples during the measurements at the two Belgian sites. The data of Sherman et al. (1998) also refer to dry sand conditions, but moisture values were not measured. Beach slope may have an effect on cross-shore sand transport as measured by Sherman et al (1998). As they did not adjust their data, the effect of beach slope is most likely negligibly small. Beach slope was almost flat during the measurements at the Belgian sites, where sand transport was in the longshore direction.

A large influence on the variability between observed and predicted transport rates could be attributed to the spatial distribution of the different sand traps. It is well known that aeolian sand transport has a spatial-temporal character. During a transport event, one trap could capture more sand than another trap if, for example, wind forces and sand transport are in the form of streamers or streaks. Thus, shear velocity can vary spatial-temporally due to varying wind conditions or even the threshold velocity can vary locally and in time due to a varying grain size or different surface characteristics. In practice, shear velocity

can only be determined at one or two locations. Eventually, this has an impact on the calculation of sand transport rates. Figure 2-10 shows the relation between the variability of the observed transport rates and shear velocity. The variability is determined by the standard deviation. Higher shear velocities cause larger variability of the observed transport rates. It seems that this variation also follows a relationship of the type (u_*^3-$u_{*,th}^3$) with an R^2 equal to 0.54. Most of our transport rates were measured during longshore wind conditions. Poortinga et al. (2015) found that on a wide beach on the island of Ameland, The Netherlands, the largest variability of sand transport rates was found for alongshore events. Variability can be reduced by increasing the sampling time provided that the wind conditions are constant (de Vries et al., 2012 and Keijsers et al., 2014).

In this study, we assumed that the estimates of shear velocity are closely to the true values. However, it is possible that the actual shear velocities related to the saltating particles vary substantially from the shear velocities, derived from vertical wind profiles due to roughness effects and measurement scatter (Bauer et al., 1992). Therefore, we suggest that in future research the shear velocity would be better estimated based on the effective grain roughness ($k_{s,grain}$). The influence of moisture content and beach armoring and other bed surface properties (e.g. shells) appear to be a critical factor in degrading the performance of aeolian models. Future work should be based on designing a workable and predictive model that can account for these influences.

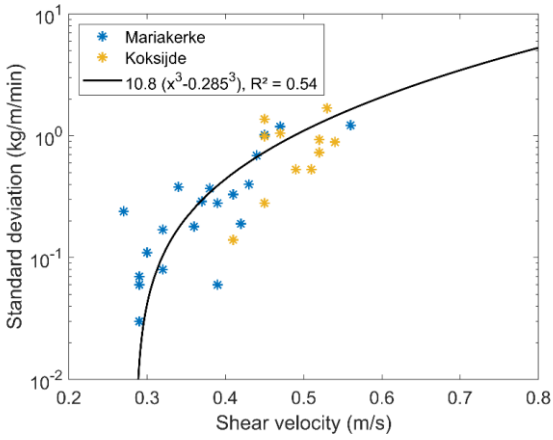

Figure 2-10. *Relation between standard deviation of observed transport rates and shear velocity.*

2.7 Conclusions

Wind-blown transport rates of beach sand have been measured at two Belgian sites using mechanical sand traps and cup anemometers to measure the wind speeds. These data sets and other data sets from the literature have been used to test six aeolian sand transport equations.

Several conclusions can be made based on this study:

1. The measured sand transport rates at the two Belgian sites show a good correlation with the shear velocity to power 3 minus the threshold shear velocity to power 3.

2. A modified Bagnold model, which has been proposed by Van Rijn (2018), proves to be the best model to predict aeolian transport of dry sand. It has an almost one-to-one relation between observed and predicted transport rates. The model shows to be very consistent with the observed transport rates. The model of Kok et al. (2012) also performs rather well.

3. The threshold model of Bagnold (1954) and the model of Kawamura (1951) produces the poorest results. The threshold Bagnold model underestimates transport rates, while the Kawamura model overestimates transport rates. Both models correlate weakly with our observations.

4. Variability between observed and predicted transport rates is mainly caused by the spatial-temporal character of aeolian sand transport. It seems that this variation is related to shear velocity by a cubic relationship. This cubic relationship is also described by the modified Bagnold model.

2.8 Acknowledgements

This research is carried out in the project CREST (Climate Resilient coaST), funded by the Strategic Basic Research (SBO) program of the Flanders Innovation & Entrepreneurship. We thank the support of VLIZ (Flanders Marine Institute) for the use of their research infrastructure. We would like to acknowledge the following people who helped during the measurement campaigns: Annelies Vandenbulcke, Evelien Brand, Janus Van Massenhove, Stijn Willemse, Vincent Gruwez, Ine Vandebeek, Anne-Lise Montreuil, Samuel Van Ackere, Tina Mertens, Toon Verwaest, Matthias Wyffels, Francesca Ortenzio and Sebastiaan Dan. We would like to thank Leonardo Duarte Campos

for his hard work and help during the measurement campaign in Koksijde, November 2016 and the opportunity to use his collected transport rates.

Chapter III

Dune evolution at decadal timescales and its relation with potential aeolian transport

Abstract

Long-term changes in dune volume at the Belgian coast are analyzed based on measured data by airborne surveys available from 1979. For most of the 65 km long coastal stretch, dune volume increases linearly in time at a constant rate. Dune growth varies between 0–12.3 $m^3/m/year$ with an average dune growth of 6.2 $m^3/m/year$, featuring large variations in longshore directions. Based on a wind data set from 2000–2017, it is found that potential aeolian sediment transport has its main drift from the west to southwest direction (onshore to oblique onshore). Based on a modified Bagnold model, onshore potential aeolian sediment transport ranges to a maximum of 9 $m^3/m/year$, while longshore potential aeolian sediment transport could reach up to 20 $m^3/m/year$. We found an important correlation between observed and predicted dune development at decadal timescales when zones with dune management activities are excluded. Most of the predicted data are within a factor of two of the measured values. The variability in potential transport is well related to the variability in dune volume changes at the considered spatial–temporal scale, suggesting that natural dune growth is primarily caused by aeolian sediment transport from the beach. It also suggests that annual differences in forcing and transport limiting conditions (wind and moisture) only have a modest effect on the overall variability of dune volume trends.

Keywords: Aeolian sediment transport, Dune development, Belgian Coast, Decadal timescales, Annual timescales

Chapter published as: Strypsteen, G., Houthuys, R. and Rauwoens, P. (2019). Dune evolution at decadal timescales and its relation with potential aeolian transport. *Journal of Marine Science and Engineering, 7*(10), 357.

3.1 Introduction

Coastal dunes provide safety against flooding during storm events. They also have functions for recreation and nature conservation. Compared to hard engineering structures like sea dykes, coastal dunes are in favor because they are primarily being built by natural aeolian processes (Nickling & Davidson-Arnott, 1990; Delgado-Fernandez & Davidson-Arnott, 2009; Baas et al., 2006). However, natural coastal dunes are dynamic features and the disadvantage, therefore, is that the provided safety level is variable in time (de Vries et al., 2012). Long-term coastal dune development is a net result of combined storm wave erosive and aeolian processes. It is the net result which determines if the dunes are eroding or growing. Predicting and evaluating these processes is a prerequisite for many management activities. In the past few decades, a substantial amount of research has been carried out on dune erosion which can be simulated with good accuracy. Yet, predictions on aeolian sediment transport from the beach towards the dunes, leading to dune recovery, are still difficult to make (Vellinga, 1986; Steetzel, 1993; van Rijn, 2013; Delgado-Fernandez, 2011). This study examines how annual to decadal variations in wind climate (indirect potential aeolian transport) correlate with annual to decadal variations in dune volume along the Belgian coast. Decadal variations are of interest because they describe the general coastline development.

Coastal dune development studies generally focus on the measurement of short-term transport processes in the timescale of hours to days (Strypsteen et al., 2017; Sarre 1989; Dingler et al., 1992; Jackson & Nordstrom, 1997; Nordstrom et al., 1996; Bauer et al., 1990). Sometimes, at these timescales, a one to one relation is found between predicted and observed values (Strypsteen et al., 2019). Coastal dune development is also frequently studied by the measurement of long-term topographical elevation variations in the timescale of months to years (Sarre, 1989; Law & Davidson-Arnott, 1990; Delgado-Fernandez, 2011; Pye & Blott, 2008; Brodie et al., 2019). Primarily, these topographical elevation changes are related to calculated potential transport rates (Keijsers et al., 2014). Long-term aeolian sediment transport from the beach towards the coastal dunes are generally predicted by integrating hourly meteorological data such as wind speed and direction from standard meteorological stations, into sediment transport equations (e.g. Bagnold, 1954; Kadib, 1965; Hsu, 1974; McKee, 1980; Kroon & Hoekstra, 1990). Unfortunately, at these timescales, the calculated potential sediment input in the dunes from the beach frequently do not agree with volume observations in the dunes (e.g. Sarre, 1989; Law & Davidson-Arnott, 1990). Keijsers et al. (2014) and de Vries et al. (2012) studied aeolian transport and dune behavior on annual to decadal timescales and found no significant correlation. Both found greater correlation between dune behavior and erosive events by storms. Though, for their study at the Dutch coast, Keijsers et al. (2014) found stronger correlations between time series of potential sediment transport and dune volume on wider beaches ($>$ 200 m). This suggests

potentially stronger correlations at the Belgian coast, where beach widths are generally wider (between 150 m and 400 m). The wider beaches at the Belgian coast are primarily created by massive sand nourishments to cope with future flooding risks and hazards. Especially since the 1990s, nourishments are used to keep the sediment budgets along the coast positive. The nourished sand is naturally distributed in the coastal zone.

When coastal dune development and its relation with potential aeolian sediment transport is studied on decadal timescales, the effects of erosive and accretive years should eventually average out. Annual differences would then be observed as small perturbations on the trend at decadal timescales. Potential transport should then, hypothetically, be well related to dune behavior at the considered spatial–temporal scale. This would suggest that dune growth (at locations not suffering too much from dune erosion) is primarily caused by aeolian sediment transport from the beach.

The purpose of this paper is:

1. To gain insight into long-term dune development at the Belgian coast. This study is based on the analysis of airborne photogrammetric and airborne laser scanner (LiDAR) data of the dunes from 1979–2018.

2. To gain insight in annual potential aeolian sediment transport quantities and how it behaves on decadal timescales (long-term). Annual potential aeolian sediment transport along the Belgian coastline is estimated by the use of a modified Bagnold model, which has been validated by short-term field data of aeolian sediment transport rates (Strypsteen et al., 2019), applied to a wind data set from 2000–2017.

3. To gain insight in the correlation between observed and predicted dune volume on an *annual* timescale. Year-to-year variations (between elevation measurements) in potential transport and dune volume changes are compared.

4. To gain insight into the correlation between observed and predicted dune volume on decadal timescales. Trend analysis on predicted and measured dune volume is conducted for comparisons on a decadal timescale.

5. To explain longshore variations of the correlations by distinguishing between ‘natural’ and ‘managed’ beach sections of the Belgian coast featuring dunes.

3.2 Regional setting

Located between France and the Netherlands (Figure 3-1), the modest 65 km long Belgian coast was historically characterized by sandy beaches, backed by wide sand dunes, mudflats and tidal marshes (Vandebroek et al., 2017). However, over the last 50 years, these marshes and mudflats were modified by draining and diking them to develop agriculture, habitation and major economical recreation (Charlier & De Meyer, 1995). Nowadays, besides many coastal areas worldwide, the Belgian coast also faces increasing challenges due to coastal erosion, sea-level rise, and an increased risk of flooding.

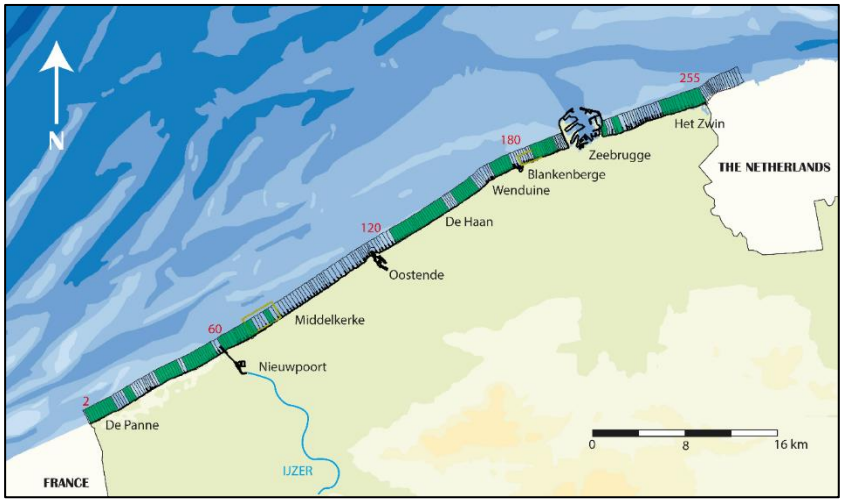

Figure 3-1. *The 65 km long Belgian coast is located at the North Sea, between the French and the Dutch border and is divided into 254 coastal sections. The river 'IJzer' flows into the North Sea at Nieuwpoort. The green areas indicate the locations with vegetated coastal dunes.*

The Belgian coast is southwest-northeast orientated with a mean of 62° to the North (Figure 3-2). Local variations from the mean coastal orientation are found especially around the harbor mouths (Ostend (30 km) and Zeebrugge (50 km)), and the nature reserve 'het Zwin', on the border with the Netherlands.

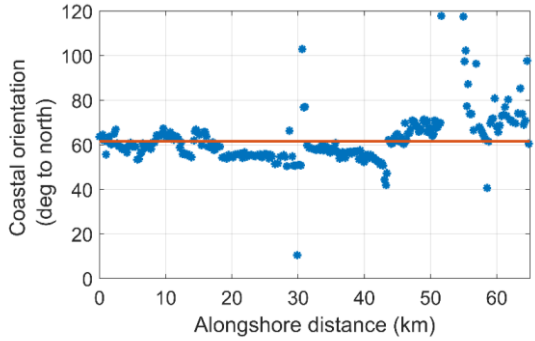

Figure 3-2. *Coastal orientation of the Belgian coast. It represents the orientation of foredunes or dykes. The mean coastal orientation is 62° with respect to the North (red line).*

The Belgian coast consists of sandy beaches, which are generally up to 400 m wide in the southwest and only 150 m in the northeast (Figure 3-3). Beach width is defined here as the horizontal distance between mean low-water level (+1.39 m TAW[1]) and dune foot (+6.89 m TAW). During springtide, beach width can range from 100 m to 600 m (Lebbe et al., 2008). The upper beach width, defined as the horizontal distance between mean high-water level (+4.39 m TAW) and dune foot (+6.89 m TAW), ranges from 30 m to 100 m. The beaches along the entire coastline are very gently sloping, although the slope increases from west to east (Figure 3-3). Due to the construction of the jetties (approximately 3 km in length) of Zeebrugge harbor (between 52–55 km alongshore), the beach width is relatively large, causing a very mild beach slope in that region.

[1] TAW is the Belgian reference level (Tweede Algemene Waterpassing) and is located around mean water level at low low tide springs.

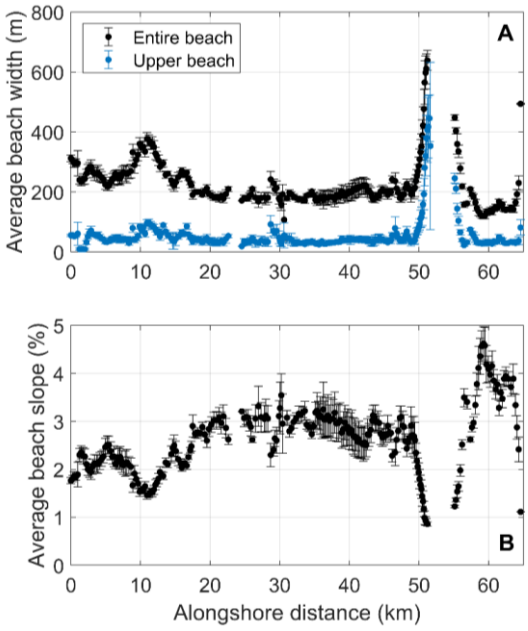

Figure 3-3. *A) Average beach width along the Belgian coast based on airborne surveys from 2000–2017. Beach width is the horizontal distance between the average low-water level and the dune foot. Upper beach width is the horizontal distance between the average high-water level and the dune foot or a hard defense structure. B) Average beach slope along the Belgian coast based on airborne surveys from 2000–2017. Error bars indicate the standard deviation.*

Due to a natural gradient and an increase in nourishments towards the Northeast, the sand becomes gradually coarser along the coast, from 150 µm in the west to up to 400 µm in the east (Vandebroek et al., 2017). Figure 3-4 shows the median grain size variation along the Belgian coast. It is from a unique data set from the year 2000 that covers the entire Belgian coast (Verwaest et al., 2008). Three to four samples were taken at the surface on the upper beach and were analyzed for grain size after removal of organic material. On the basis of the available measurement data, the coast is divided into zones in which the nature of the beach sand is assumed to be homogeneous. In total, 16 zones are distinguished. The black line represents the 16 homogeneous zones with each having a different grain size. The corresponding standard deviation is also shown (black bars).

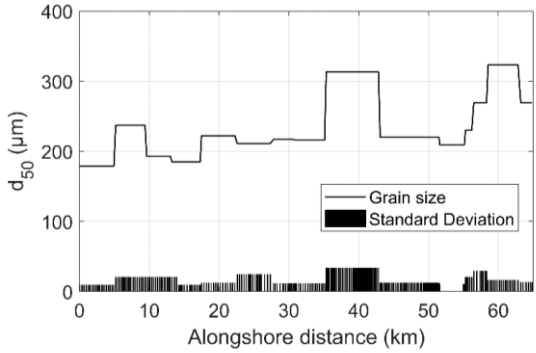

Figure 3-4. *The grain size variation along the Belgian coast. There is an increase from France (0 km) to the Netherlands (65 km).*

Approximately half of the Belgian coast consists of vegetated coastal dunes (Figure 3-5) which vary in height between +5 m TAW and +30 m TAW and with most ranging between +7 and +15 m TAW (Haerens et al., 2012). According to Lebbe et al. (2008), the width of the Belgian dunes narrow down from 2 km west of the IJzer estuary to a few hundred meters eastwards of the IJzer. Landward of the dunes, an outstretched and extensive coastal lowland is present at elevations between +1 and +4 m TAW (Haerens et al., 2012). The remaining part of the Belgian coast, especially around coastal cities, is being protected by harbors, groynes, seawalls, and sea dykes (Figure 3-5). The height of the sea dykes is approximately + 9 m TAW.



Figure 3-5. *Typical sights at the Belgian coast. Left: natural beach-dune system at Koksijde (11 km from the French border). Right: managed beach-dyke system at Mariakerke (26 km from the French border).*

3.3 Methods

3.3.1 Dune volume changes along the Belgian coast

Since 1979, the Belgian government has been monitoring the eastern part of the coastline, and since 1983 the entire coastline by annually or bi-annually surveying cross-shore bathymetric profiles and collecting airborne photogrammetric and, since 1999, airborne Laser Scanner (LiDAR) data (International Marine & Dredging Consultants (IMDC), 2010; Houthuys, 2012). The surveys took place at different times per year. Determining and managing the seawall safety level was the initial idea to monitor and survey the coastal morphology in Belgium (Deronde et al., 2009). The available data allow specific morphological analyses. Demonstrated by numerous studies, LiDAR data is able to accurately represent beach topography over large stretches of coastline (Revellt et al., 2016; Sallenger et al., 2003; White & Wang, 2003). Sequentially, LiDAR surveys allow to very accurately monitor temporal shoreline changes (Stockdon et al., 2002). Concerning the Belgian coast, LiDAR data covers the intertidal beach up to the sea-fronting dunes. For this study, the focus lies on the dunes. The Belgian coast is represented by a system of coastal sections adopted by the Flemish government, defined by fixed boundaries, which are also used in this study (Vandebroek et al., 2017). There are 277 coastal sections, each approximately 250 m wide, where morphology is monitored and surveyed. Section 1 is located, however, in France and sections 256 to 277 are located in the Netherlands. Hence, this study focusses on sections 2 to 255 (Figure 3-1).

In the 1980s, on the basis of elevation boundaries, the Belgian coast was also divided into five cross-shore horizontal elevation slices (International Marine & Dredging Consultants (IMDC), 2010; Houthuys, 2012). Following Figure 3-6, slice 1 comprises the intertidal beach with elevations between +1.39 and +4.39 m TAW, slice 2 is the dry beach with elevations between +4.39 and +6.89 m TAW, slice 3 represents the dune area above +6.89 m TAW, slice 4 is the shoreface with elevations between -4.11 m and +1.39 m TAW, and slice 5 is the sea bottom below -4.11 m TAW. Initially, these elevations were defined by the department of mobility and public works (MOW) relative to the Z vertical datum (-4, 1.5, 4.5, and 7 m Z). Later, these were converted to the TAW vertical datum by subtracting 0.11 m. The elevations are conventional boundaries and have not been derived on the basis of tidal water level variations (Vandebroek et al., 2017).

The dune volume is defined as the volume of sand above the dune foot level and is bounded by fixed vertical planes constituting a fixed landward limit. The dune foot level along the Belgian coast was defined at +6.89 m TAW. The term "dune volume" has been defined purely based on bounding planes. It results that a dune volume can also be calculated in areas with a seawall or with artificially

raised touristic berms, where no vegetated dunes are found. It is noticed that the landward limit is either positioned at the foot of the seawall or on the top or even at the landward side of the first dune ridge. However, the varying landward reference is not of relevance given that most morphological changes occur in the area included in the section boundaries.

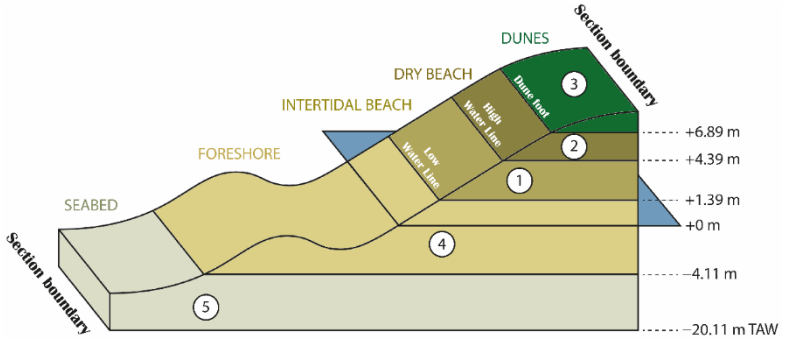

Figure 3-6. *The definition of the dune volume (number 3), where the dune foot level starts at +6.89 m TAW. Figure adapted from Vandebroek et al. (2017).*

Figure 3-7 gives an overview of all the available dune volume data at the Belgian coast. Blank bars indicate no performed LiDAR flights and thus no available survey data. Some regions, especially the dune regions, experience a growth in time (yellow to red color). Other regions, in particular the regions that are diked, remain stable in time.

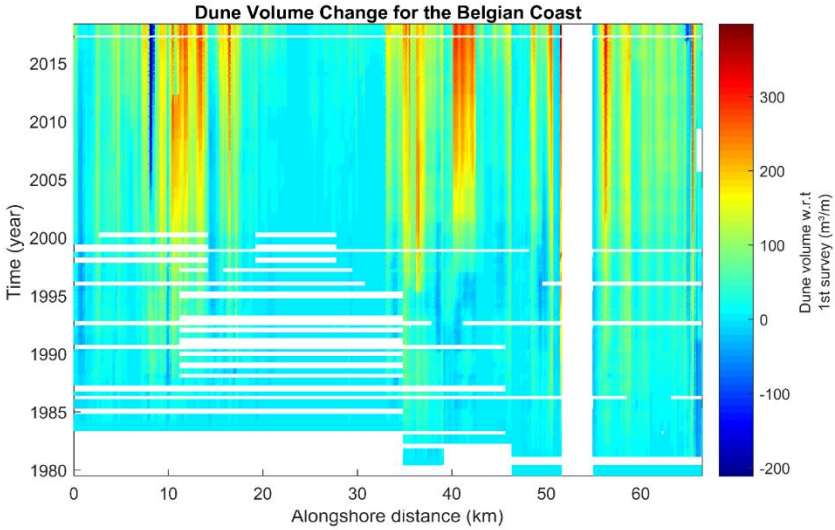

Figure 3-7. *Overview of available data on dune volume with respect to the first survey along the Belgian coast, based on the annual surveys (positive values = deposition; negative values = erosion; 0 = stable). The term dune volume has been defined purely based on bounding planes. Dune volume can also be calculated in areas with a seawall or with artificially raised touristic berms, where no vegetated dunes are found.*

3.3.2 Calculation procedure of potential transport

Dune growth could be best explained by potential aeolian sediment input from the beach in the dunes. By applying a time series of regional wind data to aeolian transport equations, potential aeolian transport can be calculated (Delgado-Fernandez & Davidson-Arnott, 2011; Kroon & Hoekstra, 1990). It should be mentioned that potential transport is the maximum transport that can be achieved. All winds above the threshold velocity can transport sand if factors such as precipitation and surficial moisture which negatively influence aeolian sediment transport are disregarded (Arens, 1997). Validated by short-term field campaigns (Strypsteen et al., 2019), where wind speeds and saturated aeolian transport rates were measured, a modified Bagnold model (van Rijn, 2018) is used to calculate annual aeolian sand transport and is formulated by:

$$q = \begin{cases} 3600 \cdot \alpha_B \cdot \sqrt{\frac{d_{50}}{d_{50,ref}}} \cdot \frac{\rho_{air}}{g} \cdot \left[(u*)^3 - (u_{*,cr})^3\right], & u* > u_{*,cr} \\ 0, & u* < u_{*,cr} \end{cases} \quad (3.1)$$

where q = saturated mass flux (kg/m/h); d_{50} = median particle size (µm); $d_{50,ref}$ = 250 µm; ρ_{air} = density of air (1.2 kg/m³); g = acceleration of gravity (9.81

m/s^2); u_* = shear velocity (m/s); $u_{*,cr}$ = threshold shear velocity (m/s); α_B = Bagnold factor (1.5 – 3.5). The coefficient α_B ranges from 1.5 to 3.5 and is depending on the surface sediments. A value of $\alpha_B = 2$ represents naturally graded sands, which is used in the calculation of potential transport (see also Section 2.2). Apart from the wind speed, Equation (3.1) assumes conditions where all parameters are considered constant in time, making the transport variability solely depending on the variability in wind speed (de Vries et al., 2012).

The critical shear velocity of dry sand is defined as:

$$u_{*,cr} = 0{,}11 \cdot \sqrt{\left[\left(\frac{\rho_s}{\rho_{air}} - 1\right) \cdot g \cdot d_{50}\right]} \tag{3.2}$$

where ρ_{air} = density of air (1.2 kg/m^3); ρ_s = absolute density of sand grains (2650 kg/m^3); g = 9.81 m/s^2; d_{50} = median particle size (m).

The shear velocity, u_*, is the main driving factor in most transport formulae (Sherman & Li, 2012; Valance et al., 2015). Determining the shear velocity, u_*, requires either measurement of the velocity profile or knowledge of the aerodynamic roughness length (Davidson-Arnott & Law, 1996). A time series of hourly mean wind speed and wind direction were obtained from a meteorological station maintained by Ostend Airport. The station is about 1 km inland from the coastline and measured at a height of 4 m (Figure 3-1). The wind data is available since the year 2000. It is likely that the roughness length varies significantly spatial-temporally (Strypsteen et al., 2017). This makes it inappropriate to use any of the frequently used transport formulae (Davidson-arnott & Law, 1996).

Hsu (1974) suggested a straightforward equation for the prediction of aeolian sediment transport from hourly routine wind observations at meteorological stations. This equation is based on the relationship between the bed shear velocity, u_*, and wind speed at a certain height above the surface, taken from field data from numerous study areas. This relationship for the dry beach area is given by $u_* = 0.040 \cdot U_{2m\text{-}10m}$, where U_{2m} and U_{10m} is the wind speed at 2 m and 10 m above the surface respectively. This relationship is also the average value what Strypsteen et al. (2017) found. In the potential aeolian sand transport calculations, the wind shear velocity, u_*, is constant throughout the hour, in spite of the fact that this is practically not the case. Normally distributed fluctuations around the mean wind speed, would cause in theory a larger amount of sediment to be transported by wind than would be given here (Sarre, 1989). According to Sarre (1989), these inaccuracies and underestimations of potential aeolian transport are not important. Other transport limiting factors in coastal areas are of more importance, such as: surface moisture, vegetation and beach dimensions (de Vries et al., 2012).

Potential sediment transport will also be influenced by the fetch effect (Lynch et al., 2007; Delgado-Fernandez, 2010). Delgado-Fernandez (2010) described the fetch effect as an increase in sediment transport rate in the downwind direction until an equilibrium is reached. Longer fetch lengths often lead to higher transport rates under certain wind conditions. The limit where an equilibrium is reached is defined as the critical fetch. Critical fetch distance is not considered in this paper, since it is in the order of 10-50 m for wind speeds up to 15 m/s (Spies & McEwan, 2000) and it is smaller than the average upper beach width at the Belgian coast.

Applying measured wind time series produces the total transport by summation of all calculated transport rates q_i (Equation (3.2)). It is of great importance that potential aeolian sediment transport is being modified according to the angle of wind approach along the shoreline in order to compare predicted with observed dune volume changes (Nickling & Davidson-Arnott, 1990). The predicted net sediment input by wind in the dunes (in m^3/m) becomes:

$$Q_{cross\text{-}shore} = \frac{1}{\rho_b} \sum_{i=1}^{n} q_i \sin[\alpha\text{-}O] = \frac{1}{\rho_b} \sum_{i=1}^{n} q_i \sin[dd_j] \tag{3.3}$$

Parallel or longshore winds should be modified by the cosine of the transport direction:

$$Q_{longshore} = \frac{1}{\rho_b} \sum_{i=1}^{n} q_i \cos[dd_j] \tag{3.4}$$

where the angle, dd_j, is the difference between the wind direction α and the coastal orientation, O (Figure 3-8); n equals the total amount of hours in the measured time series, while assuming a bulk density of sand of 1600 kg/m^3 (ρ_b) (e.g. van Rijn, 2018; Rijn & Walstra, 2003). Hence, predicted sediment transport can be compared to observed dune volume changes in consecutive periods were (oblique) onshore winds were exceeding the threshold velocity.

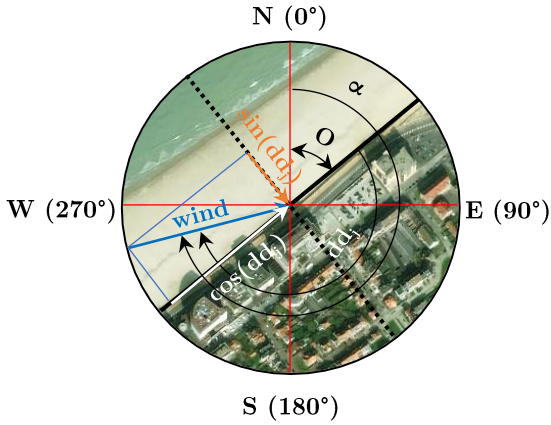

Figure 3-8. *Orientation (O) of the Belgian coastline and calculation procedure of potential transport. The orange arrow shows the onshore direction of sediment transport towards the dunes and is used to explain dune behavior. The angle α is the wind direction (with respect to the north) and the angle dd_j is the difference between the wind direction and coastal orientation O.*

3.4 Results and discussion

3.4.1 Spatial-temporal variability in dune volume changes: linear trends

As an illustrative example of an analysis at a natural dune system, Figure 3-9 shows the dune volume at section 50 of the Belgian coast. It is found that dune volume increases to a good approximation at a constant rate in time (8.14 m^3/m/year with a correlation of 0.99). To assess if this is valid for all coastal dunes, the decadal trend in the calculation of dune volume changes is based on linear analysis. Fitting linear trendlines for all the coastal sections can test to which extent this linearity in time is valid for the entire Belgian coastline. Linear trends are calculated for the entire period between 1979-2018 and/or for the most recent trend. The correlation coefficient was calculated for all dune sections experiencing dune growth or dune erosion. Figure 3-10 shows that higher correlation coefficients occur more for dune growth than for dune erosion. It is found that 80% of all coastal dunes with dune growth (total of 93%) have correlation coefficients higher than or equal to 0.9, which yields an overall average dune growth of 6.20 m^3/m/year. This percentage is decreasing for smaller correlation coefficients. Similar observations are found by de Vries et al. (2012). For the negative rates of dune volume change (7% of all coastal dunes), the occurrence of a lower correlation coefficient increases. These calculations show that a substantial part of the Belgian coastal dunes is excellently

represented using a linear dune growth model in time. Figure 3-11 indicates that the locations of the coastal dunes, with correlation coefficients larger than 0.9, are distributed over the total stretch of the Belgian coast. Figure 3-11 also shows the annual dune development per dune section for the entire Belgian coastline. It is observed that in most areas, dunes are growing. The annual dune growth ranges between 0 and 12.3 $m^3/m/year$, based on the observations between 1979-2018. Dune growth rates at the Holland coast have been calculated in the order 0-40 $m^3/m/year$, which is in the same order of magnitude (de Vries et al., 2012).

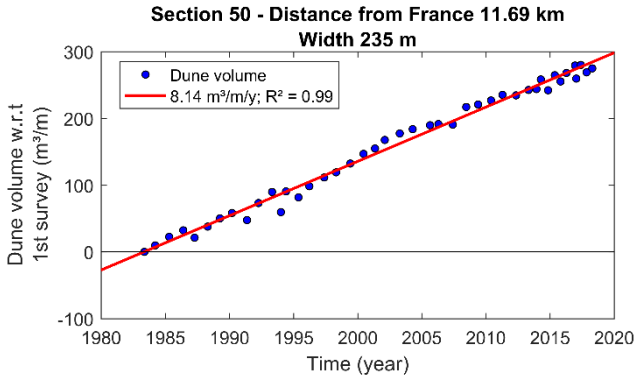

Figure 3-9. *Example of dune volume in time combined with a linear fit (correlation of determination $R^2 = 0.99$) for coastal section 50 (natural dunes).*

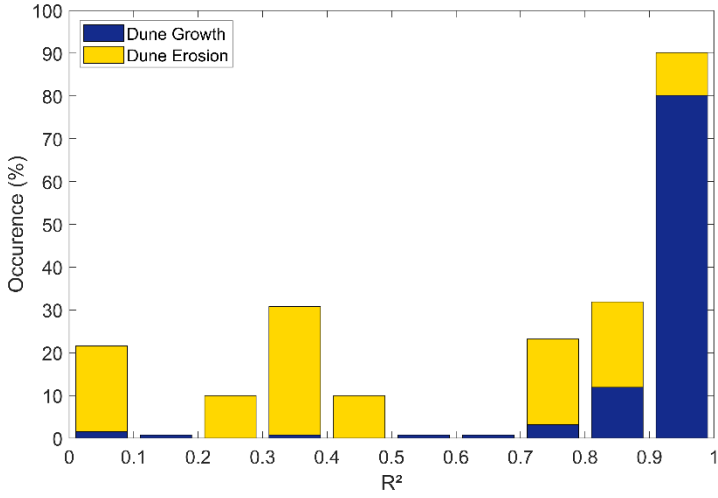

Figure 3-10. *Density of occurrence of linear dune behavior. Of the dune sections, 80% show correlation coefficients larger than or equal to 0.9.*

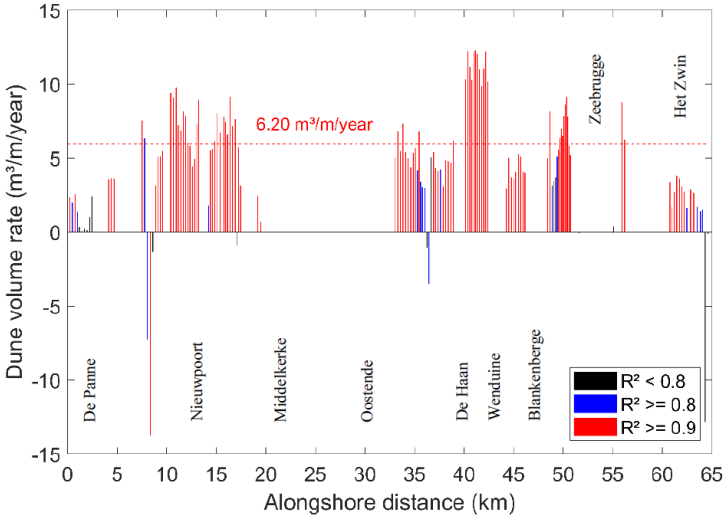

Figure 3-11. *Dune behavior along the Belgian coast. Red bars indicate the places where the correlation coefficient of the linear trend analysis is higher than or equal to 0.9. The red dashed line represents the average annual dune growth for correlations higher than or equal to 0.9.*

In some beach sections along the Belgian coast, management activities are carried out which have a direct influence on dune development. In the following paragraphs, some typical management strategies and their effect on dune behavior are described in more detail.

3.4.2 Typical management strategies and their effect on dune behavior

3.4.2.1 Influence of dune foot reinforcement

Figure 3-12 shows dune volume changes between 1983 and 2018 for section 8. In the past, section 8, close to the French border, experienced intense dune erosion during storm events. For coastal safety, a dune foot reinforcement (concrete dyke) was constructed in the period 1976–1979. In 1990, this concrete dyke was extended on the east side after a severe storm surge. Massive erosion in the coastal zone was caused by heavy storms at the beginning of 1990 and storms in the period 1993–1994. In a part of section 8, a concrete wall was erected in 1994 above the dune foot reinforcement (Figure 3-13). Sand was also applied above the dune foot from the low-water line. Sand was again supplied after the storms of 1-2 January 1995, 19 February 1996, 29 August 1996 and 29 October 1996. Due to the influence of dune foot reinforcement, the dune volume of section 8 does not experience a linear trend in time. The natural behavior of

the dune has been completely blocked. As such, dune reinforcements are not suitable for climate-resilient flood protection.

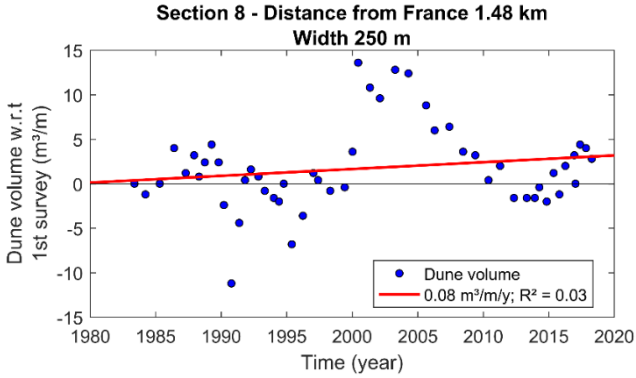

Figure 3-12. *Decadal dune evolution of the coastal dunes at section 8.*



Figure 3-13. *Concrete revetment and wall, built to reinforce the dune foot in section 8.*

3.4.2.2 Effect of dune blowouts

Since the airborne surveys started (year 1983), the dunes of section 36 experienced a gradual linear growth in time due to aeolian sand input from the beach (Figure 3-14). In the beginning of the 1990s, dune erosion started to occur due to the formation of a dune blowout (Figure 3-15). The formation of dune blowouts tends to start at patches of bare sand, where vegetation does not grow. Wind speeds above the threshold erodes into those patches, blowing the sand out of the system. Note that the sand is feeding the dunes further inland. Because they are not covered by the LiDAR measurement, this effect is not captured. These blowouts often occur on stabilized vegetated dunes. Dune

erosion was highest between 2000–2005. Since 2005, the intensity of dune erosion has decreased to 7.26 $m^3/m/year$.

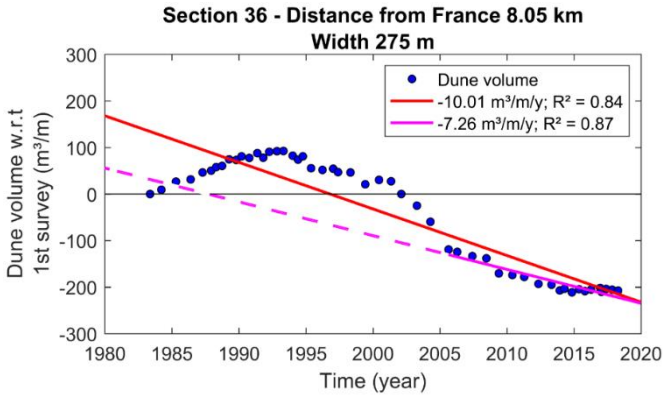

Figure 3-14. *Decadal dune evolution of the coastal dunes at section 36. The solid magenta line indicates the recent dune trend.*



Figure 3-15. *Dune blowouts at sections 36 to 38.*

3.4.2.3 Influence of dune foot protection measures

Figure 3-16 shows dune volume changes between 1983 and 2018 for section 72. In section 72 and a part of section 73, a dune foot protection measure was constructed in 1944 in the form of a concrete wall (Figure 3-17) because this area experienced severe dune erosion. As an indication, the location of the dune foot of the adjacent section (section 71) is approximately 25 m further inland of the wall. Section 72 experienced fairly linear dune growth until 1993. Major dune erosion happened due to the heavy storms in the 1990s. Afterwards, the dunes experienced slow dune erosion or were basically stable as the dune foot could not grow further seawards. Primary embryo dune growth is difficult to develop at the dune foot and most volume variations are generally found in the dune foot region.

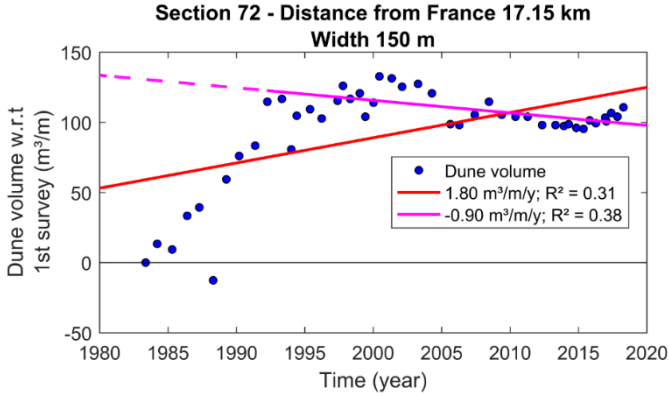

Figure 3-16. *Decadal dune evolution of the coastal dunes at section 72. The solid magenta line indicates the recent dune trend.*



Figure 3-17. *Concrete wall as a dune foot protection measure in section 72.*

3.4.2.4 Combined influence of nourishments and brushwood fences

Section 160 (Figure 3-18), located 41 km from the French border, was fairly stable since measurements started. However, the heavy spring storms of 1990 had particularly affected the coastal dunes in this part of the Belgian coast. Due to those storms, large-scale beach nourishments were needed. These works were carried out during the period of 1992–2000 and attributed to the creation of wide beaches and by the subsequent plantation of brushwood fences (Figure 3-19). The widening of the beaches enhanced aeolian sand being blown to the dunes causing a linear growth of 12.18 m^3/m/year which is well above the average dune growth rate. The sand trapping efficiency of brushwood fences varies from site to site and is particularly high if the availability of sand is large (Ruz & Anthony, 2008)

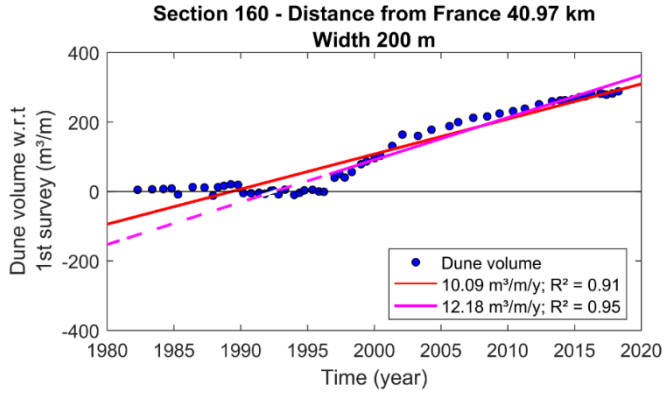

Figure 3-18. *Decadal dune evolution of the coastal dunes at section 160. The solid magenta line indicates the recent dune trend.*



Figure 3-19. *The dunes at section 160, showing the plantation of brushwood fences.*

3.4.2.5 Influence of excavation works

At the Dutch border, section 254 is the last section of the Belgian coast. In section 254, the tidal channel 'the Zwingeul' is present (Figure 3-20). Because of its free movement, this section has large annual fluctuations in sand beach volume. The dunes grow fairly linear in time till the year 2016. In the year 2016, large dune erosion occurred in this section because of large excavation works. Since then, the dunes are continuously eroding with a rate of -12.84 m^3/m/year (Figure 3-21).

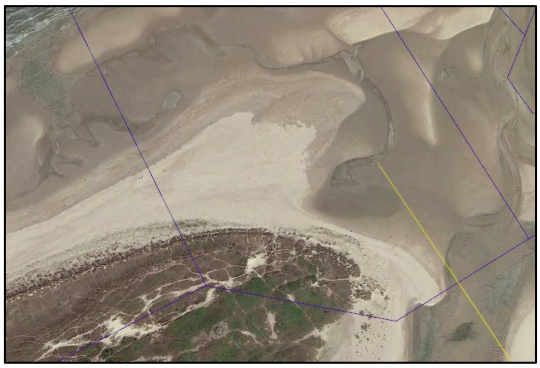

Figure 3-20. *Tidal channel 'the Zwingeul' (sections 254 and 255).*

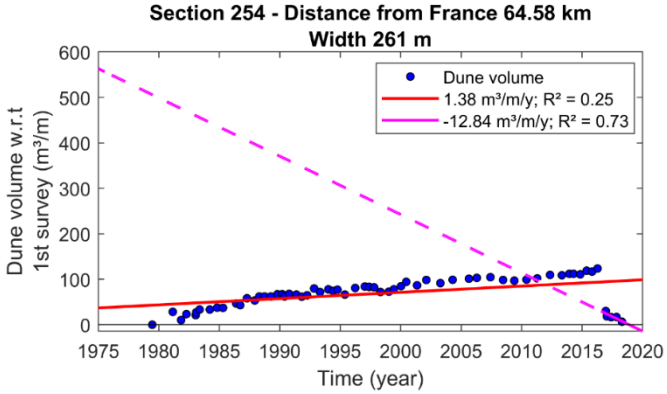

Figure 3-21. *Decadal dune evolution of the coastal dunes at section 254. The solid magenta line indicates the recent dune trend.*

3.4.3 Potential aeolian sediment transport

It is well known that dune growth is primarily governed by aeolian sediment processes. Therefore, expectations are that dune volume variability does correlate with variability in wind conditions. Potential aeolian sediment transport is calculated per coastal dune section between the dates where a LiDAR flight is conducted using the representative median grain size and coastal orientation. Hourly wind data is available since the year 2000 at Ostend Airport (middle of the coastline and approximately 1 km inland) and is used to calculate the time series of potential transport. The wind sensor is located 4 m above the surface. Figure 3-22 shows the measured wind data at the weather station of Ostend Airport for the period 2000–2017 in the form of a wind rose. The red line represents the mean direction of the Belgian coastline. Measured

over that period, a large west to southwest component of the wind is found. West to southwestern winds are oblique onshore to longshore with respect to the Belgian coastline.

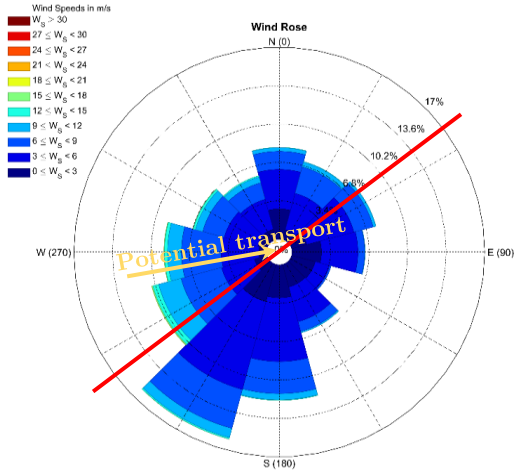

Figure 3-22. *Measured wind speed (W_s) and wind direction at Ostend Airport weather station for the period 2000–2017. The red line represents the Belgian coastline direction. The potential transport drift is also given.*

Figure 3-23 shows the annual potential transport and transport direction for the period 2000–2017 derived from measurements at Ostend Airport weather station based on a grain size of 310 µm and coastal orientation of 57° (section 103). Figure 3-23 indicates considerable temporal variability, caused by annual variations in wind climate. Annual variations are approximately between 0.5 times and 1.6 times the mean transport rate meaning that potential transport is occasionally three times larger for some years than other years. The average direction of potential transport over the period of 17 years is 260° with a standard deviation of 14° implying that the direction is constant. Potential transport has an oblique onshore character with respect to the coastline (Figure 3-22). The larger parallel component (longshore) of the potential transport drift is directed towards the northeast (the Netherlands), while the normal component (onshore) is directed towards the southeast.

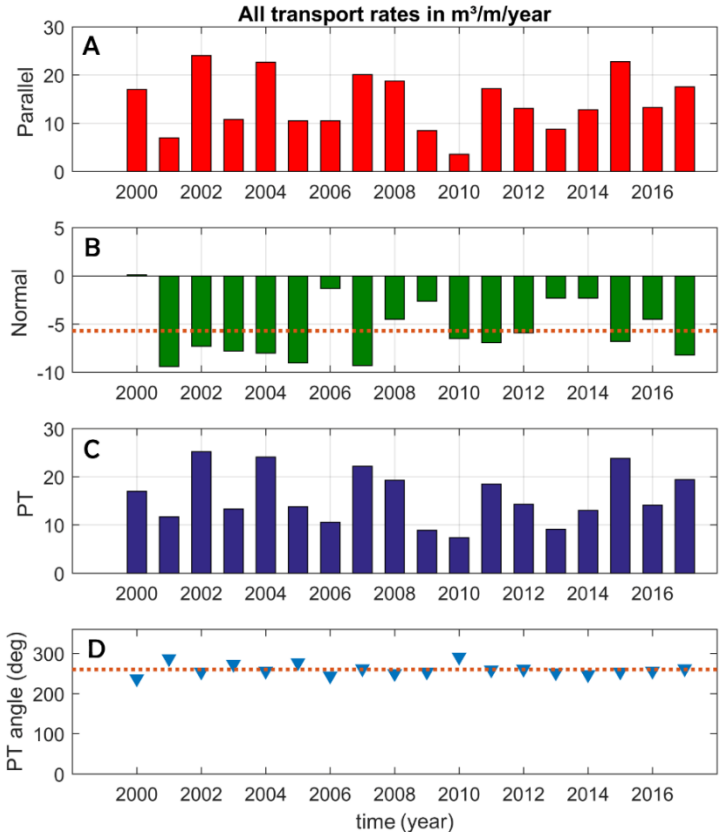

Figure 3-23. *A) Annual potential longshore transport for the period 2000-2017. B) Annual potential cross-shore (or normal) transport for the period 2000-2017. Positive is offshore transport, negative is onshore transport. C) Annual potential transport (PT) for the period 2000–2017. All transport rates are given in m³/m/year. D) The angle of potential transport is fairly constant with an average value of 260 degrees to the north.*

Interpreting the results on a decadal timescale, all potential transport rates are cumulatively summed. Potential dune volume changes because of aeolian sediment transport appears to vary linearly in time with a constant rate which in return explains the decadal linear dune growth (Figure 3-24). Considering all coastal dune sections within the period of 2000-2017, Figure 3-25 indicates that onshore potential transport maximum ranges to 9 m^3/m/year (average = 5.2 m^3/m/year), while longshore potential transport could maximum reach up to 20 m^3/m/year (average = 18.7 m^3/m/year) assuming dry beach sand. In return this gives a mean total potential transport of approximately 20 m^3/m/year. Longshore transport is relatively constant along the coastline (4.9% deviation of the mean). Onshore transport has some longshore variations due to a varying

coastline orientation, especially behind the protruding point of Wenduine (43 km) where transport is lower due to a more north–northeast coastal orientation. It also implies that longshore transport is almost three to four times higher than onshore transport. This would explain why brushwood fences are so efficient for enhancing dune growth locally.

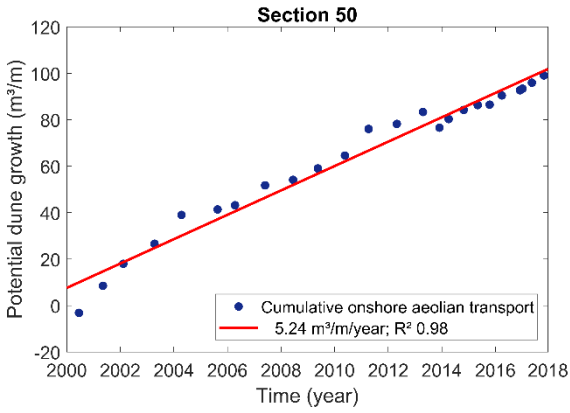

Figure 3-24. *Decadal evolution of potential dune growth at Section 50 of the Belgian coast.*

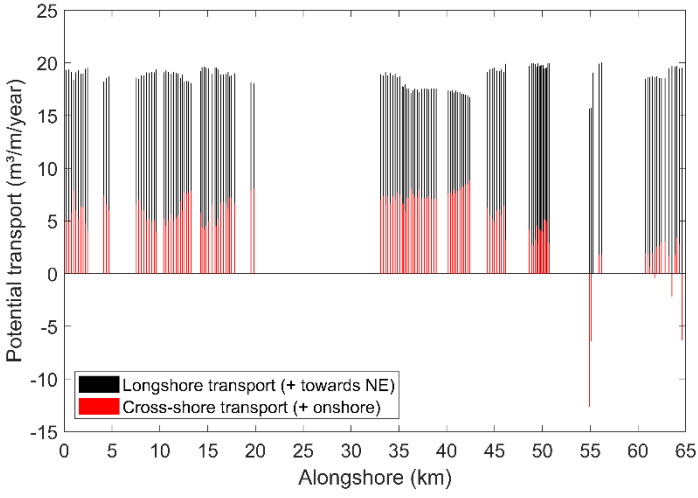

Figure 3-25. *Annual potential longshore and onshore aeolian sediment transport, based on the period between 2000-2017.*

3.4.4 Correlation between potential transport and dune volume changes

3.4.4.1 Correlation on annual timescales

More wind induces more aeolian sediment transport and intuitively, therefore more dune growth is expected (de Vries et al., 2012). To find a correlation between variation in potential transport and dune volume change on an annual timescale, the Pearson correlation coefficient is calculated. In this procedure, three methods are applied to calculate the correlation coefficient:

- Method 1: The first method compares dune erosion and dune growth with corresponding potential transport. Net potential transport is calculated based on the full wind rose (onshore and offshore winds).

- Method 2: The second method compares dune erosion and dune growth with corresponding potential transport based solely on onshore winds. It is assumed here that offshore winds do not extract sediment from the dune seawards. As mentioned before, dunes are, besides aeolian processes, also influenced by marine erosive processes.

- Method 3: The third and last method compares only the periods with dune growth with the corresponding potential transport based solely on onshore winds. Offshore winds are not used in the calculation procedure.

A positive correlation implies that an increase in potential transport causes an increase in dune volume. A negative correlation implies the opposite. However, the three methods gave similar results. No important correlation (positive or negative) is found between potential transport and dune volume change on an annual timescale, considering all sections with coastal dunes. The poor correlation could be attributed to:

- According to Equation (3.1), potential aeolian sediment transport is related to the cube of shear velocity, meaning that high winds above the threshold contribute exponentially to the annual sum of potential transport (Equation (3.4)). Although these winds are able to transport large amounts of sediment, they tend to create high water levels and long wave run-ups as well.

- Between consecutive LiDAR flights, dune erosion and dune growth can occur. Even during strong aeolian transport events, a single dune-erosion event can undo any dune growth that happened before that storm.

- The duration between two consecutive LiDAR flights is also too long, resulting in a coarse spatial-temporal data set.

- Dune volume changes can be influenced by the sediment supply and sediment availability from the marine zone (de Vries et al., 2012, Pye & Blott, 2008). Transport limiting factors, such as sediment size and distribution, beach geometry and moisture can be of more importance than the driving wind speed.

3.4.4.2 Correlation on decadal timescales

Decadal timescales are of interest because it is the most appropriate timescale for engineering purposes and coastline development. On decadal timescales, potential dune volume appears to grow linear in time with a similar magnitude like observed dune volume (see Section 3.4.3). It is of particular interest if both are correlated at this spatial-temporal scale. For all coastal dune sections, the decadal trend of potential dune volume changes is based on linear analysis. Linearity is calculated for the entire period between 2000-2017. It is found that in 93% of all coastal dune sections, the potential dune volume trend has a correlation higher than 0.90.

Figure 3-26 shows the comparison between observed and predicted dune development on decadal timescales. The yellow dots show the places were regular managing activities are carried out. About 75% of all predicted data are within a factor 2 of the measured values. Interpreting the results show that the modified Bagnold model based on Equation (3.1) (van Rijn, 2018) yields a good performance when observed values are compared to predicted dune development rates.

Figure 3-27 shows the alongshore extent of the observed and predicted dune development rates along the Belgian coastline. The variability in potential transport is well correlated to the variability in dune volume changes at the considered spatial–temporal scale. The general variability, on a decadal timescale, between observed and predicted rates could be partly attributed to the management activities at certain sections along the coast. It is uncertain how many of the dune regions are managed. An attempt has been made to know which dune regions are managed. Based on historical images from Google Earth, approximately 50% of the coastal dunes are managed. Most of these activities include regular plantation of brushwood fences, especially where observed linear dune behavior is higher than the predicted values (under the line of perfect agreement). Other discrepancies include the ones discussed in Section 3.4.4.1. The locations including dune foot protection measures, dune foot reinforcements, and dune blowouts, are mostly the locations where predicted values are higher than the observed values. When the managed zones are excluded from the data set, the best fit line slope is approximately one, and the RMSE (Root Mean Square Error) value is 2.9 m^3/m/year. Most (90%) of the

predicted data are within a factor of two of the measured values. This is a high score, given all variabilities and non-uniformities involved in aeolian processes (wind field, sand composition, bed relief, surface roughness). The finding of potentially stronger correlations compared to the literature (e.g. Keijsers et al., 2014 and de Vries et al., 2012) at the Belgian coast are most likely caused by the generally wider beach widths (between 150 and 400 m). Keijsers et al. (2014) also found stronger correlations between the time series of potential sediment transport and dune volume on wider beaches (> 200 m) at the Dutch coast. This indicates that natural dune behavior can be predicted with a reasonable accuracy on decadal timescales, and it suggests that annual differences in forcing and transport limiting conditions (wind speed and surface conditions) only have a slight effect on the overall variability of dune volume trends.

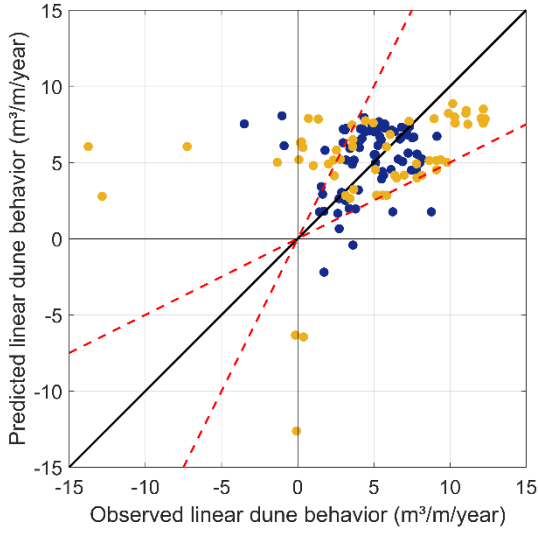

Figure 3-26. *Comparison between observed and predicted linear dune development. Diagonal lines represent the one-to-one correspondence. Red dashed lines show the factor of two variance. Yellow dots represent the locations where managing activities are carried out.*

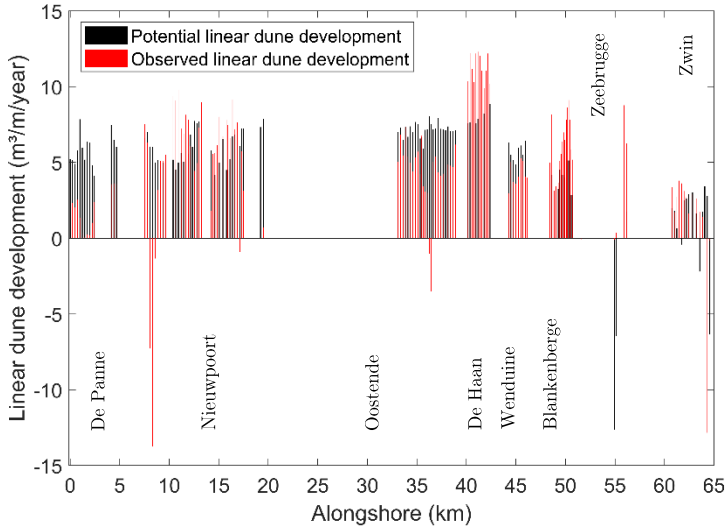

Figure 3-27. *Annual predicted and observed dune volume change along the Belgian coast on a decadal timescale. Red and black bars indicate the observed and predicted values of dune development, respectively.*

3.5 Conclusions

Long-term temporal and spatial dune trends along the Belgian coast are analyzed using a data set of annual and bi-annual beach–dune LiDAR surveys, conducted between 1979–2018. Furthermore, potential aeolian sediment transport along the Belgian coast is calculated based on a wind data set from 2000–2017. On the basis of this analysis we conclude that:

1. Along the Belgian coast, concerning the coastal sections with vegetated dunes (approximately half of the coast), it is found that the dunes grow at a constant rate. Linear regression analysis shows that 80% of the dune sections have linear correlations higher than 0.9. There is alongshore variability in linear dune growth rates at the Belgian coast and they are found to be in the order of 0–12.3 m^3/m/year. An average dune growth of 6.2 m^3/m/year has been found.

2. Considering all coastal dune sections within the period of 2000–2017, onshore potential aeolian sediment transport ranges up to 9 m^3/m/year (average = 5.2 m^3/m/year), while longshore potential aeolian sediment transport could reach up to 20 m^3/m/year (average = 18.7 m^3/m/year). This means that total potential transport along the Belgian coastline is, on average, 20 m^3/m/year.

The main direction of aeolian sediment transport on the Belgian coast is from west to southwest. West to southwestern winds are oblique onshore to longshore with respect to the Belgian coastline. The larger parallel component (longshore) of the potential transport drift is directed towards the northeast (the Netherlands), while the normal component (onshore) is directed towards the southeast (hinterland).

3. There was no significant relationship between annual wind and dune volume change in the alongshore direction. However, a significant correlation is found between potential and observed dune volume development on a decadal timescale, indicating that dune growth is primarily caused by aeolian sediment transport from the beach. Most of the predicted data are within a factor of two of the measured values. The finding of potentially stronger correlations at the Belgian coast are most likely caused by the wider beaches (between 150 m and 400 m) due to the massive sand nourishments to keep the sediment budgets along the Belgian coast positive. It also suggests that annual differences in forcing and transport limiting conditions (wind speed and surface conditions) only have a slight effect on the overall variability of dune volume trends.

3.6 Acknowledgments

This publication is the result of research part of the project CREST (Climate REsilient coaST), funded by the Strategic Basic Research (SBO) program of the Flanders Innovation and Entrepreneurship. We thank the support of Coastal Division of the Flemish Government, Department of Mobility and Public Works, to make it possible to use the data of dune volume and wind.

Chapter IV

Downwind evolution of aeolian saltation across an artificially constructed coastal berm

Abstract

This study reports on a field experiment designed to carry out simultaneous measurements of wind and sediment transport across a human-constructed high berm with a steep seaward cliff that is backed by a dyke. In front of the dyke, a trench is excavated to prevent aeolian sand being blown to the hinterland. Two sets of measurements were carried out, one with oblique onshore and one with winds directly onshore. Over-steepened velocity profiles and thus large shear velocities were measured at the steep cliff during the onshore wind event compared to the back beach due to flow compression and acceleration. The fetch effect has been measured across the flat berm where maximum transport was achieved at a distance of 20 to 35 m of the berm lip. The fetch effect is characterized with an overshoot during the oblique onshore wind event. Sand flux rapidly increases towards a maximum value followed by a decrease to a lower equilibrium value which was approximately half of the maximum mass flux obtained at the critical fetch distance. The evolution of the vertical mass flux profiles downwind causes the exponential decay rate β to increase almost linear with increasing fetch length further away from the berm lip, until an equilibrium decay rate is achieved. This means that the distribution of particle trajectories changes similarly until it is stable for different transport events on a flat dry beach surface. Based on this study, the steep cliff in front of the human-constructed coastal berm is very sensitive to erosion due to aeolian sand transport. Sand being eroded from the berm lip is deposited in front of the dyke and in the trench.

Keywords: Aeolian flux profiles, Wind flow, Field measurements, Human-constructed beach, Fetch effect

---

Chapter submitted as: Strypsteen, G., De Sloover, L., De Wulf, A., and Rauwoens, P. (2019). Downwind evolution of aeolian saltation across an artificially constructed coastal berm. *Aeolian Research*.

4.1 Introduction

Although we have good qualitative understandings of the mechanics of aeolian sediment transport, prediction models for aeolian sediment transport in coastal environments remains a challenge (Davidson-Arnott et al., 2005; Bauer et al., 2012; Lynch et al., 2016). The combined physical interaction between variable wind flow, changing topography and supply-limiting factors such as beach characteristics, surface moisture and armoring effects makes it hard to predict sediment transport (Delgado-Fernandez, 2011). Field measurements often do not agree with predicted rates of sand flux (Sherman et al., 1998; Sherman et al., 2013). In the last decades, a substantial amount of research has focused on these supply limiting factors and tend to decrease the amount of sand flux at a variety of temporal and spatial scales.

The fetch effect and evolution of aeolian saltation across a beach surface is equally important in modelling sand transport processes. It is a typical example of a disequilibrium situation of aeolian transport on a spatial scale. Delgado-Fernandez (2010) has made an extensive review of the fetch effect observed in coastal and agricultural environments in the past decades. Fetch length is defined as the length where wind can blow over a surface without any obstructions (Gillette et al., 2006). However, the fetch effect is the increase of sand flux in the downwind wind direction across a beach surface until a maximum is achieved (Davidson-Arnott et al., 2005; Delgado-Fernandez, 2010). Literature suggests that this maximum is achieved exponentially after a certain critical fetch distance (Bauer & Davidson-Arnott, 2003; Stout, 1990; Davidson-Arnott et al., 2008). The critical fetch distance varies for different wind speeds and moisture contents, where distances of 10 m to more than 300 m are reported (Lynch et al., 2007; Davidson-Arnott et al., 2008; Lynch et al., 2016; Gillette et al., 1996). Shao & Raupach (1992) report that the fetch effect is characterized with an overshoot. Sand flux rapidly increases towards a maximum value followed by a decrease to a lower equilibrium value. This maximum increases for increasing wind speeds, but the critical fetch distance remains constant. Spies & McEwan (2000) found the same effect in their numerical simulations, but increasing wind speeds produced longer critical fetch distances. Delgado-Fernandez (2010) reports that the overshoot effect has not yet been observed in field experiments on beaches.

Regarding the evolution of vertical flux profiles downwind, relationships between the coefficients of aeolian flux (decay rate β) and fetch distance is not well established in literature (Dong et al., 2004). Furthermore, literature is typically scarce about this topic and is mostly based on wind tunnel experiments. Field assessments are necessary to find relationships between the coefficients of aeolian flux profiles and fetch distance in coastal environments. Frequently, the fetch effect is assessed with mass fluxes rather than the coefficients of the vertical flux profile.

Short-term field experiments on the fetch effect and evolution of saltation across a flat beach surface along the wind direction is studied on a managed beach-dyke environment in Belgium. The beach has an extensive, flat berm that is uniform due to bull-dozing activities with a steep cliff in front of it, which provides a nice experimental situation. The paper reports on the effects of beach form (cliff in front of a wide, flat berm) and fetch on the subsequent aeolian sediment transport during two wind events without rainfall.

The general objective of this paper is to examine the fetch effect and saltation evolution across a flat uniform beach surface. Three research goals are set:

1. To quantitatively study the vertical flux profile of aeolian sand transport blowing over a flat beach with increasing fetch length;

2. To define a relationship between the vertical decay coefficient β of the flux profile and the fetch length;

3. To relate aeolian sediment flux to topographical volume changes.

4.2 Methods

4.2.1 Study site

A two-week monitoring campaign was carried out on the human-constructed high flat berm of a beach at Mariakerke, Ostend, Belgium, in November 2017. This coastal section (section 103) is Southwest-Northeast oriented and uniform in the longshore direction (Figure 4-1). Locally, variations in topography, surface roughness and sediment characteristics occur which influence aeolian sand transport fluxes (Nordstrom et al., 2011). The study area is in the macro-tidal regime ranging between 3.5 m at neap and 5 m at spring tide (Haerens et al., 2012). The beach is relatively wide up to 250 m to 300 m. It consists mainly of quartz sand with a mean diameter of 310 µm. The sand does not contain very fine material (fraction < 63 µm). The study area is an artificial beach which has been nourished on both dry beach and shoreface in the year 2014. It is also backed by a hard dyke structure and promenade. On top of the dyke, a temporarily shore-parallel wall, consisting of Jersey Blocks, was erected to prevent sand blowing inland. In the backshore, the beach is characterized by a relatively low slope (1:50) (Strypsteen et al., 2017).

Preparing this beach against winter storms, the coastal town involves excavators and bulldozers to create an artificial plateau (high flat berm) at 7.5 m TAW (Belgium Ordnance Datum) thereby removing an excess of sand from the higher beach seawards and resulting in a steep cliff at a distance 50 m to 60 m from the dyke (Figure 4-2). At the toe of the dyke a trench has been dug as an extra

measure to limit wind-driven sand transport towards the hinterland (Figure 4-3). At the beginning of the measurement campaign the upper beach was relatively flat and horizontal, yielding a nice experimental situation without topographic irregularities and other surface complexities of natural beaches.

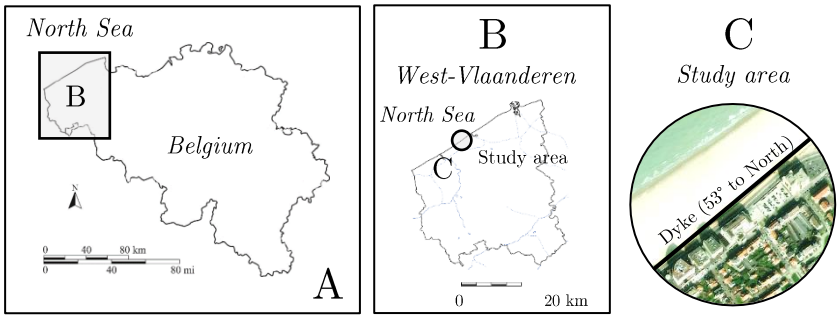

Figure 4-1. *Location of the study area.*

In the study area, prevailing winds blow from SW direction and are characterized by light and moderate breezes with speeds ranging from 3-8 m/s. However, in terms of aeolian sand transport, the dominant strong to very strong breezes (> 10 m/s) occur mostly between November and February and are from WSW to NW directions. These dominant winds could also have severe threatening conditions for the occurrence of storm surge (Montreuil et al., 2016). According to Haerens et al. (2012), storm surges are recorded at least once a year when water levels and onshore wave heights could reach 5 m TAW and 3 m respectively.

All sand transport event experiments described in this paper were conducted under northwesterly winds (onshore and oblique onshore winds). As the measurement of aeolian transport requires strong winds above the threshold of 6 m/s (Strypsteen et al. 2017; Snacken, 1956) and a dry beach surface, suitable conditions were very limited during the two-week field campaign. Two separate data sets were collected featuring beneficial circumstances.

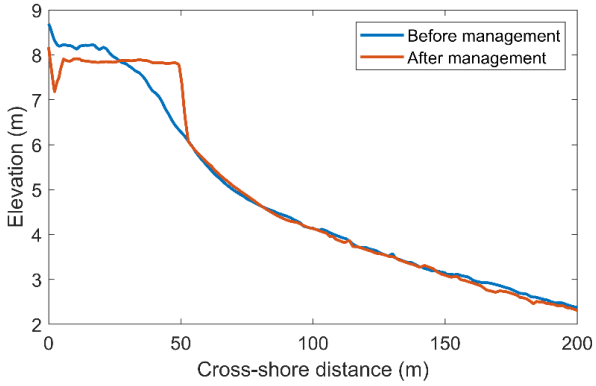

Figure 4-2. *Topography before and after preparation of the study area against winter storms. Excavators and bulldozers manipulate the upper beach by removing an excess of sand from the upper beach seawards and digging a trench at the dyke toe.*



Figure 4-3. *Left panel shows the trench at the dyke toe. Right panel shows the study site at Mariakerke with aeolian sand transport during strong onshore winds. (Photograph taken on 12 November 2017)*

4.2.2 Experimental design

The data used in this paper were collected in the winter period of 2017. On November 12 and November 18, 2017 detailed data on aeolian sand transport were obtained. Figure 4-4 gives an overview of the locations where the equipment was installed. On the upper beach (high flat berm), two 3-m high meteorological stations were positioned at distances of 10 m (M_{dyke}) and 45 m (M_{cliff}) from the dyke crest (Figure 4-5a). Four rotating cup anemometers (Vector Instruments A100R) were mounted at 0.15, 0.30, 0.51 and 1.94 m elevation, respectively. The station was also equipped with a wind vane 1.94 m above the surface (Vector Instruments W200P) and a temperature sensor. The data were automatically recorded and stored on a CR800 Campbell Scientific datalogger. The wind speeds were recorded once every 20 seconds. The temperature sensor recorded once every 10 minutes. The temporal variability in transport intensity was recorded with two saltiphone sensors (Eijkelkamp) placed at 10 m (S_{dyke}) and 45 m (S_{cliff}) from the dyke crest, approximately 10 cm above the surface (Figure 4-5b). The saltiphone sensors were also connected to the CR800 Campbell datalogger and registered the amount of hits per second (#counts/sec). Every 20 seconds, the cumulative value was recorded and stored on the datalogger. These sensors consist of a 0.3 m long, 0.02 m wide tube and can freely move along their vertical axes, according to wind direction. Detailed descriptions about its design, testing and deployment are given by Spaan & Van Den Abeele (1991). Additional to the measured field data, quantitative data on precipitation was collected from a nearby measuring station at Klemskerke (station number: P02_008), 9.36 km inland from the study site.

Deviations on the wind speed measurements, due to any form of turbulence, was eliminated by averaging the measurements over 10-minute periods. Based on the wind speeds recorded at the four cup anemometers, shear velocities were derived by calculating the slope of the regression line of the log-linear wind profile. The following equation was used:

$$u_z = \frac{u_*}{\varkappa} \ln\left(\frac{z}{z_0}\right) \tag{4.1}$$

Where u_z is the wind speed (m/s) at height z (m), u_* is the shear velocity (m/s), $\varkappa$ is the Von Karman constant (taken as 0.40) and z_0 is the aerodynamic roughness length (m).

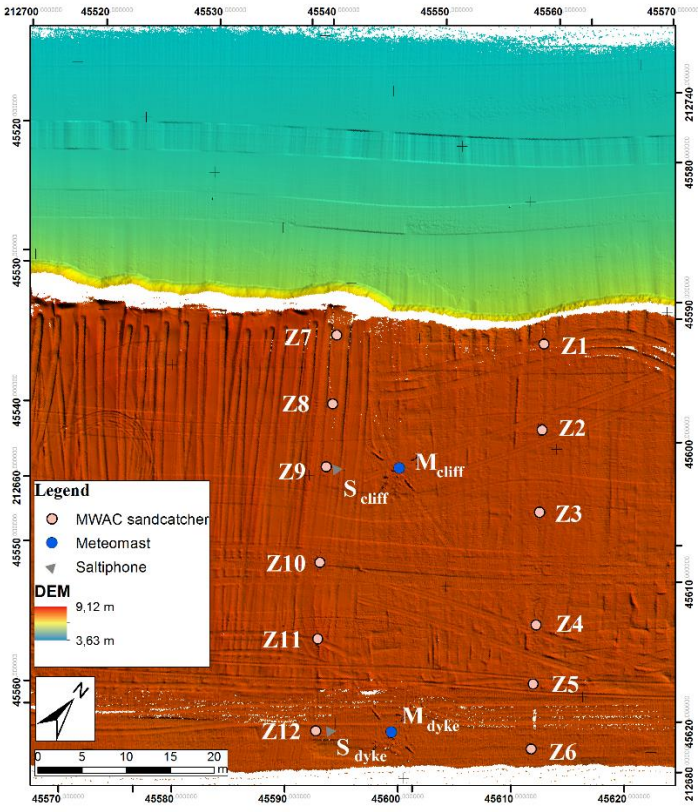

Figure 4-4. *Plan view of the study site with the location of the equipment. 12 Modified Wilson And Cook (MWAC) sand traps were placed at the upper beach together with two meteorological stations and two saltiphones. Coordinates refer to the Lambert 72 coordinate system. The topography is from field surveys conducted on November 7, 2017.*

During sand-blowing events, 12 Modified Wilson And Cook (MWAC) sand traps were exposed to the wind to determine the rate of aeolian sand transport (Z_1-Z_6 and Z_7-Z_{12}). These sand traps (Figure 4-5c) have been extensively used in numerous studies where, in which efficiencies of between 42% and 120% were reported (e.g. Van Pelt et al., 2009; Sterk & Raats, 1996; Goossens & Offer, 2000; Poortinga et al., 2013; Youssef et al., 2008). The sand trap is equipped with a vane to ensure that the bottle inlet was always orientated towards the wind. The traps collected sediment in seven plastic bottles from 0.065 to 1.00 m above the surface. Saltation, defined by wind speed and grain size, is the dominating transport mode during aeolian sand transport (Pye & Tsoar, 2013). Saltation involves sand grains following ballistic trajectories as they hop from one place to another across the beach surface. However, when aeolian sand transport occurs, the saltating layer seldom reaches heights above 25 cm (Van

Dijk et al., 1996; Poortinga et al., 2014). Therefore, only the four lowermost bottles were used in the MWAC sand traps at a of height 6.5, 13.5, 21.0 and 28.5 cm above the surface. Each bottle has a glass inlet and outlet tube with a diameter of 8 mm (≈ 50 mm^2 or 5.10^{-5} m^2). The mass of sand collected in the bottle is divided by the inlet tube area and exposed time (in minutes) to provide transport rates in $kg/m^2/min$. The MWAC sand traps were placed on two cross-shore lines on the flat berm, between the steep cliff and the dyke (Figure 4-4). They were placed 7 m to 12 m from each other to ensure they had no influence on each other.

Topography was surveyed with a mobile laser scanner equipped SPV (Special Purpose Vehicle), in combination with a high-grade INS (Inertial Navigation System) and an RTK-GNSS, on November 7, November 13 and November 20, covering the upper beach and intertidal zone. Also changes in beach surface elevations at the meteorological stations were recorded daily.

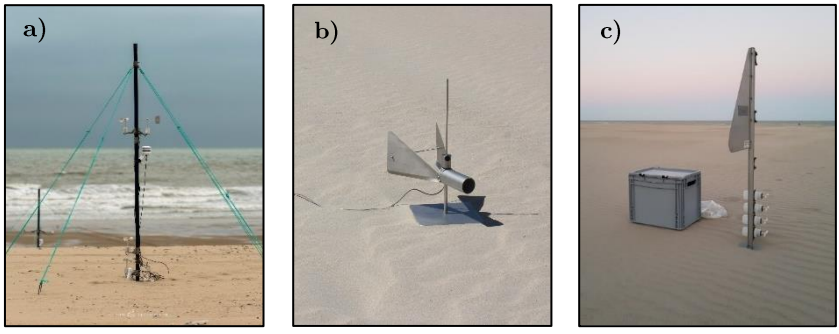

Figure 4-5. *a) Meteorological station with four anemometers, a wind vane and a temperature sensor. b) Saltiphone sensor. c) MWAC sand trap deployed at the beach surface.*

4.2.3 Vertical distribution of aeolian mass flux

The vertical distribution of sediment saltation transport can be best described by an empirical exponential decay function (Ellis et al., 2009; Horikawa & Shen, 1960; Williams, 1964; Bauer & Davidson-Arnott, 2014; Poortinga et al., 2014):

$$q_z = q_0 \cdot e^{-\beta . z} \tag{4.2}$$

Where q_z is the sediment mass transported at height z above the surface ($kg/m^2/min$), q_o is the extrapolated saltating sediment mass transported at the surface ($kg/m^2/min$) and β is the decay rate (m^{-1}), a measure of the vertical concentration gradient (Van Dijk et al., 1996). Generally, this non-linear multiparameter decay model yield high correlation coefficients ($R^2 > 0.9$), because the fitted coefficients (q_o and β) are not directly related to physical

aeolian parameters such as grain size, roughness, and shear velocity (Bauer & Davidson-Arnott, 2014). Therefore, it is not surprising that a large range in the values of the fitted coefficients are found in literature (Li et al., 2008; Ellis et al., 2009; Dong et al., 2011). Bauer & Davidson-Arnott (2014) noted that there are all manner of uncertainties associated with properly analyzing mass flux profiles. Yet, there are no clear answers on how to do it correctly. A point of discussion is if adopting the best fit (such as largest R^2) for different regression models adequately represents the underlying physics of saltation. One major issue is also deciding which is the dependent and independent variable. When analyzing trap data with elevation, Ellis et al. (2009), Namikas (2003) and Rasmussen & Mikkelsen (1991) stated that elevation should be the independent variable (x abscissa) and mass flux the dependent variable (y ordinate). Other authors also used this principle when analyzing trap data (Strypsteen et al., 2017; Campos, 2018; Poortinga et al., 2014). However, as is often the case in Earth surface studies, the dependent and independent variables are often reversed, giving different regression results (Greeley et al., 1996; Gerety & Slingerland, 1983; Liu et al., 2006; Dong & Qian, 2007; Liu & Dong, 2004; Bauer & Davidson-Arnott, 2014). Sometimes, this latter employed method to derive flux profiles is ambiguously described in the author's texts and brings up a lot of uncertainties.

Bauer & Davidson-Arnott (2014) state that there are two ways of analyzing flux profiles. If the purpose is to predict the magnitude of sediment flux in a given time interval and if the lowermost trap data is accurate, then the protocol of Ellis et al. (2009) could be used. Ellis et al. (2009) suggests to apply the non-linear exponential fitting procedure. The challenge with the method of Bauer & Davidson-Arnott (2014) is that non-linear regression using the transport rate data in that way optimizes the fit to the two lowermost transport rates because they are by far the largest values. Thus, the regression fit always prioritizes those two lower data points because it minimizes the squared errors. When the mechanics of saltation processes and the vertical flux profiles are studied, performing the second way of analyzing vertical flux profiles is more relevant. Bauer & Davidson-Arnott (2014) suggest performing a linear regression analysis on log-transformed data. Performing this method would give very different regression coefficients because this approach would better accommodate the points higher in the flux profile. The higher points may hold information that could be important in understanding the mechanics of saltation. Furthermore, this method is also used when the lowermost trap values are in question.

The use of MWAC sand traps, of course, have limitations, especially with regards to their size. Most sand transport occurs close to the bed surface (take below 5 cm). The lowest bottle of the sand traps captures sand just above this bed load transport. This means that there is very little data available about what happens close to the bed. Ellis et al. (2009) performed non-linear regression analysis on the trap data of Dong & Qian (2007) and found that when trap compartments are placed higher above the surface (bed reference level higher),

the relationship between the regression coefficients becomes log-linear. When aeolian sand transport is measured across the entire saltation layer (starting at the surface), the relationship is almost linear. When measurements are taken higher above the surface, a small error in determining β would have greater impacts in estimating q_0. Thus, this has major implications for determining the total mass flux, which could be under- or overpredicted.

In this study, the total saltating mass is obtained from the data-fitted parameters q_0 and β by the integration of Equation (4.2):

$$Q_s = \int_0^\infty q_z \cdot dz = \frac{q_0}{\beta} \tag{4.3}$$

where Q_s is the total mass transported by saltation (kg/m/min), assuming that saltating particles start moving immediately above the surface, z = 0 m (Horikawa & Shen, 1960). Creep transport was not included in the analysis.

4.3 Results and discussion

4.3.1 Grain sizes

During the measurement campaign, samples were taken from the trapped sand and sand surface beneath the traps in order to determine particle size distribution. Figure 4-6 shows the grain size distribution of samples taken at the surface at sand trap Z_6 (near the dyke) and Z_7 (near the cliff). The grain size distributions match closely together indicating that the upper high berm is fairly uniform in grain size. The mean surface grain size for the study site is found to be 310 $\pm$ 16 µm. The grain size of the trapped sand varies with elevation above the surface and is not equal to the surface grain size. The grain size seems to decrease just above the surface. Higher above the surface, grain size tends to increase again. Similar conclusions are found by Farrell et al. (2012) and Yang et al. (2019). They found that an inflection occurs between 4 to 40 cm above the surface. Below this inflection, median grain size decreases with elevation in the near bed region which is dominated by reptation and saltation. Above the inflection, a coarsening of median grain size with elevation occurs. The height of the inflection point above the surface tends to increase with wind velocity by a power function (Yang et al., 2019).

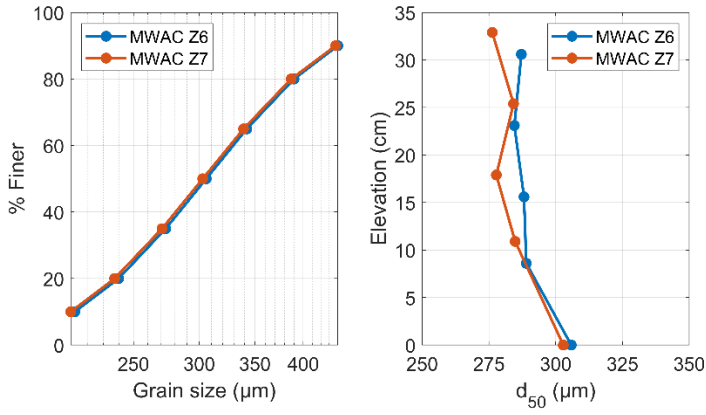

Figure 4-6. *Grain size distribution of surface samples, and median grain size of trapped sand with height above the surface at the study site for sand traps Z_6 and Z_7.*

4.3.2 Aeolian sand transport events

Figure 4-7 displays the time series of wind speed and wind direction (A and B), rainfall and cumulative rainfall (C), and saltation intensity recorded by the saltiphones S_{cliff} and S_{dyke} (D). During the measuring period (8/11 – 21/11), wind speed varied between 0 and 15 m/s. Temperature fluctuated between 7 and 12 °C. The greatest wind velocities occurred on between 12/11 and 14/11. Aeolian sand transport occurred in four periods when the wind started blowing over the threshold for dry sand movement of 6 m/s on November 10/11, November 12/13, November 18/19 and November 21. Despite a lot of rainfall during the experiment (cumulative precipitation of 25.9 mm) especially in the first week of the campaign, aeolian sand transport was observed and measured during two transport events with the MWAC sand traps on two days: November 12 and November 18. The transport events occurred between consecutive rain showers when the beach sand was sufficiently dry to be transported by wind.

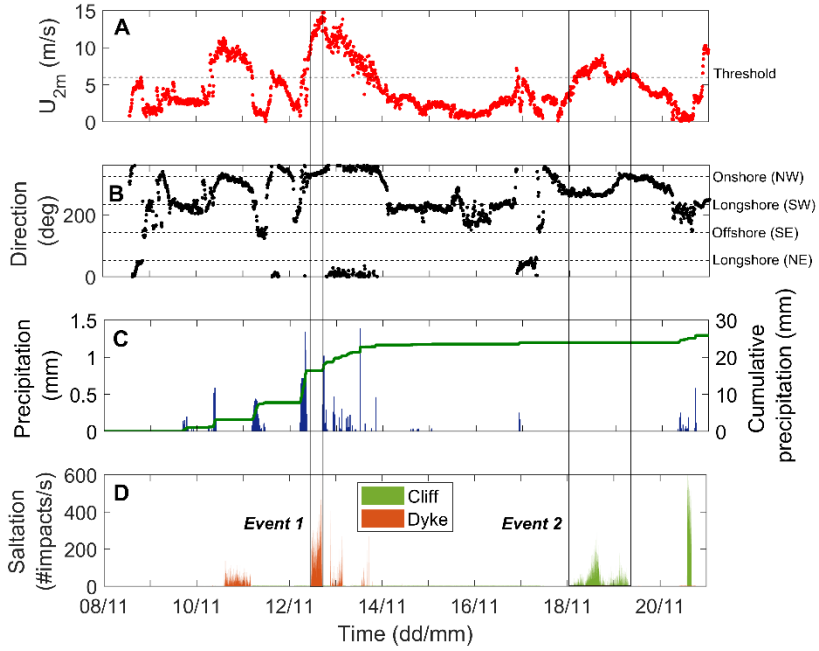

Figure 4-7. *A) 10-min average records of wind speed at 2 m. The dashed line represents the threshold of movement (6 m/s). B) 10-min average records of wind direction. Offshore winds occur when wind direction is between 53 and 233 degrees. Wind speed and direction refers to the data obtained from* M_{cliff}. *C) Precipitation and cumulative precipitation. D) Saltation intensity at* M_{dyke} *and* M_{cliff}, *10 cm above the surface, recorded once every 20 seconds. Two aeolian transport events were measured with the MWAC sand traps (Event 1 and Event 2).*

On November 12, during *Event 1*, aeolian transport was measured from 13:20 until 15:41 (≈ 2 hours sample duration) with an average wind direction of 11° from dyke normal and an average wind speed of 12.75 m/s (measured at M_{cliff}). The onshore wind direction remained relatively steady during *Event 1*. On November 18, during *Event 2*, aeolian transport was measured from 07:00 until 07:48 of the next day (≈ 24 hours sample duration) with an average wind direction of 60° from dyke normal and an average wind speed of 6.64 m/s (measured at M_{cliff}). The wind direction during *Event 2* was obliquely onshore to alongshore with moderate breezes. The wind data refers to the meteorological station positioned at the cliff (M_{cliff} in Figure 4-4).

In the following sections, firstly, information about the wind flow across the berm and characterization of vertical mass flux profiles are given, followed by the downwind trends in saltation evolution and mass flux across the flat berm. This forms a basis for the interpretation of the evolution of vertical flux profiles.

4.3.3 Wind flow across an artificially constructed coastal flat berm

Figure 4-8 shows the vertical wind speed distribution above the surface at 15h00 for *Event 1* and *Event 2* in a semi-logarithmic graph. The regression procedure of the logarithmic law of Equation (4.1) is also shown. Onshore wind with an average wind speed of 12.75 m/s occurred during *Event 1*, moving across the flat berm towards the dyke. There is strong modification of the onshore wind across the berm surface due to the steep cliff in front of the berm lip (from the foreshore), such that the near-surface boundary layer experiences flow compression and acceleration up the cliff leading to the lip. This creates a speed-up bulge in the near surface region immediately downwind of the berm lip, and therefore modification of the vertical wind speed profile at M_{cliff}. As a consequence, the shear velocities are very large at the cliff, possibly more than expected based on the log-linear relationship. Strypsteen et al. (2017) found a relationship between shear velocity and U_{2m} (wind speed at 2 m above the surface) on the same study site. The ratio u_*/U_{2m} is about 0.025 for wind conditions below the threshold value increasing to 0.06 at a wind velocity of about 15 m/s. This suggests that shear velocity should averagely be equal to 0.70 m/s during *Event 1* (at M_{cliff}). The wind speed profiles downwind (i.e. closer to the dyke) have equilibrated more to normal. In short, the slowing down of the near-surface wind field at the back of the beach is caused by the steep slope in front of the berm lip that causes an unusual boundary layer response at the leading edge of the berm. Bauer et al. (1990) showed precisely the same trend during field measurements on a steep, natural beach with a high berm above a steeply sloping foreshore. Their seaward tower (at the berm lip) had an over-steepened vertical wind speed profile due to flow compression and near surface flow acceleration, which led to abnormally large shear velocities. In the downwind direction, the boundary layer adjustments led to more equilibrated wind speed profile that yielded normal shear velocities. Smyth & Hesp (2015) did numerical simulations (CFD) of shear velocity distribution across beach scraped ridges and sand dyke structures with different onshore wind directions. They found that shear velocity from the beach during onshore winds for all these structures experienced a reduction at the foot of the structure. This reduction seems to be related to the stoss slope. Steeper stoss slopes (similar to the cliff in this study) had the greatest reduction in shear velocity. The wind flow then experienced acceleration across the slope until a maximum is reached at the crest of the structure. Perfect onshore winds experienced the highest wind speed acceleration in the study of Smyth & Hesp (2015). In the lee of the structures, the shear velocity showed different patterns but generally they decreased again to a normal state.

Opposed to *Event 1*, the wind speed profiles measured during *Event 2* at the cliff and the dyke meteorological station on the back beach were in the same order of magnitude. Oblique onshore wind (60 degrees of dyke normal) with an

average wind speed of 6.64 m/s occurred during *Event 2*. The according available fetch distance is double in length compared to that of *Event 1* (100 m compared to 50 m). There is almost no modification of the oblique onshore wind and boundary layer across the steep cliff in front of the berm lip. The flow compression and acceleration effects are negligible compared to *Event 1*, because the wind speed and stoss slope of the cliff is much lower. Smyth & Hesp (2015) showed that oblique onshore winds experience less flow acceleration than onshore winds.

It should be noted that the deceleration and acceleration effects at the toe and near the crest of the structures computed by Smyth & Hesp (2015) are much stronger than the effects measured for example on natural dunes by Arens et al. (1995) and Wiggs et al. (1996), which is most likely caused by the sharp transitions in the profile of the artificial structure. In natural field conditions these transitions will be smoother resulting in less strong deceleration and acceleration effects.

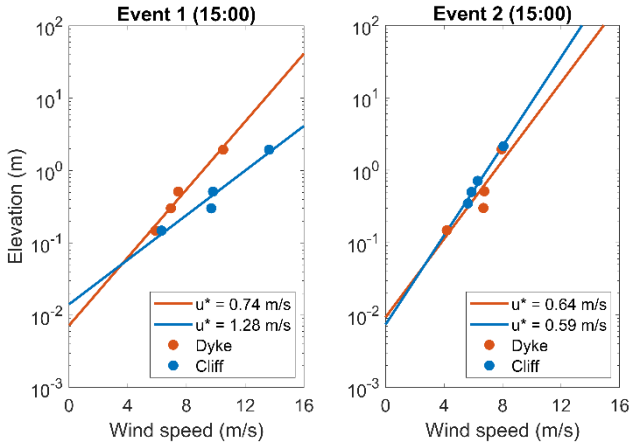

Figure 4-8. *Selected vertical wind profiles for Event 1 and 2 at 15:00 on 12/11/2017.*

Temporal fluctuations in wind speed at the two locations were similar as shown in Figure 4-9. However, as mentioned above, the flow velocity varies spatially across the berm. Shear velocities were consistently greater at the berm lip than at the back of the berm during strong onshore winds (*Event 1*). During weaker oblique onshore winds (*Event 2*), shear velocities were in the same order of magnitude at the back of the berm and at the berm lip. The wind vane measurements show no difference between the two locations, indicating that the flow field was fairly constant in its approach.

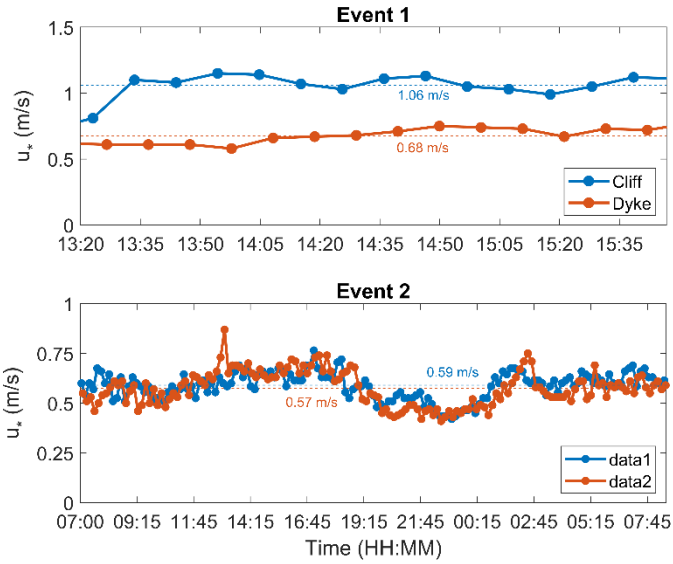

Figure 4-9. *Shear velocities during Event 1 and 2 using the regression procedure of the logarithmic law of Equation (4.1).*

4.3.4 Vertical flux profile characterization

Figure 4-10 shows the results from regression analysis carried out on trap data of MWAC Z_6 during *Event 1* (location in Figure 4-4). Mass flux and trap elevations were used as the dependent and independent variables and vice versa to determine the regression coefficients (q_0 and β). The exponential decay relationship, described in Equation (4.2) is used. The recommended non-linear method is to use elevation as the independent variable (cf. Ellis et al., 2009, Namikas, 2003 and Rasmussen & Mikkelsen, 1991). The log-linear method described by Bauer & Davidson-Arnott (2014), where elevation is chosen as the dependent variable is also used. Figure 4-10 indicates that the exponential decay function based on four points produces excellent statistical results for both methods ($R^2 = 0.97$). The magnitude of error when mass flux rather than elevation is used as the independent variable is negligible, even when a log-linear regression is used. As Bauer & Davidson-Arnott (2014) suggest to perform a linear regression analysis on log-transformed data to accommodate for the points higher in the flux profile, the method of Ellis et al. (2009) can also be used here to study vertical flux profiles. The negligible error between both methods can be attributed to the lack of transport data near the bed, as the lowermost trap data typically dominate the flux profile when the exponential decay model is fitted. Consequently, the non-linear exponential decay regression procedure is used to analyze the flux profiles from the trap data collected in this study. Furthermore, an integration of the vertical flux profile based on the four-point

regression approach lies close to the predicted transport values. Strypsteen et al. (2019) used their MWAC trap data to compare with predicted values based on a modified Bagnold model. They concluded that there is a one-to-one ratio between observed and computed values. They strengthened their study with trap data from Campos (2018) and Sherman et al. (1998). The latter authors used passive mechanical traps that spanned the entire saltation layer from surface to heights of 30 cm and 45 cm above the surface. Therefore, it is concluded that the MWAC sand traps, used here in this study, are a robust measure of the total flux and flux profile.

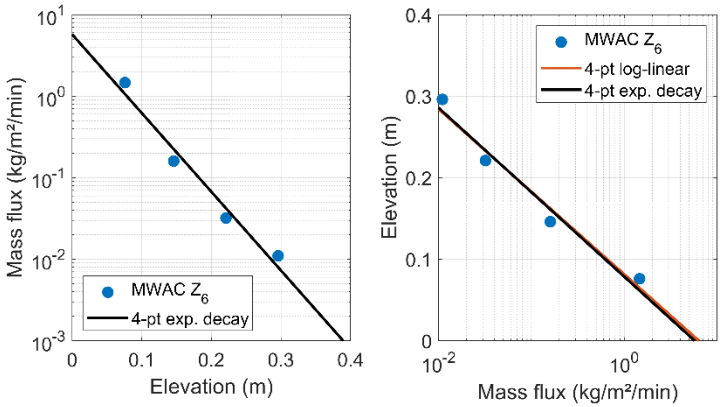

Figure 4-10. *Vertical flux profiles for MWAC Z_1 during Event 1. The left figure shows the regression line from the four-point exponential decay model (Equation (4.2)), where elevation is the independent variable. The right figure shows the regression based on the exponential decay model and log-linear model. Herein is elevation the dependent variable.*

4.3.5 Fetch effect across a human-constructed coastal flat berm

Measured mass fluxes are presented in Table 4-1 and normalized in Figure 4-11. Normalized flux is calculated based on the deviation of the mass flux at each MWAC trap in the transect Z_1 to Z_6 and Z_7 to Z_{12} and maximum mass flux in the transect Z_1 to Z_6 and Z_7 to Z_{12} accordingly. During *Event 1*, aeolian sand transport was in the form of streamers (right image on Figure 4-3). The two-hour transport event revealed a rapid change in topography during onshore moderate wind conditions (Figure 4-12). The effective fetch distance is approximately equal to the cross-shore distance of the berm, as winds were perpendicular onshore (11° to dyke normal). During *Event 1*, Figure 4-11 indicates increasing sand transport over the first half of the upper flat beach with increasing fetch distance (Z_1 to Z_4 and Z_7 to Z_{11}), followed by a decrease in sand transport towards of the dyke (Z_4 to Z_6 and Z_{11} to Z_{12}). The rates of trapped sand are confirmed by the observed topographic changes shown in Figure 4-12.

Surface elevation was measured on November 7th and November 13th. Two transport events occurred between the two topographical surveys (Figure 4-7). However, only low transport was observed during the pre-event due to a moist beach surface. In return, this almost did not affect the berm topography. Therefore, the surface elevation changes between the two surveys can be largely attributed to *Event 1*. The increase and decrease of transport rates are excellently related to erosion and deposition respectively (Figure 4-12). The observed growth in sand transport in the downwind direction may be attributed to the downwind fetch effect described by authors such as Anderson & Haff (1991), Cahill et al. (1996), Lynch et al. (2016), Law & Davidson-Arnott (1990) and Delgado-Fernandez (2010). The fetch effect is described as an increase in sediment transport rate with distance downwind until maximum transport rate is reached at the critical fetch distance. The critical fetch distance during *Event 1* is approximately 35 m, until it decreases again towards the dyke. The rapid decrease in sand flux in front of the dyke is likely caused by any pressure effects localized to the trench in front of the dyke and the dyke itself. The range of deposition of sand in front of the dyke is similar to the deposition of sand in front of the steep cliff as pressure effects are also present there (Figure 4-12).

Table 4-1. *Regression parameters for the non-linear exponential regression procedure and total mass flux for Event 1 and Event 2.*

MWAC	q_0 (kg/m/min)	β (m^{-1})	R^2	RMSE (kg/m/min)	Q_s (kg/m/min)
Event 1					
Z_1	0.28	7.00	0.863	0.02	0.04
Z_2	7.63	8.39	0.992	0.15	0.91
Z_3	22.53	12.19	0.999	0.16	1.75
Z_4	36.13	17.78	0.999	0.31	2.03
Z_5	25.69	21.66	0.992	0.39	1.19
Z_6	5.74	22.23	0.972	0.21	0.26
Z_7	0.21	5.63	0.804	0.02	0.04
Z_8	5.21	9.07	0.999	0.02	0.57
Z_9	18.27	10.97	0.999	0.12	1.67
Z_{10}	39.23	14.00	0.998	0.39	2.80
Z_{11}	68.43	17.27	0.991	0.80	3.96
Z_{12}	6.41	22.57	0.990	0.30	0.28
Event 2					
Z_1	0.78	4.61	0.910	0.05	0.19
Z_2	6.62	22.29	0.998	0.08	0.30
Z_3	3.61	27.62	1000	0.00	0.13
Z_4	4.08	31.72	0.999	0.03	0.13
Z_5	4.81	30.38	0.988	0.06	0.16
Z_6	2.90	36.15	0.999	0.00	0.08
Z_7	0.83	6.39	0.876	0.06	0.13
Z_8	9.25	19.55	1.000	0.04	0.47
Z_9	3.42	25.50	0.996	0.03	0.13
Z_{10}	7.17	25.78	0.995	0.06	0.28
Z_{11}	1.98	19.98	0.903	0.12	0.10
Z_{12}	6.66	26.97	0.999	0.06	0.25

Figure 4-11 shows also the normalized transport in the downwind direction for *Event 2*. For *Event 2*, the wind was highly oblique (and rather weak) which means that each of the trap positions had a much longer fetch distance upwind. The effective fetch distance is approximately equal to two times the cross-shore distance of the berm, as winds were 60 degrees to dyke normal. An increase in sand transport was measured between the first two upwind traps (Z_1 - Z_2 and Z_7 - Z_8), followed by a decrease to a lower equilibrium value in the downwind direction. The critical fetch distance where maximum transport is achieved is approximately 20 m and is lower than that achieved in *Event 1* (35 m). There is supporting field evidence of Davidson-Arnott & Law (1990) showing a strong linear correlation between wind speed and critical fetch length. Stronger wind events need more distance to develop an equilibrium flux profile and vice versa (cf. *Event 1*). However, the measurements of *Event 2* clearly indicate the overshoot effect described by Shao & Raupauch (1992). The overshoot effect is typically described by a rapid increase in sand flux towards a maximum until it decreases again to a lower equilibrium sand flux. This is due to relaxation and deepening of the boundary layer which distributes the total shear more evenly in the vertical (i.e. it is not as concentrated in the near-surface layer). Wind tunnel studies by Shao & Raupauch (1992) indicate that this lower equilibrium value is typically a bit lower than half of the maximum sand flux. Similar observations are found by numerical simulations carried by Spies & McEwan (2000). Our field measurements validated this effect. However, there are some minor differences in sand flux between traps behind the maximum sand flux. These spatial differences between traps is dependent on the complex interaction between local and contextual factors (Bauer et al., 2009) and could be explained due to the observed presence of armoring effects and shell pavement caused by sediment sorting at the sediment surface of the upper beach (e.g. Hoonhout & de Vries, 2017).

Moreover, Figure 4-12 shows that sand originating from the foreshore is deposited locally at the foot of the cliff due to flow separation immediately in front of the lip causing a reduction in shear as simulated by Smyth & Hesp (2015).

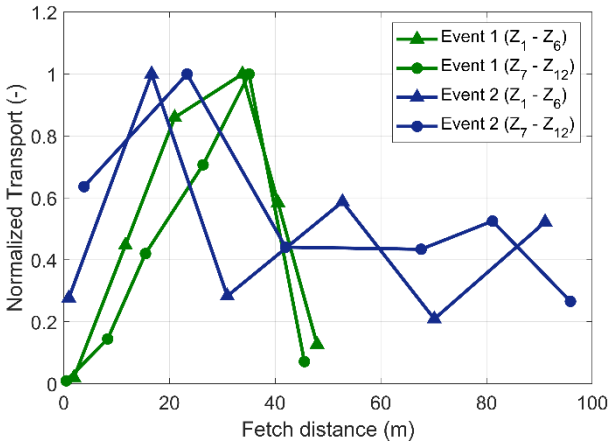

Figure 4-11. *Evolution of sand transport downwind from the lip of the berm for Event 1 and Event 2.*

As mentioned before, the wind flow across a steep cliff accelerates and is maximum at the crest, especially during strong onshore winds (*Event 1*). The critical threshold for sand transport ($u_{*,t}$ = 0.29 m/s based on the Bagnold equation) was always exceeded at the two meteorological stations, even though sand was not being transported continuously. Sand fluxes close to the berm lip were small and increased in the downwind direction. High shear velocities do not coincide with high transport rates, because the upwind sand traps were at the beginning of the fetch and sand coming from upwind seem to be deposited locally in front of the berm lip. Bauer et al. (1990) showed the same trend on a similar study site. Abnormally high shear velocities due to flow compression at the seaward side of a high berm led to small transport rates at the berm lip, whereas farther downwind the fluxes were much closer to what was predicted by the Bagnold equation.

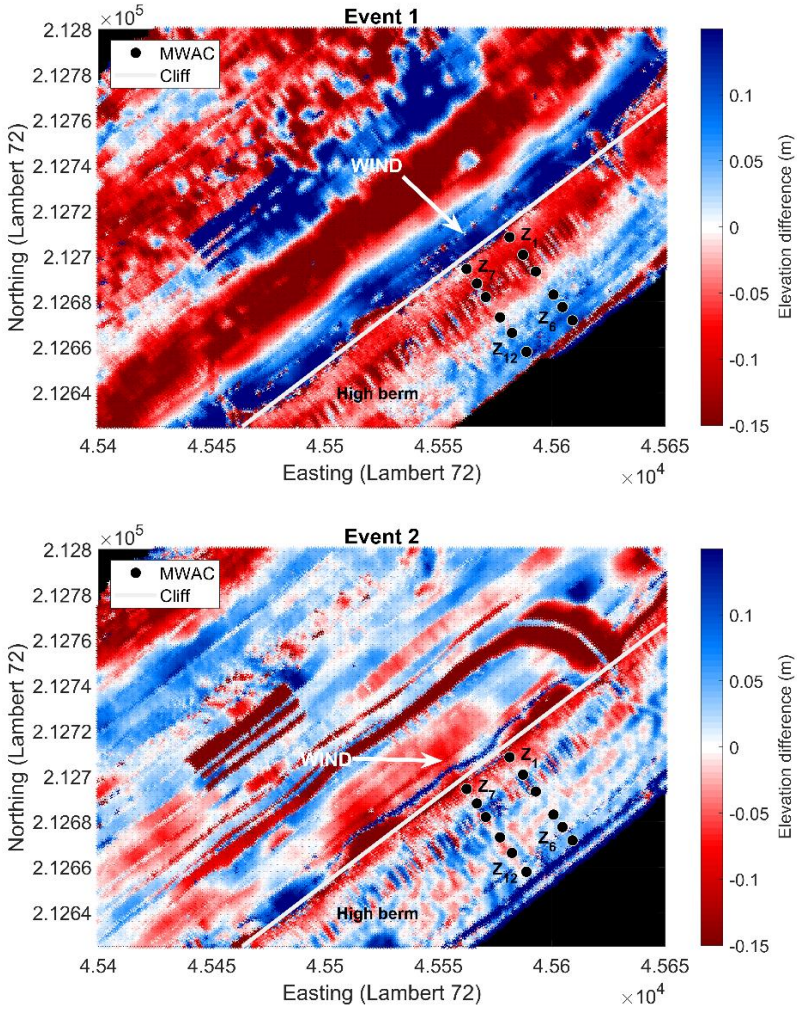

Figure 4-12. *Topographic elevation changes caused by transport Event 1 and Event 2. Red color indicates erosion, while blue color indicates deposition.*

4.3.6 Downwind evolution of vertical flux profiles

Our measurements, given in Figure 4-13, show that the exponential decay rate, β, increases with increasing cross-shore distance further away from the cliff. The increase of the decay rate is confirmed for both transport events. However, for *Event 2* the vertical decay rate seems to reach an equilibrium value β_c. Combining both events present a better understanding. Therefore, the calculated fetch distance F is related with the decay rate β for the different transport events. The effective fetch distance and decay rate are normalized with the critical fetch distance F_c and equilibrium decay rate β_c respectively.

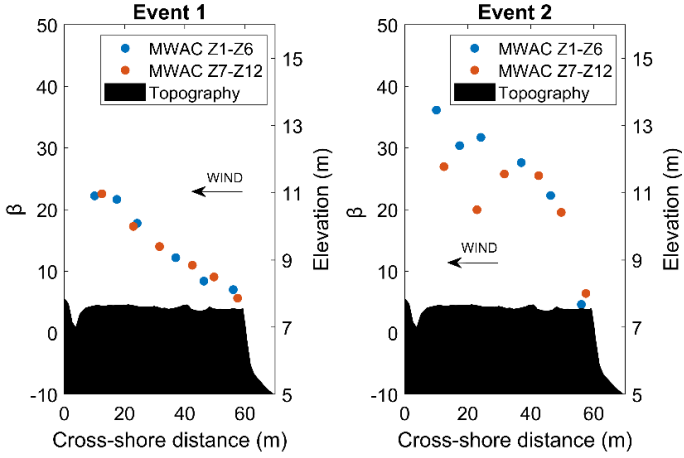

Figure 4-13. *Relationship between the vertical decay rate, β, and cross-shore distance. 0 m is the location of the dyke crest.*

The critical fetch distance is the distance where maximum sand transport is achieved. Our field observations indicate that the critical fetch distance of *Event 1* and *Event 2* equals approximately 35 m and 20 m respectively (Figure 4-11). To confirm this result, the linear relationship of Davidson-Arnott & Law (1990) between critical fetch distance and wind speed is used to calculate the critical fetch distance. Although this expression is based one set of three measurements over a short period of time with poorly documented conditions, it does give an indication of what the critical fetch distance should be. Their expression is as follows:

$$F_c = (4.38 \cdot U) - 8.23 \tag{4.4}$$

Where F_c is the critical fetch length, in m and U the wind speed, in m/s. Stronger wind events need more distance to develop a maximum mass flux and vice versa. During *Event 1*, the average wind speed was 12.75 m/s, resulting in a critical fetch length of about 49 m according to Equation (4.4). During *Event 2*, the

average wind speed was 6.64 m/s, resulting in a critical fetch length of 21 m. Based on our field observations the critical fetch distance for *Event 2* matches the theoretical value based on Equation (4.4). However, the theoretical critical fetch distance of *Event 1* is 14 m longer than the observed value of 35 m. Most likely due to any pressure effects localized at the trench in front of the dyke, and a short available fetch (berm width of 58 m) the critical fetch distance was not achieved during *Event 1*. Therefore, the normalization of the effective fetch distance is done with the critical fetch distance of 49 m and 21 m respectively based on Equation (4.4).

The normalization of the exponential decay rate β is done with the critical or equilibrium decay rate β_c. The measurement campaign of 29 September 2016, on the upper flat beach of the same study area with longshore winds and thus large fetch, is used to determine the equilibrium decay rate β_c. Figure 4-14 shows the instrument locations and variation of the vertical decay rate with fetch distance. The same MWAC sand traps are placed in a cross-shape position with four bottles at elevations of 6.5, 13.5, 21.0 and 28.5 cm above the surface. One trap array is parallel, and the other perpendicular to the wind direction. The decay rate β is calculated based on Equation (4.2) for the longshore array A3 – E3 for two consecutive experiments. The measured wind speed had an average value of 6.82 m/s, similar to *Event 2*. Due to a very large fetch length, the decay rate is almost constant with an average of 28.11 ± 2.71 m^{-1} for experiment 1, and, 26.70 ± 2.38 m^{-1} for experiment 2 respectively. The equilibrium decay rate implies a relatively stable distribution of saltating particle trajectories. The values of the calculated decay rates are in the same order of magnitude as the ones observed during *Event 1* and *Event 2* (Table 4-1). Herein, the equilibrium decay rate β_c is chosen as 27 m^{-1}.

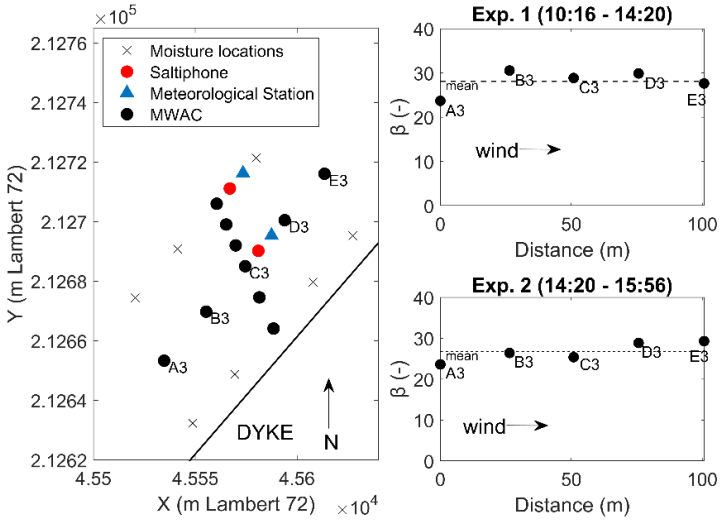

Figure 4-14. *Variation of the vertical decay rate, β, and fetch distance during longshore winds on 29 September 2016 on the study site.*

Figure 4-15 compares the normalized decay rate, β/β_c, with the normalized fetch distance, F/F_c for *Event 1* and *Event 2*. β_c is the critical or equilibrium decay rate of the flux profile (i.e. 27 m^{-1}), while F_c is the critical fetch length (i.e. 49 m and 21 m). Figure 4-15 shows that the exponential decay rate β increases almost linear with increasing fetch length further away from the berm lip until an equilibrium decay rate is achieved. The linear increase of the decay rate is confirmed for *Event 1* and *Event 2* and has high statistical correspondence (R^2 = 0.98). Both data sets collapse on the same curve when normalized properly. It shows the fetch effect in a different way than usually done with mass fluxes. It also states that for both transport events, the decay rate increases at a same rate. Meaning that the probability distribution of particle trajectories changes similarly for different transport events on a flat dry beach surface. It seems that when equilibrium transport mass flux is achieved (cf. Figure 4-11) an equilibrium decay rate is also achieved. More variation is found for *Event 2* during the highly oblique onshore wind conditions most likely because the sand traps were not installed in one transect parallel with the wind direction.

Total mass flux is computed as q_0/β (cf. Equation (4.3)). Due to the fetch effect and the increase in decay rate with fetch distance, q_0 would also have to increase until it becomes constant with constant decay rate (equilibrium state). In the equilibrium state, saltation is fully developed and traditional transport equations may be used.

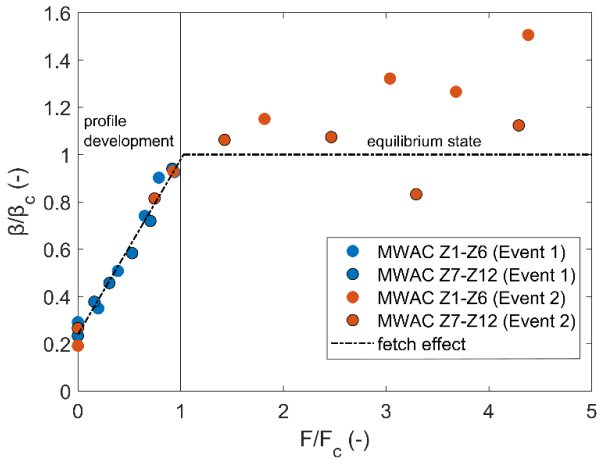

Figure 4-15. *The increase of decay rate as a function of increasing fetch length (β_c=27 m^{-1}).*

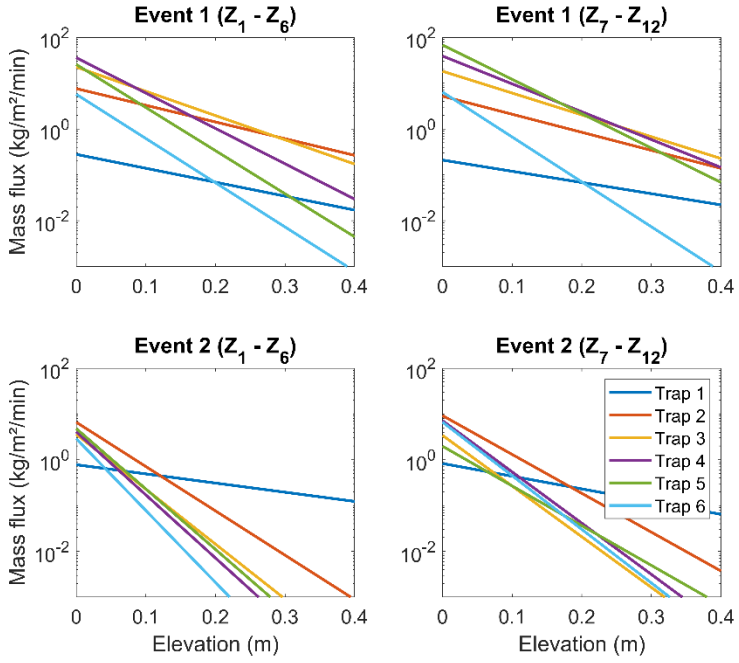

Figure 4-16. *Vertical flux profile development for Event 1 and Event 2 in the transect Z_1 – Z_6 and Z_7 – Z_{12}. Trap 1 corresponds with the most upwind sand trap, while Trap 6 corresponds with the most downwind sand trap.*

Figure 4-16 shows the vertical flux profiles in semi-logarithmic graphs for both events based on the fitted data (q_0 and β) shown in Table 4-1. Emphasis is placed on *Event 2*, where the fetch effect is combined with an overshoot (larger available fetch length) and where the development of the vertical flux profiles with fetch length is shown. In the beginning of the fetch the slope, (β) and y-intercept (q_0) of the flux profile is small (Trap 1) but with increasing fetch, the slope and y-intercept of the flux profile increases until a maximum mass flux is reached (maximum q_0 and β). Subsequently, the y-intercept of the flux profile decreases while the slope remains constant (overshoot). On Figure 4-16 it can be seen that the flux profiles from *Event 2* (Trap 3 – Trap 6) cluster together, indicating an equilibrium flux profile and thus constant mass flux (equilibrium state). To extend the knowledge of vertical flux profile development with increasing fetch distance on a flat dry sand surface detailed experiments in wind tunnels are highly recommended.

4.4 Conclusions

This study describes the downwind evolution of aeolian saltation across a human-constructed coastal high berm with a steep seaward cliff that is backed by a dyke. A data set (sand transport and wind) is gathered and analyzed in the context of fetch distance from the seaward lip of the berm which is the dominant control on the vertical profiles of wind speed and sediment mass flux. Two transport events were measured during moderate onshore to oblique onshore wind conditions. Over-steepened velocity profiles and thus large shear velocities were measured at the steep cliff during the onshore wind event compared to the back beach due to flow compression and acceleration. Despite these large shear velocities at the berm lip, not much sand was transported at the lip due to a lack of sand upwind. In return, the fetch effect has been measured across the flat berm where maximum transport was achieved at a distance of 20 to 35 m of the berm lip. The overshoot effect is observed during the oblique onshore wind event where the available fetch length was much larger. The equilibrium mass flux was approximately half of the maximum mass flux obtained at the critical fetch distance. The evolution of the vertical mass flux profiles downwind causes the exponential decay rate β to increase almost linearly with increasing fetch length further away from the berm lip until an equilibrium decay rate is achieved. Traditional transport equations may be used in the equilibrium state, where saltation is fully developed with sand particles having a relatively stable distribution. Based on this study, the steep cliff in front of the human-constructed coastal berm is found to be very sensitive to erosion. Sand being eroded from the berm lip is deposited in front of the dyke and in the trench.

4.5 Acknowledgments

This publication is the result of research carried out in the project CREST (Climate REsilient coaST), funded by the Strategic Basic Research (SBO) program of the Flanders Innovation & Entrepreneurship. We thank the support of VLIZ (Flanders Marine Institute) for the purchase of research infrastructure. We would like to acknowledge Jeffrey Verbeurgt, Annelies Vandenbulcke, Bart De Wit and Samuel Van Ackere from Ghent University for the topographic measurements and processing. Furthermore, we would like to express sincere gratitude to the extensive anonymous reviews, which has helped greatly for the current form of this paper.

Chapter V

Aeolian sand transport across a shell-fragmented beach: a field study

Abstract

When studying aeolian sediment transport in coastal zones, often a location is chosen where the number of supply-limiting factors is minimal to ensure better comparison between predicted and observed transport rates. However, as is often the case in a natural coastal environment, the beach contains bed irregularities caused by wind action, patches of pebbles, beach wrack, shells and shell-fragments, vegetation and beach litter. The effect of largely scattered shell pavement on aeolian sand transport on the upper beach of a natural beach-dune system was studied during a short-term field experiment in the winter of 2016 in Belgium. The coverage of shell pavement on the upper beach increased towards the dunes and was highest just in front of the dune foot. Continuous sand transport occurred during strong highly oblique onshore wind and was measured during two experiments. During the two experiments, spatial variations in aeolian sand transport indicate that there was a consistent decrease in transport rate with distance downwind. Within 162 m, aeolian sand transport decreased by factor of 10 from the high waterline in the direction of the dunes. The negative gradient in transport caused local deposition of sand on the upper beach in the form of mobile rippled sand strips. This accumulation of sand acted as a new source area for aeolian transport to the dunes when the intertidal beach was inundated. However, as this region is also very sensitive to wave run-up, the accumulated sand may be removed again from the upper beach. The vertical distribution and median grain size of airborne sand particles across the shell-fragmented beach remained constant.

Keywords: Aeolian transport, Shell pavement, Field measurement, Fetch length, Natural beach

Chapter submitted as: Strypsteen, G., and Rauwoens, P. (2019). Aeolian sand transport across a shell-fragmented beach: a field study. *Journal of Coastal Research*.

5.1 Introduction

When studying aeolian sediment transport in coastal zones, a location is often chosen where the number of supply-limiting factors is minimal (e.g. moisture, shells, vegetation) to ensure better comparison between predicted and observed transport rates. However, as is often the case in a natural coastal environment, the beach contains bed irregularities caused by wind action, patches of pebbles, beach wrack, shells and shell-fragments, vegetation and beach litter. The effect of these small-scale bed features is frequently disregarded when conducting field experiments, even sometimes called insignificant (Nordstrom et al., 2011). Large percentages of shells and shell-fragments are mostly found on the upper part of natural beaches outside the wave action zone and on beaches with nourished sand. Shells can protect the beach surface against erosion of the sand particles. Across this complex part of the beach (back beach), potential transport rates commonly deviate from observed values (Sherman et al., 1998). Many natural beaches contain an abundance of shells and shell fragments/hash due to pounding and fracturing in the surf zone. Literature on this topic is rather scarce. Most available literature on aeolian sediment transport across shells is studied in wind tunnel experiments (e.g. Van Der Wal, 1999 and McKenna et al., 2012). Sometimes, observations in the field are described but are not directly measured as total mass fluxes with vertical sand traps (e.g. Hoonhout & de Vries, 2017). Direct field studies on transport rates due to the impact of shells and shell pavements are limited. Nordstrom et al. (2011) did a short-term field study on the effect of beach wrack on the upper beach parallel with the dunes on rates of transport and found that mass fluxes downwind of the wrack line exhibited a great reduction (3.2% and 12.7% of upwind amounts). Van Der Wal (1999) studied the effect of shells on the wind-induced transport of Dutch beach sand in a wind tunnel and found that the percentage of sand blown off during the test was calculated for each of the experiments. The transport rate was reduced by a factor of 1.5 for samples with a percentage of shells of 10% and by a factor of 3 for samples with a percentage of shells of 20% to 30%. Shell pavements were formed during the wind tunnel experiments with shell-rich beach samples. McKenna et al. (2012) also conducted a wind tunnel study on the effect of various types of shells (most commonly found on beaches) on the erosion of sand. It was observed that the shells (crushed, small and large) were organized into chains and clusters with the long axis of many of the shells appearing to be aligned with the wind flow. The threshold wind velocity and shear velocity were found to increase by about 15% to 25% for a cover of 15% and about 35% to 45% for a cover of 43%. The amount of erosion after the test (in kg/m^2) was recorded showing almost no erosion for the largest cover values of 40% both for small and large shells. Erosion is reduced by a factor of 5 to 10 by increasing the cover of shell from about 15% to about 30-40%. Crushed shells are less effective than small/large shells. The sand transport is estimated to be reduced by about 40% for a cover of 15% and about 95% for a cover of 40%.

This study presents detailed measurements of aeolian sand transport rates, wind conditions, and grain size distributions during a two-day measurement campaign in the winter of 2016 on the natural upper beach of Koksijde, Belgium. The experiment was designed to study the influence of shell pavement (various types of shells) on sand transport rates during strong and highly oblique onshore wind. Understanding local aeolian transport processes ultimately helps improving predictions of aeolian sediment transport in coastal areas over short to long-term timescales.

5.2 Study site

Detailed field measurements on aeolian sand transport rates, wind conditions, and grain size distributions were conducted on the upper beach of Koksijde (section 50) in Belgium on November 24-25, 2016. Koksijde beach is located on the southwest side of the Belgian coast, close to the French border (Figure 5-1). The beach of Koksijde is natural and consists of sand ($d_{50} = 220$ µm) with small-scale bed irregularities (ripples) and many shell hash and shell fragments with heights ranging between a few millimeters to 30 mm on the upper beach (Figure 5-2). Due to wave uprush, many patches of crushed, small and large shells were present in a region 40 m in front of the dune foot. The location is a dissipative macro-tidal environment, oriented along southwest to northeast direction. The intertidal beach is relatively horizontal with a minor slope of approximately 1% and is characterized by ridge and runnels topography (Speybroeck et al., 2008; Voulgaris et al., 1998). The tide in this area is semi-diurnal with a large neap to spring variation ranging between 3.5 m and 5 m (Haerens et al., 2012). The width of the intertidal beach is large and ranges between 250 m and 500 m at neap and spring tide respectively. In the study area, prevailing winds blow from SW direction and are characterized by light and moderate breezes with speeds ranging from 3-8 m/s. However, in terms of aeolian sand transport, the dominant strong to very strong breezes ($>$ 10 m/s) occur mostly between November and February and are from WSW to NW directions. These dominant winds could also have severe threatening conditions for the occurrence of storm surge (Montreuil et al., 2016). According to Haerens et al. (2012), storm surges are recorded at least once a year when water levels and onshore wave heights could reach 5 m TAW and 3 m respectively. The upper beach width, defined as the distance between the dune foot (+6.89 m TAW) and mean high water line (+4.39 m TAW) is approximately 60 m. The experiments were carried out near the transition of the intertidal beach and the upper beach, in a zone free of groins where dunes back the beach.

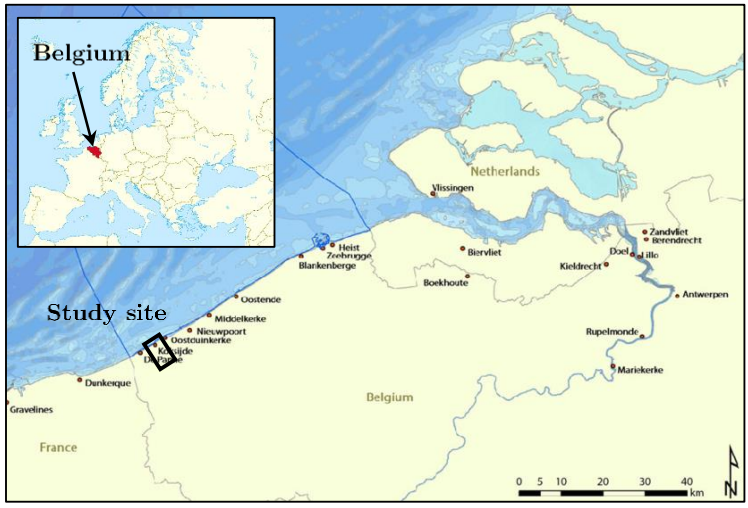

Figure 5-1. *Location and orientation of the study site.*



Figure 5-2. *Meteorological station with eight anemometers, a wind vane and a temperature sensor connected to a buried CR800 Campbell Scientific datalogger. On the beach surface, many shell hash and fragments are present of different size (crushed, small and large).*

5.3 Methodology

5.3.1 Instrumentation

Aeolian sediment transport rate measurements were performed in a transect parallel to the wind direction which was highly oblique onshore. The spatial variation in sediment transport rate was measured in downwind direction on November 24, 2016 starting close to the high waterline, across the upper beach, towards the dune foot (Figure 5-3). Nine Modified Wilson And Cook (MWAC) vertical sand traps were exposed to the wind to determine the rate of aeolian sand transport (Figure 5-4). They are extensively used in numerous studies where efficiencies of between 42% and 120% were reported (e.g. Van Pelt et al., 2009; Sterk & Raats, 1996; Goossens & Offer, 2000; Poortinga et al., 2013; Youssef et al., 2008). They have the advantage of being easily installed when quick decisions have to be made during transport events. During the campaign, the sand traps were placed approximately 20 m apart from each other. The traps collected sediment in plastic bottles at a of height 6.5, 13.5, 21.0, 28.5 and 54.0 cm above the surface. The sand trap was equipped with a vane to ensure that the bottle inlet was always orientated towards the wind. Each bottle had a glass inlet and outlet tube with a diameter of 8 mm (≈ 50 mm^2 or 5.10^{-5} m^2). The mass of sand collected in the bottle was divided by the inlet tube area and exposed time (in minutes) to provide transport rates in kg/m^2/min. The samples collected in the MWAC bottles were analyzed for grain size distribution. Topography was also measured along the transect at the beginning of the experiment.

Transport intensity was measured on 24 and 25 November in combination with the measurement of wind conditions and temperature. Saltating sand grains were counted using two high-frequency saltiphone sensors placed at 5 cm and 15 cm above the sand surface (Figure 5-4). The instruments only detected a small (vertical) portion of the horizontal flux. Two vanes at the back of the tube ensured proper positioning of the microphone in the wind. Saltating particles larger than 50 microns would mostly hit the microphone and produce high-frequency noise, which can be distinguished from other noises caused by wind and rain. Every 20 seconds, the cumulative number of impacts was recorded and stored on a CR800 Campbell Scientific datalogger. Detailed descriptions about its design, testing and deployment are given by Spaan & Van Den Abeele (1991). Saturation of the impact sensor (oversampling) may occur in specific conditions: very close to the bed and/or in strong wind conditions with high particle concentrations. At low wind conditions, the transport layer may be so small (thin), that most of the particles will pass underneath the location of the lowest sensor (undersampling).

Wind speed and wind direction were measured using eight cup anemometers (Vector Instruments A100R) and a wind vane (Vector Instruments W200P) on

a 3 m high meteorological station positioned on the upper beach (Figure 5-2). The cup anemometers were positioned at eight elevations above the shell-fragmented surface: 0.04, 0.22, 0.49, 0.91, 1.29, 1.67, 2.02 and 2.40 m respectively. The wind vane was installed at an elevation 2.02 m. The wind speed data was recorded once every 20 seconds and saved on the CR800 Campbell Scientific datalogger. The wind speed measurements were used to calculate the aerodynamic roughness length, z_0, and wind shear velocity, u_*, derived from the vertical log-wind profile. Furthermore, measurements on air temperature were performed at 10-minute intervals.

At three moments during the experiment where sand transport rates were measured, surficial moisture content (upper 6 cm) was measured with an ML3 ThetaProbe Soil Moisture Sensor. The moisture content was measured at the locations near each MWAC sand trap.

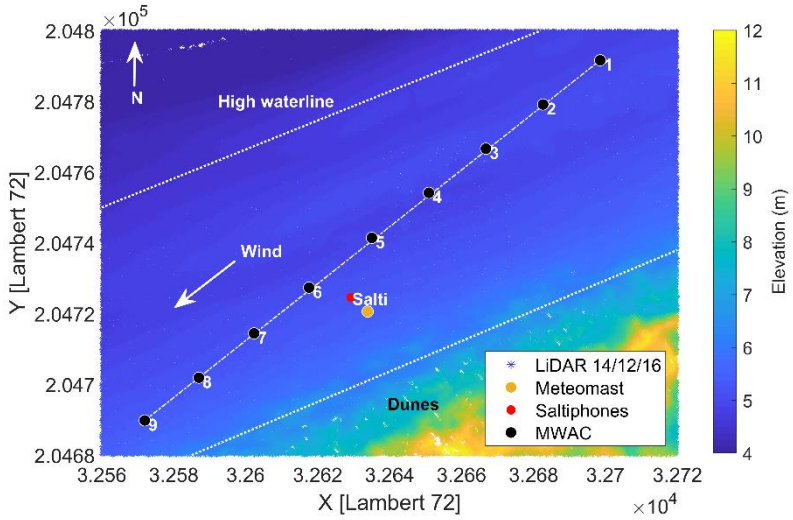

Figure 5-3. *Overview of measurement locations. The topography is obtained from the LiDAR flight three weeks after the campaign (14/12/2016). All the instruments are located on the upper beach. The meteorological station is located in the middle of the experiment near the embryo dunes. The dotted lines represent the high waterline (+4 m TAW) and dune region. The MWAC sand traps are positioned parallel with the wind direction. During the whole experiment, the wind direction was from northeast, highly oblique onshore.*



Figure 5-4. *The Modified Wilson And Cook sand trap (MWAC) and saltiphones, measuring sand transport on the beach of Koksijde, 24 November 2016. Note the presence of different sized shell fragments.*

5.3.2 Data analysis

Shear velocities are derived based upon 10-minute averaged values of wind speed at eight heights above the surface by calculating the slope of the regression line of the log-linear wind profile following the law of the wall:

$$U_z = \frac{u*}{\varkappa} \cdot \ln\left(\frac{z}{z_0}\right) \tag{5.1}$$

where U_z is the wind speed at elevation z above the surface, $\varkappa$ is the von Karman's constant (taken as 0.4), and z_0 is the roughness length of the surface, which is $k_s/30$ during non-transport conditions, with k_s being the equivalent roughness length of Nikuradse (Nikuradse, 1933). The critical shear velocity of dry sand (Bagnold, 1941) is calculated and defined as:

$$u_{*,cr} = 0{,}11 \cdot \sqrt{\left[\left(\frac{\rho_s}{\rho_{air}} \text{-} 1\right) \cdot g \cdot d_{50}\right]} \tag{5.2}$$

where ρ_{air} = density of air (1.2 kg/m^3); ρ_s = absolute density of sand grains (2650 kg/m^3); g = 9.81 m/s^2; d_{50} = mean particle size (m).

The MWAC sand traps captured sand in four to five bottles at different elevations above the surface. The sand collected in each bottle was weighed and divided by the inlet tube area and exposed time (in minutes). The inlet tube has a diameter of 8 mm ($\approx$ 50 mm^2 or 5.10^{-5} m^2). The unit of the transport rates are given in kg/m^2/min. The vertical distribution of sediment saltation transport can be best described by an empirical exponential decay function

(Ellis et al., 2009; Horikawa & Shen, 1960; Williams, 1964; Bauer & Davidson-Arnott, 2014; Poortinga et al., 2014):

$$q_z = q_0 \cdot e^{-\beta z} \tag{5.3}$$

where q_z is the sediment mass transported at height z above the surface (kg/m²/min), q_o is the extrapolated saltating sediment mass transported at the surface (kg/m²/min) and β is the decay rate (m^{-1}), a measure of the vertical concentration gradient (Van Dijk et al., 1996). The total saltating mass transport can be obtained by the integration of Equation (5.3):

$$Q_s = \int_0^{\infty} q_z \cdot dz = \frac{q_0}{\beta} \tag{5.4}$$

where Q_s is the total mass transported by saltation (kg/m/min), assuming that saltating particles start moving immediately above the surface, z = 0 m (Horikawa & Shen, 1960).

Validated by short-term field campaigns (Strypsteen et al., 2019), where wind speeds and saturated aeolian transport rates were measured, a modified Bagnold model (van Rijn, 2018) is used to give an indication of saturated or maximum aeolian sand transport during the experiment:

$$q = \begin{cases} 60 \cdot \alpha_B \cdot \sqrt{\frac{d_{50}}{d_{50,ref}}} \cdot \frac{\rho_{air}}{g} \cdot \left[(u_*)^3 - (u_{*,cr})^3 \right], & u_* > u_{*,cr} \\ 0, & u_* < u_{*,cr} \end{cases} \tag{5.5}$$

where q = saturated mass flux (kg/m/min); d_{50} = particle size (220 µm); $d_{50,ref}$ = 250 µm; ρ_{air} = density of air (1.2 kg/m³); g = 9.81 m/s²; u_* = shear velocity (m/s); $u_{*,cr}$ = threshold shear velocity (m/s); α_B = Bagnold factor (1.5 – 3.5). The coefficient α_B ranges from 1.5 to 3.5 and is depending on the surface sediments. A value of α_B = 2 represents naturally graded sands, which is used in the calculation of potential transport.

5.4 Results and discussion

The conditions during the field campaign were dry, sunny weather with strong winds of up to 14.6 m/s (measured at a height of 2.02 m). Temperature reached a maximum of 9°C during the campaign. The average wind speed over the entire experiment was 9.1 m/s (or u_* = 0.51 m/s) which was always above the threshold of movement based on Equation (5.2) ($u_{*,cr}$ = 0.24 m/s) (Figure 5-5). Wind direction was highly oblique towards the dunes with an average direction of 70 degrees to the North or 8 degrees out of longshore direction. Tide ranged between 0 and +4 m TAW. Aeolian sand transport was in the form of

continuous streamers and occurred during the entire campaign. Particle counts, measured with the saltiphones ranged between zero and the saturation value (8000 counts per 20 seconds). Obviously, the lowest saltiphone recorded more impacts than the upper saltiphone. The lower saltiphone experienced saturation of the impact sensor (oversampling) because of the high particle concentrations. Figure 5-6 shows that, apart from the saturated values, the data gathered by both saltiphones correlate linearly. The higher positioned saltiphone registered 10% of the transport measured at the lower positioned saltiphone.

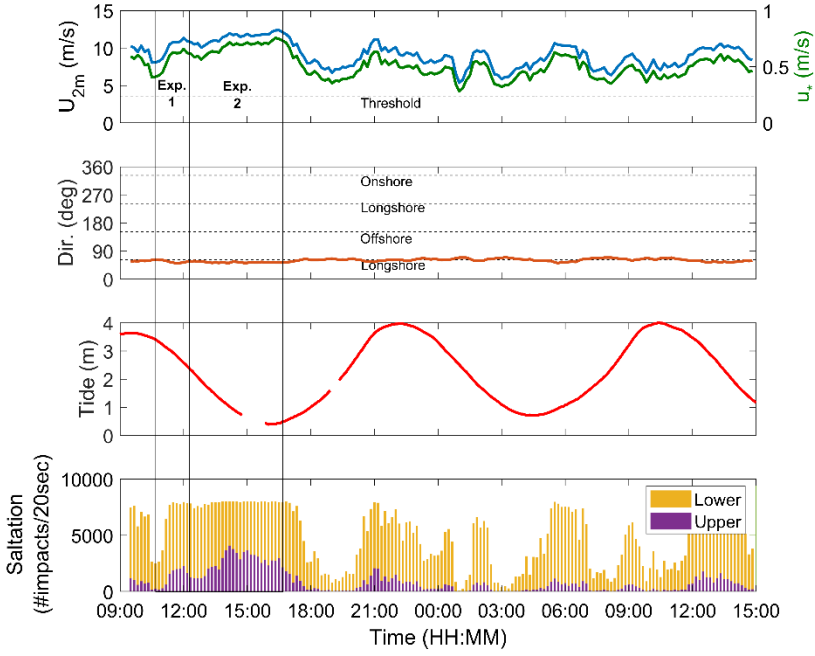

Figure 5-5. *10-minute time series of wind speed, shear velocity, wind direction, tide and saltation impacts over the entire field experiment conducted on November 24-25, 2016.*

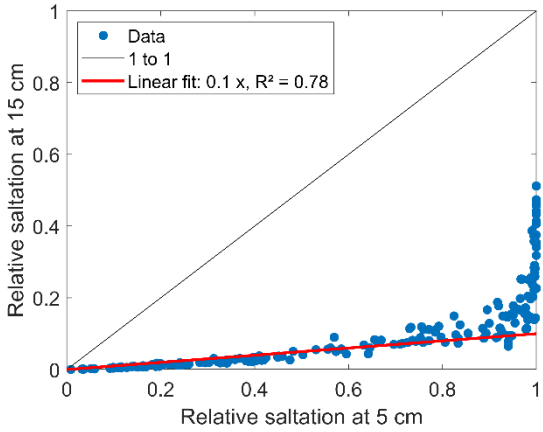

Figure 5-6. *Comparison between the registrations of the two saltiphones.*

The MWAC sand traps were exposed to aeolian sand transport during two experiments on November 24 (Figure 5-5). Experiment 1 started from 10:55 until 12:40, resulting in a sampling time of approximately 1h45min. During the first experiment, average wind speed and shear velocity was 10.4 m/s and 0.60 m/s respectively. Approximately one hour before the first experiment started (9:30), high water occurred, meaning that the intertidal beach was completely saturated with water, resulting in moisture contents up to 25%. Aeolian transport started directly from the high waterline during Experiment 1 (Figure 5-7). Experiment 2 started from 12:40 until 16:55, following Experiment 1 consecutively (4h15min sampling time). Average wind speed and shear velocity during the second experiment was 11.5 m/s and 0.68 m/s respectively. In terms of wind conditions, Experiment 2 was more intense. Aeolian transport started further upwind during Experiment 2 due to the drying out of the upper part of the intertidal beach. During the entire field experiment, shear velocities were generally high due to the many shell fragments on the surface (Figure 5-2). Figure 5-8 shows that the bed roughness height, k_s varies between 20 and 90 mm at the upper beach. Based on the fieldwork of Owen (1964) and Sherman and Farrell (2008), the effective bed roughness is in the range of 10 to 100 mm. Figure 5-8 indicates that the roughness height, k_s, increases with shear velocity. Field & Pelletier (2018) found that the aerodynamic roughness, z_0 (equal to $k_s/30$) increases as a power law with shear velocity due to saltating particles. Figure 5-8 shows the power regression fit (see also Figure 2-5 in Chapter 2).



Figure 5-7. *Aeolian sand transport commences directly at the high waterline on November 24, 2016 during Experiment 1.*

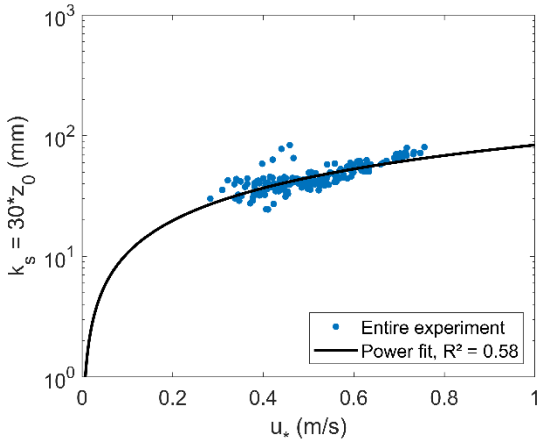

Figure 5-8. *Bed roughness for different shear velocities during the entire experiment.*

The entire experiment was accompanied with periods of high particle count (Figure 5-5). The peaks occurring in the wind speed seem to correspond with the peaks found in the particle count. Figure 5-9 shows that there is overall strong linear relation between potential transport based on Equation (5.5) and particle count measured by the two saltiphones. This indicates that the variation of particle count follows the variation of the wind speed seamlessly, since Equation (5.5) uses parameters that are constant in time, except for the wind speed (shear velocity).

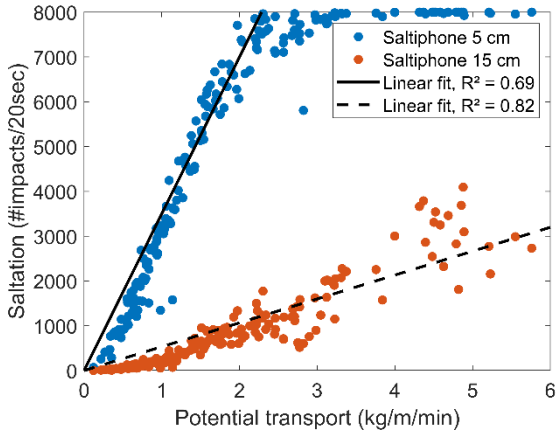

Figure 5-9. *Relation between overall particle count and potential transport.*

Significant spatial variations are found along the transect with distance downwind. Figure 5-10 shows that the highest transport rates are found close to the high waterline and the lowest close to the dune region during both experiments. Minor patches of shells were present near the high waterline. The general observed trend is that mass flux decreases downwind over a distance of 162 m. Two processes are likely to be relevant during aeolian sand transport across shells: trapping impacting sand grains (hampering saltation) or causing fully elastic collissions (enhancing saltation) (Hoonhout & de Vries, 2017). Due to the consistent decrease of mass flux downwind, the process of hampering is dominant over the enhancement proces.

Fetch distance was not unrestricted at all traps, especially the traps close to the high waterline (MWAC 10 to 8). It could be possible that the fetch effect occurred at the first sand traps since the high waterline was approximately 40 m upwind and sand transport commenced there. The fetch effect is a typical example of a disequilibrium situation of aeolian transport on a spatial scale. Delgado-Fernandez (2010) has an extensive review of the fetch effect observed in coastal and agricultural environments in the past decades. The fetch effect is the increase of sand flux in the downwind wind direction across a beach surface until a maximum is achieved (Davidson-Arnott et al., 2005; Delgado-Fernandez, 2010). According to Bauer & Davidson-Arnott (2003), this maximum is achieved exponentially after a certain critical fetch distance. The critical fetch distance varies for different wind speeds and moisture contents, where distances of 10 m to more than 300 m are reported (Lynch et al., 2007; Davidson-Arnott et al., 2008; Lynch et al., 2016; Gillette et al., 1996). Strypsteen et al. (2019) found that the decay coefficient β used in Equation (5.3) linearly increases downwind to an equilibrium value when the critical fetch distance is reached. Figure 5-10 indicates that the decay coefficient is relatively constant ($\beta = 21.8 \pm 2.3$), meaning that the critical distance would have been reached at the

beginning of the upwind sand traps or a distance before. Experiment 1 started when the intertidal zone was completely wet and sand transport started at the high waterline. It is possible that maximum transport was achieved at MWAC 9 (or 20 m downwind distance in Figure 5-10). Maximum potential transport according to Equation (5.5) during Experiment 1 is 2.7 kg/m/min. As Shao & Raupach (1992) and Strypsteen et al. (2019) reported, they found that the fetch effect is characterized with an overshoot. Sand flux rapidly increases towards a maximum value followed by a decrease to a lower equilibrium value hence, sand transport decreases after a distance of 20 m downwind. Sand transport started further upwind from the high waterline during Experiment 2. As wind speeds were also slightly higher than during Experiment 1, the lower overshoot equilibrium value could already been achieved. Since no transport rate measurements were performed further upwind, this was an assumption. Maximum potential transport according to Equation (5.5) during Experiment 2 is 4.2 kg/m/min. The constant decay rate also indentifies that the vertical distribution of sand particles are not influenced by the roughness elements. Moreover, the median particle size (d_{50}) of saltating particles above the surface remains constant along the transect during both experiments (Figure 5-10).

The significant reduction of aeolian sand transport further downwind (from 40 m onwards) is caused by a combination of an increase in bed roughness due to the shells and morphological feedback with the wind. Spatial variations between traps is caused by local differences in bed surface properties (amount and distribution of the shells at the surface). Figure 5-10 shows that between 80 m and 100 m there is larger decrease in sand transport (large negative gradient). The larger decrease is caused due to wetter surface conditions in combination with shell cover (12% compared to 2% surface moisture) in that relatively small region. It appears that in that region a runnel is present as indicated by the topography. Due to a further increase of the roughness elements downwind (based on visiual observations), the impacting grains are being trapped. Therefore, saltation is being hampered to almost zero transport in the region just in front of the dunes. In the region in front of the dunes, more and larger shells were present. According to McKenna et al. (2012), transport is reduced by a factor of 5 to 10 by increasing the cover of shell from about 15% to about 30-40%. Large shells are also more effective in hampering saltation than crushed shells which was typically found above the high waterline. Our measurements suggest that aeolian sand transport is reduced by a factor 10 over a distance of 162 m from the high waterline to the dune front due to the combinational influence of shells and moisture. To extend the knowledge of the bed roughness elements and sand transport of sandy beaches, wind tunnel and field experiments are highly recommended. There is pressing need for detailed, short-duration experiments in wind tunnels and at field sites with a flat, mobile sand surface in the upper transport regime to study the influence of shell cover and/or moisture on aeolian transport.

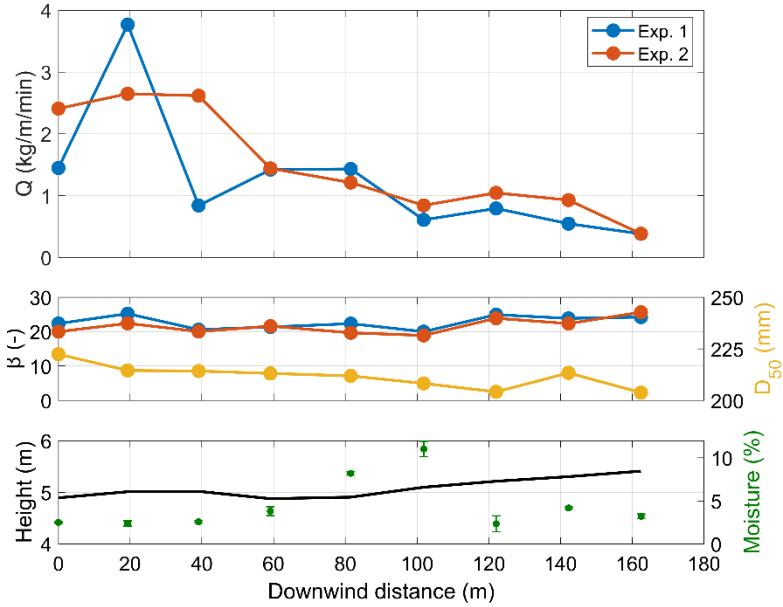

Figure 5-10. *Upper graph shows the measured mass fluxes downwind during Experiment 1 and 2. Left to right is MWAC 1 to MWAC 9. Middle graph shows the calculated decay coefficient β based on Equation (1.3) and median grain size d_{50}. Lower graph shows the beach profile at the beginning of the field campaign together with the variation of surface moisture.*

The decrease in mass flux causes a local deposition of sand on the upper beach in front of the dunes. This accumulation of sand is observed on top of the shell pavement in the form of large rippled sand strips with well sorted sand (Figure 5-11). Commencing of sand strips is a very complex process. Usually, these sand strips are mainly dependent on the wind direction and form mostly during highly oblique to alongshore winds (Hage et al. 2018). Van der Wal (1998) also found moving patches of well sorted sand on shell pavement on the beach of Ameland in the Netherlands. Sand strips are often present during strong aeolian events on beaches with high surface moisture and roughness elements (Nield et al., 2011). The sand strips do not enter the dunes directly, but slowly move across the surface downwind. Nield et al. (2011) and Hage et al. (2018) observed that mobile sand strips migrate with speeds ranging from 0.18 m/h to 1.24 m/h. Different environmental conditions are needed to be favorable for aeolian sand to reach the dunes. Hoonhout & de Vries (2017) observed similar findings on the Sand Motor and discussed that aeolian transport is a phased process. Aeolian sand from the intertidal beach is being deposited just above the high waterline which coincides with a berm and shell pavement. This area acts as a temporary source of sand to be transported by wind during different environmental conditions to the dunes. However, it is also possible that swash

uprush during storm events may remove the sand accumulated on the backbeach (Delgado-Fernandez & Davidson-Arnott, 2009). The location of large patches of roughness elements on the beach is very influencial as lower situated patches make the accumulated sand there more vulnerable to loss by waves (Nordstrom et al., 2011).



Figure 5-11. *Deposition of sand on the upper beach in the form of large rippled sand strips visible on top of the shell pavement.*

5.5 Conclusions

Direct field studies on sand transport rates due to the impact of shells and shell pavement have been limited. The effect of large scattered shell pavement on aeolian sand transport on the upper beach of a natural beach-dune system is examined during a short-term (hours) field experiment in the winter of 2016 in Belgium. The shell pavements consisted of crushed, small and large shells where coverage increased towards the dunes and was highest just in front of the dune foot. During highly oblique onshore wind with a maximum wind speed of 14.6 m/s two experiments were conducted where sand transport rates are measured with vertical sand traps. During the two experiments, spatial variations in aeolian sand transport indicated that there was a consistent decrease in transport with distance downwind. Within 162 m, aeolian sand transport decreased by factor 10 from the high waterline in the direction of the dunes. The decrease in mass flux caused for a local deposition of sand on the upper beach in the form of large rippled sand strips. The sand strips were not entering the dunes directly, but slowly moved across the surface downwind. This accumulation of sand acted as a new source area for aeolian transport to the dunes when the intertidal beach was inundated. However, this region was also very sensitive to wave uprush, whereas the accumulated sand may be removed again from the upper beach. Aeolian sand transport across the roughness elements did not influence the vertical distribution of sand particles as the decay

rate of the vertical flux profiles remained constant. Consequently, the median particle size above the surface remained constant along the transect.

5.6 Acknowledgements

This publication is the result of research carried out in the project CREST (Climate REsilient coaST), funded by the Strategic Basic Research (SBO) program of the Flanders Innovation & Entrepreneurship. We thank the support of VLIZ (Flanders Marine Institute) for the purchase of research infrastructure.

Chapter VI

Conclusions

This thesis concludes with addressing the research questions formulated in the introductory chapter (Chapter 1).

Research Objective A: Evaluating the relationship between aeolian sand transport rate and wind speed on the Belgian coast (Chapter 2).

An extensive data set has been obtained through field experiments on two study sites in Belgium with different beach morphologies (natural and artificial). By simultaneously measuring wind speeds at different altitudes above the surface and sand transport rates, the forcing (shear velocity) and the result (sand flux) are correlated under various circumstances of wind speeds and wind direction.

The research questions and answers related to this objective are:

1. Which mathematical aeolian model can be proposed, showing a good relation between observed and predicted saturated sand transport rates?

   A modified Bagnold model, which has been proposed by Van Rijn (2018), proves to be the best model to predict aeolian transport of dry sand. It has a near one-to-one relation between observed and predicted sand transport rates. The model shows to be very consistent with the observed sand transport rates and is in fact a modified Bagnold-equation for saturated (equilibrium) transport of dry sand in air. The model is cubic related to the wind shear velocity, whereas it includes the term (u_*^3-$u_{*,th}^3$). The derivation of the mathematical model is theoretically based on general dimensional analysis for sand transport in water. The aeolian model of Kok (2012) is a close second. Variability between observed and predicted transport rates is mainly caused by the spatial-temporal character of aeolian sand transport. It seems that this variation is related to shear velocity by a cubic relationship. This

cubic relationship is also described by the modified Bagnold model proposed by Van Rijn (2018).

2. Which often used aeolian models perform poor in the relation between observed and predicted saturated sand transport rates?

   The model of Bagnold (1954), which is often used to do long-term aeolian budget calculations, and the model of Kawamura (1951) produce the poorest results. The model of Bagnold (1954) underestimates sand transport rates, while the model of Kawamura (1951) overestimates sand transport rates. Both models match weakly to our observations.

Research Objective B: Characterizing the temporal variability and relative magnitude of annual aeolian sediment transport on the Belgian coast (Chapter 3).

In order to study the temporal variability and relative magnitude of annual aeolian sediment transport on the Belgian coast, potential aeolian sand transport is calculated per coastal section using the modified Bagnold model proposed by Van Rijn (2018). For each coastal section, the representative median grain size and coastal orientation is used. Hourly wind data, from 2000-2017, at Ostend Airport is used as forcing input parameter (middle of the coastline and approximately 1 km inland).

The research questions and answers related to this objective are:

1. What is the amount of annual cross- and longshore potential aeolian sediment transport along the Belgian coast?

   Considering all coastal sections within the period of 2000-2017, onshore potential aeolian sediment transport ranges maximum to 9 $m^3/m/year$ (average = 5.2 $m^3/m/year$), while longshore potential aeolian sediment transport could reach up to 20 $m^3/m/year$ (average = 18.7 $m^3/m/year$). Total potential aeolian transport along the Belgian coast is approximately 20 $m^3/m/year$. On decadal time-scales, it appears that potential aeolian sediment transport varies linear in time. Longshore aeolian transport could be three to four times larger than cross-shore aeolian transport.

2. What is the main direction of annual aeolian sediment transport along the Belgian coast?

   The main drift of aeolian sediment transport on the Belgian coast is from western and southwestern direction. West to southwestern winds

are oblique onshore to longshore with respect to the Belgian coastline. The larger parallel component (longshore) of the potential transport drift is directed towards NE (the Netherlands), while the normal component (onshore) is directed towards SE (hinterland).

3. What is the frequency and variation of aeolian sediment transport events along the Belgian coast?

   The entire wind speed data set of 17 years at an hourly basis is analyzed, comprising +150,000 hours. Threshold wind speeds varied between 5.5 and 7.3 m/s with an average of 6 m/s (height of 2 m above the surface). All winds below the average threshold wind speed of 6 m/s are so called light breezes and represent the first wind class. The other six wind classes, above the average threshold wind speed, ranged from moderate breezes to fresh gales with wind speeds from 6-8 m/s to higher than 16 m/s respectively. 67% of all winds were below the threshold, meaning that there is only 33% chance on annual potential aeolian sand transport. Potential annual aeolian sediment transport indicates considerable spatial-temporal variability caused by annual variations in wind climate and beach characteristics (e.g. bedforms, grain size, roughness elements). Annual variations are approximately between 0.5 times and 1.6 times mean transport rate, meaning that potential transport, occasionally, is 3 times larger for some years than other years.

Research Objective C: Identifying trends in dune behavior on the Belgian coast (Chapter 3).

Temporal and spatial dune behavior along the Belgian coast is analyzed using a unique 38-year data set of annual and bi-annual airborne photogrammetric and, since 1999, airborne Laser Scanner (LiDAR) topographical data. Spatial and temporal variability in dune behavior is then correlated with potential sediment input from the beach in the period between 2000 and 2017.

The research questions and answers related to this objective are:

1. What is the spatial-temporal variability in dune volume changes along the Belgian coast?

   Along the Belgian coast, concerning the coastal sections with vegetated dunes (approximately half of the coast), it is found that dunes grow linearly in time with a constant rate on a decadal timescale. The majority of these coastal sections have a constant dune growth rate. It is found that 80% of all coastal dunes with dune growth have correlation coefficients higher than or equal to 0.9. However, there is

alongshore variability in linear dune growth rates at the Belgian coast and they are found to be in the order 0-12.3 $m^3/m/year$. An average dune growth of 6.2 $m^3/m/year$ is found.

2. What is the correlation between observed and predicted dune volume on an annual timescale along the Belgian coast?

   No significant relationship between annual wind and annual dune volume change is found in the alongshore direction. The poor correlation could be mainly attributed to the coarse spatial-temporal data set of the LiDAR flights. The duration between two consecutive LiDAR flights is too long. Furthermore, between consecutive LiDAR flights, dune erosion and dune growth can occur. Even during strong aeolian transport events, a single dune-erosion event can undo any dune growth that happened prior to that storm. Dune volume changes are also influenced by the sediment supply and sediment availability from the marine zone. Transport limiting factors, such as sediment size and distribution, beach geometry and moisture can be of greater importance than the driving wind speed.

3. What is the correlation between observed and predicted dune volume on decadal timescales along the Belgian coast?

   A significant correlation is found between potential and observed dune volume development on a decadal timescale, indicating that dune growth is primarily caused by aeolian sediment transport from the beach. Most of the predicted data are within a factor of two of the measured values. The finding of potentially stronger correlations at the Belgian coast are most likely caused by the wider beaches (between 150 m and 400 m) due to the massive sand nourishments to keep the sediment budgets along the Belgian coast positive. It also suggests that annual differences in forcing and transport limiting conditions (wind speed and surface conditions) only have a slight effect on the overall variability of dune volume trends.

4. What are the longshore variations of the correlations by distinguishing between 'natural' and 'managed' beach sections of the Belgian coast featuring dunes?

   The general variability, on a decadal timescale, between observed and predicted dune volume could be partly attributed to the managing activities at certain sections along the coast. It is uncertain how many of the dune regions are managed, but it is estimated to be around 50%. Most of these activities include regular plantation of brushwood fences, especially where observed linear dune behavior is higher than the predicted values. The locations including dune foot protection

measures, dune foot reinforcements, and dune blowouts, are mostly the locations where predicted values are higher than the observed values. When the managed zones are excluded from the data set, the best fit line slope between observed and predicted dune volume is approximately 1, and the RMSE value is 2.9 $m^3/m/year$. Most of the predicted data are within a factor 2 of the measured values. This indicates that natural dune behavior can be predicted with a reasonable accuracy on decadal timescales.

Research Objective D: Examining the downwind evolution of aeolian saltation across an artificially constructed coastal high berm with a steep seaward cliff, backed by a dyke. (Chapter 4).

This study describes the downwind evolution of aeolian saltation across a human-constructed coastal high berm with a steep seaward cliff that is backed by a dyke. In front of the dyke, a trench is excavated to limit aeolian sand to the hinterland. A data set (sand transport and wind) is gathered and analyzed in the context of fetch distance from the seaward lip of the berm, which is the dominant control on the vertical profiles of wind speed and sediment mass flux. Two transport events were measured during moderate onshore to oblique onshore wind conditions. Some general patterns could be distinguished during the transport events.

The research questions and answers related to this objective are:

1. How does the total mass flux of aeolian sand vary over a flat beach with increasing fetch length?

   The fetch effect has been measured across the flat berm where maximum transport was achieved at a distance of 20 to 35 m of the berm lip. The fetch effect is characterized with an overshoot during the oblique onshore wind event (larger available fetch). Sand flux rapidly increases towards a maximum value followed by a decrease to a lower equilibrium value which was approximately half of the maximum mass flux obtained at the critical fetch distance.

2. What is the relationship between the vertical decay coefficient β of the flux profile and the fetch length?

   The evolution of the vertical mass flux profiles downwind causes the exponential decay rate β increase almost linear with increasing fetch length further away from the berm lip, until an equilibrium decay rate is achieved. Traditional transport equations may be used in the

equilibrium state, where saltation is fully developed with sand particles having a relatively stable distribution.

3. What is the influence of a steep cliff and dyke structure?

   Over-steepened velocity profiles and thus large shear velocities were measured at the steep cliff during an onshore wind event compared to the back beach due to flow compression and acceleration. Despite these large shear velocities at the berm lip, not much sand was transported at the lip due to a lack of sand upwind. Based on this study, the steep cliff in front of the human-constructed coastal berm is very sensitive to erosion. Sand being eroded from the berm lip is deposited in front of the dyke and in the trench. This specific beach topography is a general good solution to minimize sand transport to the hinterland, but only serves temporally.

Research Objective E: Studying the effect of shells on aeolian sand transport across a shell-fragmented beach (Chapter 5).

Direct field studies on sand transport rates due to the impact of shells and shell pavement have been limited. This study presents detailed measurements of aeolian sand transport rates, wind conditions, and grain size distributions during a two-day measurement campaign in the winter of 2016 on the natural upper beach of Koksijde, Belgium. The experiment was designed to study the influence of shell pavement (with various types of shells) on sand transport rates during strong and highly oblique onshore wind. Understanding local aeolian transport processes ultimately helps improve predictions of aeolian sediment transport in coastal areas over short to long-term timescales.

The research questions and answers related to this objective are:

1. What is the downwind evolution of the total mass flux of aeolian sand across a shell-fragmented beach?

   The shell pavements consisted of crushed, small and large shells where coverage increased towards the dunes and was highest just in front of the dune foot. During highly oblique onshore wind with a maximum wind speed of 14.6 m/s two experiments were conducted where sand transport rates were measured with vertical sand traps (MWAC). During the two experiments, spatial variations in aeolian sand transport indicated that there was a consistent decrease in transport with distance downwind. Within 162 m, aeolian sand transport decreased by factor 10 from the high waterline in the direction of the dunes. The decrease in mass flux caused for a local deposition of sand

on the upper beach in the form of large rippled sand strips. The sand strips were not entering the dunes directly, but slowly moved across the surface downwind. This accumulation of sand acted as a new source area for aeolian transport to the dunes when the intertidal beach was inundated. However, this region was also very sensitive to wave uprush, whereby the accumulated sand may be removed again from the upper beach.

2. How does the vertical distribution and grain size of airborne sand particles vary across a shell-fragmented beach?

   Aeolian sand transport across the roughness elements did not influence the vertical distribution of sand particles as the decay rate of the vertical flux profiles remained constant. Consequently, the median particle size above the surface remained constant along the transect.

Chapter VII

Future Research

This thesis ends with a chapter about recommendations and open issues for future research. A brief description about improvements for monitoring techniques is given, as well as a description of how a comprehensive predictive model for aeolian sand transport in coastal areas might look like. This chapter is finishing with relevant future research about the influence of climate change on coastal dune behavior.

7.1 Recommendations for future monitoring techniques

Major uncertainties about dune initiation, dune growth, and dune migration on short-term timescales (weeks to months) and long-term timescales (years) are still present today. In future research, measuring the variability in transport limiting factors is equally and/or even more of interest than measuring the varying wind velocities. Especially when long-term sediment transport predictions are considered. Delgado-Fernandez & Davidson-Arnott (2009) presented some techniques to monitor long-term aeolian sediment transport in coastal environments. They used a camera-system to monitor the overall weather and wave conditions, bar welding, beach morphology, and the frequency and magnitude of erosional events. Moreover, rectified images were used to extract moisture maps, beach dimensions, fetch distances and vegetation cover. Smit et al. (2017) also presented a new method to measure spatial-temporal variation in surface moisture with an infrared terrestrial laser scanner. Williams et al. (2018) and Montreuil et al. (2018) presented some new methods to detect aeolian streamers from images. However, given enough resources (i.e. financially), a static terrestrial laser scanner (e.g. time-of-flight-pulse-based Riegl® VZ-2000 LiDAR) with improved methods for measuring morphological and volumetric changes as a result of individual transport events would be a very good technique to measure process dynamics at the meso-scale for the purpose of knowing how coastal dunes grow. It could be installed on a stable weather-proof frame on a high point above the beach. These high spatial-temporal data would help our understanding of coastal processes on land (intertidal and upper beach).

Very few detailed field studies on aeolian sediment transport are available, especially on different locations on the beach and/or dunes. These detailed studies should mainly focus on measuring wind velocities, wind directions, surface shear velocities, bed roughness, and rates of sediment transport. Bed irregularities should be measured over a distance of at least 100 m upstream of the sand traps/wind mast. When measuring the much needed short-term aeolian sediment transport, attention should be paid to instrumentation use. There are various instruments on the market to measure aeolian sediment transport. Most of them are sand traps, impact detectors, and optical sensors. However, there is no consensus of which one is optimal for a typical aeolian study. The use of passive vertical sand traps, like MWAC sand traps, can sometimes be limited because of issues such as scouring around the base, unsteady rotation due to turbulence, blocked inlets, and relatively poor temporal and spatial resolution (Ellis et al., 2009). Furthermore, MWAC sand traps only measure sediment transport from approximately 5 cm above the beach surface. Most of the total transport occurs in the first few centimeters above the surface (Bagnold, 1954). It would be of interest to introduce a self-rotating vertical sand trap that measures the whole transport column from surface to a certain distance above the surface.

It should be acknowledged that alongshore winds have chances of inputting a reasonable amount of sand to the dunes because of wind deflection close to the dune toe (Bauer et al., 2012). This process is not correclty quantified as yet, and it would be interesting to see how many moving bedforms (e.g. mobile sand strips) formed at the upper beach during alongshore winds actually end up welding to the dune toe area.

Instead of using one or two meteorological stations in the study area, vertical wind profiles should be monitored adjacent to a sand trap to measure to spatial-temporal behavior of the wind field. Furthermore, Spies et al. (1995) argued the significance of shear velocity in a blowing sand cloud. The shear velocity is difficult to determine from measured wind profiles when wind-blown sand occurs, especially at high wind velocities (Dong et al., 2003). When wind-blown sand occurs, the wind profile is altered. Usually, it is assumed that estimates of shear velocity are close to the true values. However, it is possible that the actual shear velocities related to the saltating particles vary substantially from the shear velocities, derived from vertical wind profiles due to roughness effects, damping of turbulence, and measurement scatter (Bauer et al., 1992; Li et al., 2010). Furthermore, it is not yet fully clear what is the effective bed roughness for aeolian sand transport (dynamic grain roughness, form-related roughness or both). The influence of moisture content and beach armoring and other bed surface properties (e.g. shells or shell fragments) also appear to be a critical factor in degrading the performance of aeolian models. Future work should be based on designing a workable and predictive model that can account for these influences.

7.2 A comprehensive predictive model for aeolian sand transport

7.2.1 Introduction

To deal with storms, seasonal and decadal variations, restoration and maintenance of coastal beach and dune systems require knowledge of aeolian transport processes for the prediction of system response to wind forces over short to long-term timescales. Accurate aeolian sand transport equations are of utmost importance for modern geomorphology and coastal engineering practices. Many aeolian equations are available for the prediction of the transport of loose grains along a surface of dry and clean sand without vegetation (e.g. Bagnold, 1954; Kawamura, 1951; Zingg, 1953; Owen, 1964; Kadib, 1965; Hsu, 1974; Lettau & Lettau, 1978 and Sørensen, 2004). Most equations are strongly related to a power of the bed-shear velocity (u_*) and to lesser extent to the grain size and composition. One or more empirical coefficients are included based on calibration using data from wind tunnel and field experiments. Although sand transport by wind is easily observable, reliable and accurate data sets of sand transport rates are still scarcely available due to measuring difficulties. Mostly, relatively simple mechanical trapping systems are being used, but reported efficiencies are often below 50%, differing from site to site and sometimes even unknown. Hence, corrections are not always possible resulting in biased calibration data. Using such data sets imply that the calibrated models are inadequate yielding poor model performance. Sherman et al. (1998) and Sherman & Li (2012) have shown that six models substantially overpredict the measured sand transport rates of high-quality data sets. Similar results were obtained by Horikawa et al. (1984) and Dong et al. (2003). Reasons for discrepancies are discussed in detail by Sherman et al. (2013). Important sources of error are the grain size and composition of the bed (uniform versus graded), horizontally non-uniform sand surface conditions related to grain size, relief, crusting and shells, moisture variations and saturation length scales. However, the major source of error most likely is the bed shear velocity and associated bed roughness height. This latter parameter consists of several contributions, being the static and dynamic grain roughness, form-related roughness if bed forms (ripples) are present, and roughness of isolated elements resting on the surface (shells, pebbles, stones, etc.). It is common practice to determine the bed shear velocity from the slope of measured velocity profile data using $\varkappa = 0.4$ (Von Karman coefficient). These shear velocities may be significantly too large as discussed by Li et al (2010). High concentrations of saltating particles may lead to the damping of turbulence which can be expressed as a reduction of the $\varkappa$-coefficient (range of 0.25 to 0.4 based on Li et al (2010)). Similar effects have been extensively observed and described for sediment-laden water flows (van Rijn, 1993). Taking this effect into account, the bed-shear velocities are substantially reduced resulting in smaller predicted

sand transport rates (less overprediction, Sherman et al., 2013). A problem of the methods proposed by Li et al (2010) and Sherman et al. (2013) is that the modified $\varkappa$-coefficient is related to the sand transport rate, which is a priori unknown and thus requiring iterative computations. Another problem of the model application proposed by Sherman et al. (2013) is the use of measured bed shear velocities requiring detailed wind velocity measurements at different levels above the sand surface. Most accurate estimates of the bed-shear velocity even require the use of sophisticated anemometers to measure the instantaneous horizontal and vertical wind velocity components to derive the Reynold stress-term. As such, this method is in no way predictive. In principle for engineering practices, it must be possible to get a reasonable estimate of the aeolian sand transport rate at a particular site based on wind velocity data from a nearby meteorological station and available grain size data from local samples. Yet, such comprehensive predictive model is not available.

7.2.2 General predictive roughness model

The transport of particles by wind occurs in different transport regimes, which depend on the particle size and wind speed. Particles at a flat beach surface are set into motion if the wind speed exceeds the threshold value for initiation of motion. At low wind speed just beyond the threshold condition most particles will move by rolling, sliding and hopping along the sand surface. This transport regime is known as creep and reptation. For increasing wind speeds the particles are lifted from to bed to make a kind of ballistic trajectory which is known as saltating transport, primarily dominated by gravitational and aerodynamical forces. The impact of the saltating particles with the sand surface may result in particle rebounds, but may also mobilize and eject other particles into saltation. Saltating particles may be susceptible to turbulent velocity fluctuations in the near-bed layer, particularly when small-scale bed bedforms (ripples) are present or are developing along the sand surface. The powerful vortices developing in the lee zone behind the ripple crests may intensify the pickup of sand particles resulting in larger transport rates. Small particles ($<$ 150 µm) may be continuously supported by turbulent motions and travel in suspension over longer distances. These processes with creep, reptation, saltation and developing ripples predominantly occur in the lower wind transport regime with wind speeds in the range of 5 to 10 m/s. Ripples will be gradually smoothed out in the upper transport regime with wind speeds larger than about 10 m/s as more and more particles are travelling in suspension (Belly, 1964).

The bed roughness, of relevance, for aeolian sand transport in the lower wind regime with bed forms is different from that in the upper wind regime without bed forms. Four types of bed roughness parameters can be distinguished:

- static grain roughness during low wind speeds with rolling, sliding and hopping particles and is characterized by the larger particles (d_{90}) of the sand surface;

- dynamic grain roughness during wind conditions with saltating particles creating small-scale vortices due to the differences between wind velocity and particle velocity;

- form roughness due to the presence of small-scale bed forms (ripples) creating vortices in the lee zones behind the bed form crests

- additional static roughness due to the larger roughness elements resting on the bed surface creating vortices in their lee zones (shells, stones, debris, etc.).

A predictive sand transport equation for aeolian transport requires the use of a bed-roughness predictor, but it is not yet clear what type of roughness is the dominant factor for sand transport. To compute the sand transport rate, the bed shear velocity (u_*), and thus the bed roughness height (k_s) are required as input parameters. If measured velocity profile data is available, these parameters can be derived from the measured data. However, the shear velocity derived from the slope of the measured velocity profile is not representative for sand transport if bed forms are present. If only one wind velocity from a nearby weather station is available, the bed roughness parameter (k_s) must be predicted and can then be used to compute the bed-shear velocity. Various expressions are available to predict the k_s-value. A major drawback of these equations is that the bed roughness (k_s) is related to u_*, which depends on the bed roughness (k_s) itself. Hence, an iterative method is required to determine the k_s-value. Furthermore, there is a lack of literature on the relation between bed roughness and beach morphology. Attention in future research should be focused on these processes. To extend the knowledge of the bed roughness and sand transport of sandy beaches, wind tunnel and field experiments are required. The effective roughness of a flat sand with and without shells (cover percentage of 3 to 30%) can be studied in a wind tunnel at low wind velocities without sand transport. The dynamic grain roughness of a flat sand bed can be studied by short-duration tests in a wind tunnel at high wind velocities velocity profiles. The form drag of artificially prepared ripples can also be studied in a wind tunnel. Special field studies focusing on the effect of ripples and shells on sand transport are also highly recommended.

7.2.3 Modelling other effects

7.2.3.1 General

A fully predictive model must include the effects of sloping surfaces, limited fetch lengths, varying moisture contents, vegetation and shells. Herein, these effects are sometimes represented by simple coefficients acting on the bed-shear velocity, the threshold velocity or on the sand transport rate. Further research is required to improve and extend the knowledge. Some processes can be studied

in wind tunnels (effect of bed slope, moisture and shells), but other processes can be better studied at field sites (vegetation, saturation). A brief description of these effects is made in the next sections.

7.2.3.2 Adjustment/saturation length scale

Transport conditions (u_* and $u_{*,cr}$) may vary in space due to variations of environmental parameters. As a result, the actual sediment transport rate will often differ from the equilibrium (potential) transport rate. When transport conditions change, the transport rate adjusts/adapts to the new conditions within a certain distance. The distance over which the sediment transport adjusts to new equilibrium conditions is known as the adjustment or saturation length scale (L_{ad}) and depends on the particle size and wind speed. Experiments in wind tunnels and at field sites with dry, loose sand surfaces have shown that the saltation layer development takes place at very short timescales (10 s) (Belly, 1964). During saltation, the average horizontal velocity of the grains may be of the order of 3 to 10 m/s. A spatial change in transport conditions may cause changing mass fluxes over a distance of 30 to 100 m for dry, loose sand. The field work of Davidson-Arnott et al. (2008) at a Canadian beach with sand of 0.26 mm shows an adjustment length (the distance at which the transport reaches a maximum) of about 100 to 150 m. Similar length scales (100 to 150 m) can be derived from the work of Dong et al. (2012). The adjustment length scale of dry sand is different from that of wet sand. Relatively high transport rates were measured by Davidson-Arnott et al. (2008) in conditions with offshore winds when sand supplied from the dry upper beach was transported over a damp, hard surface on the lower foreshore. Thus, the transport rate may exceed that for dry sand if the sand supply comes from a dry upwind zone and the sand particles are transported over a moist and hardpacked surface. These high transport rates are probably caused by the lower drag losses for sand grains impacting with the hard surface. Where surface moisture is very high, some saltating grains may adhere to the surface on impact resulting in smaller transport rates. Where bedforms such as ripples or low dunes are present on a wet sand surface, grains resting on the surface in the lee of the bed forms may become wet resulting in higher threshold values leading to smaller transport rates. In these conditions the transport rate will be smaller than for dry sand.

7.2.3.3 Wind speed acceleration

Wind normal to the beach accelerates along the slope of the foredune and is maximum at the dune crest level. The influence of topography on wind speed is prominent. The speed-up effect increases with height of the foredune. An increase in height from the beach to the dune crest of about 10 m causes an increase in windspeed of about 20% to 40% (Arens et al., 1995) in the case that the wind speed is measured at the beach (reference value). This will result in an increase of the sand-carrying capacity. A further increase in foredune height

> 10 m appears to have limited influence, probably because the increase in height (acceleration) is compensated by an increase in roughness due to the presence of irregularities at the dune crest.

7.2.3.4 Moisture content

Wind-induced sand transport is strongly affected by moisture content and related cohesion. Cohesion between particles increases the surface resistance against erosion (critical shear velocity). Cohesion may result from the presence of moisture, salt, algae, clay, organic matter and calcareous materials. Even low levels of moisture may effectively reduce the transport rate of dry sand. However, intensive rainfall may also increase the sand transport rate by splash effects promoting saltation processes. Moisture content may be the direct result of precipitation, water spray, wave uprush near the water line or capillary action (adhesive forces; surface tension forces). Moisture fraction is generally defined as: mc = mass water of sample/mass dry sand of sample (moisture content is moisture fraction x 100%). Moisture content of a saturated sample can be computed by the expression $mc_{saturated} = [\varepsilon/(1-\varepsilon)][\rho/\rho_s]x100\%$ with ε = porosity factor (0.35-0.45 for sand); ρ = water density ($\cong$ 1000 kg/m^3); ρ_s = sand density ($\cong$ 2650 kg/m^3), yielding $mc_{saturated}$= 20%-30%. Generally, moisture contents are in the range of 0 to 10%, as the pores are not fully saturated with water. Let us assume that a sand particle with diameter D is covered by a thin water film with thickness δ except at the particle contact points; any other pore water is absent. The volume of the water film is: $V_{wf} = 1.33\pi\ [(0.5D+\delta)^3-(0.5D)^3]$ and the mass is: $M_{wf}=\rho V_{wf}$. The volume of the sand particle is: $V_{sand}=1.33\pi(0.5D)^3$ and the mass is $M_{sand}=\rho_s V_{sand}$. The mass ratio of water and dry sand defined as the moisture fraction is: $mc= M_{wf}/M_{sand} = \rho[(0.5D+\delta)^3-(0.5D)^3]/[\rho_s(0.5D)^3]$. Using: D = 200 μm for sand, δ = 0.01D = 2 μm, it follows that: mc $\cong$ 0.025 (2.5%). Thus, a thin water film with thickness equal to 2 μm surrounding a sand particle of 200 μm yields a moisture content of about 2.5%. A water film of 1 μm yields a moisture content of 1%. Dry sand has a moisture content < 0.25% (Han et al., 2011). In conditions with a moisture content > 2.5%, the sand transport rate is strongly reduced to a very small value. In conditions with mc = 10% (near the water line), the surface is so saturated that aeolian transport reduces to almost zero, even under very strong winds. Field experiments (Davidson-Arnott et al., 2008) show that the moisture content at a certain location and thus the critical shear velocity can change rapidly over a period of minutes to hours due to drainage and/or drying by wind and sun. Based on this, the wind-driven sediment transport is highly variable in space and usually intermittent in time.

The field work of Davidson-Arnott et al. (2008) at a Canadian beach with sand of 0.26 mm shows large variations of the critical wind speeds: $U_{wind,cr,min}$ = 5 m/s (lowest wind speed with sediment transport) and $U_{wind,cr,max}$ = 9 m/s (highest wind speed without sediment transport) mainly due to variations of the

moisture content. The mean critical wind speed defined as $0.5(U_{wind,cr,min}+U_{wind,cr,max})$ was found to increase with moisture content (about 30% for a moisture content increasing from 0 to 4%). Han et al., 2009 and Han et al. (2011) studied the effect of moisture content on the critical shear velocity. The effect of moisture is negligibly small for moisture content $< 0.25\%$.

7.2.3.5 Shells

Shells (calcium carbonate) can protect the beach surface against erosion of the sand particles. Van der Wal (1998) studied the effect of shells on the wind-induced transport rate of beach sand. Beach sand samples were taken from 5 sites along the Dutch coast and tested in a wind tunnel. The d_{50} varied in the range of 0.21 to 0.35 mm. The percentage of shells (> 2 mm) varied in the range 1 to 30%. A tray with (length = 1.22 m; width = 0.33 m; height = 0.03 m) was filled with weighed oven-dried sand and placed in the middle of the test section. The sample surface was smoothed and levelled to the tray edges. The wind speed was gradually increased over one minute to about 11 m/s and kept at this speed for another minute. Then, the wind speed was gradually returned to zero over one minute. After the experiment, the sand was reweighed. The percentage of sand blown off during the test was calculated for each of the experiments. The transport rate was reduced by a factor of 1.5 for samples with a percentage of shells of 10% and by a factor of 3 for samples with a percentage of shells of 20% to 30%. Shell pavements were formed during the wind tunnel experiments with shell-rich beach samples. Samples containing very coarse gravels and stones also showed pavement effects. Large percentages of shell are mostly found on the upper part of natural beaches outside the wave action zone and on beaches with nourished sand.

7.2.3.6 Vegetation

The effects of vegetation on wind-blown sand can be described as (Wolfe & Nickling, 1993): i) vegetation extracts momentum from the air flow resulting in larger roughness; ii) vegetation elements are obstacles for saltating sand grains, and iii) vegetation reduces part of the surface where sand transport takes place. Vegetation is herein identified as grass-type plants with a maximum height of about 0.5 m. The shear velocity can be determined from wind velocity measurements outside the roughness layer (say 2 times the plant height) to eliminate the local velocity variations occurring between the plants. Both the shear velocity and overall effective bed roughness will increase due to the presence of the vegetation. Two approaches are possible to account for the effect of vegetation on the sand transport rate by : i) increase of the threshold value as the sand grains are hiding between the vegetation and the application of the total bed-shear velocity for sand transport (Musick & Gilette, 1990; Musick et al., 1993; Raupach et al., 1993), and ii) reduction of bed-shear velocity acting on the sand grains between the vegetation and the application of the standard threshold shear velocity (Raupach, 1992).

7.3 Dune behavior due to climate change

It seems that the dunes along the Belgian coast can grow due to the occurrence of dominant westerly winds (onshore to oblique onshore). The evolution and development of coastal dunes generally depend on sediment supply, beach morphology, vegetation growth, and climate variables such as wind conditions, sea level and wave conditions (Short & Hesp, 1982; Pye, 1990; Hesp, 2002). When one of these factors change, it has the potential to change dune development. Therefore, the influence of climate change will have direct consequences for dune development. The extent to which the Belgian dunes are still stable relative to predicted climate scenarios is something that should be studied in future research. It does illustrate the importance of current research work. For example, Keijsers et al. (2016) studied the effect of climate change on coastal dune evolution in the Netherlands by using a cellular model of dune, beach, and vegetation development. They concluded that sea level rise mainly determines the direction of dune development.

Appendix A

Dune behavior along the Belgian coast

This appendix belongs to Chapter 3, dealing with decadal dune behavior along the Belgian coast. Since 1979, the Belgian government has been monitoring the eastern part of the coastline, and since 1983 the entire coastline by annually or bi-annually surveying cross-shore bathymetric profiles and collecting airborne photogrammetric and, since 1999, airborne Laser Scanner (LiDAR) data (International Marine & Dredging Consultants (IMDC), 2010; Houthuys, 2012). Concerning the Belgian coast, LiDAR data covers the intertidal beach up to the sea-fronting dunes. The Belgian coast is represented by a system of coastal sections adopted by the Flemish government, defined by unchanging boundaries, which are also used in this study (Vandebroek et al., 2017). There are 277 coastal sections, each approximately 250 m wide, where morphology is monitored and surveyed. However, section 1 is located in France and sections 256 to 277 are located in the Netherlands. Hence, Chapter 3 focused on sections 2 to 255.

The dune volume is defined as the volume of sand above the dune foot level and is bounded by fixed vertical planes constituting an unchanging landward limit. The dune foot level along the Belgian coast was defined at +6.89 m TAW (Belgian Ordnance datum). The term "dune volume" has been defined purely based on bounding planes. It dictates that a dune volume can also be calculated in areas with a seawall or with artificially raised touristic berms, where no vegetated dunes are found. It is noted that the landward limit is either positioned at the foot of the seawall or on the top or even at the landward side of the first dune ridge. However, the varying landward reference is not of relevance, given that most morphological changes occur in the area included in the section boundaries.

The figures below give an overview of all the available dune volume data at the Belgian coast per coastal section having vegetated dunes (approximately half of the coast). The solid magenta line indicates the recent dune trend, while the solid red line indicates the dune trend for the entire measuring period. Each figure mentions the section number and distance from the French border. The section width is also given.

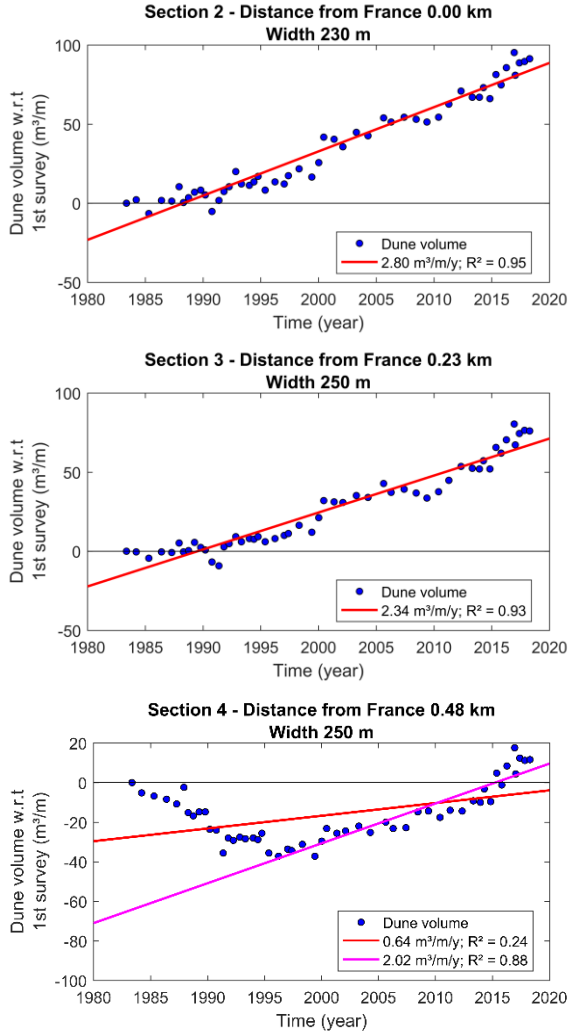

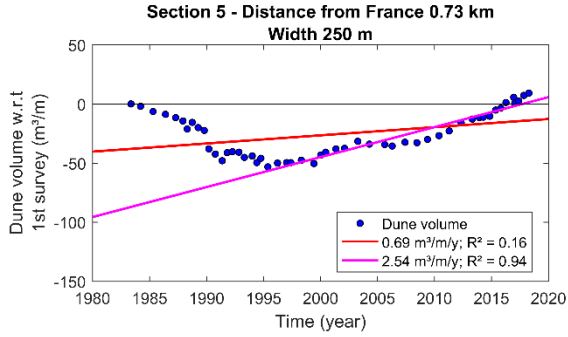
Section 5 - Distance from France 0.73 km
Width 250 m
Dune volume w.r.t 1st survey (m³/m)
Time (year)
Dune volume
0.69 m³/m/y; R² = 0.16
2.54 m³/m/y; R² = 0.94

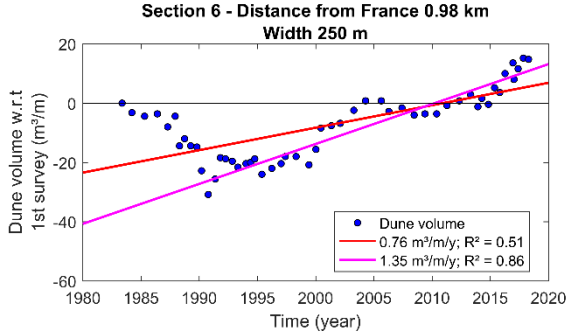
Section 6 - Distance from France 0.98 km
Width 250 m
Dune volume w.r.t 1st survey (m³/m)
Time (year)
Dune volume
0.76 m³/m/y; R² = 0.51
1.35 m³/m/y; R² = 0.86

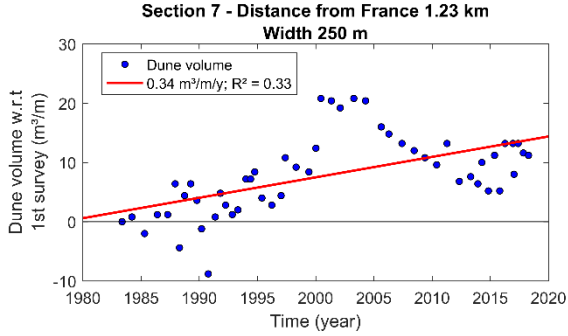
Section 7 - Distance from France 1.23 km
Width 250 m
Dune volume w.r.t 1st survey (m³/m)
Time (year)
Dune volume
0.34 m³/m/y; R² = 0.33

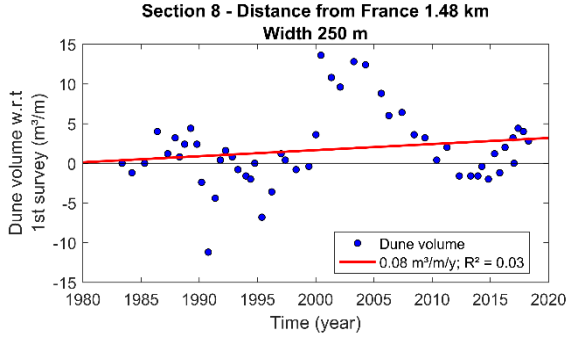
Section 8 - Distance from France 1.48 km
Width 250 m
Dune volume w.r.t 1st survey (m³/m)
Time (year)
Dune volume
0.08 m³/m/y; R² = 0.03

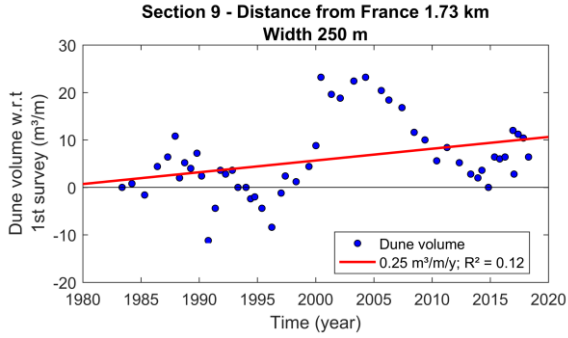
Section 9 - Distance from France 1.73 km
Width 250 m
Dune volume w.r.t 1st survey (m³/m)
Time (year)
Dune volume
0.25 m³/m/y; R² = 0.12

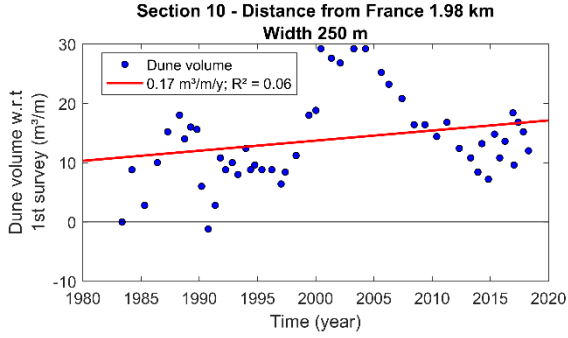
Section 10 - Distance from France 1.98 km
Width 250 m
Dune volume w.r.t 1st survey (m³/m)
Time (year)
Dune volume
0.17 m³/m/y; R² = 0.06

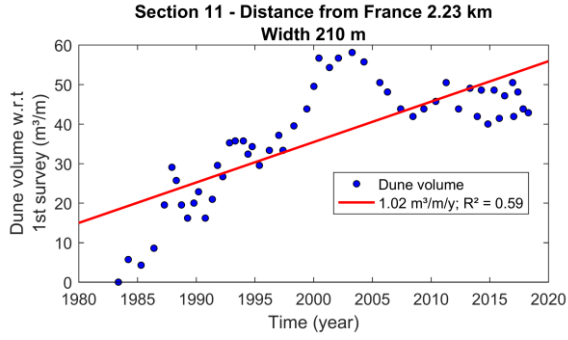
Section 11 - Distance from France 2.23 km
Width 210 m
Dune volume w.r.t 1st survey (m³/m)
Time (year)
Dune volume
1.02 m³/m/y; R² = 0.59

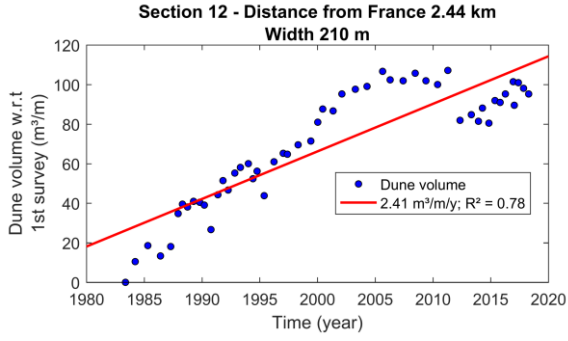
Section 12 - Distance from France 2.44 km
Width 210 m
Dune volume w.r.t 1st survey (m³/m)
Time (year)
Dune volume
2.41 m³/m/y; R² = 0.78

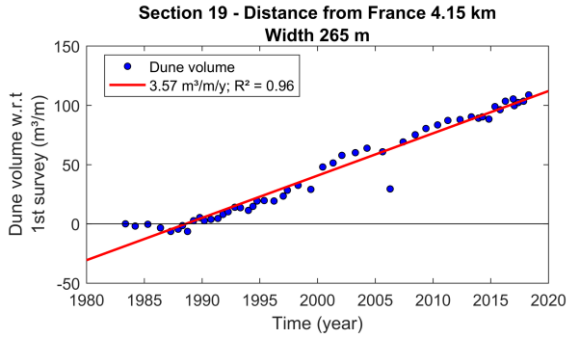
Section 19 - Distance from France 4.15 km
Width 265 m
Dune volume
3.57 m³/m/y; R² = 0.96
Dune volume w.r.t 1st survey (m³/m)
Time (year)

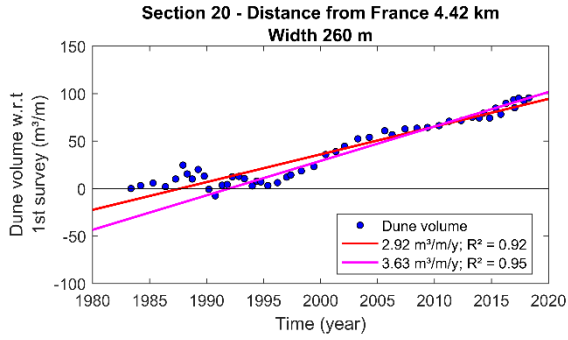
Section 20 - Distance from France 4.42 km
Width 260 m
Dune volume
2.92 m³/m/y; R² = 0.92
3.63 m³/m/y; R² = 0.95
Dune volume w.r.t 1st survey (m³/m)
Time (year)

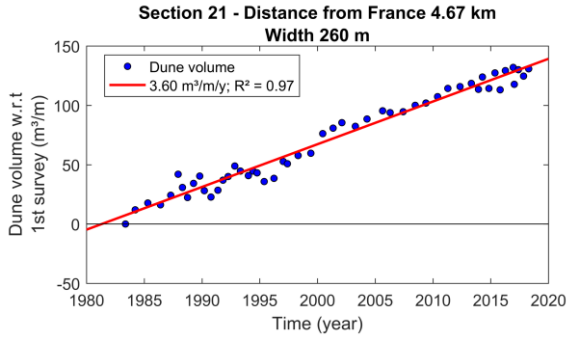
Section 21 - Distance from France 4.67 km
Width 260 m
Dune volume
3.60 m³/m/y; R² = 0.97
Dune volume w.r.t 1st survey (m³/m)
Time (year)

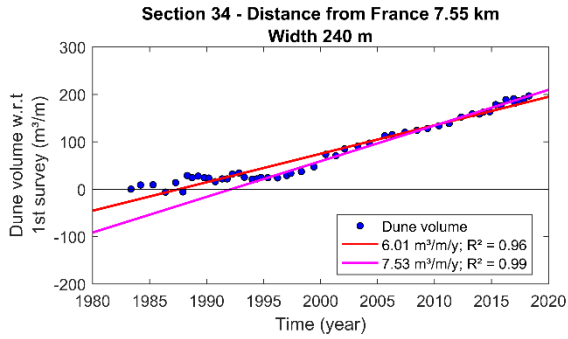
Section 34 - Distance from France 7.55 km
Width 240 m
Dune volume
6.01 m³/m/y; R² = 0.96
7.53 m³/m/y; R² = 0.99
Dune volume w.r.t 1st survey (m³/m)
Time (year)

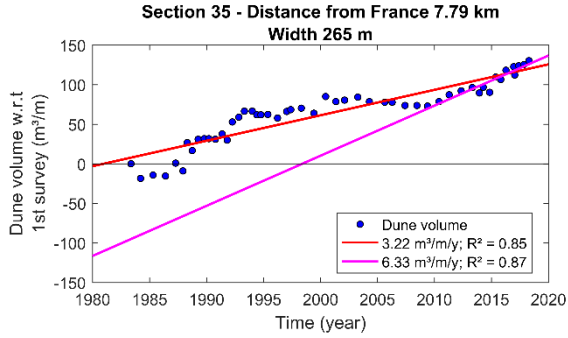
Section 35 - Distance from France 7.79 km
Width 265 m
Dune volume w.r.t 1st survey (m³/m)
Time (year)
Dune volume
3.22 m³/m/y; R² = 0.85
6.33 m³/m/y; R² = 0.87

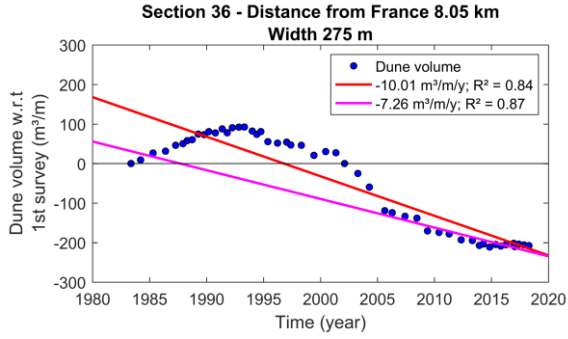
Section 36 - Distance from France 8.05 km
Width 275 m
Dune volume w.r.t 1st survey (m³/m)
Time (year)
Dune volume
-10.01 m³/m/y; R² = 0.84
-7.26 m³/m/y; R² = 0.87

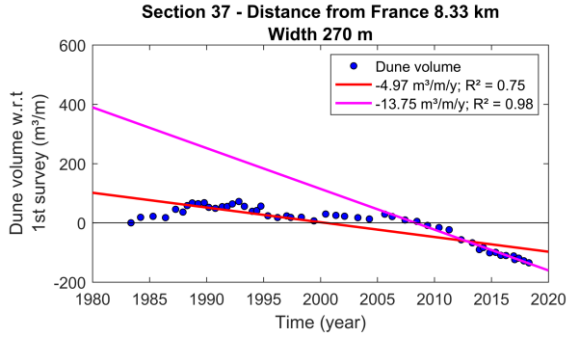
Section 37 - Distance from France 8.33 km
Width 270 m
Dune volume w.r.t 1st survey (m³/m)
Time (year)
Dune volume
-4.97 m³/m/y; R² = 0.75
-13.75 m³/m/y; R² = 0.98

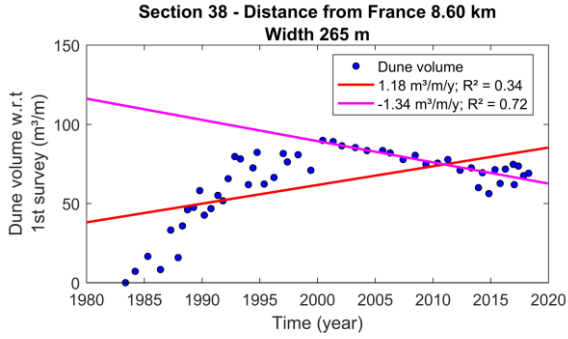
Section 38 - Distance from France 8.60 km
Width 265 m
Dune volume w.r.t 1st survey (m³/m)
Time (year)
Dune volume
1.18 m³/m/y; R² = 0.34
-1.34 m³/m/y; R² = 0.72

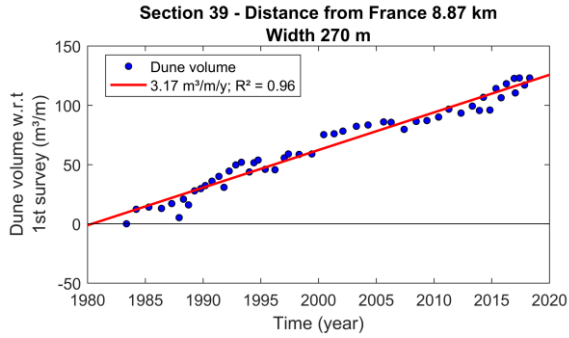
Section 39 - Distance from France 8.87 km
Width 270 m
Dune volume
3.17 m³/m/y; R² = 0.96
Dune volume w.r.t 1st survey (m³/m)
Time (year)

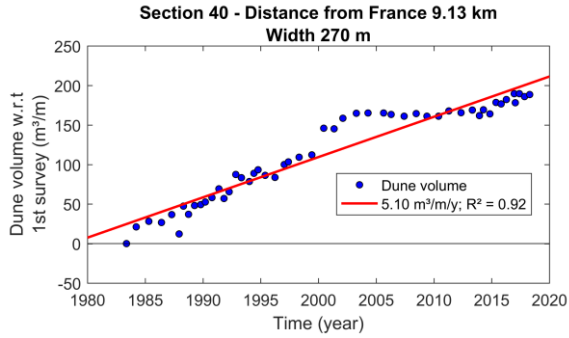
Section 40 - Distance from France 9.13 km
Width 270 m
Dune volume
5.10 m³/m/y; R² = 0.92
Dune volume w.r.t 1st survey (m³/m)
Time (year)

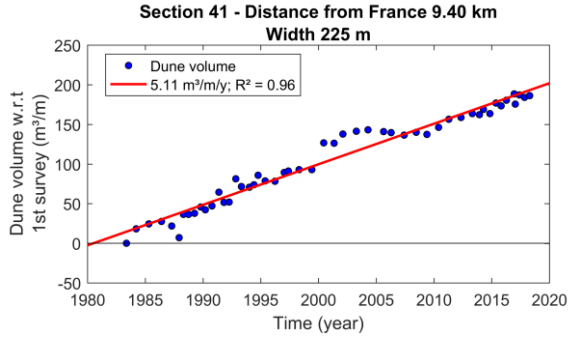
Section 41 - Distance from France 9.40 km
Width 225 m
Dune volume
5.11 m³/m/y; R² = 0.96
Dune volume w.r.t 1st survey (m³/m)
Time (year)

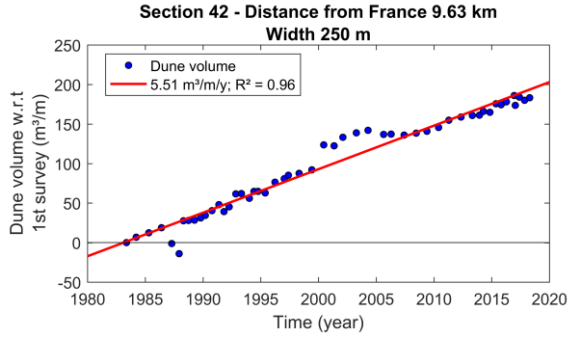
Section 42 - Distance from France 9.63 km
Width 250 m
Dune volume
5.51 m³/m/y; R² = 0.96
Dune volume w.r.t 1st survey (m³/m)
Time (year)

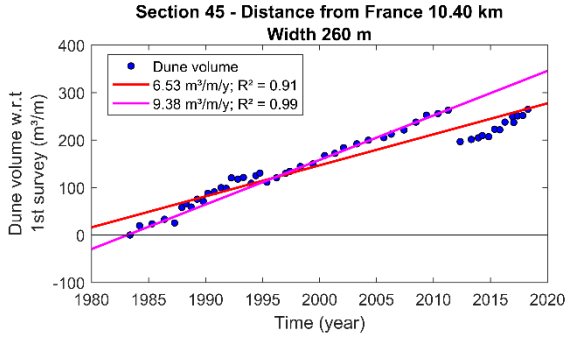
Section 45 - Distance from France 10.40 km
Width 260 m
Dune volume
6.53 m³/m/y; R² = 0.91
9.38 m³/m/y; R² = 0.99
Dune volume w.r.t 1st survey (m³/m)
Time (year)

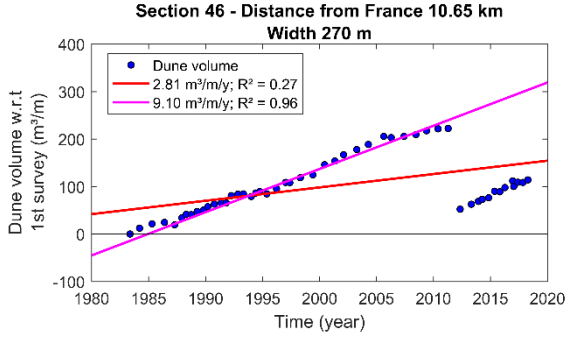
Section 46 - Distance from France 10.65 km
Width 270 m
Dune volume
2.81 m³/m/y; R² = 0.27
9.10 m³/m/y; R² = 0.96
Dune volume w.r.t 1st survey (m³/m)
Time (year)

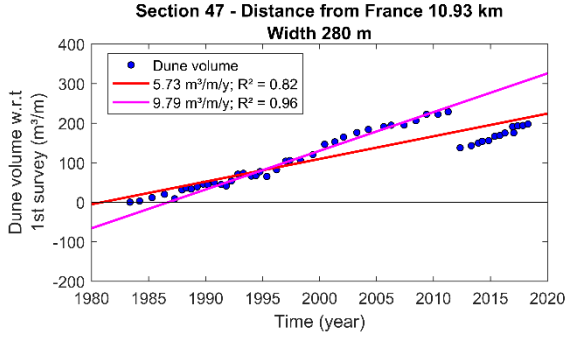
Section 47 - Distance from France 10.93 km
Width 280 m
Dune volume
5.73 m³/m/y; R² = 0.82
9.79 m³/m/y; R² = 0.96
Dune volume w.r.t 1st survey (m³/m)
Time (year)

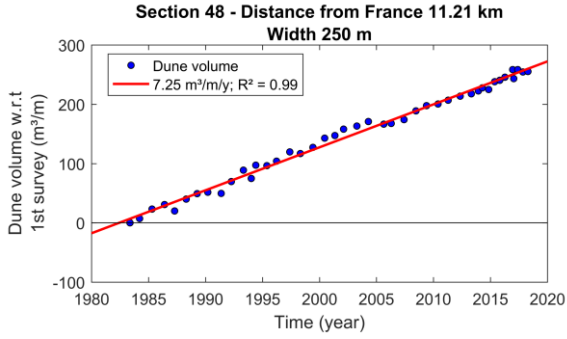
Section 48 - Distance from France 11.21 km
Width 250 m
Dune volume
7.25 m³/m/y; R² = 0.99
Dune volume w.r.t 1st survey (m³/m)
Time (year)

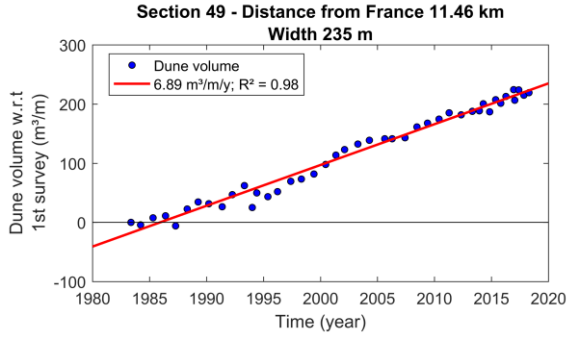
Section 49 - Distance from France 11.46 km
Width 235 m
Dune volume
6.89 m³/m/y; R² = 0.98
Dune volume w.r.t 1st survey (m³/m)
Time (year)

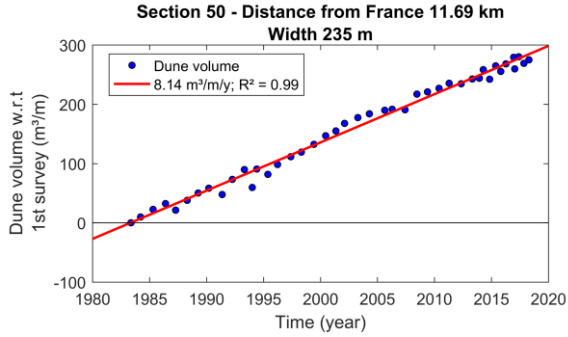
Section 50 - Distance from France 11.69 km
Width 235 m
Dune volume
8.14 m³/m/y; R² = 0.99
Dune volume w.r.t 1st survey (m³/m)
Time (year)

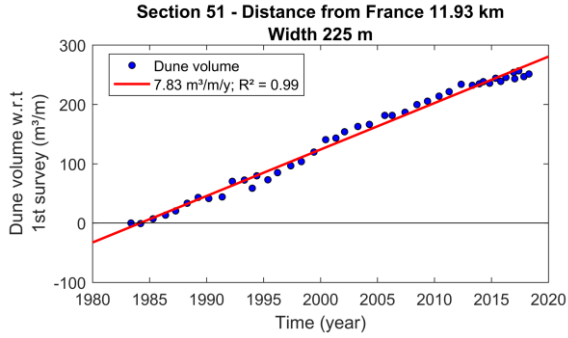
Section 51 - Distance from France 11.93 km
Width 225 m
Dune volume
7.83 m³/m/y; R² = 0.99
Dune volume w.r.t 1st survey (m³/m)
Time (year)

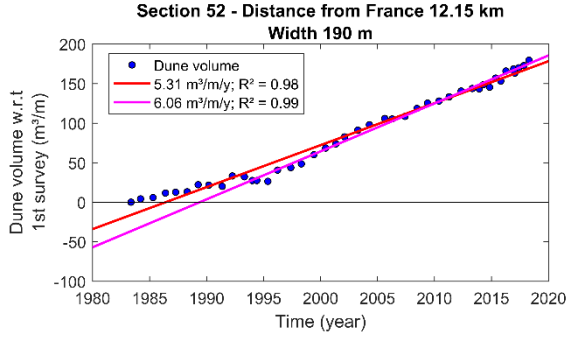
Section 52 - Distance from France 12.15 km
Width 190 m
Dune volume
5.31 m³/m/y; R² = 0.98
6.06 m³/m/y; R² = 0.99
Dune volume w.r.t 1st survey (m³/m)
Time (year)

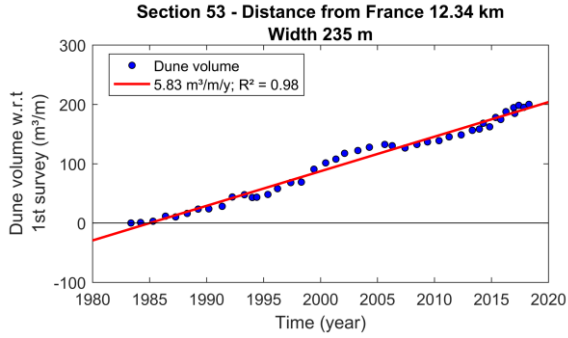
Section 53 - Distance from France 12.34 km
Width 235 m
Dune volume
5.83 m³/m/y; R² = 0.98
Dune volume w.r.t 1st survey (m³/m)
Time (year)

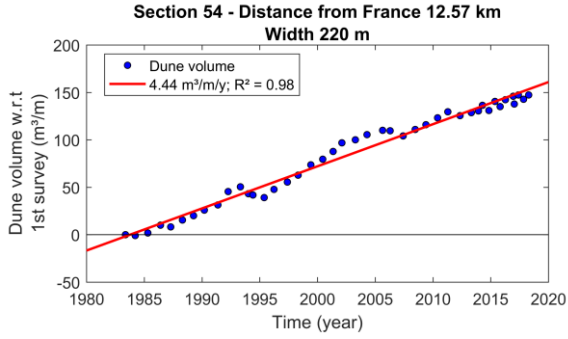
Section 54 - Distance from France 12.57 km
Width 220 m
Dune volume
4.44 m³/m/y; R² = 0.98
Dune volume w.r.t 1st survey (m³/m)
Time (year)

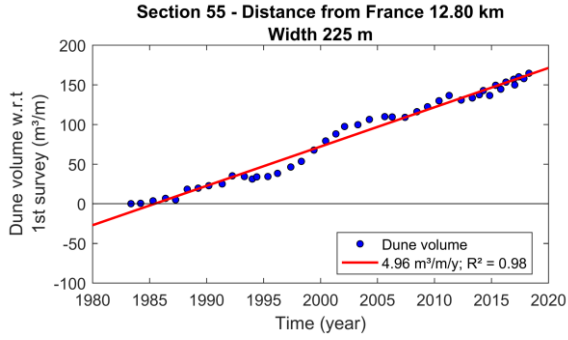
Section 55 - Distance from France 12.80 km
Width 225 m
Dune volume
4.96 m³/m/y; R² = 0.98
Dune volume w.r.t 1st survey (m³/m)
Time (year)

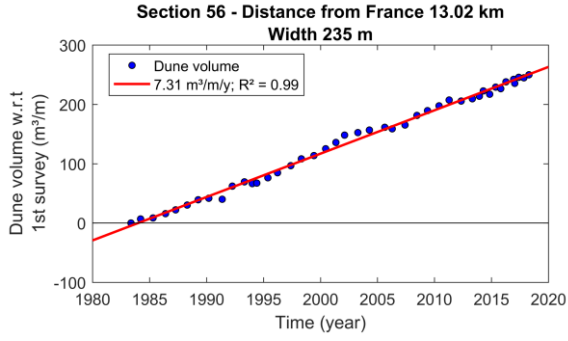
Section 56 - Distance from France 13.02 km
Width 235 m
Dune volume
7.31 m³/m/y; R² = 0.99
Dune volume w.r.t 1st survey (m³/m)
Time (year)

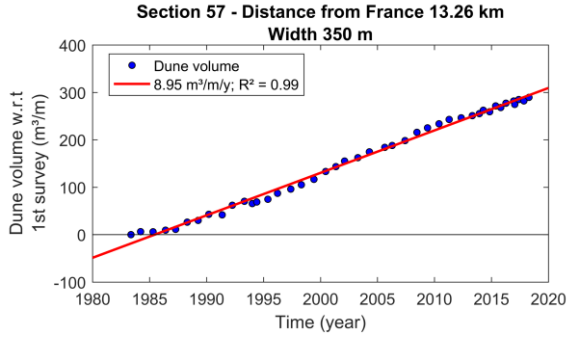
Section 57 - Distance from France 13.26 km
Width 350 m
Dune volume
8.95 m³/m/y; R² = 0.99
Dune volume w.r.t 1st survey (m³/m)
Time (year)

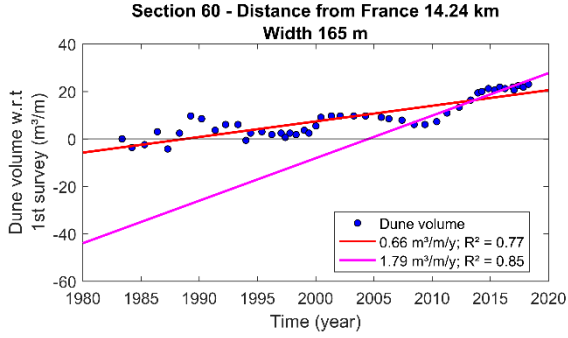
Section 60 - Distance from France 14.24 km
Width 165 m
Dune volume
0.66 m³/m/y; R² = 0.77
1.79 m³/m/y; R² = 0.85
Dune volume w.r.t 1st survey (m³/m)
Time (year)

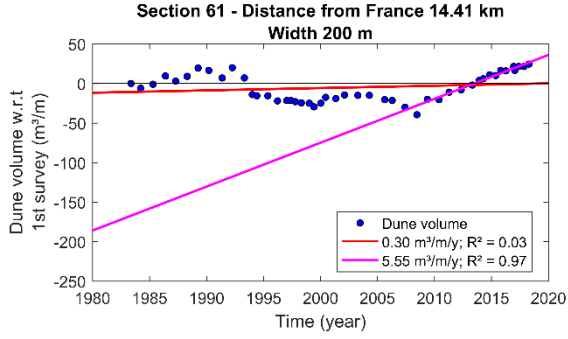
Section 61 - Distance from France 14.41 km
Width 200 m
Dune volume
0.30 m³/m/y; R² = 0.03
5.55 m³/m/y; R² = 0.97
Dune volume w.r.t 1st survey (m³/m)
Time (year)

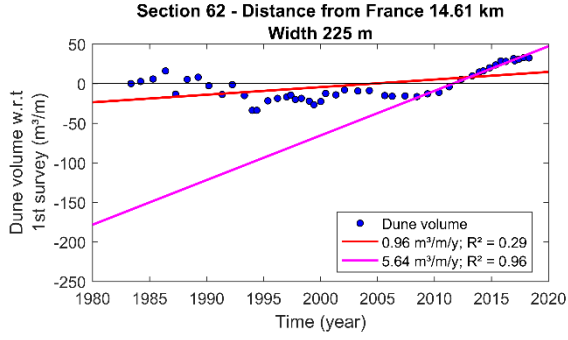
Section 62 - Distance from France 14.61 km
Width 225 m
Dune volume
0.96 m³/m/y; R² = 0.29
5.64 m³/m/y; R² = 0.96
Dune volume w.r.t 1st survey (m³/m)
Time (year)

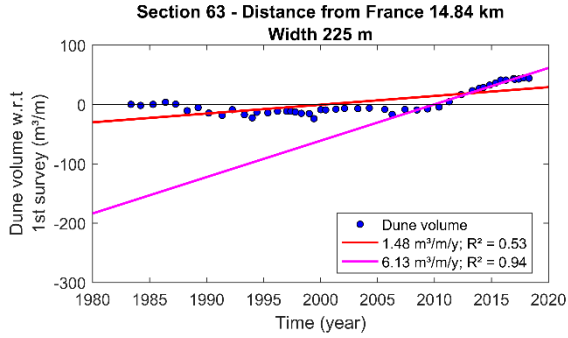
Section 63 - Distance from France 14.84 km
Width 225 m
Dune volume w.r.t 1st survey (m³/m)
Time (year)
Dune volume
1.48 m³/m/y; R² = 0.53
6.13 m³/m/y; R² = 0.94

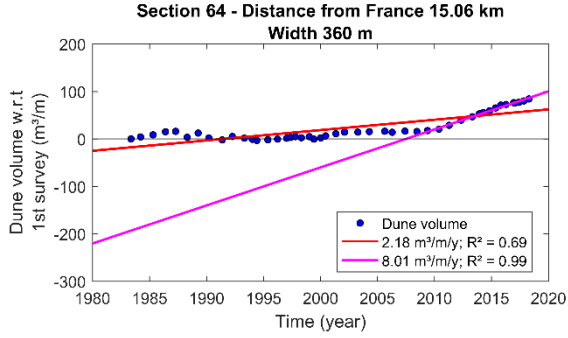
Section 64 - Distance from France 15.06 km
Width 360 m
Dune volume w.r.t 1st survey (m³/m)
Time (year)
Dune volume
2.18 m³/m/y; R² = 0.69
8.01 m³/m/y; R² = 0.99

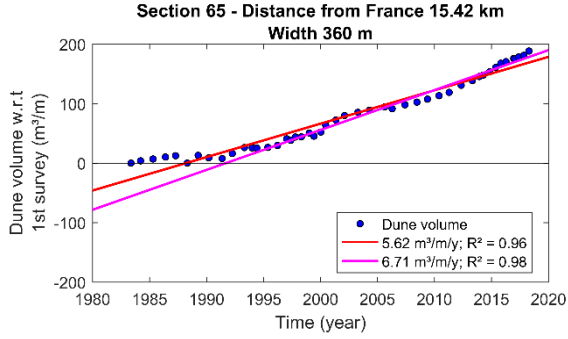
Section 65 - Distance from France 15.42 km
Width 360 m
Dune volume w.r.t 1st survey (m³/m)
Time (year)
Dune volume
5.62 m³/m/y; R² = 0.96
6.71 m³/m/y; R² = 0.98

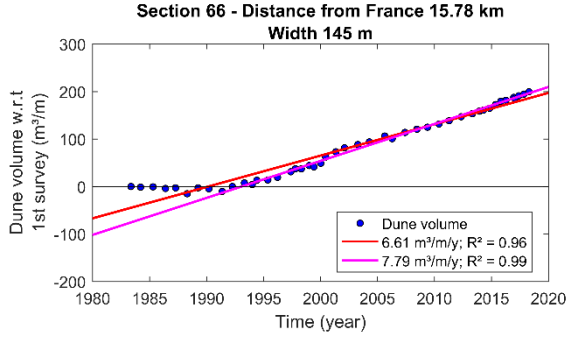
Section 66 - Distance from France 15.78 km
Width 145 m
Dune volume w.r.t 1st survey (m³/m)
Time (year)
Dune volume
6.61 m³/m/y; R² = 0.96
7.79 m³/m/y; R² = 0.99

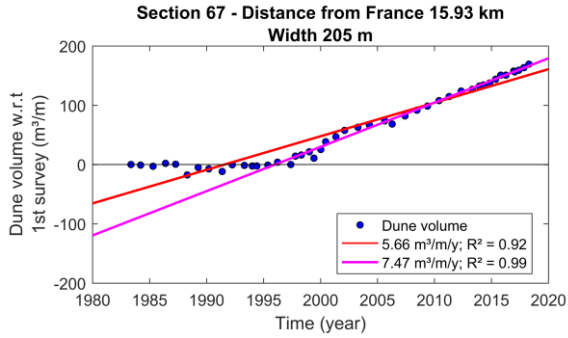
Section 67 - Distance from France 15.93 km
Width 205 m
Dune volume w.r.t 1st survey (m³/m)
Time (year)
Dune volume
5.66 m³/m/y; R² = 0.92
7.47 m³/m/y; R² = 0.99

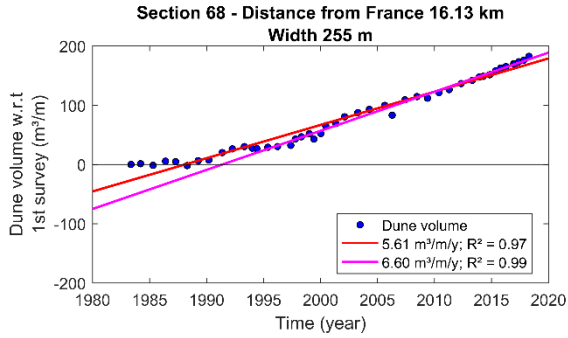
Section 68 - Distance from France 16.13 km
Width 255 m
Dune volume w.r.t 1st survey (m³/m)
Time (year)
Dune volume
5.61 m³/m/y; R² = 0.97
6.60 m³/m/y; R² = 0.99

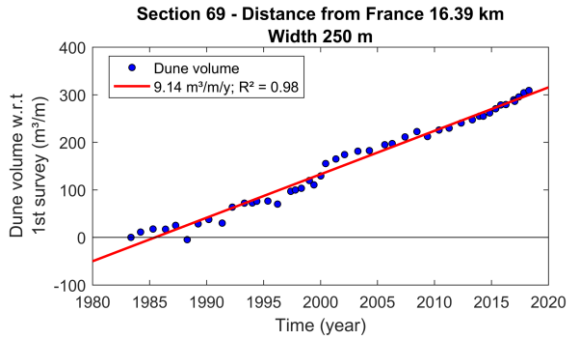
Section 69 - Distance from France 16.39 km
Width 250 m
Dune volume w.r.t 1st survey (m³/m)
Time (year)
Dune volume
9.14 m³/m/y; R² = 0.98

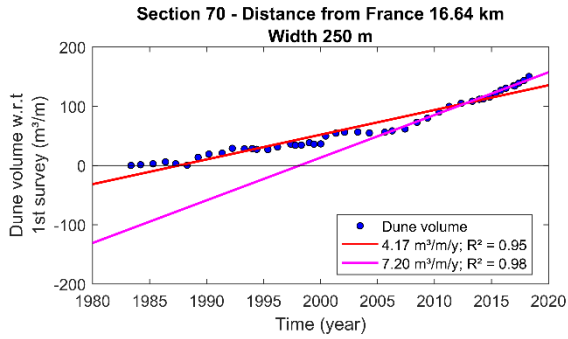
Section 70 - Distance from France 16.64 km
Width 250 m
Dune volume w.r.t 1st survey (m³/m)
Time (year)
Dune volume
4.17 m³/m/y; R² = 0.95
7.20 m³/m/y; R² = 0.98

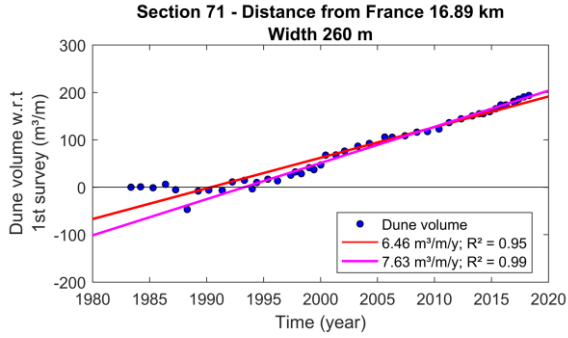
Section 71 - Distance from France 16.89 km
Width 260 m
Dune volume w.r.t 1st survey (m³/m)
Time (year)
Dune volume
6.46 m³/m/y; R² = 0.95
7.63 m³/m/y; R² = 0.99

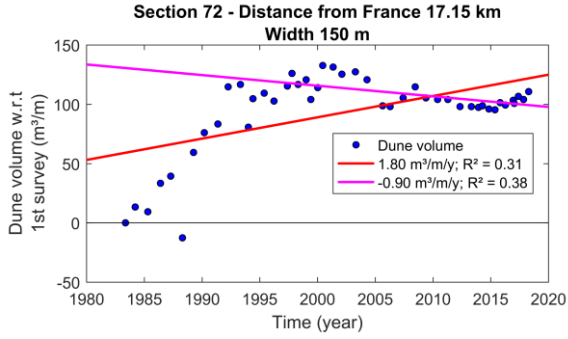
Section 72 - Distance from France 17.15 km
Width 150 m
Dune volume w.r.t 1st survey (m³/m)
Time (year)
Dune volume
1.80 m³/m/y; R² = 0.31
-0.90 m³/m/y; R² = 0.38

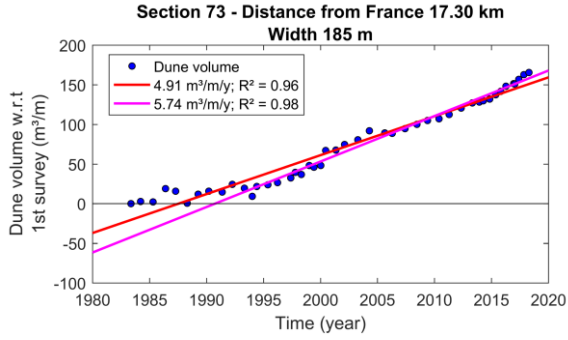
Section 73 - Distance from France 17.30 km
Width 185 m
Dune volume w.r.t 1st survey (m³/m)
Time (year)
Dune volume
4.91 m³/m/y; R² = 0.96
5.74 m³/m/y; R² = 0.98

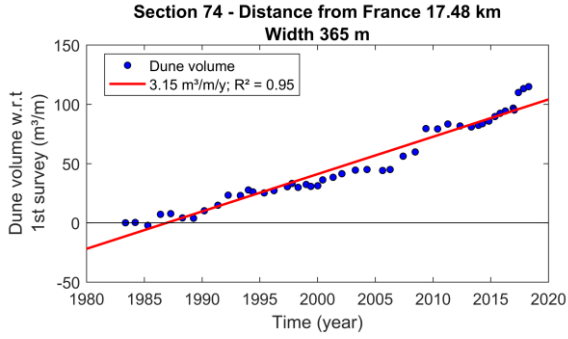
Section 74 - Distance from France 17.48 km
Width 365 m
Dune volume w.r.t 1st survey (m³/m)
Time (year)
Dune volume
3.15 m³/m/y; R² = 0.95

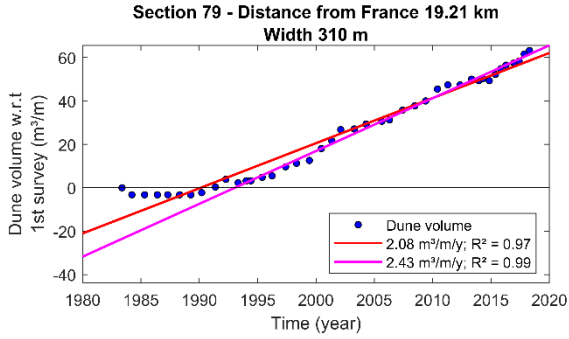
Section 79 - Distance from France 19.21 km
Width 310 m
Dune volume w.r.t 1st survey (m³/m)
Time (year)
Dune volume
2.08 m³/m/y; R² = 0.97
2.43 m³/m/y; R² = 0.99

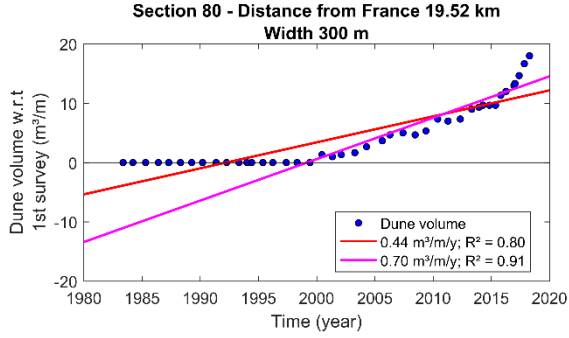
Section 80 - Distance from France 19.52 km
Width 300 m
Dune volume w.r.t 1st survey (m³/m)
Time (year)
Dune volume
0.44 m³/m/y; R² = 0.80
0.70 m³/m/y; R² = 0.91

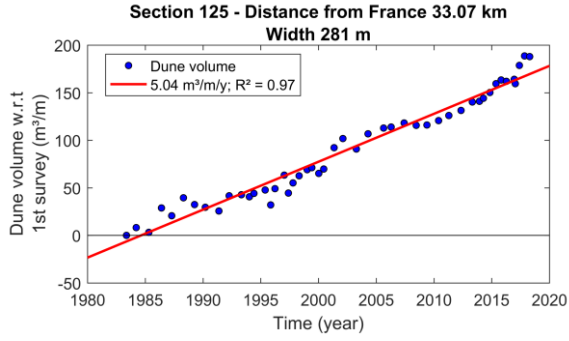
Section 125 - Distance from France 33.07 km
Width 281 m
Dune volume w.r.t 1st survey (m³/m)
Time (year)
Dune volume
5.04 m³/m/y; R² = 0.97

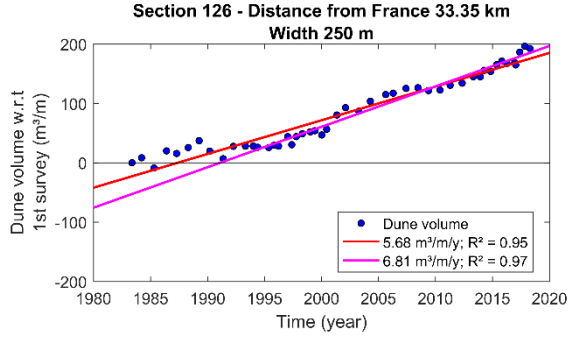
Section 126 - Distance from France 33.35 km
Width 250 m
Dune volume w.r.t 1st survey (m³/m)
Time (year)
Dune volume
5.68 m³/m/y; R² = 0.95
6.81 m³/m/y; R² = 0.97

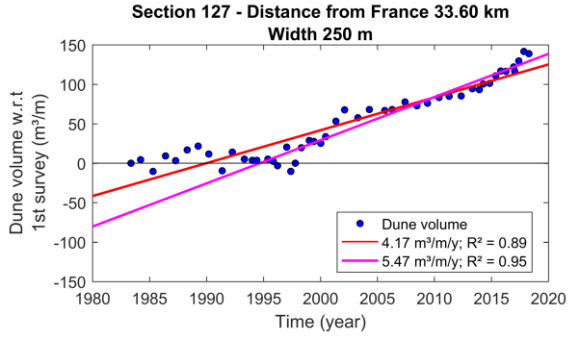
Section 127 - Distance from France 33.60 km
Width 250 m
Dune volume w.r.t 1st survey (m³/m)
Time (year)
Dune volume
4.17 m³/m/y; R² = 0.89
5.47 m³/m/y; R² = 0.95

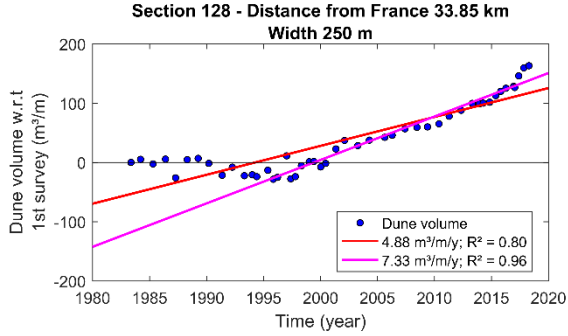
Section 128 - Distance from France 33.85 km
Width 250 m
Dune volume w.r.t 1st survey (m³/m)
Time (year)
Dune volume
4.88 m³/m/y; R² = 0.80
7.33 m³/m/y; R² = 0.96

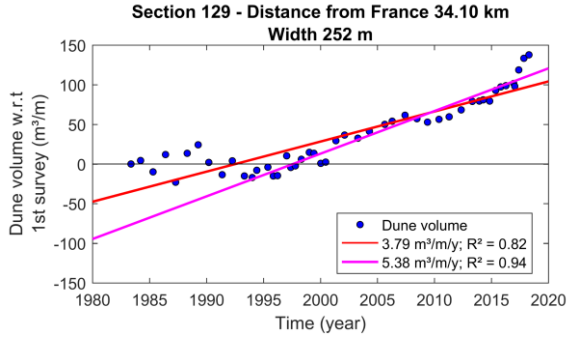
Section 129 - Distance from France 34.10 km
Width 252 m
Dune volume w.r.t 1st survey (m³/m)
Time (year)
Dune volume
3.79 m³/m/y; R² = 0.82
5.38 m³/m/y; R² = 0.94

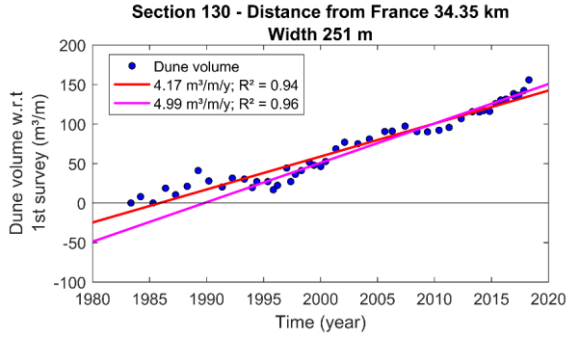
Section 130 - Distance from France 34.35 km
Width 251 m
Dune volume w.r.t 1st survey (m³/m)
Time (year)
Dune volume
4.17 m³/m/y; R² = 0.94
4.99 m³/m/y; R² = 0.96

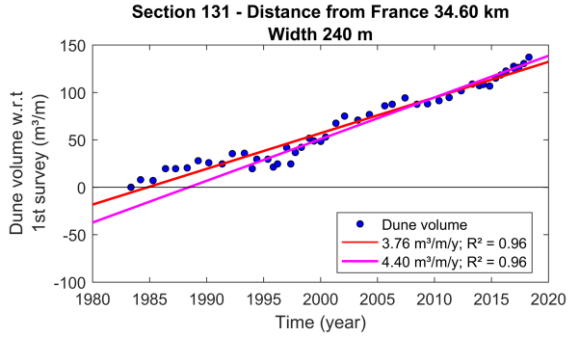
Section 131 - Distance from France 34.60 km
Width 240 m
Dune volume w.r.t 1st survey (m³/m)
Time (year)
Dune volume
3.76 m³/m/y; R² = 0.96
4.40 m³/m/y; R² = 0.96

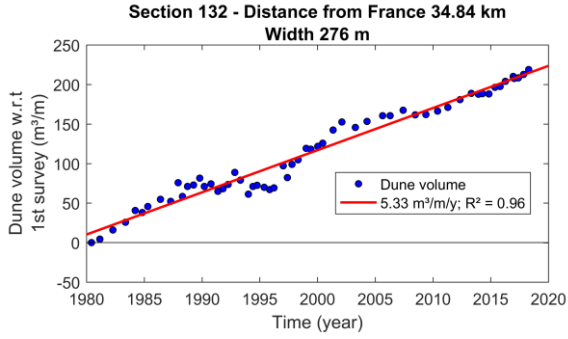
Section 132 - Distance from France 34.84 km
Width 276 m
Dune volume w.r.t 1st survey (m³/m)
Time (year)
Dune volume
5.33 m³/m/y; R² = 0.96

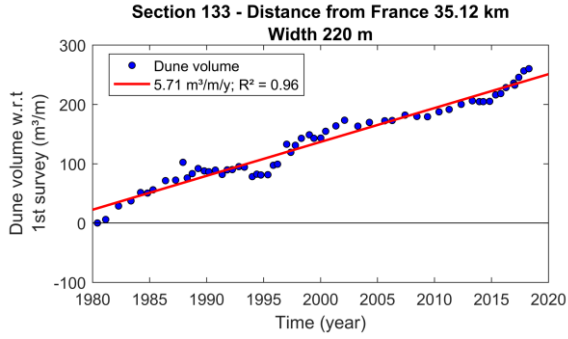
Section 133 - Distance from France 35.12 km
Width 220 m
Dune volume w.r.t 1st survey (m³/m)
Time (year)
Dune volume
5.71 m³/m/y; R² = 0.96

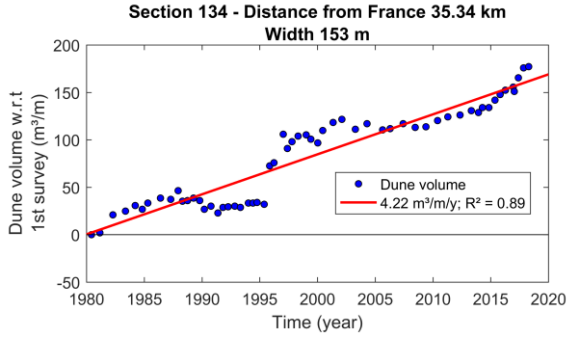
Section 134 - Distance from France 35.34 km
Width 153 m
Dune volume w.r.t 1st survey (m³/m)
Time (year)
Dune volume
4.22 m³/m/y; R² = 0.89

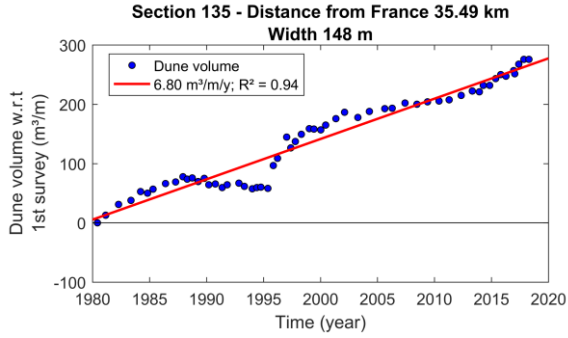
Section 135 - Distance from France 35.49 km
Width 148 m
Dune volume
6.80 m³/m/y; R² = 0.94
Dune volume w.r.t 1st survey (m³/m)
Time (year)

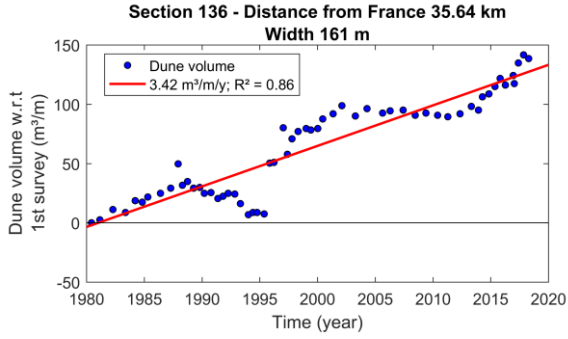
Section 136 - Distance from France 35.64 km
Width 161 m
Dune volume
3.42 m³/m/y; R² = 0.86
Dune volume w.r.t 1st survey (m³/m)
Time (year)

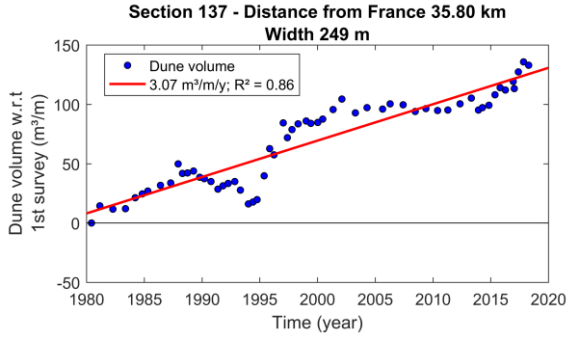
Section 137 - Distance from France 35.80 km
Width 249 m
Dune volume
3.07 m³/m/y; R² = 0.86
Dune volume w.r.t 1st survey (m³/m)
Time (year)

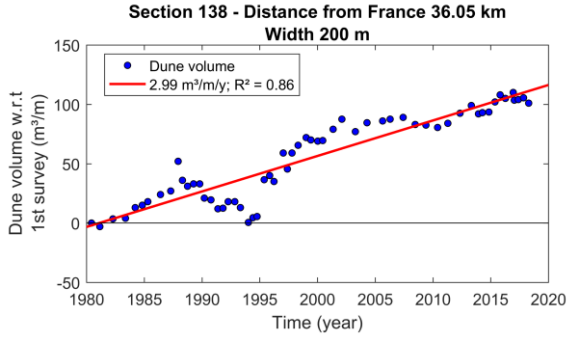
Section 138 - Distance from France 36.05 km
Width 200 m
Dune volume
2.99 m³/m/y; R² = 0.86
Dune volume w.r.t 1st survey (m³/m)
Time (year)

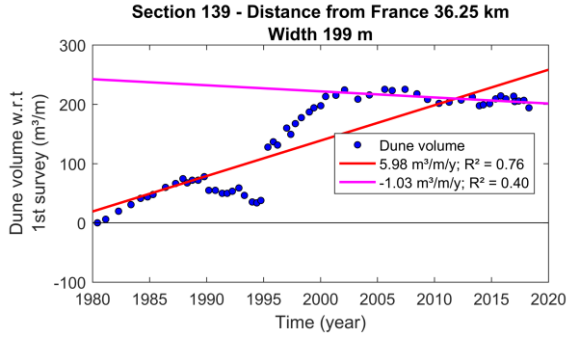
Section 139 - Distance from France 36.25 km
Width 199 m
Dune volume w.r.t 1st survey (m³/m)
Time (year)
Dune volume
5.98 m³/m/y; R² = 0.76
-1.03 m³/m/y; R² = 0.40

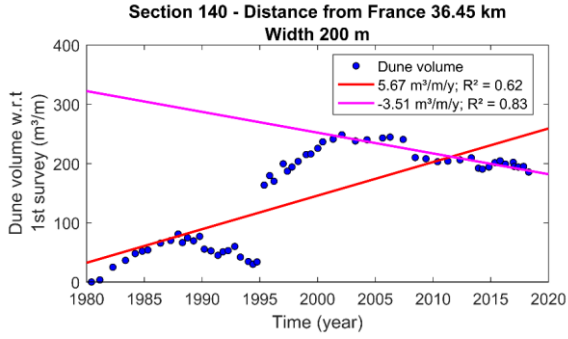
Section 140 - Distance from France 36.45 km
Width 200 m
Dune volume w.r.t 1st survey (m³/m)
Time (year)
Dune volume
5.67 m³/m/y; R² = 0.62
-3.51 m³/m/y; R² = 0.83

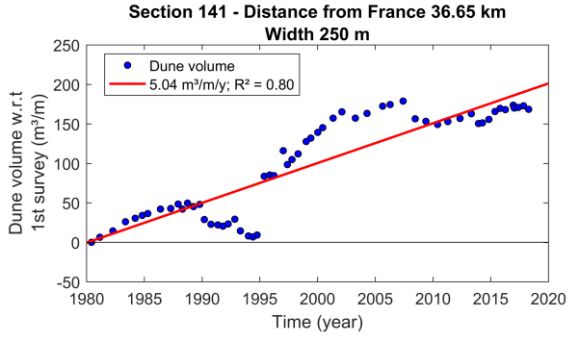
Section 141 - Distance from France 36.65 km
Width 250 m
Dune volume w.r.t 1st survey (m³/m)
Time (year)
Dune volume
5.04 m³/m/y; R² = 0.80

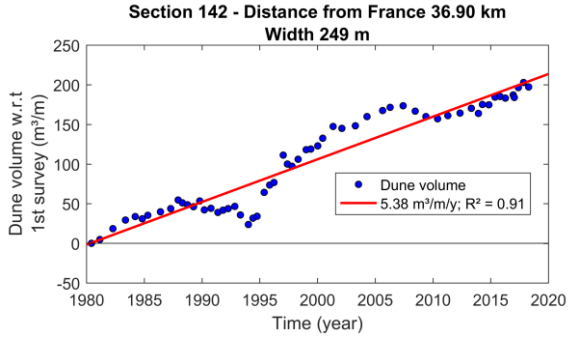
Section 142 - Distance from France 36.90 km
Width 249 m
Dune volume w.r.t 1st survey (m³/m)
Time (year)
Dune volume
5.38 m³/m/y; R² = 0.91

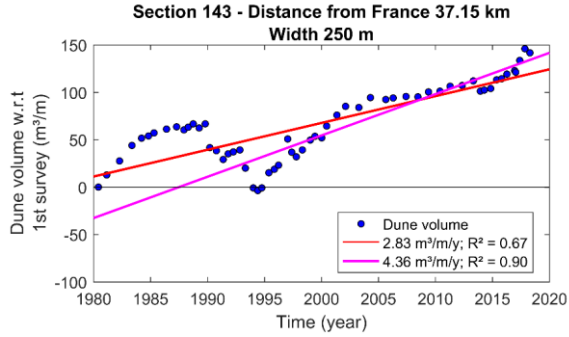
Section 143 - Distance from France 37.15 km
Width 250 m
Dune volume w.r.t 1st survey (m³/m)
Time (year)
Dune volume
2.83 m³/m/y; R² = 0.67
4.36 m³/m/y; R² = 0.90

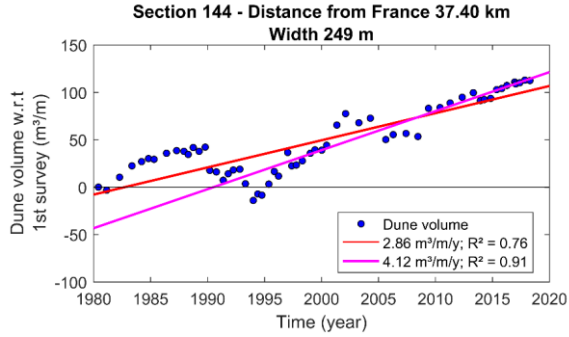
Section 144 - Distance from France 37.40 km
Width 249 m
Dune volume w.r.t 1st survey (m³/m)
Time (year)
Dune volume
2.86 m³/m/y; R² = 0.76
4.12 m³/m/y; R² = 0.91

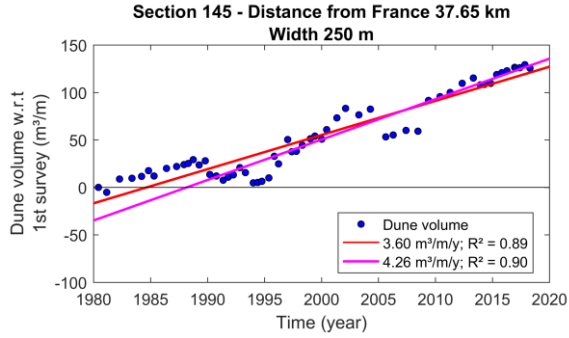
Section 145 - Distance from France 37.65 km
Width 250 m
Dune volume w.r.t 1st survey (m³/m)
Time (year)
Dune volume
3.60 m³/m/y; R² = 0.89
4.26 m³/m/y; R² = 0.90

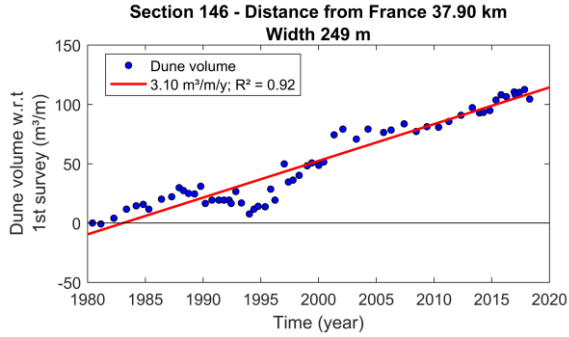
Section 146 - Distance from France 37.90 km
Width 249 m
Dune volume w.r.t 1st survey (m³/m)
Time (year)
Dune volume
3.10 m³/m/y; R² = 0.92

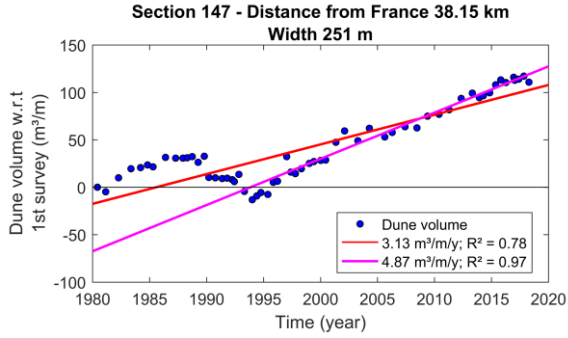
Section 147 - Distance from France 38.15 km
Width 251 m
Dune volume w.r.t 1st survey (m³/m)
Time (year)
Dune volume
3.13 m³/m/y; R² = 0.78
4.87 m³/m/y; R² = 0.97

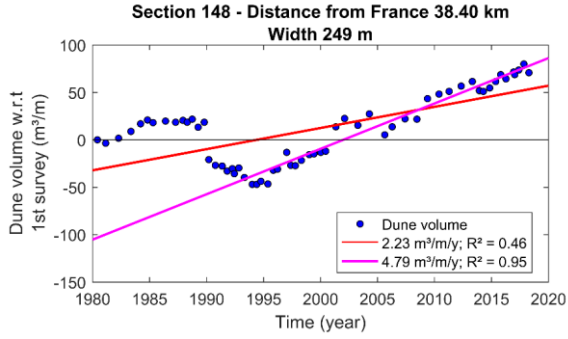
Section 148 - Distance from France 38.40 km
Width 249 m
Dune volume w.r.t 1st survey (m³/m)
Time (year)
Dune volume
2.23 m³/m/y; R² = 0.46
4.79 m³/m/y; R² = 0.95

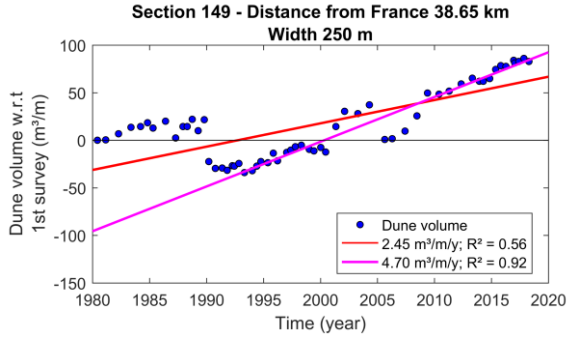
Section 149 - Distance from France 38.65 km
Width 250 m
Dune volume w.r.t 1st survey (m³/m)
Time (year)
Dune volume
2.45 m³/m/y; R² = 0.56
4.70 m³/m/y; R² = 0.92

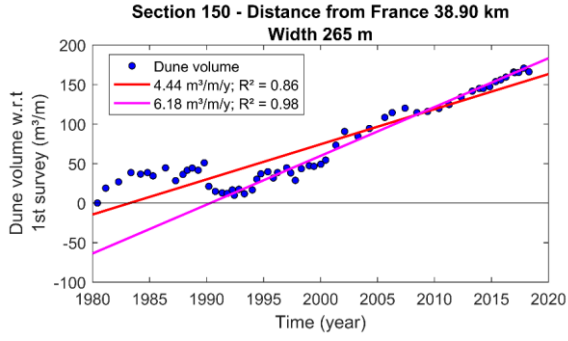
Section 150 - Distance from France 38.90 km
Width 265 m
Dune volume w.r.t 1st survey (m³/m)
Time (year)
Dune volume
4.44 m³/m/y; R² = 0.86
6.18 m³/m/y; R² = 0.98

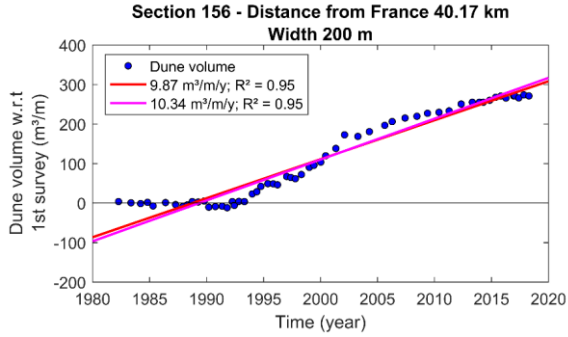
Section 156 - Distance from France 40.17 km
Width 200 m
Dune volume
9.87 m³/m/y; R² = 0.95
10.34 m³/m/y; R² = 0.95
Dune volume w.r.t 1st survey (m³/m)
Time (year)

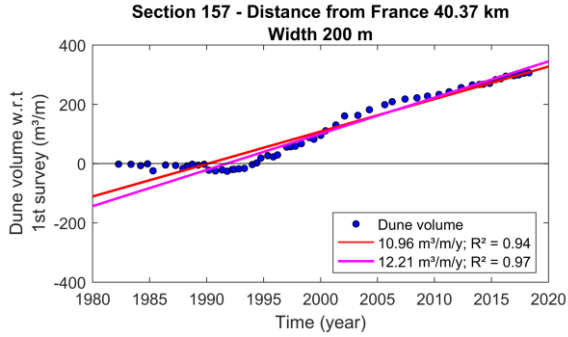
Section 157 - Distance from France 40.37 km
Width 200 m
Dune volume
10.96 m³/m/y; R² = 0.94
12.21 m³/m/y; R² = 0.97
Dune volume w.r.t 1st survey (m³/m)
Time (year)

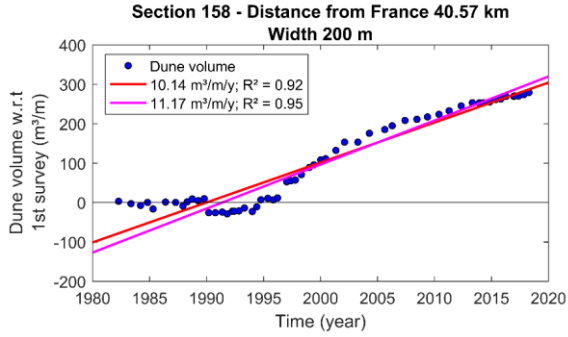
Section 158 - Distance from France 40.57 km
Width 200 m
Dune volume
10.14 m³/m/y; R² = 0.92
11.17 m³/m/y; R² = 0.95
Dune volume w.r.t 1st survey (m³/m)
Time (year)

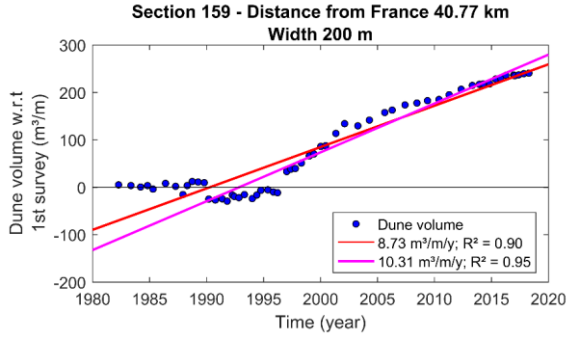
Section 159 - Distance from France 40.77 km
Width 200 m
Dune volume
8.73 m³/m/y; R² = 0.90
10.31 m³/m/y; R² = 0.95
Dune volume w.r.t 1st survey (m³/m)
Time (year)

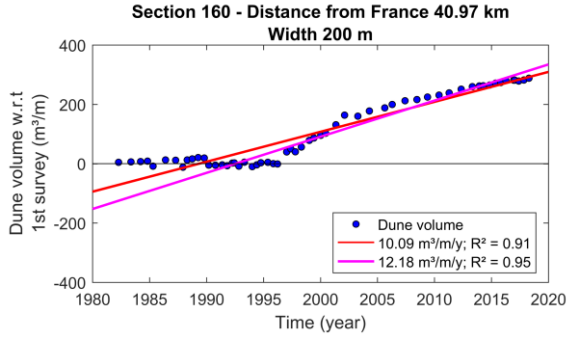
Section 160 - Distance from France 40.97 km
Width 200 m
Dune volume w.r.t 1st survey (m³/m)
Time (year)
Dune volume
10.09 m³/m/y; R² = 0.91
12.18 m³/m/y; R² = 0.95

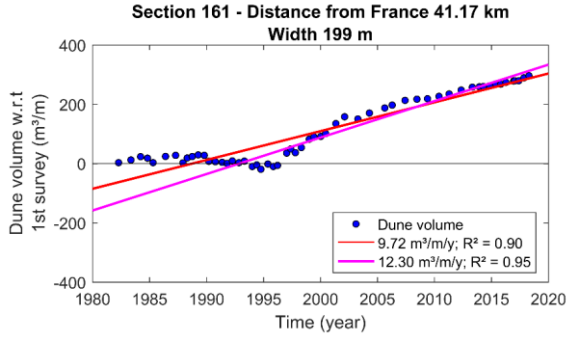
Section 161 - Distance from France 41.17 km
Width 199 m
Dune volume w.r.t 1st survey (m³/m)
Time (year)
Dune volume
9.72 m³/m/y; R² = 0.90
12.30 m³/m/y; R² = 0.95

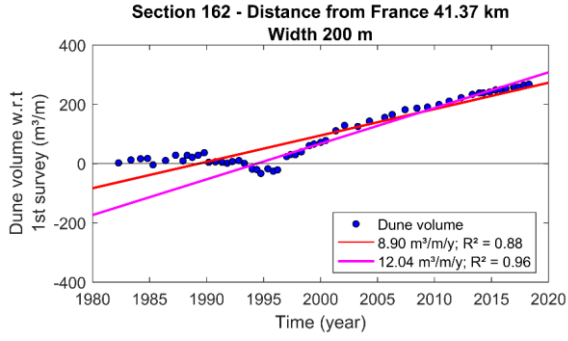
Section 162 - Distance from France 41.37 km
Width 200 m
Dune volume w.r.t 1st survey (m³/m)
Time (year)
Dune volume
8.90 m³/m/y; R² = 0.88
12.04 m³/m/y; R² = 0.96

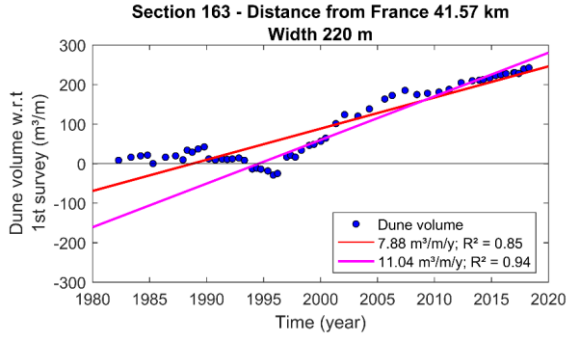
Section 163 - Distance from France 41.57 km
Width 220 m
Dune volume w.r.t 1st survey (m³/m)
Time (year)
Dune volume
7.88 m³/m/y; R² = 0.85
11.04 m³/m/y; R² = 0.94

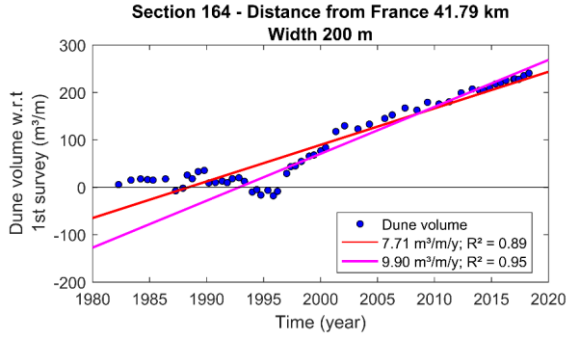
Section 164 - Distance from France 41.79 km
Width 200 m
Dune volume w.r.t 1st survey (m³/m)
Time (year)
Dune volume
7.71 m³/m/y; R² = 0.89
9.90 m³/m/y; R² = 0.95

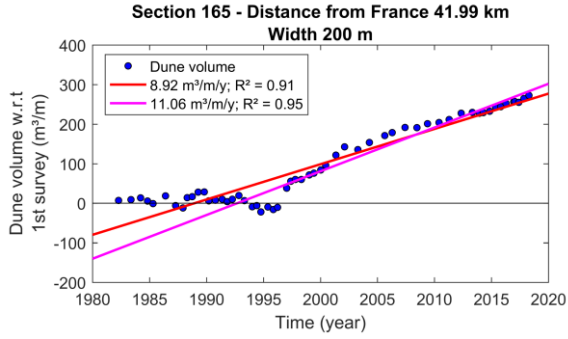
Section 165 - Distance from France 41.99 km
Width 200 m
Dune volume w.r.t 1st survey (m³/m)
Time (year)
Dune volume
8.92 m³/m/y; R² = 0.91
11.06 m³/m/y; R² = 0.95

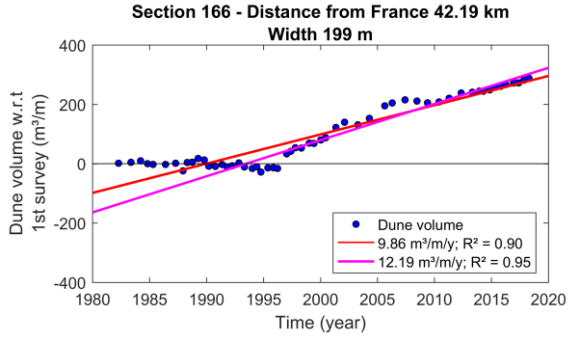
Section 166 - Distance from France 42.19 km
Width 199 m
Dune volume w.r.t 1st survey (m³/m)
Time (year)
Dune volume
9.86 m³/m/y; R² = 0.90
12.19 m³/m/y; R² = 0.95

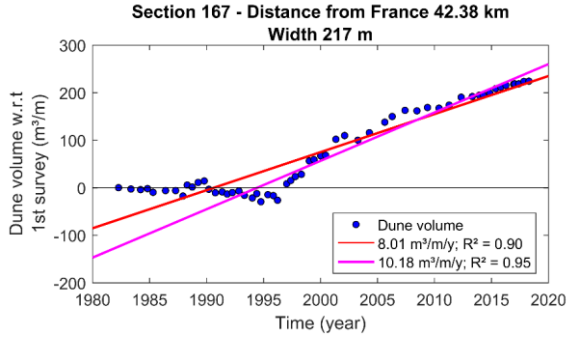
Section 167 - Distance from France 42.38 km
Width 217 m
Dune volume w.r.t 1st survey (m³/m)
Time (year)
Dune volume
8.01 m³/m/y; R² = 0.90
10.18 m³/m/y; R² = 0.95

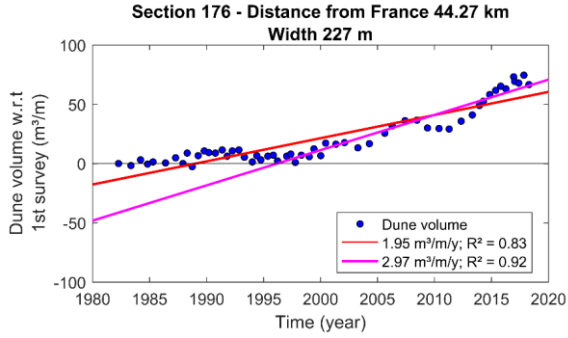
Section 176 - Distance from France 44.27 km
Width 227 m
Dune volume w.r.t 1st survey (m³/m)
Time (year)
Dune volume
1.95 m³/m/y; R² = 0.83
2.97 m³/m/y; R² = 0.92

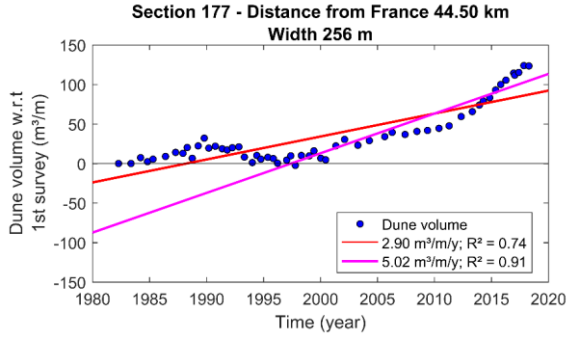
Section 177 - Distance from France 44.50 km
Width 256 m
Dune volume w.r.t 1st survey (m³/m)
Time (year)
Dune volume
2.90 m³/m/y; R² = 0.74
5.02 m³/m/y; R² = 0.91

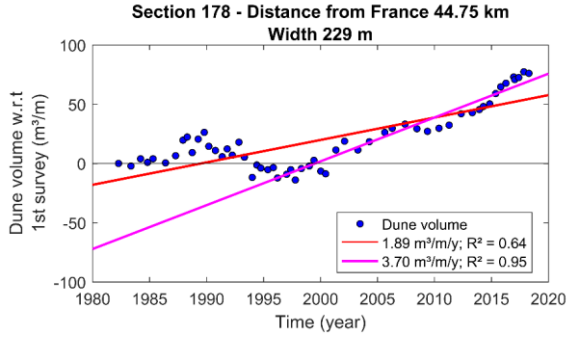
Section 178 - Distance from France 44.75 km
Width 229 m
Dune volume w.r.t 1st survey (m³/m)
Time (year)
Dune volume
1.89 m³/m/y; R² = 0.64
3.70 m³/m/y; R² = 0.95

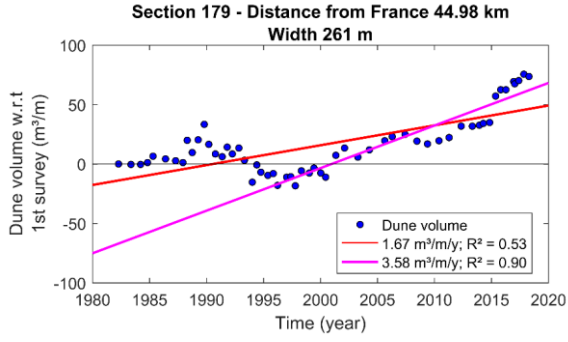
Section 179 - Distance from France 44.98 km
Width 261 m
Dune volume w.r.t 1st survey (m³/m)
Time (year)
Dune volume
1.67 m³/m/y; R² = 0.53
3.58 m³/m/y; R² = 0.90

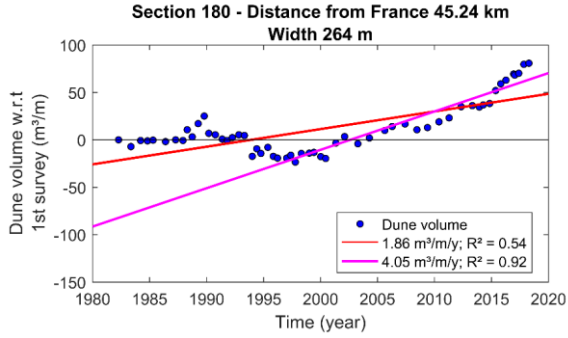
Section 180 - Distance from France 45.24 km
Width 264 m
Dune volume w.r.t 1st survey (m³/m)
Time (year)
Dune volume
1.86 m³/m/y; R² = 0.54
4.05 m³/m/y; R² = 0.92

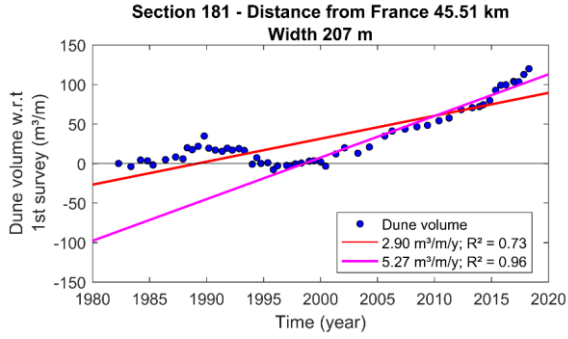
Section 181 - Distance from France 45.51 km
Width 207 m
Dune volume w.r.t 1st survey (m³/m)
Time (year)
Dune volume
2.90 m³/m/y; R² = 0.73
5.27 m³/m/y; R² = 0.96

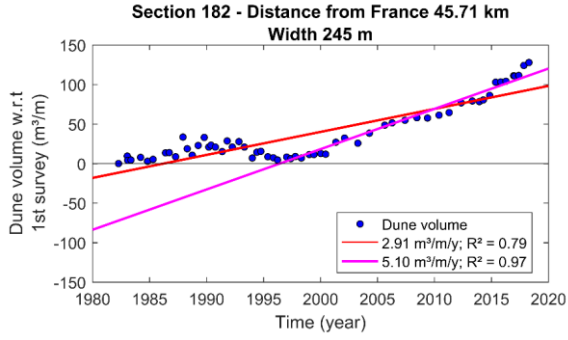
Section 182 - Distance from France 45.71 km
Width 245 m
Dune volume w.r.t 1st survey (m³/m)
Time (year)
Dune volume
2.91 m³/m/y; R² = 0.79
5.10 m³/m/y; R² = 0.97

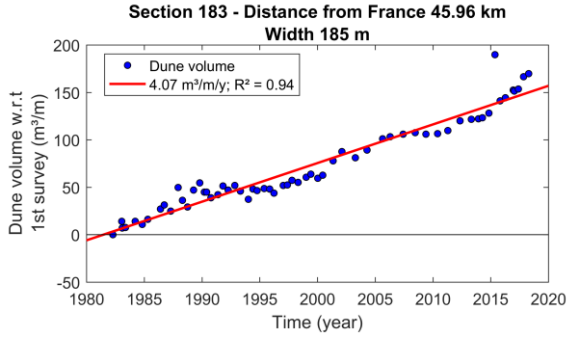
Section 183 - Distance from France 45.96 km
Width 185 m
Dune volume w.r.t 1st survey (m³/m)
Time (year)
Dune volume
4.07 m³/m/y; R² = 0.94

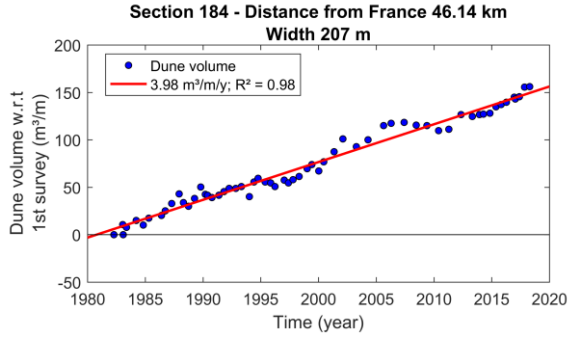
Section 184 - Distance from France 46.14 km
Width 207 m
Dune volume
3.98 m³/m/y; R² = 0.98
Dune volume w.r.t 1st survey (m³/m)
Time (year)

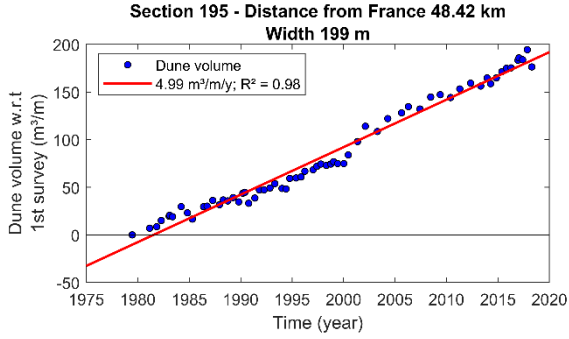
Section 195 - Distance from France 48.42 km
Width 199 m
Dune volume
4.99 m³/m/y; R² = 0.98
Dune volume w.r.t 1st survey (m³/m)
Time (year)

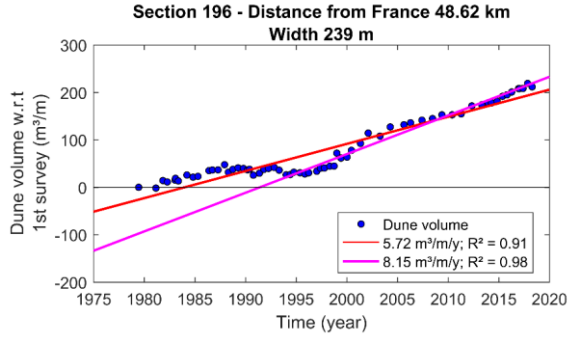
Section 196 - Distance from France 48.62 km
Width 239 m
Dune volume
5.72 m³/m/y; R² = 0.91
8.15 m³/m/y; R² = 0.98
Dune volume w.r.t 1st survey (m³/m)
Time (year)

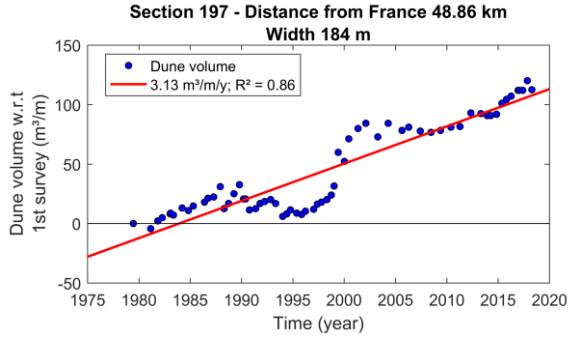
Section 197 - Distance from France 48.86 km
Width 184 m
Dune volume
3.13 m³/m/y; R² = 0.86
Dune volume w.r.t 1st survey (m³/m)
Time (year)

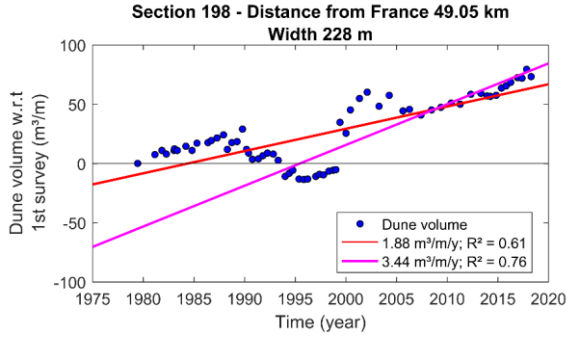
Section 198 - Distance from France 49.05 km
Width 228 m
Dune volume w.r.t 1st survey (m³/m)
Time (year)
Dune volume
1.88 m³/m/y; R² = 0.61
3.44 m³/m/y; R² = 0.76

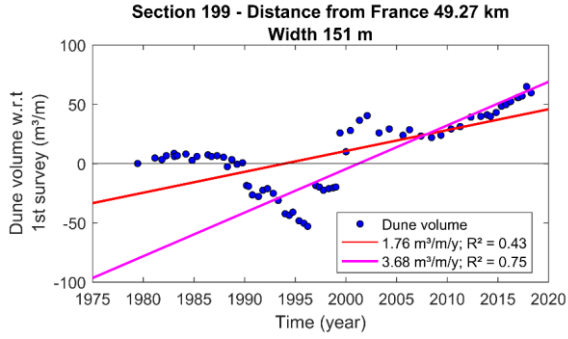
Section 199 - Distance from France 49.27 km
Width 151 m
Dune volume w.r.t 1st survey (m³/m)
Time (year)
Dune volume
1.76 m³/m/y; R² = 0.43
3.68 m³/m/y; R² = 0.75

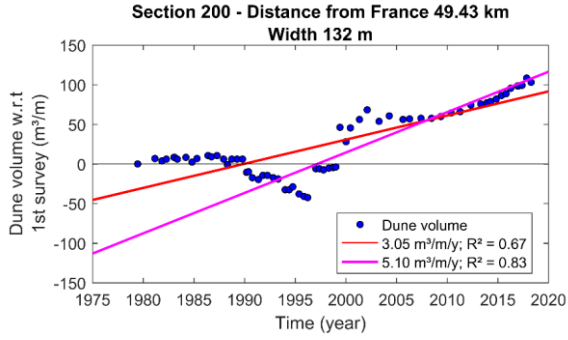
Section 200 - Distance from France 49.43 km
Width 132 m
Dune volume w.r.t 1st survey (m³/m)
Time (year)
Dune volume
3.05 m³/m/y; R² = 0.67
5.10 m³/m/y; R² = 0.83

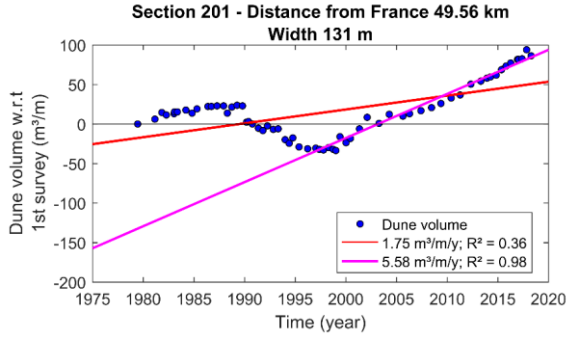
Section 201 - Distance from France 49.56 km
Width 131 m
Dune volume w.r.t 1st survey (m³/m)
Time (year)
Dune volume
1.75 m³/m/y; R² = 0.36
5.58 m³/m/y; R² = 0.98

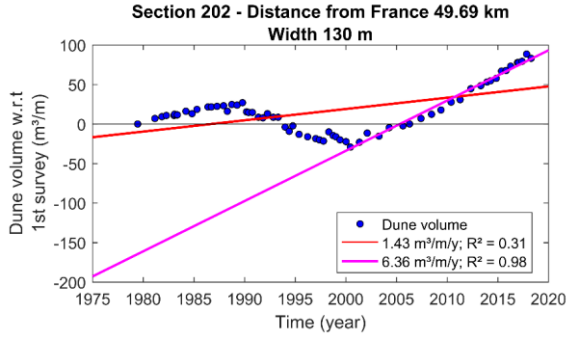
Section 202 - Distance from France 49.69 km
Width 130 m
Dune volume w.r.t 1st survey (m³/m)
Time (year)
Dune volume
1.43 m³/m/y; R² = 0.31
6.36 m³/m/y; R² = 0.98

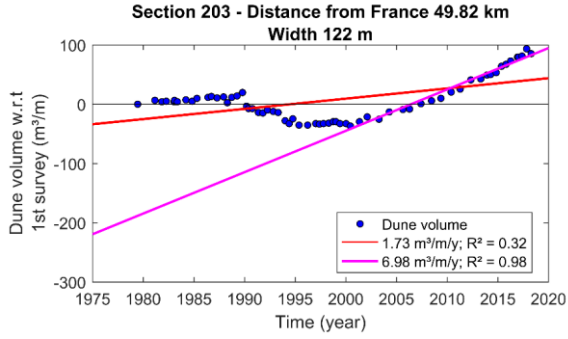
Section 203 - Distance from France 49.82 km
Width 122 m
Dune volume w.r.t 1st survey (m³/m)
Time (year)
Dune volume
1.73 m³/m/y; R² = 0.32
6.98 m³/m/y; R² = 0.98

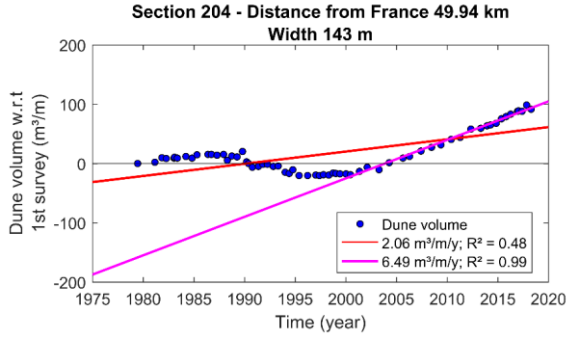
Section 204 - Distance from France 49.94 km
Width 143 m
Dune volume w.r.t 1st survey (m³/m)
Time (year)
Dune volume
2.06 m³/m/y; R² = 0.48
6.49 m³/m/y; R² = 0.99

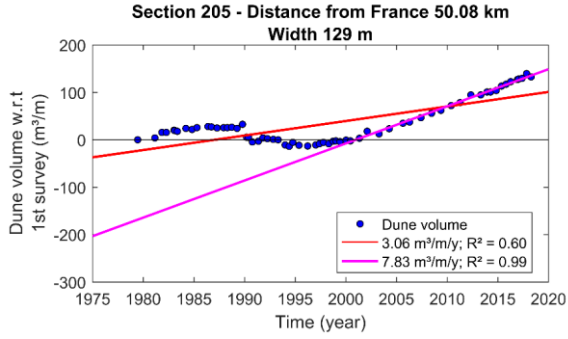
Section 205 - Distance from France 50.08 km
Width 129 m
Dune volume w.r.t 1st survey (m³/m)
Time (year)
Dune volume
3.06 m³/m/y; R² = 0.60
7.83 m³/m/y; R² = 0.99

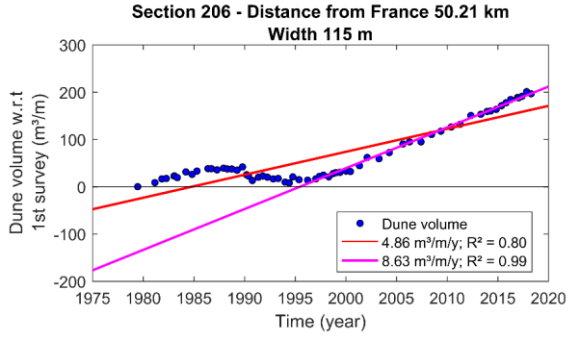
Section 206 - Distance from France 50.21 km
Width 115 m
Dune volume w.r.t 1st survey (m³/m)
Time (year)
Dune volume
4.86 m³/m/y; R² = 0.80
8.63 m³/m/y; R² = 0.99

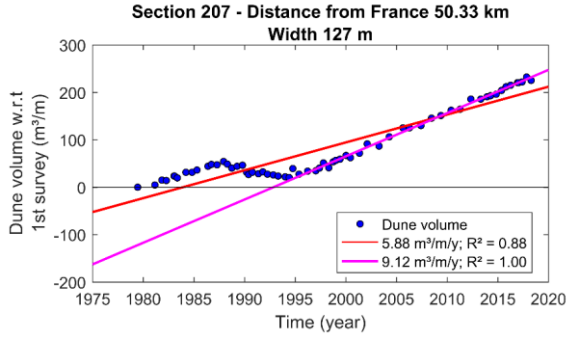
Section 207 - Distance from France 50.33 km
Width 127 m
Dune volume w.r.t 1st survey (m³/m)
Time (year)
Dune volume
5.88 m³/m/y; R² = 0.88
9.12 m³/m/y; R² = 1.00

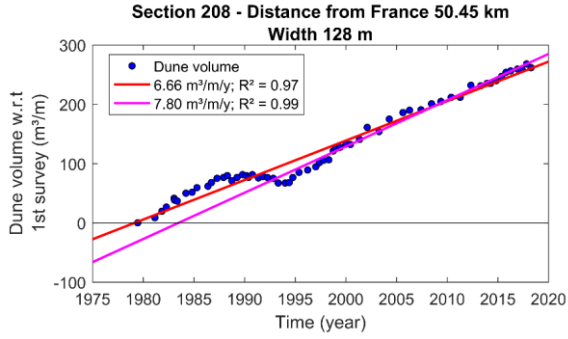
Section 208 - Distance from France 50.45 km
Width 128 m
Dune volume w.r.t 1st survey (m³/m)
Time (year)
Dune volume
6.66 m³/m/y; R² = 0.97
7.80 m³/m/y; R² = 0.99

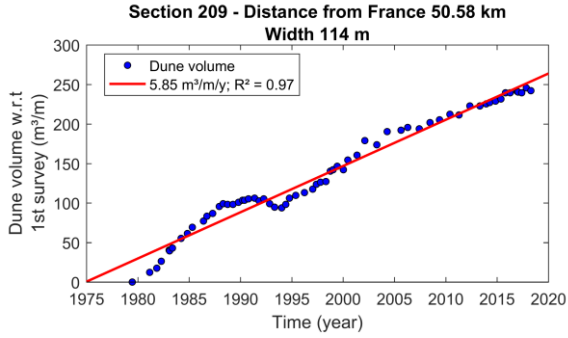
Section 209 - Distance from France 50.58 km
Width 114 m
Dune volume w.r.t 1st survey (m³/m)
Time (year)
Dune volume
5.85 m³/m/y; R² = 0.97

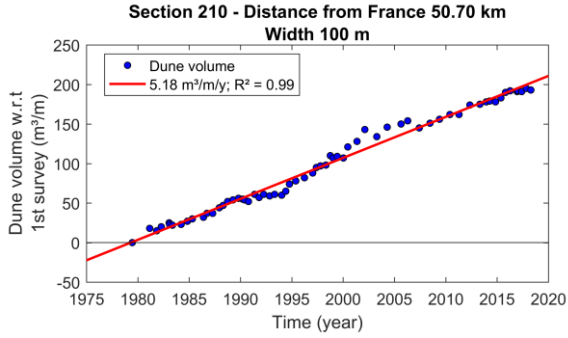
Section 210 - Distance from France 50.70 km
Width 100 m
Dune volume
5.18 m³/m/y; R² = 0.99
Dune volume w.r.t 1st survey (m³/m)
Time (year)

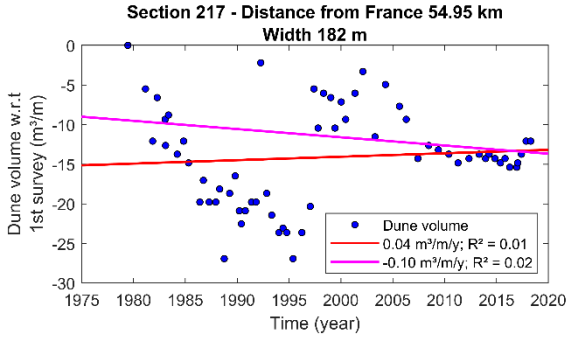
Section 217 - Distance from France 54.95 km
Width 182 m
Dune volume
0.04 m³/m/y; R² = 0.01
-0.10 m³/m/y; R² = 0.02
Dune volume w.r.t 1st survey (m³/m)
Time (year)

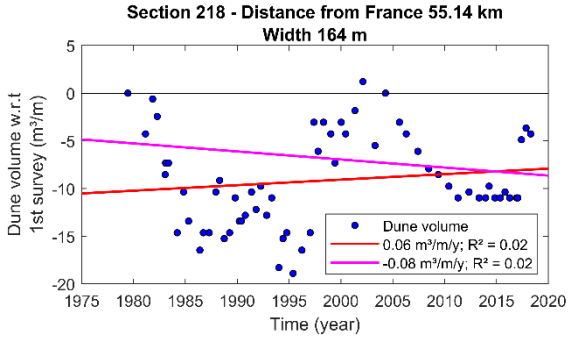
Section 218 - Distance from France 55.14 km
Width 164 m
Dune volume
0.06 m³/m/y; R² = 0.02
-0.08 m³/m/y; R² = 0.02
Dune volume w.r.t 1st survey (m³/m)
Time (year)

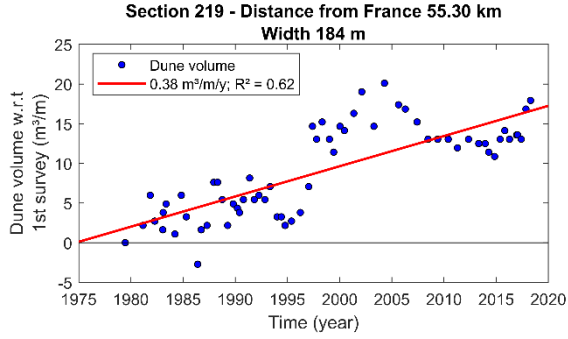
Section 219 - Distance from France 55.30 km
Width 184 m
Dune volume
0.38 m³/m/y; R² = 0.62
Dune volume w.r.t 1st survey (m³/m)
Time (year)

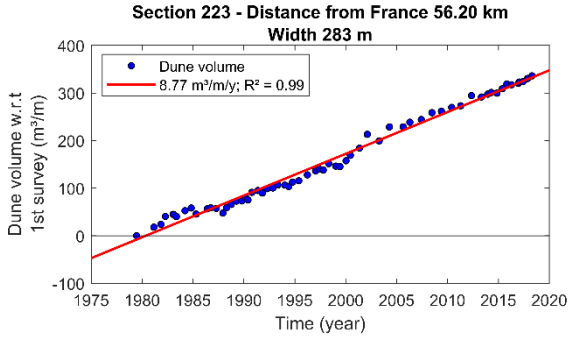
Section 223 - Distance from France 56.20 km
Width 283 m
Dune volume
8.77 m³/m/y; R² = 0.99
Dune volume w.r.t 1st survey (m³/m)
Time (year)

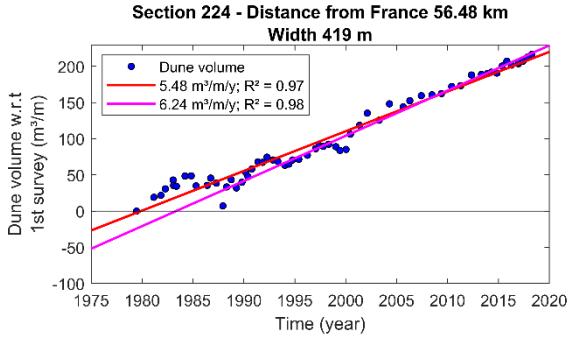
Section 224 - Distance from France 56.48 km
Width 419 m
Dune volume
5.48 m³/m/y; R² = 0.97
6.24 m³/m/y; R² = 0.98
Dune volume w.r.t 1st survey (m³/m)
Time (year)

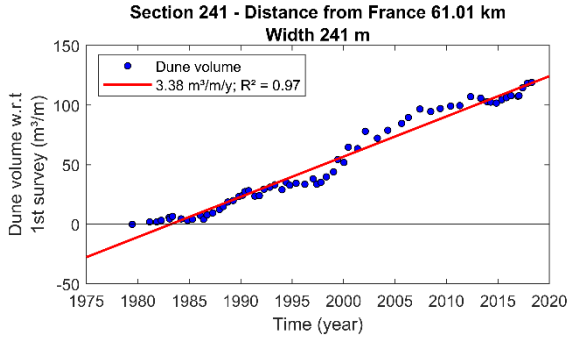
Section 241 - Distance from France 61.01 km
Width 241 m
Dune volume
3.38 m³/m/y; R² = 0.97
Dune volume w.r.t 1st survey (m³/m)
Time (year)

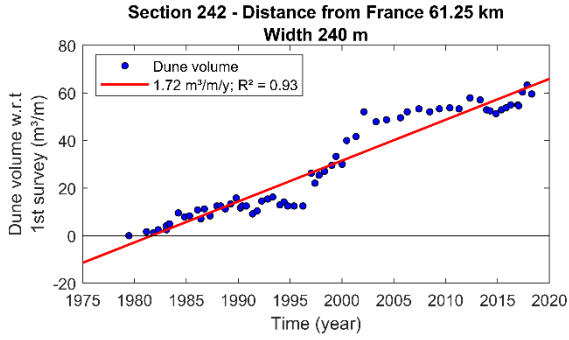
Section 242 - Distance from France 61.25 km
Width 240 m
Dune volume
1.72 m³/m/y; R² = 0.93
Dune volume w.r.t 1st survey (m³/m)
Time (year)

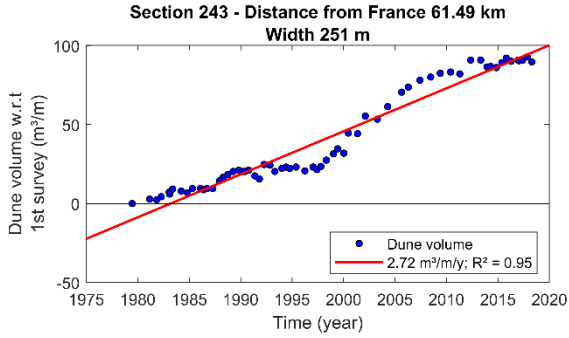
Section 243 - Distance from France 61.49 km
Width 251 m
Dune volume w.r.t 1st survey (m³/m)
Time (year)
Dune volume
2.72 m³/m/y; R² = 0.95

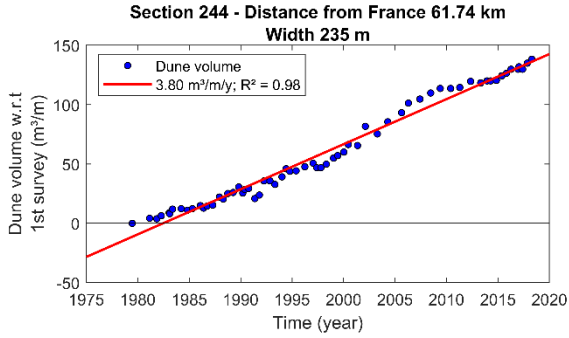
Section 244 - Distance from France 61.74 km
Width 235 m
Dune volume w.r.t 1st survey (m³/m)
Time (year)
Dune volume
3.80 m³/m/y; R² = 0.98

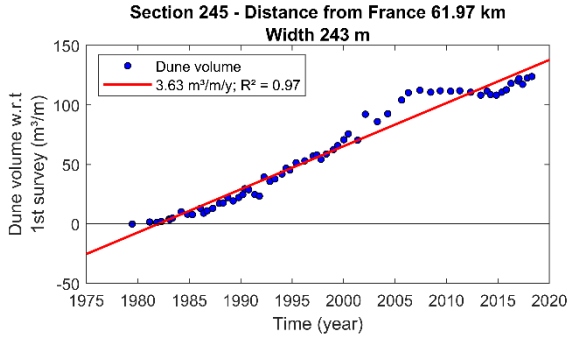
Section 245 - Distance from France 61.97 km
Width 243 m
Dune volume w.r.t 1st survey (m³/m)
Time (year)
Dune volume
3.63 m³/m/y; R² = 0.97

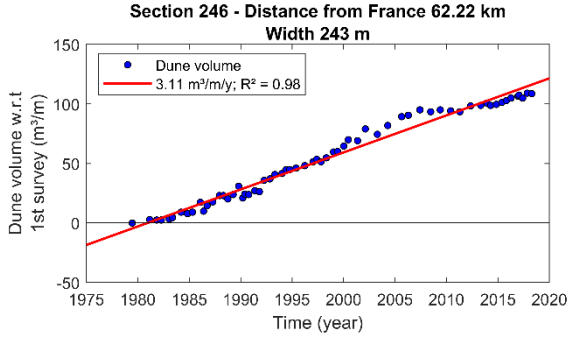
Section 246 - Distance from France 62.22 km
Width 243 m
Dune volume w.r.t 1st survey (m³/m)
Time (year)
Dune volume
3.11 m³/m/y; R² = 0.98

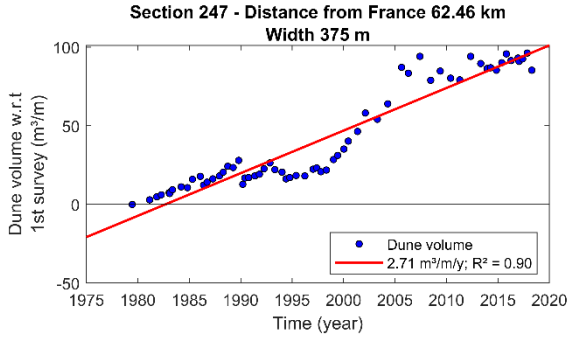
Section 247 - Distance from France 62.46 km
Width 375 m
Dune volume w.r.t 1st survey (m³/m)
Time (year)
Dune volume
2.71 m³/m/y; R² = 0.90

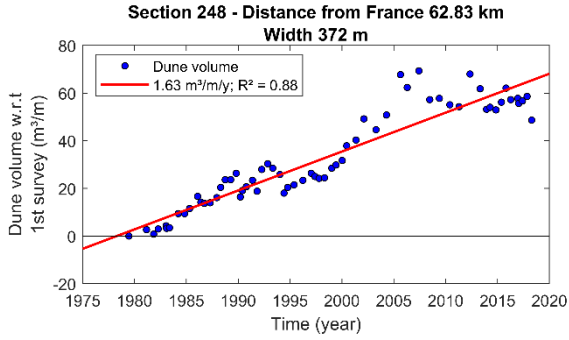
Section 248 - Distance from France 62.83 km
Width 372 m
Dune volume w.r.t 1st survey (m³/m)
Time (year)
Dune volume
1.63 m³/m/y; R² = 0.88

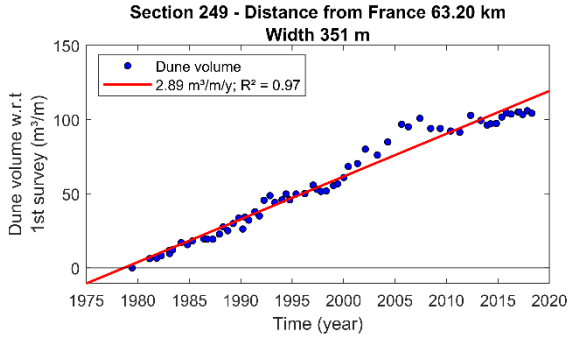
Section 249 - Distance from France 63.20 km
Width 351 m
Dune volume w.r.t 1st survey (m³/m)
Time (year)
Dune volume
2.89 m³/m/y; R² = 0.97

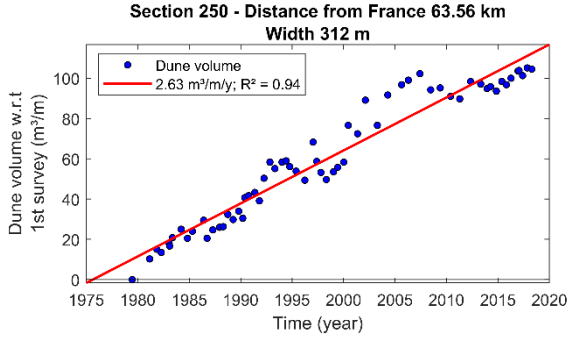
Section 250 - Distance from France 63.56 km
Width 312 m
Dune volume w.r.t 1st survey (m³/m)
Time (year)
Dune volume
2.63 m³/m/y; R² = 0.94

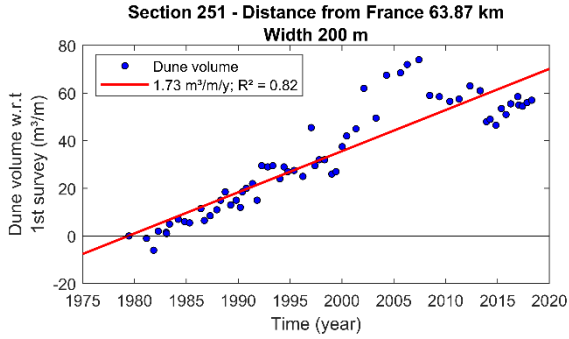
Section 251 - Distance from France 63.87 km
Width 200 m
Dune volume
1.73 m³/m/y; R² = 0.82
Dune volume w.r.t 1st survey (m³/m)
Time (year)

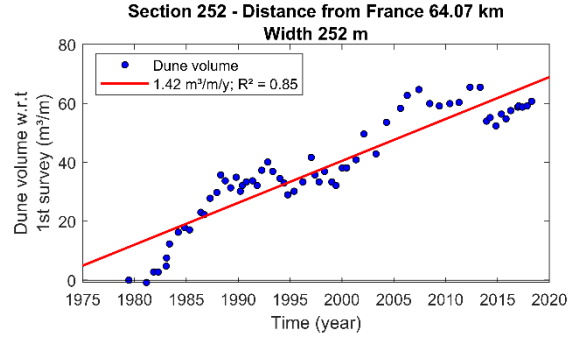
Section 252 - Distance from France 64.07 km
Width 252 m
Dune volume
1.42 m³/m/y; R² = 0.85
Dune volume w.r.t 1st survey (m³/m)
Time (year)

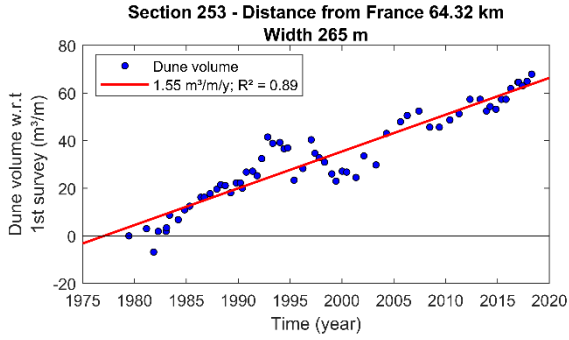
Section 253 - Distance from France 64.32 km
Width 265 m
Dune volume
1.55 m³/m/y; R² = 0.89
Dune volume w.r.t 1st survey (m³/m)
Time (year)

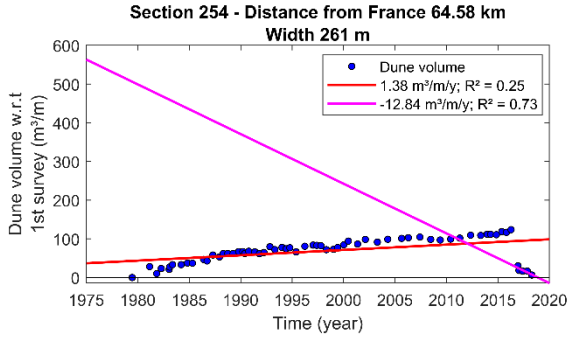
Section 254 - Distance from France 64.58 km
Width 261 m
Dune volume
1.38 m³/m/y; R² = 0.25
-12.84 m³/m/y; R² = 0.73
Dune volume w.r.t 1st survey (m³/m)
Time (year)

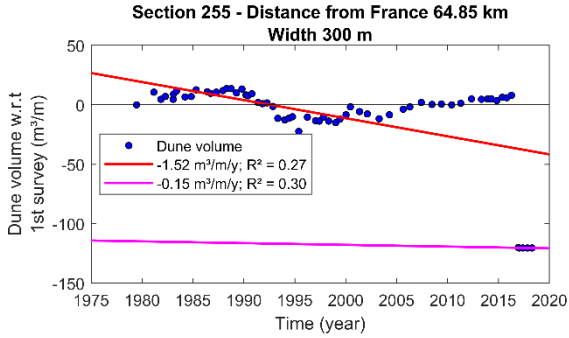
Section 255 - Distance from France 64.85 km
Width 300 m
Dune volume w.r.t 1st survey (m³/m)
Time (year)
Dune volume
-1.52 m³/m/y; R² = 0.27
-0.15 m³/m/y; R² = 0.30
50
0
-50
-100
-150
1975
1980
1985
1990
1995
2000
2005
2010
2015
2020

References

Anderson, R.S., & Haff, P.K. (1991). Wind modification and bed response during saltation of sand in air. *Acta Mechanica Supplementum*, *1*, 21–51.

Anthony, E.J., Vanhee, S., & Ruz, M.H. (2006). Short-term beach-dune sand budgets on the North Sea coast of France: Sand supply from shoreface to dunes, and the role of wind and fetch. *Geomorphology*, *81*(3–4), 316–329.

Arens, S.M. (1996). Rates of aeolian transport on a beach in a temperate humid climate. *Geomorphology*, 17(1–3), 3–18.

Arens, S.M. (1997). Transport rates and volume changes in a coastal foredune on a Dutch Wadden island. *Journal of Coastal Conservation*, *3*(1), 49–56.

Arens, S.M., Van Kaam-Peters, H.M.E., & Van Boxel, J.H. (1995). Air flow over foredunes and implications for sand transport. *Earth Surface Processes and Landforms*, *20*, 315–332.

Baas, A.C.W., & Sherman, D.J. (2006). Spatiotemporal Variability of Aeolian Sand Transport in a Coastal Dune Environment. *Journal of Coastal Research*, *22*(5), 1198–1205.

Bagnold, R.A. (1937). The size-grading of sand by wind. *Proceedings of the Royal Society of London. Series A, Mathematical and Physical Sciences*, 250–264.

Bagnold, R.A. (1941). *The Physics of Blown Sand and Desert Dunes*. London: Methuen.

Bagnold, R.A. (1954). *The Physics of Blown Sand and Desert Dunes, 2nd Edition*. Methuen, London.

Bauer, B.O., Davidson-Arnott, R.G.D., Hesp, P.A., Namikas, S.L., Ollerhead, J., & Walker, I.J. (2009). Aeolian sediment transport on a beach: Surface moisture, wind fetch, and mean transport. *Geomorphology*, *105*(1–2), 106–116.

Bauer, B.O., & Davidson-Arnott, R.G.D. (2003). A general framework for modeling sediment supply to coastal dunes including wind angle, beach geometry, and fetch effects. *Geomorphology*, *49*(1), 89–108.

Bauer, B.O., & Davidson-Arnott, R.G.D. (2014). Aeolian particle flux profiles and transport unsteadiness. *Journal of Geophysical Research: Earth Surface*, *119*, 2448–2459.

Bauer, B.O., Davidson-Arnott, R.G.D., Walker, I.J., Hesp, P.A., & Ollerhead, J. (2012). Wind direction and complex sediment transport response across a beach-dune system. *Earth Surface Processes and Landforms*, *37*(15), 1661–1677.

Bauer, B.O., Sherman, D.J., Nordstrom, K.F., & Gares, P.A. (1990). Aeolian transport measurement and prediction across a beach and dune at Castroville, California. *Coastal Dunes, Form and Process*, Chichester: Wiley, 39–55.

Bauer, B.O., Sherman, D.J., & Wolcott, J.F. (1992). Sources of Uncertainty in Shear Stress and Roughness Length Estimates Derived from Velocity Profiles. *The Professional Geographer*, *44*(4), 453–464.

Belly, P.Y. (1964). *Sand Movement by Wind*. Technical Memorandum No. 1.

Brodie, K., Conery, I., Cohn, N., Spore, N., & Palmsten, M. (2019). Spatial Variability of Coastal Foredune Evolution, Part A: Timescales of Months to Years. *Journal of Marine Science and Engineering*, *7*(5), 124.

Cahill, T.A., Gill, T.E., Reid, J.S., Gearhart, E.A., & Gillette, D.A. (1996). Saltating particles, playa crusts and dust aerosols at Owens (dry) Lake, California. *Earth Surface Processes and Landforms*, *21*(7), 621–639.

Campos, L.D. (2018). *Quantification Methods for Aeolian Sand Transport on Beaches (PhD Thesis)*, University of Twente, The Netherlands.

Charlier, R.H., & De Meyer, C.P. (1995). New Developments on Coastal Protection along the Belgian Coast. *Journal of Coastal Research*, *11*(4), 1287–1293.

Chepil, W.S. (1945). Dynamics of wind erosion: I. Nature of movement of soil by wind. *Soil Science*, *60*(4), 305-320.

Chepil, W.S., & Milne, R.A. (1941). Wind erosion of soils in relation to size and nature of exposed area. *The Journal of Agricultural Science*, *21*, 479–487.

Davidson-Arnott, R.G.D., & Law, M.N. (1996). Measurement and Prediction of Long-Term Sediment Supply to Coastal Foredunes. *Journal of Coastal Research*, *12*(3), 654–663.

Davidson-Arnott, R.G.D., & Law, M.N. (1990). Seasonal patterns and controls on sediment supply to coastal foredunes, Long Point, Lake Erie. In: Nordstrom, K.F., Psuty, N.P., Carter, R.W.G. (Eds.), *Coastal Dunes: Forms and Processes*, 177–200.

Davidson-Arnott, R.G.D., MacQuarrie, K., & Aagaard, T. (2005). The effect of wind gusts, moisture content and fetch length on sand transport on a beach. *Geomorphology*, *68*(1–2), 115–129.

Davidson-Arnott, R.G.D., Yang, Y., Ollerhead, J., Hesp, P.A., & Walker, I.J. (2008). The effects of surface moisture on aeolian sediment transport threshold and mass flux on a beach. *Earth Surface Processes and Landforms*, *33*, 55–74.

de Vries, S., Arens, S.M., de Schipper, M.A., & Ranasinghe, R. (2014). Aeolian sediment transport on a beach with a varying sediment supply. *Aeolian Research*, *15*, 235–244.

de Vries, S., Southgate, H.N., Kanning, W., & Ranasinghe, R. (2012). Dune behavior and aeolian transport on decadal timescales. *Coastal Engineering*, *67*, 41–53.

de Winter, R. C., & Ruessink, B. G. (2017). Sensitivity analysis of climate change impacts on dune erosion: case study for the Dutch Holland coast. *Climatic Change*, *141*(4), 685–701.

Delgado-Fernandez, I. (2010). A review of the application of the fetch effect to modelling sand supply to coastal foredunes. *Aeolian Research*, *2*(2–3), 61–70.

Delgado-Fernandez, I. (2011). Meso-scale modelling of aeolian sediment input to coastal dunes. *Geomorphology*, *130*(3–4), 230–243.

Delgado-Fernandez, I., & Davidson-Arnott, R. (2009). Sediment Input to Foredunes Description and Frequency of Transport Events at Greenwich Dunes, PEI, Canada. *Journal of Coastal Research*, *1*(56), 302–306.

Delgado-Fernandez, I., & Davidson-Arnott, R.G.D. (2011). Meso-scale aeolian sediment input to coastal dunes: The nature of aeolian transport events. *Geomorphology*, *126*(1–2), 217–232.

Deronde, B., Houthuys, R., Henriet, J.P., & Van Lancker, V. (2009). Monitoring of the sediment dynamics along a sandy shoreline by means of airborne hyperspectral remote sensing and LIDAR: a case study in Belgium. *Earth Surface Processes and Landforms*, 34(July 2007), 155–161.

Dingler, J.R., Hsu, S.A., & Reiss, T.E. (1992). Theoretical and measured aeolian sand transport on a barrier island, Louisiana, USA. *Sedimentology*, *39*, 1031–1043.

Dong, Z., Lu, J., Man, D., Lv, P., Qian, G., Zhang, Z., & Luo, W. (2011). Equations for the near-surface mass flux density profile of wind-blown sediments. *Earth Surface Processes and Landforms*, *36*, 1292–1299.

Dong, Z., Liu, X., Wang, H., & Wang, X. (2003). Aeolian sand transport: a wind tunnel model. *Sedimentary Geology*, *161*, 71–83.

Dong, Z., Lv, P., Zhang, Z., Qian, G., & Luo, W. (2012). Aeolian transport in the field: A comparison of the effects of different surface treatments. Journal of Geophysical Research, 117(D9), 1-9

Dong, Z., & Qian, G. (2007). Characterizing the height profile of the flux of wind-eroded sediment. *Environmental Geology*, *51*(5), 835–845.

Dong, Z. Wang, H., Liu, X., & Wang, X. (2004). The blown sand flux over a sandy surface: A wind tunnel investigation on the fetch effect. *Geomorphology*, *57*(1–2), 117–127.

Durán, O., Claudin, P., & Andreotti, B. (2011). On aeolian transport: Grain-scale interactions, dynamical mechanisms and scaling laws. *Aeolian Research*, *3*(3), 243-270.

Ellis, J.T., Li, B., Farrell, E.J., & Sherman, D.J. (2009). Protocols for characterizing aeolian mass-flux profiles. *Aeolian Research*, *1*(1–2), 19–26.

Ellis, J.T., & Sherman, D.J. (2013). Fundamentals of Aeolian Sediment Transport: Wind-Blown Sand. *Treatise on Geomorphology*, *11*, 85–108.

Field, J.P., & Pelletier, J.D. (2018). Controls on the aerodynamic roughness length and the grain-size dependence of aeolian sediment transport. *Earth Surface Processes and Landforms*, *43*(12), 2616–2626.

Gerety, K.M., & Slingerland, R. (1983). Nature of the saltating population in wind tunnel experiments with heterogenous size-density sands. *Developments in Sedimentology*, *38*, 115–131.

Gillette, D.A., Herbert, G., Stockton, & Al., E. (1996). Causes of the fetch effect in wind erosion. *Earth Surface Processes and Landforms*, *21*, 641–659.

Gillette, D.A., Herrick, J.E., & Herbert, G.A. (2006). Wind characteristics of Mesquite Streets in the northern Chihuahuan Desert, New Mexico, USA. *Environmental Fluid Mechanics*, *6*(3), 241-275.

Goossens, D., & Offer, Z.Y. (2000). Wind tunnel and field calibration of five aeolian dust samplers. *Atmospheric Environment*, *34*(7), 1043–1057.

Greeley, R., Blumberg, D.G., & Williams, S.H. (1996). Field measurements of the flux and speed of wind-blown sand. *Sedimentology*, *43*(1), 41–52.

Greeley, R., & Iversen, J.D. (1985). *Wind as a Geological Process on Earth, Mars, Venus and Titan (4th ed.; C.P.S. Series, Ed.)*. Cambridge, London, New York, New Rochelle, Melbourne, Sydney: Cambridge University Press.

Haerens, P., Bolle, A., Trouw, K., & Houthuys, R. (2012). Definition of storm thresholds for significant morphological change of the sandy beaches along the Belgian coastline. *Geomorphology*, *143–144*, 104–117.

Hage, P.M., Ruessink, B.G., & Donker, J.J.A. (2018). Determining sand strip characteristics using Argus video monitoring. *Aeolian Research*, *33*, 1–11.

Han, Q., Qu, J., Liao, K., Zhu, S., Zhang, K., Zu, R., & Niu, Q. (2011). A wind tunnel study of aeolian sand transport on a wetted sand surface using sands from tropical humid coastal southern China. *Environmental Earth Sciences*, *64*(5), 1375–1385.

Han, Q., Qu, J., Zhang, K., Zu, R., Niu, Q., & Liao, K. (2009). Wind tunnel investigation of the influence of surface moisture content on the entrainment and erosion of beach sand by wind using sands from tropical humid coastal southern China. *Geomorphology*, *104*(3–4), 230–237.

Hesp, P.A. (1999). *The beach backshore and beyond. Handbook of Beach and Shoreface Morphodynamics, Ed. A.D.* Short (Brisbane, Australia). John Wiley and Son, 145–170.

Hesp, P.A. (2002). Foredunes and blowouts: Initiation, Geomorphology and dynamics. *Geomorphology*, *48*(1–3), 245–268.

Hesse, P.P., & Simpson, R.L. (2006). Variable vegetation cover and episodic sand movement on longitudinal desert sand dunes. *Geomorphology, 81*(3–4), 276–291.

Ho, T.D. (2012). *Experimental study of saltating particles in a turbulent boundary layer (PhD Thesis).* École doctorale Sciences de la matière (Rennes) and Université européenne de Bretagne.

Hoonhout, B., & de Vries, S. (2017). Field measurements on spatial variations in aeolian sediment availability at the Sand Motor mega nourishment. *Aeolian Research, 24*, 93–104.

Hoonhout, B., & de Vries, S. (2016). A process-based model for aeolian sediment transport and spatiotemporal varying sediment availability. *Journal of Geophysical Research: Earth Surface, 121*(8), 1555–1575.

Horikawa, K., Hotta, S., Kubota, S., & Katori, S. (1984). Field measurement of blown sand transport rate by trench trap. *Coastal Engineering in Japan, 27*, 214–232.

Horikawa, K., & Shen, H.W. (1960). *Sand Movement by Wind Action (on the characteristics of sand traps).* Technical memorandum No. 119. Beach erosion board, Corps of Engineers.

Horikawa, K. (1988). *Nearshore Dynamics and Coastal Processes: Theory, Management, and predictive Models.* Tokyo, Japan: University of Tokyo Press, 522 pp.

Houser, C. (2009). Synchronization of transport and supply in beach-dune interaction. *Progress in Physical Geography, 33*(6), 733–746.

Houser, C., Wernette, P., Rentschlar, E., Jones, H., Hammond, B., & Trimble, S. (2015). Post-storm beach and dune recovery: Implications for barrier island resilience. *Geomorphology, 234*, 54–63.

Houthuys, R. (2012). *Morfologie van de Vlaamse kust in 2011.* Agentschap Maritieme dienstverlening en Kust. Afdeling Kust: Oostende. 150 pp.

Hsu, S.A. (1974). Computing Eolian sand transport from routine weather data. *Proc. 14th Coastal Eng. Conf. II*, 1619–1626. Copenhagen.

International Marine & Dredging Consultants (IMDC). (2010). *DO4: Morfologische evolutie van de Vlaamse kust ingedeeld in morfologisch homogene kuststroken, vanaf de eerste meetvlucht tot 2009, rekening houdend met de aangevoerde zandhoeveelheden.* Oostende.

Iversen, J.D., Greeley, R., White, B.R., & Pollack, J.B. (1976). The effect of vertical distortion in the modeling of sedimentation phenomena. *Journal of Geophysical Research*, *81*, 4846–4856.

Jackson, N.L., & Nordstrom, K.F. (1997). Effects of time-dependent moisture content of surface sediments on aeolian transport rates across a beach, Wildwood, New Jersey, U.S.A. *Earth Surface Processes and Landforms*, *22*(7), 611–621.

Jackson, N.L., & Nordstrom, K.F. (1998). Aeolian transport of sediment on a beach during and after rainfall, Wildwood, NJ, USA. *Geomorphology*, *22*(2), 151–157.

Jackson, N.L., & Nordstrom, K.F. (2011). Aeolian sediment transport and landforms in managed coastal systems: A review. *Aeolian Research*, *3*(2), 181–196.

Kadib, A.A. (1965). *A function for sand movement by wind. Berkeley.*

Kawamura, R. (1951). *Study of sand movement by wind. In The reports of the Institute of Science and Technology: vol 5.* University of Tokyo, Tokyo, Japan.

Keijsers, J.G.S., de Groot, A.V., & Riksen, M.J.P.M. (2016). Modeling the biogeomorphic evolution of coastal dunes in response to climate change. *Journal of Geophysical Research: Earth Surface*, *121*, 1161–1181.

Keijsers, J.G.S., Poortinga, A., Riksen, M.J.P.M., & Maroulis, J. (2014). Spatio-temporal variability in accretion and erosion of coastal foredunes in the Netherlands: Regional climate and local topography. *PLoS ONE*, *9*(3).

Kind, R.J. (1976). A critical examination of the requirements for model simulation of wind-induced erosion/deposition phenomena such as snow drifting. *Atmospheric Environment*, *10*, 219–227.

Kok, J.F., Parteli, E.J.R., Michaels, T.I., & Karam, D.B. (2012). The physics of wind-blown sand and dust. *Reports on Progress in Physics*, *75*(10), 1–119.

Kok, J., & Renno, N. O. (2007). Physically Based Numerical Model of Wind-Blown Sand Suggests Deficiencies in Classical Saltation Theory. AGU Fall Meeting Abstracts.

Kroon, A., & Hoekstra, P. (1990). Eolian Sediment Transport on a Natural Beach. *Journal of Coastal Research*, *6*(2), 367–379.

Kuhlman, H. (1958). Quantitative measurements of aeolian sand transport. *Geografisk Tidsskrift*, *57*, 51–74.

Law, M.N., & Davidson-Arnott, R.G.D. (1990). Seasonal controls on aeolian processes on the beach and foredune. *Proceedings of the Symposium on Coastal Sand Dunes*, 49–68.

Leatherman, S. (1978). A new aeolian sand trap design. *Sedimentology*, *25*, 303–306.

Lebbe, L., Meir, N. Van, & Viaene, P. (2008). Potential Implications of Sea-Level Rise for Belgium. *Journal of Coastal Research*, *24*, 358–366.

Lettau, K., & Lettau, H. (1978). *Experimental and micrometeorological field studies of dune migration. In: Lettau, K., Lettau, H. (Eds.), Exploring the World's Driest Climate*. Center for Climatic Research, University of Wisconsin-Madison, pp. 110–147, IES Report 101.

Li, B., Sherman, D.J., Farrell, E.J., & Ellis, J.T. (2010). Variability of the apparent von Kármán parameter during aeolian saltation. *Geophysical Research Letters*, *37*(15).

Li, Z.S., Feng, D.J., Wu, S.L., Borthwick, A.G.L., & Ni, J.R. (2008). Grain size and transport characteristics of non-uniform sand in aeolian saltation. *Geomorphology*, *100*, 484–493.

Liu, X., & Dong, Z. (2004). Experimental investigation of the concentration profile of a blowing sand cloud. *Geomorphology*, *60*(3-4), 371–381.

Liu, X., Dong, Z., & Wang, X. (2006). Wind tunnel modeling and measurements of the flux of wind-blown sand. *Journal of Arid Environments*, *66*(4), 657–672.

Livingstone, I., & Warren, A. (1996). *Aeolian Geomorphology: an introduction*. Longman.

Lynch, K., Jackson, D.W.T., & Cooper, J.A.G. (2007). Aeolian fetch distance and secondary airflow effects: the influence of micro-scale variables on meso-scale foredune development. *Earth Surface Processes and Landforms*, *33*(7), 991–1005.

Lynch, K., Jackson, D.W.T., & Cooper, J.A.G. (2016). The fetch effect on aeolian sediment transport on a sandy beach: a case study from Magilligan Strand, Northern Ireland. *Earth Surface Processes and Landforms*, *41*(8), 1129–1135.

Maegley, W.J. (1976). Saltation and martial sandstorms. *Reviews of Geophysics and Space Physics*, *14*, 135–142.

McEwan, I.K., & Willetts, B.B. (2006). On the prediction of bed-load sand transport rate in air. *Sedimentology*, *41*(6), 1241–1251.

McKee, E. (1980). *A study of global sand seas*. US Geological Survey, Professional Paper.

McKenna N., C., Li, B., & Nash, D. (2012). Micro-topographic analysis of shell pavements formed by aeolian transport in a wind tunnel simulation. *Journal of Geophysical Research: Earth Surface*, *117*(4), 1–16.

Meyer-Peter, E., & Müller, R. (1948). Formulas for Bed-Load Transport. *Proceedings of International Association for Hydraulic Structures Researach - Second Meeting*, Stockholm, Sweden, 39–65.

Montreuil, A.L., Elyahyioui, J., & Chen, M. (2016). Effect of Large-Scale Atmospheric Circulation and Wind on Storm Surge Occurrence. Proceedings of the 14th International Coastal Symposium, *75*(75), 755-759.

Montreuil, A.L., Chen, M., Brand, E., Strypsteen, G., Rauwoens, P., Vandenbulcke, A., Verwaest, T. (2018). Dynamics of Surface Moisture Content on a Macro-tidal Beach. *Journal of Coastal Research*, *85*, 206–210.

Musick, H.B., & Gilette, D.A. (1990). Field evaluation of relationships between a vegetation structural parameter and sheltering against wind erosion. *Land Degradation and Rehabilitation*, *2*, 87–94.

Musick, H.B., Randall, C., & Truji, S.M. (1993). *Wind erosion in semiarid landscapes: predictive models and remote sensing methods for the influence of vegetation*.

Nakashima, Y. (1979). A fundamental study on the blown sand control. *Bulletin of the Kyshu University*, *51*, 125–183.

Namikas, S.L. (2003). Field measurement and numerical modelling of aeolian mass flux distributions on a sandy beach. *Sedimentology*, *50*(2), 303–326.

Nickling, W.G., & Davidson-Arnott, R.G.D. (1990). Aeolian sediment transport on beaches and coastal sand dunes. *Proceedings of Symposium on Coastal Sand Dunes*, 1–35.

Nield, J.M., Wiggs, G.F.S., & Squirrell, R.S. (2011). Aeolian sand strip mobility and protodune development on a drying beach: Examining surface moisture and surface roughness patterns measured by terrestrial laser scanning. *Earth Surface Processes and Landforms*, *36*(4), 513–522.

Nikuradse, J. (1933). *Stromungsgesetz in rauhren rohren, vDI Forschungshefte 361 (Englishtranslation: Laws of flow in rough pipes)*. Tech. Rep. NACA Technical Memorandum, 1292.

Nordstrom, K.F. (1994). Beaches and dunes of human-altered coasts. *Progress in Physical Geography*, *18*(4), 497–516.

Nordstrom, K.F., Jackson, N.L., Klein, A.H.F., Sherman, D.J., & Hesp, P.A. (2006). Offshore aeolian transport across a low foredune on a developed barrier island. *Journal of Coastal Research*, *22*(5), 1260–1267.

Nordstrom, K.F., Jackson, N.L., Korotky, K.H., & Puleo, J.A. (2011). Aeolian transport rates across raked and unraked beaches on a developed coast. *Earth Surface Processes and Landforms*, *36*(6), 779–789.

Nordstrom, K.F, Bauer, B.O., Davidson-Arnott, R.G.D., Gares, P.A., Carter, R.W.G., Jackson, D.W.T., & Sherman, D.J. (1996). Offshore Aeolian Transport Across a Beach: Carrick Finn Strand, Ireland. *Journal of Coastal Research*, *12*(3), 664–672.

Nordstrom, K.F., Jackson, N.L., & Korotky, K.H. (2011). Aeolian Sediment Transport Across Beach Wrack. *Journal of Coastal Research*, *59*, 211–217.

O'Brien, M.P., & Rindlaub, B.D. (1936). The transportation of sand by wind. *Civil Engineering*, *6*, 325–327.

Owen, P.R. (1964). Saltation of uniform grains in air. *Journal of Fluid Mechanics*, *20*(2), 225–242.

Pelletier, J.D., & Field, J.P. (2016). Predicting the roughness length of turbulent flows over landscapes with multi-scale microtopography. *Earth Surface Dynamics*, *4*(2), 391–405.

Poortinga, A., Keijsers, J.G.S., Visser, S.M., Riksen, M.J.P.M., & Baas, A.C.W. (2015). Temporal and spatial variability in event scale aeolian transport on Ameland, The Netherlands. *GeoResJ*, *5*, 23–35.

Poortinga, Ate. (2015). *Beach sand dynamics: measurements, models and scales (PhD Thesis)*, University of Wageningen, The Netherlands.

Poortinga, A., Keijsers, J.G.S., Maroulis, J., & Visser, S.M. (2014). Measurement uncertainties in quantifying aeolian mass flux: evidence from wind tunnel and field site data. *PeerJ*, *2*, e454.

Poortinga, A., van Minnen, J., Keijsers, J., Riksen, M., Goossens, D., & Seeger, M. (2013). Measuring Fast-Temporal Sediment Fluxes with an Analogue Acoustic Sensor: A Wind Tunnel Study. *PLoS ONE*, *8*(9).

Pye, K. (1990). *Physical and human influences on coastal dune development between the Ribble and Mersey estuaries, northwest England.* In Coastal Dunes: Form and Process, chap. 15, edited by K.F. Nordstrom, N P. Psuty, and R.W.G. Carter (pp. 339–359).

Pye, K, & Blott, S.J. (2008). Decadal-scale variation in dune erosion and accretion rates: An investigation of the significance of changing storm tide frequency and magnitude on the Sefton coast, UK. *Geomorphology*, *102*(3–4), 652–666.

Pye, K. (1983). Coastal dunes. *Progress in Physical Geography: Earth and Environment*, *7*, 531–557.

Pye, K., & Tsoar, H. (2009). *Aeolian Sand and Sand Dunes*. Springer, The Netherlands.

Rasmussen, K.R., & Mikkelsen, H.E. (1991). Wind tunnel observations of aeolian transport rates. *Aeolian Grain Transport*, *1*, 135–144.

Raupach, M.R. (1992). Drag and drag partition on rough surfaces. *Boundary-Layer Meteorology*, *60*(4), 375–395.

Raupach, M.R., Gillette, D.A., & Leys, J.F. (1993). The effect of roughness elements on wind erosion threshold. *Journal of Geophysical Research*, *98*(D2), 3023-3029.

Revell, D.L., Komar, P.D., & Sallenger, A.H. (2002). An application of LIDAR to analyses of El Niño erosion in the Netarts littoral cell, Oregon. *Journal of Coastal Research*, *18*(4), 792–801.

Rosen, P. (1979). *Eolian dynamics of a barrier island system*. Leatherman, S.P. (Editor), Barrier Islands. Academic Press, 81–98.

Ruz, M.H., & Anthony, E.J. (2008). Sand trapping by brushwood fences on a beach-foredune contact: the primacy of the local sediment budget. *Zeitschrift Für Geomorphologie, Supplementary Issues*, *52*(3), 179–194.

Ruz, M.H., & Meur-Ferec, C. (2004). Influence of high-water levels on aeolian sand transport: Upper beach/dune evolution on a macrotidal coast, Wissant Bay, northern France. *Geomorphology*, *60*(1–2), 73–87.

Sallenger, A.H., Krabill, W.B., Swift, R.N., Brock, J., Mark Hansen, J.L., Holman, R.A., Stockdon, H. (2003). Evaluation of airborne topographic LIDAR for quantifying beach changes. *Journal of Coastal Research*, *19*(1), 125–133.

Sarre, R.D. (1989). Aeolian sand drift from the intertidal zone on a temperate beach: Potential and actual rates. *Earth Surface Processes and Landforms*, *14*(3), 247–258.

Shao, Y., & Raupauch, M.R. (1992). The overshoot and equilibration of saltation. *Journal of Geophysical Research*, *97*(D18), 20559–20564.

Shao, Yaping, Lu, H., & Shag, Y. (2000). A simple expression for wind erosion threshold friction velocity. *Journal of Geophysical Research*, *105*(17), 437–443.

Sherman, D., & Hotta, S. (1990). *Aeolian sediment transport: theory and measurement.* In Book: Coastal Dunes: Form and Process, Chapter: 2. 17–37.

Sherman, D., Swann, C., & D. Barron, J. (2014). A high-efficiency, low-cost aeolian sand trap. *Aeolian Research*, *13*, 31–34.

Sherman, D.J., & Hotta, S. (1990). *Aeolian sediment transport: theory and measurement*. In K.F. Nordstrom, N. Psuty, and R.W.G. Carter (eds.) Coastal Dunes: Form and Process. Wiley, New York, 16-38.

Sherman, D.J., & Farrell, E.J. (2008). Aerodynamic roughness lengths over movable beds: Comparison of wind tunnel and field data. *Journal of Geophysical Research: Earth Surface*, *113*(2), 1–10.

Sherman, D.J., Jackson, D.W.T., Namikas, S L., & Wang, J. (1998). Wind-blown sand on beaches: An evaluation of models. *Geomorphology*, *22*(2), 113–133.

Sherman, D.J., Jackson, N.L., Nordstrom, K.F., Hesp, P.A., & Arens, S.M. (2005). *Predicting maximum and minimum aeolian sand transport rates to provide a basis for assessing management actions for beaches and dunes*. Universitat de Valencia.

Sherman, D.J., & Li, B. (2012). Predicting aeolian sand transport rates: A reevaluation of models. *Aeolian Research*, *3*(4), 371–378.

Sherman, D.J., Li, B., Ellis, J.T., Farrell, E.J., Maia, L.P., & Granja, H. (2013). Recalibrating aeolian sand transport models. *Earth Surface Processes and Landforms*, *38*(2), 169–178.

Short, A.D., & Hesp, P.A. (1982). Wave, beach and dune interactions in southeastern Australia. *Marine Geology*, *48*(3–4), 259–284.

Smit, Y., Ruessink, G., Brakenhoff, L.B., & Donker, J.J.A. (2017). Measuring spatial and temporal variation in surface moisture on a coastal beach with a near-infrared terrestrial laser scanner. *Aeolian Research*, *31*(A), 19-27.

Smyth, T.A.G., & Hesp, P.A. (2015). Aeolian Dynamics of Beach Scraped Ridge and Dyke Structures. *Coastal Engineering*, *99*, 38-45.

Snacken, F. (1956). Eolisch Zandtransport langs het Belgisch Strand. *Natuurwetenschappelijk Tijdschrijft*, *38*, 89–99.

Sørensen, M. (1991). An analytical model ofwind-blown sand transport. *Acta Mechanica, Supplementum*, *1*, 67–82.

Sørensen, M. (2004). On the rate of aeolian sand transport. *Geomorphology*, *59*(1-4), 53–62.

Spaan, W.P., & Van Den Abeele, G.D. (1991). Wind borne particle measurements with acoustic sensors. *Soil Technology*, *4*(1), 51–63.

Speybroeck, J., Bonte, D., Courtens, W., & Gheskiere, T. (2004). *Studie over de impact van zandsuppleties op het ecosysteem.* Ministerie Vlaanderen.

Speybroeck, J., Bonte, D., Courtens, W., Gheskiere, T., Grootaert, P., Landuyt, W. Van, Degraer, S. (2008). The Belgian sandy beach ecosystem: a review. *Marine Ecology*, *29*(1), 171–185.

Spies, P.J., & McEwan, I.K. (2000). Equilibration of saltation. *Earth Surface Processes and Landforms*, *25*, 437–453.

Spies, P.J., McEwan, I.K., & Butterfield, G.R. (1995). On wind velocity profile measurements taken in wind tunnels with saltating grains. *Sedimentology*, *42*, 515–521.

Statbel. (2017). *Annual rainfall in Belgium from 2006 to 2016 (in millimeters) [Chart]*. In Statista.

Steetzel, H.J. (1993). *Cross-shore Transport during Storm Surges*. TU Delft.

Sterk, G., & Raats, P.A.C. (1996). Comparison of Models Describing the Vertical Distribution of Wind-Eroded Sediment. *Soil Science Society of America Journal*, *60*, 1914–1919.

Stockdon, H., Sallenger, A., List, J., & Holman, R. (2002). Estimation of shoreline position and change using airborne topographic LIDAR data. *Journal of Coastal Research*, *18*(2), 502–513.

Stout, J. E. (1990). Wind erosion within a simple field. *Transactions of the ASAE*, *33*(5), 1597–1600.

Strypsteen, G., De Sloover, L., De Wulf, A., & Rauwoens, P. (2019). Downwind evolution of aeolian saltation across an artificially constructed coastal berm. *Geomorphology (submitted)*.

Strypsteen, G., Montreuil, A.L., & Rauwoens, P. (2017). Aeolian sand transport at the belgian coast: field campaigns and first results. *Proceedings of Coastal Dynamics*, *11*. Helsingør.

Strypsteen, G., van Rijn, L.C., & Rauwoens, P. (2019). On the relation between predicted and observed aeolian transport rates: a field study at the Belgian coast. *Aeolian Research (under Review)*.

Teurlincx, R., Van der Biest, K., Reyns, J., Verwaest, T., & Mostaert, F. (2009). *Haven van Blankenberge – vermindering van de aanzanding van de havengeul en het voorplein*. Borgerhout.

Tsoar, H., White, B., & Berman, E. (1996). The effect of slopes on sand transport-numerical modelling. *Landscape and Urban Planning*, *34*(95), 171–181.

Valance, A., Rasmussen, K.R., Ould El Moctar, A., & Dupont, P. (2015). The physics of Aeolian sand transport. *Comptes Rendus Physique*, *16*(1), 105–117.

van der Wal, D. (1998). Effects of fetch and surface texture on aeolian sand transport on two nourished beaches. *Journal of Arid Environments*, *39*(3), 533.

Van Der Wal, D. (1999). *Aeolian transport of nourishment sand in beach-dune environments (PhD Thesis)*. Amsterdam: Universiteit van Amsterdam.

Van Dijk, P.M., Stroosnijder, L., & De Lima, J.L.M.P. (1996). The influence of rainfall on transport of beach sand by wind. *Earth Surface Processes and Landforms*, *21*(4), 341–352.

Van Pelt, R.S., Peters, P., & Visser, S. (2009). Laboratory wind tunnel testing of three commonly used saltation impact sensors. *Aeolian Research*, *1*(1–2), 55–62.

van Rijn, L.C. (2018). *Aeolian transport over a flat sediment surface*. Leovanrijn-sediment, The Netherlands.

van Rijn, L.C., & Walstra, D.J.R. (2003). *Modelling of Sand Transport in DELFT3D*. WL/Delft Hydraulics, Deflt, The Netherlands, 1–154.

van Rijn, L.C. (1982). Equivalent roughness of alluvial bed. *Journal of Hydraulic Engineering*, *118*(10), 1215–1218.

van Rijn, L.C. (1993). *Principles of sediment transport in rivers, estuaries and coastal seas*. Aqua Publications: Amsterdam.

van Rijn, L.C. (2013). *Erosion of coastal dunes due to storms*. Leovanrijn-sediment, The Netherlands.

Vandebroek, E., Dan, S., Vanlede, J., Verwaest, T., & Mostaert, F. (2017). *Sediment budget for the Belgian coast: final report*. Version 2.0. FHR reports, 12_155_1. Flanders Hydraulics Research/Antea Group: Antwerp. X, 57 + 35 p. appendices.

Vellinga, P. (1986). Beach and dune erosion during storm surges. *Coastal Engineering*, *6*(4), 361–387.

Verwaest, T., Van Poucke, P., Vanderkimpen, P., Van der Biest, K., Reyns, J., Peeters, P., Mostaert, F. (2008). *Overstromingsrisico's aan de Vlaamse kust. Evaluatie van de zeewering: deel 1. Methodologie*. WL Rapporten, 718_2A. Waterbouwkundig Laboratorium/Universiteit Gent/Soresma/Haecon: Antwerpen. 83 + 142 p. appendices.

Voulgaris, G., Collins, M.B., Michel, D., Howa, H., Simmonds, D., & Huntley, D. A. (1998). Measuring and modelling sediment transport on a macrotidal ridge and runnel beach: An intercomparison. *Journal of Coastal Research*, *14*(1), 315–330.

Walter, B.A. (2012). *Wind Tunnel Studies of Shear Stress Partitioning in Live Plant Canopies (PhD Thesis)*. École Polytechnique Fédérale de Lausanne.

White, B.R. (1979). Soil transport by wind on Mars. *Journal of Geophysical Research*, *84*, 4643–4651.

White, S.A., & Wang, Y. (2003). Utilizing DEMs derived from LIDAR data to analyze morphologic change in the North Carolina coastline. *Remote Sensing of Environment*, *85*(1), 39–47.

Wiggs, G.F.S., Livingstone, I., & Warren, A. (1996). The role of streamline curvature in sand dune dynamics: Evidence from field and wind tunnel measurements. *Geomorphology*, *17*(1-3), 29–46.

Williams, G. (1964). Some aspects of the eolian saltation load. *Sedimentology*, *3*, 257–287.

Williams, I.A., Wijnberg, K.M., & Hulscher, S.J.M.H. (2018). Detection of aeolian transport in coastal images. *Aeolian Research*, *35*, 47–57.

Wolfe, S.A., & Nickling, W.G. (1993). The protective role of sparse vegetation in wind erosion. *Progress in Physical Geography*, *17*(1), 50–68.

Xian, X., Tao, W., Qingwei, S., & Weimin, Z. (2002). Field and wind-tunnel studies of aerodynamic roughness length. *Boundary-Layer Meteorology*, *104*(1), 151–163.

Yalin, M.S. (1977). *Mechanics of sediment transport*. Oxford: Pergamon Press, 298 pp.

Yang, Y.Y., Liu, L.Y., Li, X.Y., Shi, P.J., Zhang, G.M., Xiong, Y.Y., ... Han, X.J. (2019). Aerodynamic grain-size distribution of blown sand. *Sedimentology*, *66*(2), 590–603.

Youssef, F., Erpul, G., Bogman, P., Cornelis, W.M., & Gabriels, D. (2008). Determination of efficiency of Vaseline slide and Wilson and Cooke sediment traps by wind tunnel experiments. *Environmental Geology*, *55*(4), 741–750.

Zhang, C.L., Zoua, X.Y., Gonga, J.R., Liu, L.Y., & Liu, Y.Z. (2004). Aerodynamic roughness of cultivated soil and its influences on soil erosion by wind in a wind tunnel. *Soil & Tillage Research*, *75*, 53–59.

Zingg, A.W. (1953). Wind tunnel studies of the movement of sedimentary material. *Proceedings, 5th Hydraulics Conference, Studies in Engineering*, *34*, 111–135.

Curriculum Vitae

Personalia

Glenn Strypsteen
07-11-1990, Brugge, België

Education

2004 – 2006	Scholengroep Sint-Rembert Torhout, Industriële Wetenschappen
2006 – 2009	VTI-Torhout, Industriële Wetenschappen
2009 – 2013	KHBO Oostende & VUT Brno University of Technology, MSc Civil Engineering, Process of Aeolian transport using the EIS-method (cum laude)

Employment

2013 – 2014	Self-employed construction worker
2014 – 2015	Research assistant, KU Leuven Campus Bruges-Ostend, ReLiMoS
2015 – 2019	PhD student, KU Leuven Bruges Campus

List of publications

JOURNAL ARTICLES

Strypsteen, G., Van Rijn, L.C. and Rauwoens, P. (2019). On the relation between predicted and observed aeolian transport rates: a field study at the Belgian coast. Submitted to: *Aeolian Research* (under review).

Strypsteen, G., Houthuys, R. and Rauwoens, P. (2019). Dune evolution at decadal timescales and its relation with potential aeolian transport. Submitted to: *Journal of Marine Science and Engineering, 7(10), 357.*

Strypsteen, G., De Sloover, L., De Wulf, A., and Rauwoens, P. (2019). Downwind evolution of aeolian saltation across an artificially constructed coastal berm. Submitted to: *Aeolian Research.*

Strypsteen, G., and Rauwoens, P. (2019). Aeolian sand transport across a shell-fragmented beach: a field study. Submitted to: *Journal of Coastal Research.*

Van Rijn, L.C. and **Strypsteen, G.** (2019). A fully predictive model for aeolian sand transport. Submitted to: *Coastal Engineering* (accepted).

Montreuil, A.L., Chen, M., Brand, E., **Strypsteen, G.**, Rauwoens, P., Vandenbulcke, A., De Wulf, A., Dan, S., Verwaest, T. (2018). Dynamics of Surface Moisture Content on a Macro-tidal Beach. *Journal of Coastal Research*, 206-210.

Li, J., **Strypsteen, G.**, Kioumarsi, M. (2017). Assessment of Existing RC Structures by Virtue of Nonlinear FEM: Possibilities and Challenges. *Nordic Concrete Research, 57*, 1-14.

Strypsteen, G., Sierens, Z., Joseph, M., Benoot, J., Boehme, L. (2017). Freeze-Thaw Resistance of Stabilized Soils in Flanders. *The International Journal of Environmental Studies*, *74*(4), 603-612.

Sierens, Z., Benoot, J., **Strypsteen, G.**, Joseph, M., Boehme, L. (2017). Behandelde grond als potentiële zandvervanger in zandcement – mengsels. *Geotechniek*, *21*(2), 22-27. (professional oriented).

Joseph, M., De Vlieghe, F., **Strypsteen, G.**, Benoot, J. (2016). Grouted and concreted soils: residue mapping of foundation techniques in Flanders, Belgium. *International Journal of Environmental Studies*, *73*(6), 965-973.

Books

Boehme, L., Joseph, M., Sierens, Z., **Strypsteen, G.**, Benoot, J. (contr.) (2016). ReLiMoS. Ostend: Boehme Luc / RecyCon. ISBN: 9789090301174.

Conference Papers and Abstracts

Strypsteen, G., Roest, B., Rauwoens, P. (2019). Aeolian sediment input to the Belgian coastal dunes. Presented at the NCK Days 2019, Enkhuizen, 20 Mar 2019-22 Mar 2019.

Strypsteen, G., Rauwoens, P. (2019). Dune behaviour along the Belgian coast. Presented at the VLIZ Marine Science Day, Bredene.

Peuteman, J., Janssens, A., De Craemer, R., Hallez, H., Coudeville, P., Cornelly, C., Maricau, A., Degraeve, A., **Strypsteen, G.**, Rauwoens, P., Zabasta, A. (2017). Realizing an international student exchange program for Belarusian engineering students to Belgium. *Proceedings of the SEFI Annual Conference*, 1142-1149.

Strypsteen, G., Montreuil, A.L., Rauwoens, P. (2017). Aeolian sand transport at the Belgian Coast: Field Campaigns and First Results. *Proceedings of Coastal Dynamics 2017*, 502-512.

Benoot, J., Haegeman, W., François, S., Degrande, G. (2015). Dynamic behavior of silica sand under repeated cyclic loading. *Proceedings of the XVI*

ECSMGE Geotechnical Engineering for infrastructure and Development, 6, 3111-3116.

Joseph, M., Benoot, J., **Strypsteen, G.**, Boehme, L. (2015). Limed soils as a replacement for construction sand in stabilized sands. *Proceedings of the XVI ECSMGE Geotechnical Engineering for Infrastructure and Development*, *16*(1), 566-2570.

Strypsteen, G., Rauwoens, P. (2018). Aeolian sediment transport on a Belgian beach: spatio-temporal variability during alongshore winds. Presented at the International Conference on Aeolian Research, Bordeaux, 25 Jun 2018-29 Jun 2018.

Strypsteen, G., Rauwoens, P. (2018). Aeolian sediment transport characteristics at an artificially scaped beach. Presented at the EGU General Assembly, Vienna, 08 Apr 2018-13 Apr 2018.

Strypsteen, G., Rauwoens, P. (2018). Dynamic sand: Towards a resilient Belgian Coast. Presented at the VLIZ Marine Science Day, Bredene, 21 Mar 2018-21 Mar 2018.

Strypsteen, G., Rauwoens, P. (2018). Aeolian sediment transport processes in a managed beach-dike system. Presented at the NCK Days 2018, Haarlem, 21 Mar 2018-23 Mar 2018.

Strypsteen, G. (2017). Field measurements on Aeolian sediment transport at the Belgian Coast. Presented at the Research Day @ Construction Technology Cluster, Thermotechnisch Instituut, Kasteelpark 41, 3001 Leuven, 07 Jun 2017-07 Jun 2017.

Strypsteen, G., Rauwoens, P. (2017). Aeolian Sediment Flux Measurements at the Belgian Coast: Field Campaigns 2016. Presented at the NCK Days 2017, Royal Netherlands Naval Institute, Den Helder - Het Nieuwe Diep Netherlands, 15 Mar 2017-17 Mar 2017.

De Groot, A., De Vries, S., Arens, B., Bodde, W., De Winter, W., Donker, J., Duarte Campos, L., Galiforni Silva, F., Goessen, P., Hage, P., Hoonhout, B., Keijsers, A., Montreuil, A.L., Mulder, J., Nolet, C., Rauwoens, P., Riksen, M., Ruessink, G., Smit, M., Smit, Y., **Strypsteen, G.**, Van der Valk, B., Van Puijenbroek, M., Wijnberg, K., Williams, I. (2017). State of the Art of Aeolian and Dune Research on the Dutch and Belgian Coast. Presented at the NCK Days 2017, Royal Netherlands Naval Institute, Den Helder - Het Nieuwe Diep Netherlands, 15 Mar 2017-17 Mar 2017.

Strypsteen, G. (2016). Windblown sand transport: Measurements at the Belgian Coast. Presented at the Research Day @ KU Leuven Technology Campus Ostend, Ostend, Belgium, 17 Nov 2016-17 Nov 2016. (professional oriented).

Strypsteen, G., Rauwoens, P. (2016). Agglomeration of a comprehensive model for the wind-driven sand transport at the Belgian Coast. In: Geophysical Research Abstracts: vol. 18 (396-396). Presented at the EGU General Assembly, Vienna, Austria, 17 Apr 2016-22 Apr 2016.

Strypsteen, G., Rauwoens, P. (2016). Wind-blown sand in beach-foredune and beach-dike environments at the Belgian Coast. In: Book of abstracts – VLIZ Marine Scientist Day: vol. 75 (109-109). Presented at the Vliz Marine Scientist Day, Brugge, Belgium, 12 Feb 2016-12 Feb 2016.

Strypsteen, G. (2015). Agglomeration of a comprehensive model for the wind-driven sand transport at the Belgian Coast. Presented at the Research Day @ KU Leuven Technology Campus Ostend, Ostend, Belgium, 25 Nov 2015-25 Nov 2015. (professional oriented).